Highly structured polymer foams from liquid foam templates using millifluidic lab-on-a-chip techniques

Aouatef Testouri

THESE DE DOCTORAT
DE l'UNIVERSITE PARIS SUD XI

pour obtenir le grade de
DOCTEUR DE L'UNIVERSITE PARIS SUD XI
Mention: Chimie

Présentée par

Aouatef Testouri

Titre:
HIGHLY STRUCTURED POLYMER FOAMS FROM LIQUID FOAM TEMPLATES USING MILLIFLUIDIC LAB-ON-A-CHIP TECHNIQUES

Thèse soutenue au Laboratoire de Physique des Solides le 8 Octobre 2012 devant le jury composé de:

Brigitte Pansu	Présidente du jury
Cosima Stubenrauch	Rapporteur
Fatima Vaz	Rapporteur
Frédéric Leising	Rapporteur
Dominique Langevin	Directrice de thèse
Meik Ranft	Invité

ACKNOWLEDGEMENTS

" Controlling a foam by pushing a button ".
Everything began when I saw this thesis subject on the Internet, just at the moment when I was asking myself what do I want to do after my Masters degree?
I was so curious and at the same time excited to know more about that subject that I've already get a bit of an answer for my question: Seems like I want to do a PhD!
When I first went to visit the LPS, I immediately fell in love with this green, quite and lovely place. Then, when I met the people from the MOUS group, I just said to myself, I **do** want to do **a PhD** in **Orsay** although the thesis subject which I finally chose was totally different from controlling a foam! I encountered for the first time of my life a very young and energetic group of scientists, coming from all over the world, who work in a perfect synergy.

Then, I think that all the people who did a PhD know the rest of the story. Three years (in my case four) of working on your subject pass in which you learn not only about science but also about everything but science such as do-it yourself stuff, human being psychology, and especially patience.
One probably never gets again the chance to spend three years in exploring a scientific subject in an independent and playful manner and especially to have a quasi-free agenda to do things the way you like. I advice therefore, all the PhD beginners to be aware of the opportunities that the thesis can offer and to profit at most of them.

The years of working on my PhD were a mix of moments of doubt and certainty, success and failure, or timidity and self-confidence. These ups and downs helped me a lot to grow up professionally and personally. And what aided me above all, is that there were people who helped me to put in perspective the problems I encountered and supported me all through this delicate period.
I spent four amazing years full of enriching/inspiring exchanges with very interesting people who shared generously their knowledge and time with me. I learnt a lot from them and I am grateful to each one. I would like to thank the wonderful members of my team, the MOUS team, which have created a pleasant atmosphere I simply enjoyed working in during the last four years.
Firstly, I thank *Dominique Langevin* for her advices, availability and enriching discussions. I also thank *Anniina Salonen* and *Emmanuelle Rio* for personal and scientific discussions with a special thank to *Manue* for her support in my struggle against French bureaucracy, and to *Anniina* for countless coffees.

My deepest gratitude goes to *Wiebke Drenckhan*, my "direct-supervisor". She has been more than a simple supervisor for me by being always present to help. When you work with Wiebke, you have the chance to adsorb the positive energy and enthusiasm, which she radiates all around. Having both German rigour and

Italian lenience, she helped me doing things in a very severe and meticulous way, but always finding the wright words to boost spirit.

Somebody said in his thesis acknowledgement "*I will never be able to repay what the supervisor did for me. But I can and will always try to give to students what he-and many other people -have given to me*."
It is now my turn to say that I will never be able to repay what was done for me. And that I will certainly try my best to give it back to students. *Thank you Wiebke*!

I would also like to thank all the engineers from BASF (Meik ranft, Jens ferbitz, Daniel Freidank, David Hajnal, Francisco Lopez) for sharing their precious time and expertise.

I will not single out all the people who I got a chance to meet and to work with since I am afraid to forget some names. But I warmly thank every person who helped me somehow solving academic, technical, computing, administrative or personal problems.

The success of a PhD cannot be achieved without family and friends support.
Above all I would like to thank *Aych*, my husband for his unconditional support, during the whole thesis and long before, and for his patience and understanding. My dear *Aych*, I love you.
My gratitude and love for my brother and sisters is beyond words! Even if you are out of my sight, you are far from being out of my mind. Thank you for "pampering" me from my childhood until now.

Now I'll switch to French to thank people who do not speak English (or won't be able to speak it in the near future such as my 20 months-old son).

Tout d'abord je remercie ma belle-famille qui m'a énormément aidé tout le long de ma thèse. Merci *Leila* pour ta gentillesse, ta présence et tout le temps que tu m'a accordé. Je ne sais pas ce que j'aurai fait sans toi!

Ces quatres années de thèse ont été marquées par le plus merveilleux événement de ma vie, la naissance de mon fils *Anis-Zackary*. Je tiens à le remercier (même s'il ne pourra le comprendre que dans quelques années). Merci pour avoir égayé ma vie et de m'avoir donné la force de me battre pendant les moments difficiles.

Je remercie également *Ahlem*, ma quasi-soeur et mon amie d'enfance qui a toujours su trouvé les bons mots pour me remonter le moral.

Enfin (last but not least), je dédie ce travail à mes parents, les êtres qui me sont les plus chers. Je leur exprime toute ma gratitude pour tous les sacrifices qui ont fait pour moi et qu'ils continuent de faire.

TABLE OF CONTENTS

LIST OF FIGURES

LIST OF TABLES

LIST OF SYMBOLS

C: Reactant concentration
CMC: Critical Micelle concentration
γ_∞: Equilibrium surface tension
γ : Dynamic surface tension
$\boldsymbol{\phi_L}$: Liquid fraction
$\boldsymbol{\phi_{L,c}}$: Critical liquid fraction
$\boldsymbol{V_{Foam}}$: Foam volume
$\boldsymbol{V_{Liquid}}$: Liquid volume
$\boldsymbol{\rho_{Foam}}$: Foam density
$\boldsymbol{\rho_{Liquid}}$: Liquid density
$\boldsymbol{\rho_r}$: Relative density
$\boldsymbol{\rho_{Polymer}}$: Polymer density
$\boldsymbol{\Delta p}$: Pressure difference across air/liquid interface
$\boldsymbol{R_1}$: Radius of curvature
$\boldsymbol{R_2}$: Radius of curvature
$\boldsymbol{\kappa}$: Mean curvature
$\boldsymbol{P_{Index}}$**:** Polydispersity index
$\boldsymbol{R_B}$**:** Bubble radius
$\boldsymbol{D_{B:}}$ Bubble diameter
$\boldsymbol{D_{C:}}$ Capillary diameter
$\boldsymbol{\tau_{S:}}$ Solidification time
$\boldsymbol{\tau_F}$: Foaming time
$\boldsymbol{\tau_M}$: Mixing time
$\boldsymbol{Re}$: Reynolds number
$\boldsymbol{U}$: Liquid velocity
$\boldsymbol{L}$: Characteristic dimension of the system
$\boldsymbol{\eta}$**:** Dynamic viscosity
$\boldsymbol{\rho}$: Density
$\boldsymbol{Ca}$: Capillary number
Qg: Gas flow rate
$\mathbf{Q_l}$: Liquid flow rate
$\dot{\gamma}$: Shear rate
G': Storage modulus
G": Loss modulus
t: Time
$\mathbf{t_{1/2}}$: Half-life time
$\mathbf{T_G}$: Glass transition temperature
$\boldsymbol{\varepsilon}$: Strain
$\boldsymbol{\varepsilon_0}$: Densification strain
$\boldsymbol{\sigma}$: Stress
$\boldsymbol{\alpha}$: Exponent of the power law
$\boldsymbol{\beta}$: Prefactor of the power law
$\mathbf{E_F}$: Young's modulus of the foam
$\mathbf{E_P}$: Young's modulus of the polymer

K: Shear modulus
μ: Bulk modulus
ν: Poisson ratio

1 GENERAL INTRODUCTION AND APPROACH OF OUR STUDY

Polymer foams belong to the solid foam family which are versatile materials, extensively used for a large number of applications such as automotive, packaging, sport products, thermal and acoustic insulators, tissue engineering or liquid absorbents [1-5]. Composed of air bubbles entrapped in a continuous solid network, they combine the properties of the polymer with those of the foam to create an intriguing and complex material. Polymer foams not only allow one to use the wide range of interesting properties that the polymer offers, but also permits to profit from the advantageous properties of foams including lightness, low density, compressibility and high surface-to-volume ratio.

These "up-to-date" materials are at the heart of the latest high-technology applications [3, 6] thanks to their inexhaustible qualities, which leads in parallel to an increasing number of fundamental questions seeking for a better understanding of the properties of these fancy materials.

Generally, the properties of polymer foams are strongly related to their density and their structure (bubble size and size distribution, bubble arrangement, open vs. closed cells) [7]. Low density foams, for instance, have good energy absorption and are thus used in the cushioning and packaging industries. Thermal conductivity is reduced when bubble size decreases due to the suppression of convection in the gas entrapped inside the bubbles. Open-cell foams have high absorption rate and are used as sponges.

Having a good control over foam properties is thus achieved by first controlling its density and structure. With this in mind, the last decades have seen the development of a variety of foaming techniques. However, most of these techniques combine simultaneous foaming and solidification of an initially liquid mixture in a complex manner which poses a great challenge to fine-tuning and scientific understanding.

In parallel, the understanding of liquid foams has developed significantly over the last 20 years [8-10], providing an increasingly robust description of their physico-chemical and structural properties. Scientists now avail of a wide range of surface active agents (low molecular weight and polymeric amphiphiles, proteins, polymers, particles, etc.) to create stable foams from various liquids (including non-polar ones). Especially particle-stabilised foams can be "superstable", i.e. without change in foam structure over up to several months [11, 12]. Furthermore, scientists have elaborated a large number of foaming techniques which provide excellent control over bubble sizes and bubble size distributions. Bubble sizes can be tuned from tens of micrometers to several millimeters (and even meters), and bubble size distributions can range from polydisperse to extremely monodisperse [13]. Last but not least, it is now very well understood how bubbles pack together in liquid foams, i.e. how liquid content, bubble size distribution and foam structure are related [10, 14-17].

In order to build on this expertise on liquid foams, it is desirable to develop techniques in which solid foams are generated essentially in a two-step process [10] (Figure 1.1): a sufficiently stable liquid foam with well-controlled structural properties is generated in a first step, and then solidified in a second one. These two steps can either be completely separated by choosing a solidification mechanism which is initiated externally at a desired moment (UV, temperature...). Or, foaming and onset of solidification may occur simultaneously, but foam generation and solidification times need to be matched in order to make sure that the desired foam can be created in a liquid state, i.e. before the solidification freezes the movement of liquid and bubbles. With such a two-step approach, the generation of solid foams can be divided into a number of well-separated sub-tasks (Figure 1.1), which can be controlled and optimised separately.

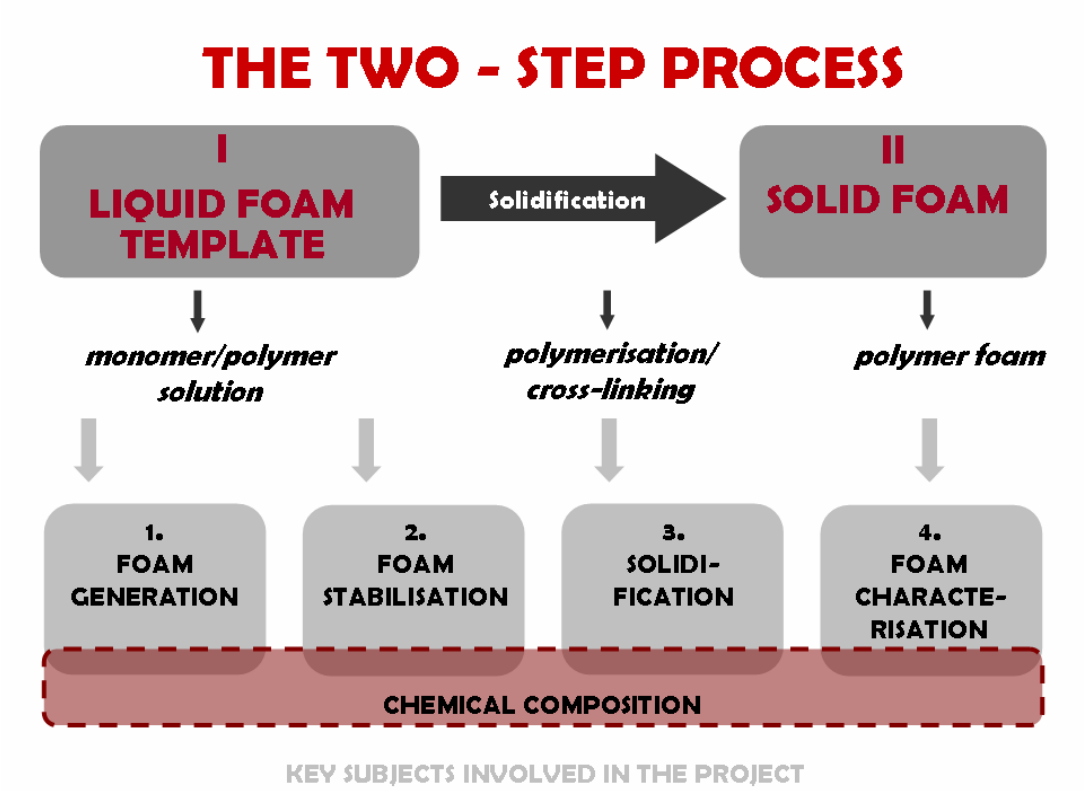

Figure 1.1: The work steps of our study. A two-step process is used to generate first a liquid foam template which is then solidified.

The transition from liquid to solid state is a sensitive issue of a great importance and therefore needs to be controlled with sufficient accuracy. It is essentially composed of three key steps: foam generation, mixing of reactants and foam solidification and requires the optimisation of foam stability in conjunction with an appropriate choice of both foaming time and solidification time. Furthermore, a good homogeneity of the polymer foam calls for a good mixing of the different reactants involved in the foaming and polymerisation. The mixing consists in

blending the different chemicals required for the generation of the final solid foam such as: surfactants, polymerising/cross-linking agent, and catalyst. This step can be performed before or during foaming.

A particularly powerful demonstration of the advantages of this two-step approach is given by solidifying monodisperse liquid foams [13], in which all bubbles have the same size. In a liquid foam, equal-volume bubbles self-order into periodic, close-packed structures under gravity or confinement [17, 18] (Figure 1.2). As such, monodisperse foams provide simultaneous control over the size and the organisation of the pores in the final solid with an accuracy which is expected to give rise to a better understanding of the structure-property relationship of porous solids and to the development of new porous materials.

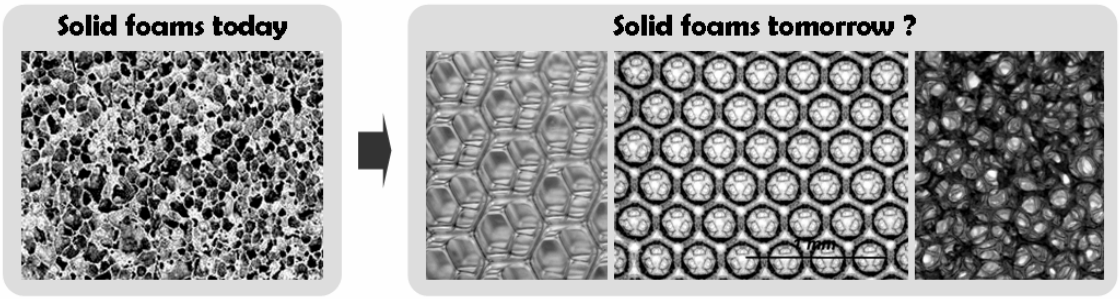

Figure 1.2: The current understanding of liquid foams presents a fruitful source for the development of techniques which provide an important degree of control over the structural properties of porous materials.

Goal of this study is therefore to establish appropriate foaming techniques for the controlled generation of monodisperse polymer foams. As such, our investigations join numerous others, which try to link the challenges of the industrial world and the exploring approach of academy. In particular, we aim to explore the new spectrum of properties, which polymer foams offer when we introduce an ordered structure into them since the most widely used polymer foams nowadays have disordered structures. The goal of our study is to demonstrate the feasibility of this approach for different classes of polymers, including biomolecular hydrogel, superabsorbent polymer and polyurethane. More specifically, the three systems studied in this thesis are:

1. Chitosan (Chapter 5) a biopolymer extensively used for many applications such as medical applications, tissue engineering and drug delivery.

2. Superabsorbent synthetic polymer (SAP) (Chapter 6), which is known for its ability to absorb up to 100 times its own weight of water. It is extensively used in disposable nappies, soil treatment, or humidity controllers.

3. Polyurethane (PU) (Chapter 7), one of the most used polymers in various applications including automotive, thermal and acoustic insulation, or cushioning.

The motivation of performing such study is different for each polymer: In the case of **Chitosan**, the production of highly controlled porous structures from biocompatible and biodegradable hydrogel proposes a new material for cell culture and scaffolding [19-21]. Producing structured foams in a **superabsorbent** medium enhances the absorption quality of the polymer by offering a homogeneous and rapid liquid uptake [22, 23] improving thus the performance of the SAP material. The most promising example of the advantages of using ordered polymer structures is monodisperse **polyurethane** foams where a modification of the foam structure leads to a noticeable change in the mechanical properties of the final foam. This is believed to improve not only the mechanical properties of polyurethane foams but also the acoustic ones.

We discuss the properties of interest for each of the polymer in the sections dedicated to their study. For each studied system, we started from the general idea of using the two-step process for the generation of the final polymer that we translated into experimental set-ups, which, in some cases, were entirely built by us. As we used these polymers for the first time, we needed to perform optimisation and feasibility studies in order to find the most suitable working parameters that fit each system.

As shown in Figure 1.1, our research was divided into four principal subjects:

1. **Foam generation** using a suitable microfluidic technique for each polymer system in which highly ordered foams are produced. Among the challenges of this step there are the control over the bubble size and the foam density (especially reaching low densities).

2. **Foam stabilisation** which aims to ensure the foam stability during the whole foaming process and sufficiently long after.

3. **Foam solidification** during which the polymerisation/crosslinking reaction occurs. The most intricate point in this step is the solidification time which has to be chosen wisely (long enough to allow bubbles organisation, and short enough to freeze the foam before its destabilisation).

4. **Foam characterisation** which provides information about the structures and the properties of the final solid foams and relationships between them. This step was not performed for all polymer systems since it requires, in some cases special techniques and experimental set-ups unavailable in our lab.

All four subjects are strongly interlinked, particularly through questions of the chemical formulation.

For the generation of the structured polymer foams we use Lab-on-a-Chip technologies (Chapter 3), which allow the “shrinking” of large-scale set-ups to micro/millimetric scales [24-26]. It permits also to perform “flow chemistry” in

which the various liquid and gaseous ingredients of the foam are injected and mixed in a purpose-designed network of the micro- and millifluidic Lab-on-a-Chip [27, 28]. We adjust this approach according to the requirements of each polymer system, i.e. the foaming and the mixing techniques are chosen to fit the properties of each system, and can be exchanged to fit the properties of the studied systems. The channel network can have mainly two designs (Figure 1.3). In the first design, solutions to-be-foamed are first mixed, then foamed, while in the second, these solutions are first foamed, then mixed.

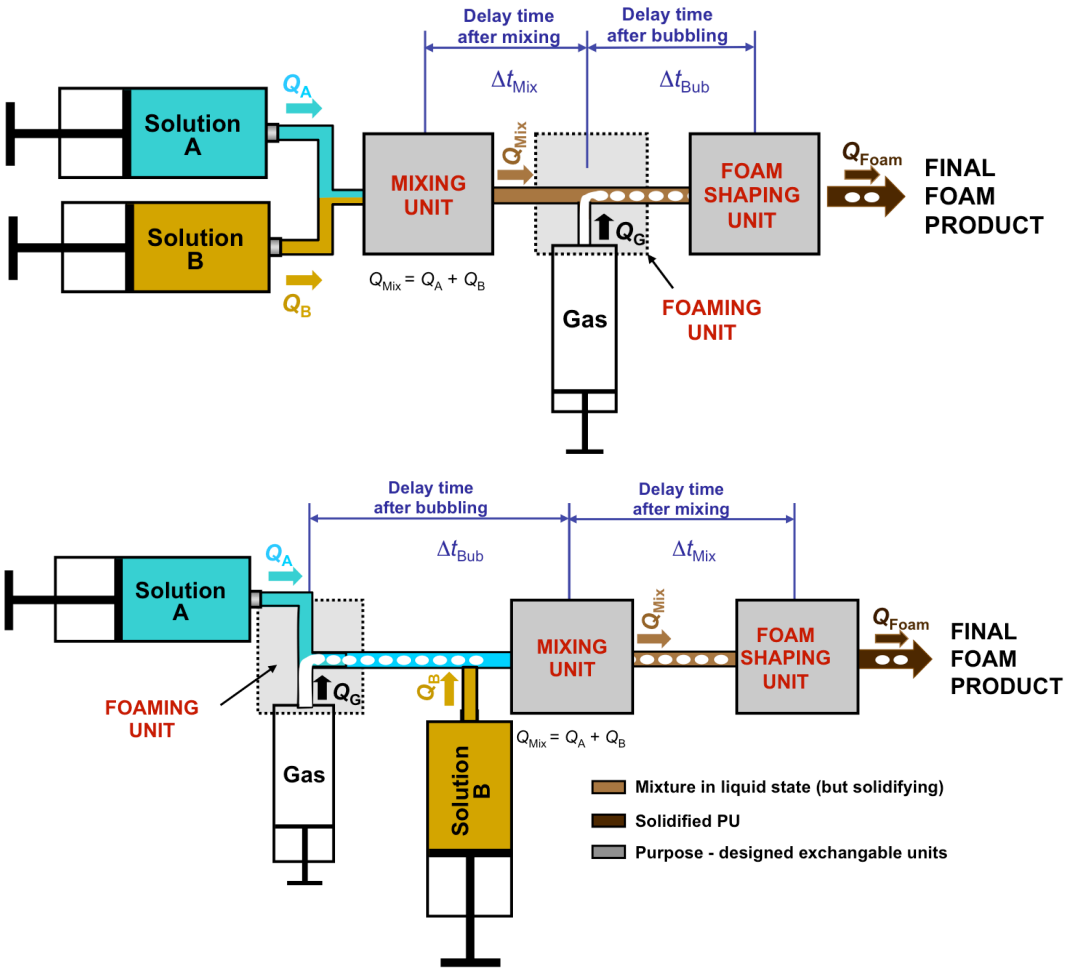

Figure 1.3: Lab-on-a-Chip channel network designs

We proposed a suitable way of generating monodisperse ordered foams according to the requirements of each studied polymer system. We also provided for each system the appropriate chemical formulations, the most adapted way of designing the foaming geometries and the most suitable working parameters. In the case of hydrogel and superabsorbent foams (Chapters 5 and 6), the work was stopped as soon as we could show how to obtain the well-controlled foam structures. As regards the PU foams, investigations of the structure-properties relationship (Chapter 7) were pursued. Figure 1.4 shows some of the ordered foams which we produced from the three polymers cited above.

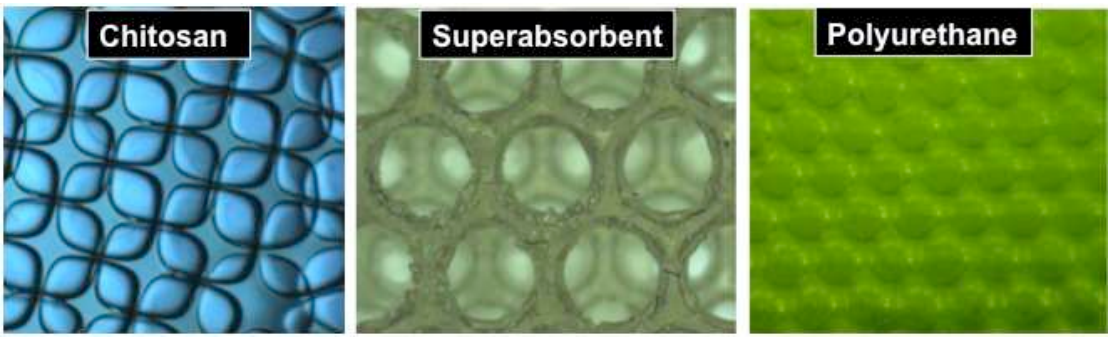

Figure 1.4: Pictures of the monodisperse ordered foams generated from the three polymer systems studied

This thesis is composed of six chapters. Chapter 2 introduces the basic notions about liquid and solid polymer foams which are of important for our study. Then, an overview about microfluidics and Lab-on-a-Chip technologies is given in Chapter 3. Chapter 4 introduces in a general way the experimental techniques used by us throughout the thesis, i.e. for the characterisation of the three studied systems. Some of these techniques will be described in more detail in the section dedicated to the study of a specific polymer system since they vary from one to another. The Chapters 5-7 describe in depth how to produce highly structured monodisperse polymer foams from liquid foam templates using Lab-on-a-Chip technologies for the three polymer systems studied by us: Chitosan, Superabsorbent and finally polyurethane. Finally, this work (Chapter 8) is concluded with a summary of the whole study and some outlook and interesting ideas to take over this work in the future are given.

BIBLIOGRAPHY

1. Gibson, L.J., *Cellular Solids.* Mrs Bulletin, 2003. **28**(04): p. 270-274.
2. Drenckhan, W., et al., *Polymer foams*, B.S. Ludwigshafen, Editor 2008.
3. Mills, N., *Polymer Foams Handbook: Engineering and Biomechanics Applications and Design Guide*2007, Oxford: Butterworth-Heinemann.
4. Lee, S.T. and N.S. Ramesh, *Polymeric foams - Mechanisms and Materials*. Polymeric foams series, ed. S.T. Lee2004, Bica Raton, Flrida, USA: CRC Press.
5. Lee, S.T., C.B. Park, and N.S. Ramesh, *Polymeric foams: science and technology*2006: CRC/Taylor & Francis.
6. Princen, H.M., *The structure, mechanics, and rheology of concentrated emulsions and fluid foams*. Encyclopedic Handbook of Emulsion Technology ed. J. Sjoblom2000: Marcel Dekker. 243.
7. Sachchida N Singh, A.B., David Eaves, *Handbook of polymer foams*, ed. D. Eaves2004: Rapra Technology Limited.
8. Weaire, D. and S. Hutzler, *The Physics of Foams*1999, Oxford: Clarendon Press.
9. Cox, S., D. Weaire, and K. Brakke, *Liquid foams - Precursors for Solid Foams*. Cellular Ceramics: Structure, Manufacturing, Properties and Applications, ed. P.C.a.M. Scheffler2005: Wiley.
10. Kraynik, A.M., *Foam structure: From soap froth to solid foams.* Mrs Bulletin, 2003. **28**(4): p. 275-278.
11. Hunter, T.N., et al., *The role of particles in stabilising foams and emulsions.* Advances in Colloid and Interface Science, 2008. **137**(2): p. 57-81.
12. Gonzenbach, U.T., et al., *Ultrastable particle-stabilized foams.* Angewandte Chemie-International Edition, 2006. **45**(21): p. 3526-3530.
13. Drenckhan, W. and D. Langevin, *Monodisperse foams in one to three dimensions.* Current Opinion in Colloid & Interface Science, 2010. **15**(5): p. 341-358.
14. Kraynik, A.M., D.A. Reinelt, and F. van Swol, *Structure of random monodisperse foam.* Physical Review E, 2003. **67**(3): p. 031403.
15. Kraynik, A.M., D.A. Reinelt, and F. van Swol, *Structure of Random Foam.* Physical Review Letters, 2004. **93**(20): p. 208301-4.
16. Hoehler, R., et al., *Osmotic Pressure and Structures of Monodisperse Ordered Foam.* Langmuir, 2007. **24**(2): p. 418-425
17. van der Net, A., et al., *Crystalline arrangements of microbubbles in monodisperse foams.* Colloids and Surfaces A: Physicochemical and Engineering Aspects, 2007. **309**(1-3): p. 117-124.
18. Jang, W.-Y., A.M. Kraynik, and S. Kyriakides, *On the microstructure of open-cell foams and its effect on elastic properties.* International Journal of Solids and Structures, 2008. **45**(7-8): p. 1845-1875.
19. Yi, H., et al., *Biofabrication with Chitosan.* Biomacromolecules, 2005. **6**(6): p. 2881-2894.
20. Testouri, A., et al., *Highly Structured Foams from Chitosan Gels.* Macromolecules, 2010. **43**(14): p. 6166-6173.

21. Poole, S., *The foam-enhancing properties of basic biopolymers.* International Journal of Food Science & Technology, 1989. **24**(2): p. 121-137.
22. Omidian, H., J.G. Rocca, and K. Park, *Advances in superporous hydrogels.* Journal of Controlled Release, 2005. **102**(1): p. 3-12.
23. van der Net, A., et al., *Highly structured porous solids from liquid foam templates.* Colloids and Surfaces a-Physicochemical and Engineering Aspects, 2009. **346**(1-3): p. 5-10.
24. Figeys, D. and D. Pinto, *Lab-on-a-Chip: A Revolution in Biological and Medical Sciences.* Analytical Chemistry, 2000. **72**(9): p. 330 A-335 A.
25. Dittrich, P.S. and A. Manz, *Lab-on-a-chip: microfluidics in drug discovery.* Nat Rev Drug Discov, 2006. **5**(3): p. 210-218.
26. Chow, A.W., *Lab-on-a-chip: Opportunities for chemical engineering.* AIChE Journal, 2002. **48**(8): p. 1590-1595.
27. Santiago V Luis, E.G.-V., *Chemical Reactions and Processes Under Flow Conditions*. S.V. Luis and E. Garcia-Verdugo ed, ed. G.A.K. James H. Clark 2009: Royal Society of Chemistry; 1st Edition. edition (November 20, 2009). 212.
28. Testouri, A., et al., *Generation of porous solids with well-controlled morphologies by combining foaming and flow chemistry on Labs-on-a-chip.* to appear in Colloid and Interface Science A, 2012.

2 LIQUID AND SOLID POLYMER FOAMS: FUNDAMENTALS

2.1 INTRODUCTION

Most solid polymer foams have been liquid in the initial stage of their formation. They are most of the time generated by different ways of solidification of pre-existing liquid foam which can be either aqueous or non-aqueous [1]. In this thesis we optimise the solidification process such that it is rapid (yet gentle) enough to freeze the liquid foam structure just after the bubbles organise and order. The solid foam is consequently the solid replica of the liquid one. This approach of their production profits from the transferable wide knowledge built on liquid foams through decades. In fact, the understanding of *liquid foams* has developed significantly over the last 20 years [1-3], providing an increasingly robust description of their physico-chemical and structural properties.
Studying liquid foams and controlling their structure and properties is a good starting point to understand and ameliorate the properties of the solid foams they will become. In this chapter we will therefore introduce the basic notions of liquid and solid foams, which are essential for the understanding of the following results. I will first begin by a presentation of the most important key ideas concerning liquid foams, since we use them as precursors for the solid ones.

2.2 FOAM STABILISATION

Liquid foams used as precursor for solid polymer foams are generally very similar to conventional aqueous liquid foams. They are usually made from monomer or polymer solutions which tend to be more viscous than aqueous solutions due to their higher molecular weight. They remain nevertheless similar in terms of foam properties [4], techniques of generation and foam aging. In particular, they have the same structural building blocks and obey to the same physical laws.

2.2.1 Surface active agents used for foam stabilisation

Liquid foams are materials made of bubbles surrounded by a liquid which contains surface active agents. The foam owes its stability to these species, called **surfactants** which are amphiphilic molecules having both hydrophilic and hydrophobic parts and tend spontaneously to go to the air/liquid interface of the bubble surface in such a way that their hydrophilic head remains inside the liquid and their hydrophobic tail direct towards air [5-10] as shown in Figure 2.1.

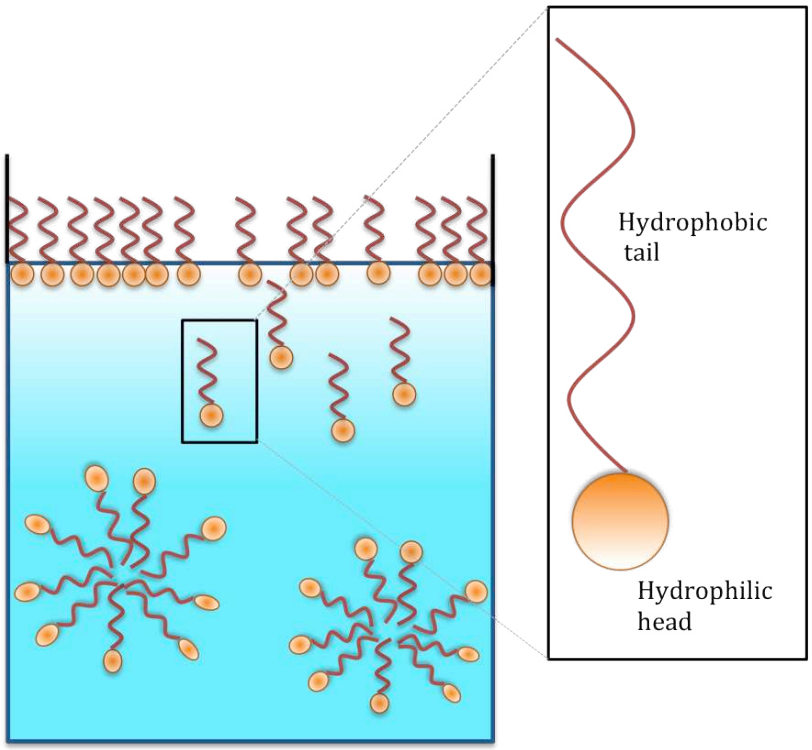

Figure 2.1: Surface active agents forming layer at the air water interface: their hydrophilic head is in the solution, whereas the hydrophobic tail is in the air. Micelles start to appear above the Critical Micelle Concentration (CMC).

There are different kinds of surfactants [7, 11-17]. Depending on whether the hydrophilic part is charged or not, one distinguishes between anionic (negatively charged), cationic (positively charged), amphoteric (having both negative and positive charges) and non-ionic surfactants (non charged). Surfactants may also be grouped into other subclasses. For example, **low molecular weight surfactants** diffuse rapidly to the interfaces and are known to be good foaming agents, but they tend to have poor long-term stability. Larger, and more complex agents, like partially hydrophobic particles [18], proteins [19, 20] or amphiphilic polymers may provide long term foam stability, but suffer from slow adsorption dynamics. It has been shown that for some systems the use of surfactants mixture can be an optimal option for the stabilisation of foams [21-24]. In this work, we use mainly non-ionic, low molecular weight surfactants for the stabilisation of the hydrogel and the superabsorbent foams (Sections 5 and 6) and amphiphilic block-copolymers for the stabilisation of polyurethane foams (Section 7).

2.2.2 Surfactant adsorption

As soon as a bubble is created in a liquid surfactant solution, the surface active molecules diffuse to the air/liquid interface where they form a monolayer [2, 6, 7]. The stability of the foam depends strongly on that of the liquid films which separate neighbouring bubbles and which consist of two narrowly-spaced monolayers of surfactants. When these films drain under gravity, they become

very thin until they rupture leading to the total collapse of the foam (Section 2.6) [15, 25, 26].
The stability of a liquid film against continuous thinning is ensured by repulsive forces between the surface-active molecules present on its two layers. These forces can be of steric or electrostatic nature [27] and are included in the *disjoining pressure*, which is the force per unit area [2, 8, 9].

When a foam undergoes rapid local stretching due to a deformation, the corresponding increase in surface area leads to a temporary decrease in the interfacial concentration of surface active molecules and consequently to an increase in the local surface tension. A gradient of surface tension is therefore created and the surfactants diffuse to populate the thinner surface in order to restore equilibrium. This is known as *Marangoni effect*, or self-healing effect [6, 7].

Since a foam has a very high surface to volume ratio, enough surface active molecules need to be added to stabilise all the air/liquid interfaces it encloses. In fact, optimal foam stability is guaranteed only when the interfaces are sufficiently covered with surface active agents. In general, the concentration has to be well above a critical concentration, ***the critical micelle concentration*** (**CMC**). Above this concentration, the surfactants start to assemble into micelles, which act as surfactant reservoirs [2, 7, 10]. We will also use it in the following as a unit of concentration of the surfactants involved in our study (Section 5, Section 6 and Section 7).

Figure 2.2a shows typical diffusion adsorption curves ("dynamic surface tension curves") at four different surfactant concentrations (A, B, C and D),

A: The surface tension is constant in time. This surface tension corresponds to the surface tension of the pure solvent ($C = 0$).
B: The surface tension decreases slightly when a small quantity of surfactant is added. The equilibrium surface tension is reached very slowly ($C = C_1$).
C: At the CMC, the interface is quickly covered by the surfactants leading to a significant and rapid drop of the surface tension ($C = C_2 > C_1$).
D: There is no change in the surface tension after adding more surfactants (**D**) but the adsorption time drops with increasing surfactant concentration ($C = C_3 > C_2$).

In fact, high surfactant concentrations are needed to stabilise rapidly the foam (air/liquid interfaces) since surfactant diffusion to the interfaces occurs more rapidly.

Figure 2.2b shows how the equilibrium surface tension γ_∞ typically varies with the logarithm of the surfactant concentration, indicating also the organisation of the surface active molecules (in the bulk and at the air/solution interface as their concentration increases) for the same four key points indicated above,

A: The solution does not contain surfactants. The surface tension is equal to the surface tension of the pure solvent.

B: As surface active agents are added, they adsorb at the air/solution interface leading to a decrease in the surface tension.
C: Molecules start to self-assemble into micelles in the bulk. The corresponding concentration is the *CMC.*
D: Above the *CMC*, the surface tension becomes independent of the surfactant concentration since the interface is saturated.

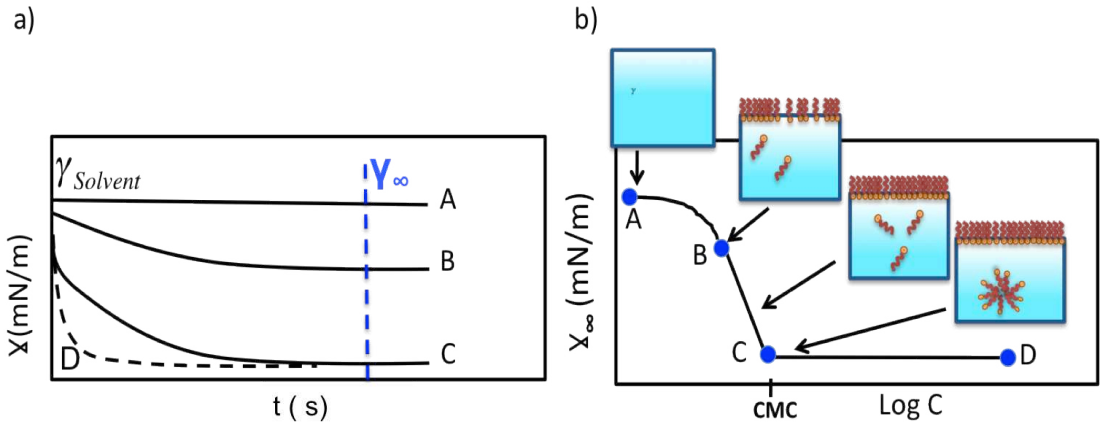

Figure 2.2: a) Dynamic surface tension curves γ (t) for different surfactant concentrations. b) Equilibrium surface tension γ_∞ versus logarithmic surfactant concentration.

2.3 THE LIQUID FOAM STRUCTURE

Bubbles contained in a liquid foam can have different shapes. These shapes depend strongly on ***the liquid fraction*** of the foam, which is given by

$$\phi_L = \frac{V_{Liquid}}{V_{Foam}}, \qquad \textbf{(2. 1)}$$

where V_{liquid} is the liquid volume and V_{Foam} the volume of the foam [7]. The liquid fraction relates the liquid and ***the foam density*** ρ_{Liquid} and ρ_{Foam}, respectively via

$$\rho_{Foam} = \phi_L \, \rho_{Liquid}. \qquad \textbf{(2. 2)}$$

According to the liquid fraction ϕ_L of the foam one can differentiate between three cases [1, 2, 28, 29] (Figure 2.3):

- In the ***high density limit*** where $\phi_L \rightarrow 1$, spherical bubbles are loosely dispersed in the liquid and separated by thick walls of liquid. They are far from each other and form a "bubbly liquid".

- Upon decreasing $\phi_L$one obtains a **wet foam** in which two touching bubbles are slightly deformed to decrease their total surface area. A thin film appears at the contact zone between these bubbles. Each foam has a well-defined ***wet limit*** at which the bubbles spherical and close-packed. The critical liquid fraction $\phi_{L,c}$ which corresponds to this limit depends on the bubble size distribution of the foam and the organisation of the bubbles. In monodisperse, ordered foams $\phi_{L,c} = 0.26$, whilst in disordered and polydisperse foams $\phi_{L,c} \approx 0.36$ [2].

- In ***a dry foam*** (generally $\phi_L < 0.1$) polyhedral bubbles are obtained. There is a very small amount of liquid surrounding the bubbles which form very thin films [30].

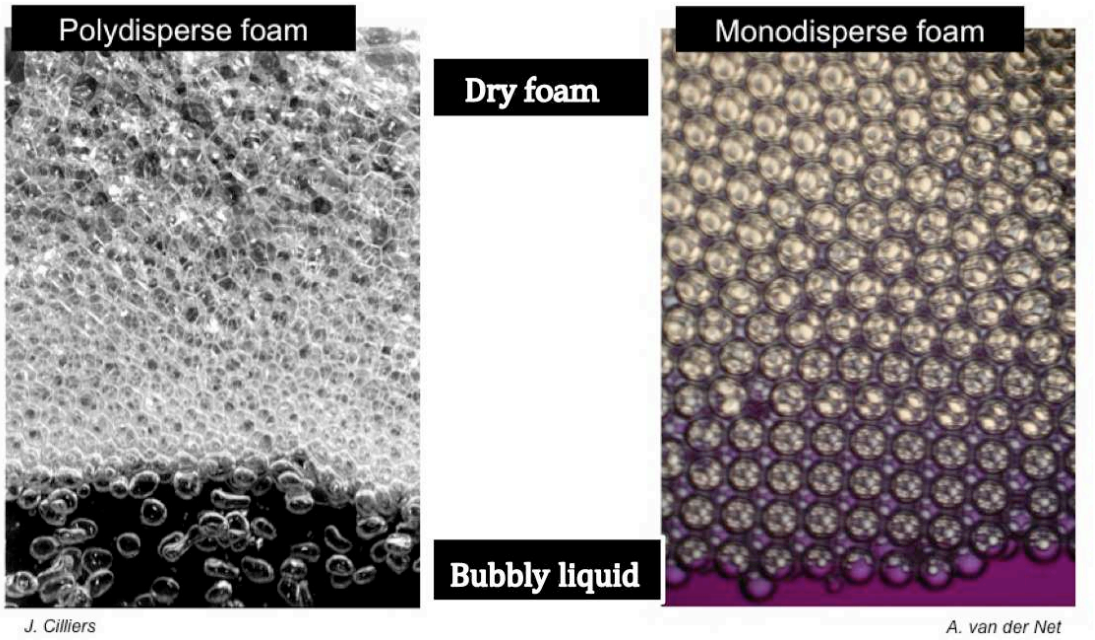

Figure 2.3: Pictures of polydisperse (LEFT) and monodisperse (RIGHT) foams showing the transition from "bubbly liquid" in the bottom part, via spherical bubbles ("wet limit") and "wet foam" in the central part to polyhedral bubbles in the upper part ("dry foam").

2.4 LAWS GOVERNING THE STRUCTURE OF FOAMS

2.4.1 The Young-Laplace law

Creating an interface costs energy. The interface therefore minimises its surface to decrease this energy and takes the "energetically least costing" shape for a given volume. In the case of an unbounded bubble this shape is a sphere. When bubbles meet, their shape changes in order to minimise their whole surface energy by sharing some elements of their structures (such as films and edges). The shape of the corresponding interfaces is captured by the **Young-Laplace law**, which relates the pressure difference Δp across the air/liquid interface to the surface tension γ and its mean curvature κ [2, 6, 7, 10].

$$\Delta p = \gamma \left(\frac{1}{R_1} + \frac{1}{R_2} \right) = \gamma \kappa \qquad \textbf{(2. 3)}$$

Here R_1 and R_2 are the two principal radii of curvature. The pressure difference across a film shared by two bubbles is given by $\Delta p = 2\gamma\kappa$ since it encloses two interfaces.

2.4.2 Plateau's laws

A close look to the elementary unit of a foam, the bubble (Figure 2.4), shows that it is a three-dimensional cell bounded by thin films which meet in Plateau borders. The latter intercept to form a vertex as shown in Figure 2.4.

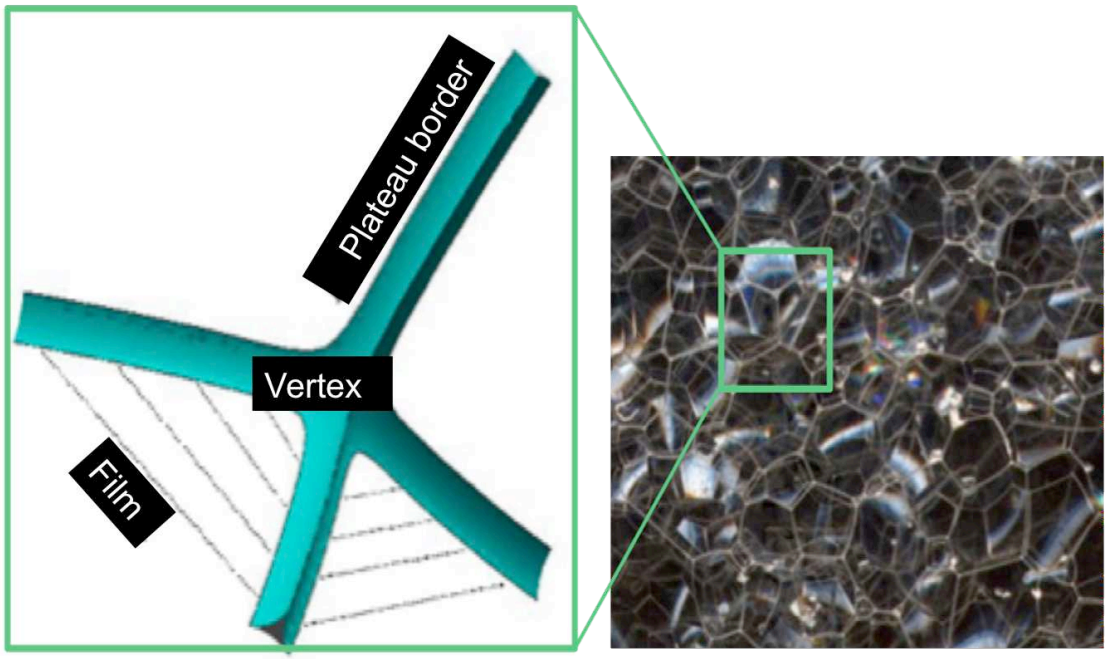

Figure 2.4: A zoom showing the building blocks of a polydisperse dry foam

In the case of dry foam, these building blocks conform to the so-called **Plateau Laws**. The films meet three at a time in the Plateau border and are separated by angles equal to 120°. These Plateau borders meet in fours at a vertex, and they do so at the Miraldi angle of 109.47° [2].

2.5 ORGANISATION OF BUBBLES IN MONODISPERSE FOAMS

In this thesis, we deal with monodisperse and polydisperse foams. The bubble size distribution of polydisperse foams tends to follow Gaussian or log-normal distributions, depending on how the foam has been obtained [28]. We shall quantify their degree of polydispersity using the normalised standard deviation or the polydispersity index P_{index} of the bubble radius R_B as follows

$$P_{Index} = \frac{\sqrt{<R_B{}^2> - <R_B>^2}}{<R_B>^2}. \qquad \textbf{(2. 4)}$$

We shall speak of monodisperse foams, when P_{index}< 5% [28]. Whilst polydisperse foams are always disordered, monodisperse foam can have ordered or disordered bubble arrangements (Figure 2.5a and Figure 2.5c). We will give in the following a brief description of each case.

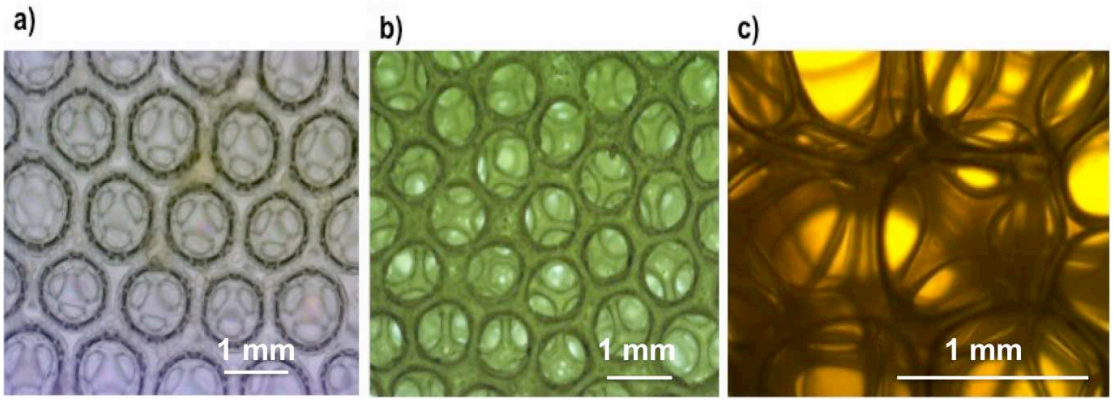

Figure 2.5 : Pictures of *a)* Monodisperse disordered foam, *b)* Polydisperse foam and *c)* Monodisperse ordered foam, at different magnifications respectively 4, 4 and 10 times.

2.5.1 Disordered monodisperse foams

Dry monodisperse foams are generally disordered containing typically around 36 different cell topologies [31]. However, experiments and simulations have proven that the average number of faces of the bubbles inside such foam is around <f>≃ 13.7. The most commonly observed bubbles are those which have 12-16 faces [31].

2.5.2 Ordered monodisperse foams

The wet foam limit

Equal-sized spherical bubbles self-organise in wet foam to form ordered structures ([29, 32-34]) which are very similar to crystalline structures of atoms in solids. The optimal foam structure in this limit corresponds to the structure which gives the densest packing [35]. Many scientists studied this problem. The first solution was given by Kepler (1611) which consists of the face centred cubic structure (fcc) with ϕ= 0.2596. However, there are different close-packed crystalline structures with the same density. Considering a triangular layer, as seen in Figure 2.6, there are three ways of stacking these layers with respect to each other. This generates different sequences of ordering to make up various types of structures such as hexagonally close-packed (HCP, ABABA, Figure 2.6a), face-centred-cubic (FCC, ABCABCA., Figure 2.6b), or random hexagonally close-packed (RHCP, ABCACABAC...). The difference between the HCP and the FCC

structures consists in the orientation of the three small bubbles of the third layer underneath.

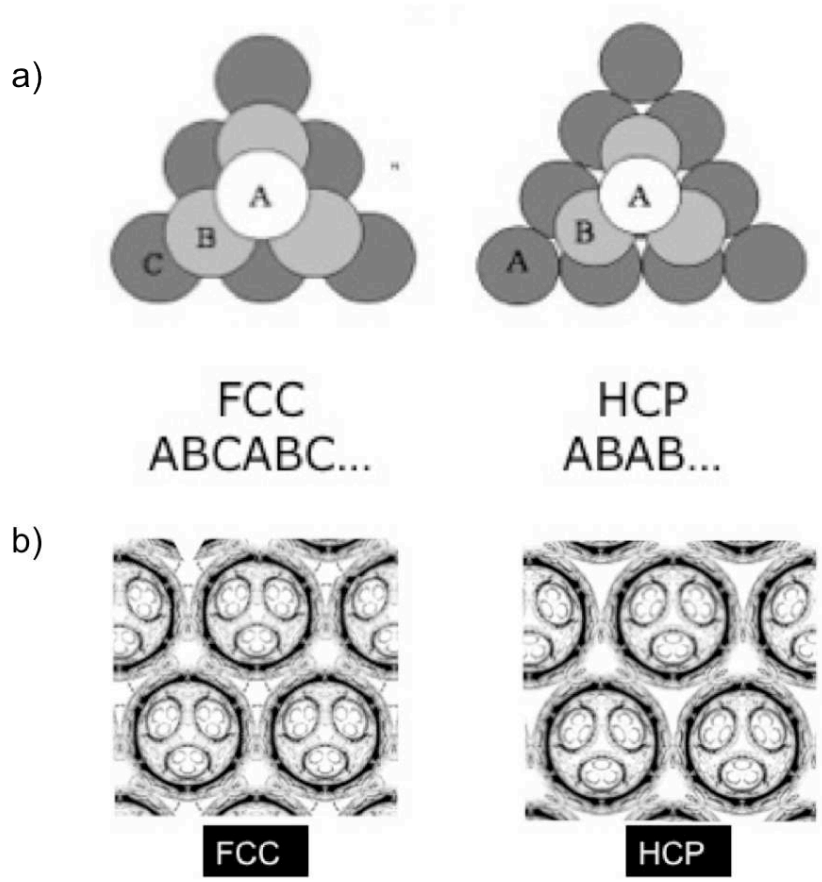

Figure 2.6: a) Examples of close-packing of three layers of bubbles and b) the corresponding results of simulation in FCC and HCP structures.

The dry foam limit

The same problem of "the perfect packing" of spheres was studied for dry monodisperse foams. It was found that the most efficient space-filling bubble structure was the slightly curved Wigner-Seitz cells of a body centred cubic structure (bcc). This structure is known as Kelvin structure since Lord Kelvin proposed it in 1887 [32]. The scientific community had to wait until 1994 to discover the Clathrate A15 structure announced by Weaire and Phelan, which has 0.3% less interfacial energy than that of Kelvin [36].
The Kelvin structure is very easy to realise experimentally while the Weaire-Phelan structure was observed experimentally only recently (by changing the container shape in order to fit the boundary conditions of this structure) [37] .

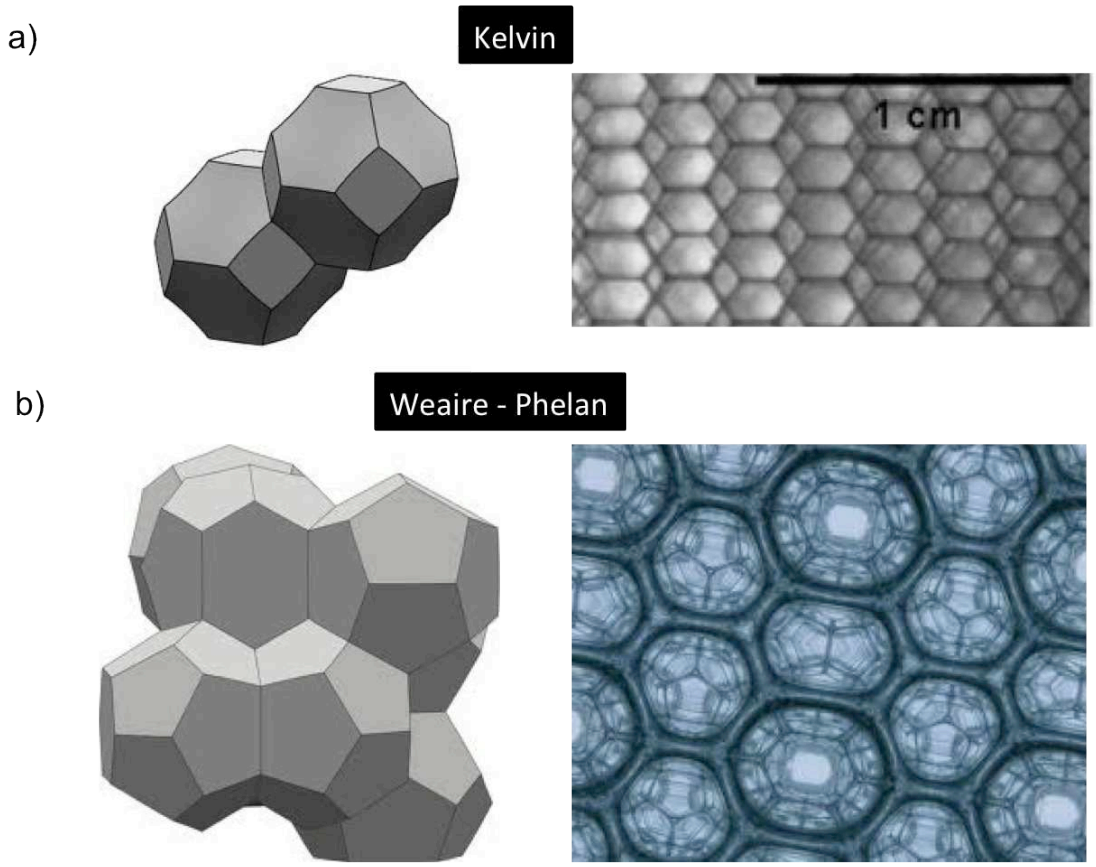

Figure 2.7: Simulation (LEFT) and experiment (RIGHT) images of the a) Kelvin structure from [32], and b) Weaire-Phelan structure from [37].

2.6 AGING OF LIQUID FOAMS

Unfortunately, liquid foams are ephemeral. Freshly created foam undergoes aging phenomena which generally lead to its total collapse and disappearance [2, 7, 38]. Among these phenomena (Figure 2.8), there are *liquid drainage* due to gravity, *coarsening* (gas diffusion between bubbles due to the pressure difference of neighbouring bubbles) and *coalescence* (rupture of thin films) [28, 39-42]. The lifetime of a foam can be increased by tuning some parameters like the bulk viscosity, the surfactant type/ concentration and the technique of foam generation. A common foam life time is typically of the order of a few minutes [27]. In the following we shall discuss each of the destabilisation mechanisms in more detail [2, 7].

Coarsening (Figure 2.8a) occurs when the gas inside the bubbles diffuses from one bubble to another through the thin liquid film due to the difference of the pressure inside the two bubbles: Bubbles of small size have a higher pressure than bubbles of bigger size. As a result, the small bubbles shrink and the volume of the larger bubbles increases. This leads to a decrease of the number of bubbles with time and an increase of the average bubble size. At the end of this process all the bubbles disappear.

Drainage (Figure 2.8b) results from the fact that gravitational forces drive the liquid downwards the foam. The liquid contained in the films is sucked by the Plateau borders then it drains along their network in the direction of gravity. This creates a liquid reservoir underneath the foam. Drainage continues until the capillary forces counterbalance the gravitational ones. This leads to a gradient of liquid fraction inside the foam where the upper part is composed of dry, close-packed polyhedral bubbles and the lower part of the foam is composed of spherical bubbles (see also Figure 2.3).

Coalescence (Figure 2.8c) consists of the rupture of the film between two neighbouring bubbles usually due to its continuous thinning because of drainage and/or external factors. This instability can induce the total collapse of the foam due to avalanches of film ruptures [43-45]. Understanding the key mechanisms which control film stability is actually an active area of research [46-49].

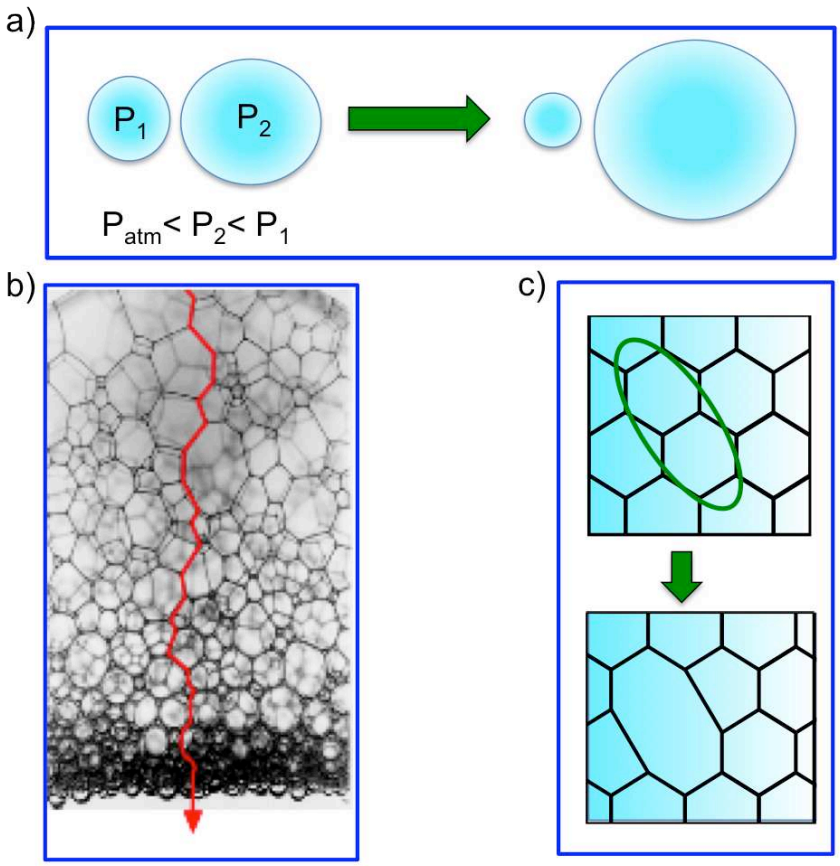

Figure 2.8: Factors leading to the destabilisation of foams a) Coarsening, b) Drainage, c) Coalescence.

2.7 SOLID POLYMER FOAMS

2.7.1 Techniques to generate solid polymer foams

Polymer foams are manufactured using different techniques [4, 50]. The most common one used in industry - and the one of interest for our study - is the ***solidification of an initially liquid foam*** typically via a ***polymerisation/crosslinking*** reaction. The different steps leading to the final polymer foam are different in the case of monodisperse and polydisperse foams. In the following, we provide a brief description of both.

Polydisperse foaming process

Polydisperse polymer foams are commonly obtained by following three key steps [50]:

- ***BUBBLE NUCLEATION***

The bubble nucleation occur thanks to blowing agents which are usually added to the initial liquid monomer or polymer phase (to be foamed). They react (dissolve/decompose/evaporate) under given conditions (heat release during exothermic reactions, pressure release, etc.) to release gas. Usually, blowing agents are used to initiate nucleation and to form bubbles inside the polymer medium. They can be chemical (reactant which release gas while reacting) or physical nature (blending air into the polymer solution). The resulting foam generally has high polydispersity.

- ***BUBBLE GROWTH***

Once the bubbles are created by one way or another, they start to grow. Bubble growth is mainly due to gas diffusion between bubbles (coarsening) and gas expansion under exothermic conditions. Surfactant molecules present in the liquid phase decrease the surface tension of the liquid and try to resist against the pressure driving force which tend to destabilise the foam (as explained in Section 2.6). During bubble growth, the liquid is drained due to gravity forces leading to a difference of density and a rearrangement of bubbles inside the foam. The drainage is slowed down by the solidification which proceeds simultaneously to bubble growth until the whole liquid phase is solidified and the final structure of the foam is obtained.

- ***BUBBLE PACKING***

Bubbles of different sizes pack in a disordered way inside the polydisperse foam
This step is detailed in Section 2.4.3.

Monodisperse foaming process

At this stage, no direct foaming technique exists on industrial scale in order to generate monodisperse foams. The goal of this study is to fill this gap using micro/millifluidic foaming techniques as it was performed by A. Van der Net with hydrogel foams [51]. In this case, the foam is generated *bubble by bubble* by

injecting the gas and the monomer or polymer solution at constant flow rates in a millifluidic device (see Section 3.2.2 for more details). No additional blowing agent is used since gas is directly injected into the polymer solution in a highly controlled manner. The monodisperse bubbles pack spontaneously to form ordered crystalline structures as seen in Section 2.5.

2.7.2 Solid polymer foam structure

Different parameters are important for the characterisation of the solid polymer foam structure. These include:

Relative density

The relative density ρ_r is the most important parameter characterizing the structure of a solid foam and of a cellular solid in general [4, 52]. It is given by

$$\rho_r = \frac{\rho_{Foam}}{\rho_{Polymer}}, \qquad \textbf{(2. 5)}$$

where, ρ_{Foam} represents the density of the foam, and $\rho_{Polymer}$ the density of the polymer from which the foam is made. Since the weight of the gas contained in the foam is negligible, the relative density ρ_r of a solid foam is equal to the liquid fraction φ_L of its liquid template.

Cell structure (open/closed cells)

Foams can have open- or closed-cell structures [4, 52]. In **open-cell foams** (Figure 2.9a) the bubbles form an interconnected network due to the breakage of the thin films separating bubbles during the solidification process. Therefore, the open-cell foams have usually low densities, they are flexible and they can expand and contract, to some extent. The open-cellness is estimated by calculating the open /closed cell ratio which can be measured by water absorption or permeation.

Closed-cell foams (Figure 2.9b) are made of bubbles with thick cell faces which lead to a high density and high elasticity. They are generally obtained by a solidification of a freshly created liquid foam which is performed fast enough to solidify the foam before that cell faces become very thin and rupture.

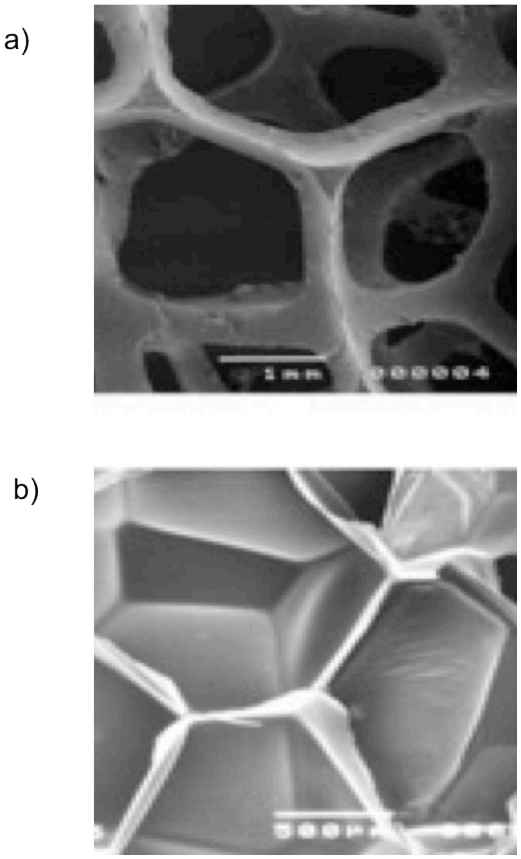

Figure 2.9: a) Open-cell foam. b) Closed-cell foam from [52]

2.8 BETWEEN LIQUID AND SOLID STATES: A VERY IMPORTANT TRANSITION

During the three steps of the transition from liquid to solid foams, there are parameters, which once tuned correctly contribute to the successful accomplishment of the whole process. We define and describe here the most important parameters.

The solidification time τ_S

Two different approaches are possible for the solidification of a liquid foam template. The first approach fully separates foaming and foam solidification using an external initiation mechanism, such as heat or light, which triggers the solidification. Even though such a procedure provides excellent control over the onset of solidification, it often suffers from inhomogeneous spreading of the initiating source through the foam.
The second approach, generally more practical, starts the solidification during the foam generation, but tunes the solidification time τ_S such that the generated foam remains sufficiently liquid to find its equilibrium structure before it solidifies. The solidification time should nevertheless be sufficiently rapid to

ensure that the foams remain stable. The solidification times can be tuned by various means, such as the concentrations of the solidifying agents or the use of catalysts.

The foaming time τ_F

The foaming time τ_F starts when the first bubble is created and ends when a given volume of a still liquid foam is obtained. The foaming time depends therefore, for a constant final foam volume, on the foaming technique and more precisely on the foaming rate.
The foaming time τ_F is a very important parameter in the transition from liquid to solid foams. If the foaming time is too short with respect to the solidification time τ_S, the foam drains and coarsens before solidifying which leads to a partial/total loss of the initial ordered foam structure. And if, on the contrary, the foaming time is too long, the solidification process starts during the foam generation. The resulting foam is heterogeneous and does not have an ordered structure since the bubbles do not have enough time to self-organise.

The foam life time

Foam stability represents the ability of a foam to preserve its initial structural properties over time. Bubbles need to be stable enough during the whole processes of foaming, mixing and solidification. Efficient surface active agents stabilising bubbles, during their formation and long after, against coalescence, coarsening and drainage are necessary to achieve a satisfactory foam stability.
Generally, measurements of foam half-life time $\tau_{1/2}$ are performed to characterise foam stability. They consist of collecting a given amount of foam and of measuring the time required to reduce the total foam height by half (see Section 4.2.2).

The mixing time τ_M

The different reactants involved in the production of polymer foams need to be well mixed in order to ensure the final foam homogeneity and stability. The mixing is generally carried out before the foaming step. In most traditional techniques, the different reagents typically surfactants, catalysts, monomer or polymer solutions and the solidifying agent are mechanically mixed and foamed while still liquid [4]. In our case, we generally perform the mixing during the creation of bubbles within the mixing unit in a specially designed Lab-on-a-Chip-device which contains both, the foaming and the mixing units.
In both cases, since normally the solidification reaction starts when the reactants are put together, the mixing time τ_M needs to be adjusted in such a way that on the one hand, it lasts long enough to ensure a good homogenisation of the chemicals. On the other hand, it has to verify the condition:

$\tau_M << \tau_S$ and that $\tau_M \leq \tau_F < \tau_S$

The principle of mixing relies on the chaotic movements of the bubbles inside zigzag shaped paths (Section 3.3 is devoted to the mixing process). The mixing "quality" needs to be characterised in order to make sure of the homogeneous dispersion of the different reagents and thus the uniform solidification.
Such characterisation is executed by tracking the pathway of neighbouring bubbles, immediately after their creation, in space and time. If the bubbles follow random paths, this will implicate a good mixing of the liquid solution surrounding them.

BIBLIOGRAPHY

1. Cox, S., D. Weaire, and K. Brakke, *Liquid foams - Precursors for Solid Foams*. Cellular Ceramics: Structure, Manufacturing, Properties and Applications, ed. P.C.a.M. Scheffler2005: Wiley.
2. Weaire, D. and S. Hutzler, *The Physics of Foams*1999, Oxford: Clarendon Press.
3. Kraynik, A.M., *Foam structure: From soap froth to solid foams.* Mrs Bulletin, 2003. **28**(4): p. 275-278.
4. Sachchida N Singh, A.B., David Eaves, *Handbook of polymer foams*, ed. D. Eaves2004: Rapra Technology Limited.
5. Hans-Jurgen Butt, M.K., *Surface and Interfacial Forces*2010: WILEY-VCH Verlag GmbH & Co. KGaA.
6. Birdi, K.S., *Surface and colloid chemistry: Principles and Applications*2010: CRC Press Taylor & Francis Group.
7. Cantat, I., et al., *Les mousses Structure et dynamique*. Collection Echelles2010, Paris: Belin.
8. Stubenrauch, C. and R. von Klitzing, *Disjoining pressure in thin liquid foam and emulsion films - new concepts and perspectives.* Journal of Physics-Condensed Matter, 2003. **15**(27): p. R1197-R1232.
9. Aronson, A.S., et al., *The influence of disjoining pressure on foam stability and flow in porous media.* Colloids and Surfaces A: Physicochemical and Engineering Aspects, 1994. **83**(2): p. 109-120.
10. Pierre-Gilles de Gennes, F.B.-W., David Quéré, *Gouttes, bulles, perles et ondes*2005: Belin.
11. Dekker, M., *Foams: Theory, Measurements, and Applications*. Surfactant Science Series, ed. R.K. Prud'homme and S.A. Khan. Vol. 57. 1995, New York: Marcel Dekker, Inc.
12. Chou, T.-H., et al., *Phase behavior and morphology of equimolar mixed cationic-anionic surfactant monolayers at the air/water interface: Isotherm and Brewster angle microscopy analysis.* Journal of Colloid and Interface Science, 2008. **321**(2): p. 384-392.
13. Eastoe, J., et al., *Interfacial Properties of a Catanionic Surfactant.* Langmuir, 1996. **12**(11): p. 2706-2711.
14. Langevin, D., *Aqueous foams: A field of investigation at the frontier between chemistry and physics.* Chemphyschem, 2008. **9**(4): p. 510-522.
15. Pugh, R.J., *Foaming, foam films, antifoaming and defoaming.* Advances in Colloid and Interface Science, 1996. **64**: p. 67-142.
16. Rodakiewicz-Nowak, J., *Surface characteristics of some anionic, cationic, and anionic--cationic surfactants.* Journal of Colloid and Interface Science, 1981. **84**(2): p. 532-535.
17. Tadros, T.F., *Applied surfactants Principles and Applications*2005: WILEY-VCH Verlag GmbH & Co.
18. Hunter, T.N., et al., *The role of particles in stabilising foams and emulsions.* Advances in Colloid and Interface Science, 2008. **137**(2): p. 57-81.

19. Murray, B.S. and R. Ettelaie, *Foam stability: proteins and nanoparticles.* Current Opinion in Colloid & Interface Science, 2004. **9**(5): p. 314-320.
20. Tcholakova, S., N.D. Denkov, and A. Lips, *Comparison of solid particles, globular proteins and surfactants as emulsifiers.* Physical Chemistry Chemical Physics, 2008. **10**(12): p. 1608-1627.
21. Binks, B.P., M. Kirkland, and J.A. Rodrigues, *Origin of stabilisation of aqueous foams in nanoparticle-surfactant mixtures.* Soft Matter, 2008. **4**(12): p. 2373-2382.
22. Sugihara, G., et al., *A Review of Recent Studies on Aqueous Binary Mixed Surfactant Systems.* Journal of Oleo Science, 2008. **57**(2): p. 61-92.
23. Lucassen-Reynders, E.H., *Surface properties of mixed anionic/cationic surfactant solutions.* Colloid & Polymer Science, 1972. **250**(4): p. 356-359.
24. Varade, D., et al., *On the origin of the stability of foams made from catanionic surfactant mixtures.* Soft Matter, 2011. **7**(14): p. 6557-6570.
25. Stubenrauch, C., *What do a foam film and a real gas have in common?* Chemphyschem, 2005. **6**(1): p. 35-42.
26. Exerova, D. and P.M. Kruglyakov, *Foam and Foam Films; Theory, Experiment, Application*. Vol. 5. 1998, Amsterdam: Elsevier Science B.V.
27. Weaire, D. and R. Phelan, *The physics of foam.* Journal of Physics-Condensed Matter, 1996. **8**(47): p. 9519-9524.
28. Drenckhan, W. and D. Langevin, *Monodisperse foams in one to three dimensions.* Current Opinion in Colloid & Interface Science, 2010. **15**(5): p. 341-358.
29. van der Net, A., et al., *The crystal structure of bubbles in the wet foam limit (vol 2, pg 129, 2006).* Soft Matter, 2006. **2**(6): p. 523-523.
30. Lambert, J., et al., *Experimental Growth Law for Bubbles in a Moderately , 3D Liquid Foam.* Physical Review Letters, 2007. **99**(5): p. 058304.
31. Kraynik, A.M., D.A. Reinelt, and F. van Swol, *Structure of random monodisperse foam.* Physical Review E, 2003. **67**(3): p. 031403.
32. Hoehler, R., et al., *Osmotic Pressure and Structures of Monodisperse Ordered Foam.* Langmuir, 2007. **24**(2): p. 418-425
33. Testouri, A., et al., *Generation of porous solids with well-controlled morphologies by combining foaming and flow chemistry on Labs-on-a-chip.* to appear in Colloid and Interface Science A, 2012.
34. van der Net, A., et al., *Crystalline arrangements of microbubbles in monodisperse foams.* Colloids and Surfaces a-Physicochemical and Engineering Aspects, 2007. **309**(1-3): p. 117-124.
35. Weitz, D.A., *Packing in the Spheres.* Science, 2004. **303**((5660)): p. 968-969.
36. Weaire, D. and R. Phelan, *A counter-example to Kelvin's conjecture on minimal surfaces.* Philosophical Magazine Letters, 1994. **69**(2): p. 107-110.
37. Gabbrielli, R., et al., *An experimental realization of the Weaire-Phelan structure in monodisperse liquid foam.* Philosophical Magazine Letters, 2012. **92**(1): p. 1-6.

38. Grassia, P., et al., *The growth, drainage and bursting of foams.* Colloids and Surfaces A: Physicochemical and Engineering Aspects, 2006. **274**(1-3): p. 110-124.
39. Ganan-Calvo, A.M., et al., *Coarsening of monodisperse wet microfoams.* Applied Physics Letters, 2004. **84**(24): p. 4989-4991.
40. Saint-Jalmes, A., *Physical chemistry in foam drainage and coarsening.* Soft Matter, 2006. **2**: p. 836 - 849.
41. Pitois, O., C. Fritz, and M. Vignes-Adler, *Liquid drainage through aqueous foam: study of the flow on the bubble scale.* Journal of Colloid and Interface Science, 2005. **282**(2): p. 458-465.
42. Carrier, V. and A. Colin, *Coalescence in draining foams.* Langmuir, 2003. **19**: p. 4535-4538.
43. Vandewalle, N., H. Caps, and S. Dorbolo, *Cascades of popping bubbles.* Physica A: Statistical Mechanics and its Applications, 2002. **314**(1-4): p. 320-324.
44. Vandewalle, N. and J.F. Lentz, *Cascades of popping bubbles along air/foam interfaces.* Physical Review E, 2001. **64**(2): p. 021507.
45. Burnett, G.D., et al., *Structure and dynamics of breaking foams.* Physical Review E, 1995. **51**(6): p. 5788.
46. Bonaccurso, E., M. Kappl, and H.-J. Butt, *Thin liquid films studied by atomic force microscopy.* Current Opinion in Colloid & Interface Science, 2008. **13**(3): p. 107-119.
47. Karakashev, S.I. and A.V. Nguyen, *Do Liquid Films Rupture due to the So-Called Hydrophobic Force or Migration of Dissolved Gases?* Langmuir, 2009. **25**(6): p. 3363-3368.
48. Lhuissier, H. and E. Villermaux, *Soap Films Burst Like Flapping Flags.* Physical Review Letters, 2009. **103**(5).
49. Saulnier, L., et al., *What Is the Mechanism of Soap Film Entrainment?* Langmuir, 2011. **27**(22): p. 13406-13409.
50. Mills, N., *Polymer Foams Handbook: Engineering and Biomechanics Applications and Design Guide*2007, Oxford: Butterworth-Heinemann.
51. van der Net, A., et al., *Highly structured porous solids from liquid foam templates.* Colloids and Surfaces A: Physicochemical and Engineering Aspects, 2009. **346**(13): p. 5-10.
52. Gibson , J.L. and M.F. Ashby, *Cellular Solids: Structure and Properties*. 2nd ed. Cambridge Solid State Science Series, ed. D.R. Clarke, S. Suresh, and I.M. Ward FRS1997, Cambridge: Cambridge University Press.

3 MILLIFLUIDIC TECHNIQUES FOR THE GENERATION OF MONODISPERSE FOAMS: BASIC CONCEPTS AND MECHANISMS

3.1 INTRODUCTION

Microfluidics is the science/technique which allows the controlled handling of components of different natures (gas, liquid and solid) in channels of at most a few hundreds of micrometres [1, 2]. Microfluidic techniques offer so many advantages and so few drawbacks that according to some authors, it is "too good to be true" [3]. The use of microfluidics has indeed revolutionised both, academic and industrial fields by improving the way of performing experiments [4-7]. Many sophisticated experimental techniques are "shrinked" and integrated in micrometric Lab-on-a-Chip while performed still with high resolution and sensitivity [6, 8]. This enables saving material, cost and analysis time.

The application of microfluidic techniques offers elegant possibilities for the generation of porous materials, especially foams, with well-controlled densities and structures [9-11]. Thanks to the modular nature of these techniques, it is possible to integrate mixing processes, chemical reactions and foam generation in a way which provides an important degree of control over each processing step. The versatility of this approach has been demonstrated for a range of materials [9, 10, 12-14].

Microfluidic Labs-on-a-Chip allow the downscaling of laboratory manipulation analysis from the metric scale to the micro scale thanks to being a miniaturised flow device. It can integrate various analytical processes including sampling, chemical reactions and mixing. Thanks to its excellent heat and mass transfer properties, it can host various reactions of different types such as organic synthesis [15] and biological cultures.

Common microfluidic devices enclose microreactors, which have channels of micrometric (or millimetric in the case of millifluidic) inner dimensions. The inlet channels ensure the transport of various reagents of different natures. Systems of different multiphasic nature such as liquid-liquid and liquid-gas systems can easily be treated inside these microreactors [16].

It is easy to control the stoichiometry of chemical reactions by simply entering automatically the flow rate of each reacting reagent. The control over the flow rates of these reagents is generally ensured by external devices (syringe pumps, flow meters, or pressure controller). The chemical reaction starts when the reagents meet inside the chip channel and allow the production of few milligrams of a desired compound.

This allows a significant gain in time and cost and motivates many of scientific fields to use Lab-on-a-Chip for multidisciplinary applications (microelectronics, biology, chemistry, physics, or engineering) [6, 8, 17-19]. Besides, microfluidics allows carrying out reactions involving dangerous reagents and exothermic reactions in a very safe manner since the reagents are used in very small quantities and are confined into the small channels of the device.

In this study, we use mostly **millifluidic techniques**; the large-scale cousin of microfluidics with channel dimensions of few hundred micrometres to few millimetres in order to generate highly ordered foams in a well-controlled manner. Different geometries are employed depending on the properties of the studied system such as viscosity, rheological behaviour or aqueous/non aqueous nature of the solutions. We also use millifluidic channel systems as microreactors containing different units where mixing and polymerisation/cross-linking reactions take place.
As our study involves different systems (biopolymer Chitosan (Section 5.4), superabsorbent polymer (Section 6.6) and polyurethane (Section 7.5)), we used and -when needed- built specific millifluidic devices for each system. Generally, they are of two sorts: in-house made and commercial millifluidic devices. The first category is fully developed in our lab and the second one is built from commercial connectors and T-junctions. For experimental details see Section 4.3.

Here we explain in the first part of the chapter (Section 3.2) the essential concepts and building blocks of micro- and millifluidic techniques as well as the mechanisms and physical phenomena behind the formation of monodisperse foams. In the second part (Section 3.3) we provide an overview mixing techniques in micro-/millifluidic systems.

3.2 GENERATION OF MONODISPERSE FOAM USING MILLIFLUIDIC TECHNIQUE

3.2.1 Useful definitions

Both, micro- and millifluidics are strongly related to fluid mechanics and rheology. They therefore involve many issues of these fields being described by key parameters such as the fluid viscosity η or the fluid velocity U, which are combined with other system-relevant parameters into dimensionless numbers. Of particular importance to our work are the Reynolds number *Re*, and the Capillary number *Ca* which we shall define here.

Reynolds number Re [1, 20, 21] is a dimensionless number which is used to characterise flow regimes by comparing the interfacial forces effects and the viscous ones. It is given by the equation

$$Re = \frac{LU\rho}{\eta} \qquad \textbf{(3. 1)}$$

where ρ is the fluid density, U is the characteristic velocity, L is the characteristic dimension of the system and η represents the dynamic viscosity.

The Reynolds number allows distinguishing between different flow regimes. According to whether it is low or high, viscous forces or inertial forces dominate the flow behaviour leading to laminar or turbulent flow, respectively.
When Re << 1 [22, 23], the flow is controlled by viscous effects and is thus smooth and laminar. In turn, when Re > 2000, the flow is turbulent and viscous effect become negligible with respect to inertial forces.

At very low Reynolds number (smaller than 1), which is the case in our work, interfacial and viscous forces dominate inertial ones. The capillary number becomes therefore the relevant parameter to characterise the flow behaviour at the micro scale.
The ***capillary number Ca*** [21] associates, for given flow conditions, the effect of viscous and interfacial tension forces [24]. It is given by

$$Ca = \frac{\eta U}{\rho \sigma} \qquad \textbf{(3. 2)}$$

with σ being the interfacial tension. For Ca << 1, the flow is dominated by interfacial tension forces, while at Ca >> 1, viscous forces dominate.

In this thesis we use a certain number of complex fluids which have Non-Newtonian properties.

A Newtonian fluid [21] is a fluid in which stress and strain are related linearly, stress going to zero for zero strain. The constant of proportionality is the viscosity.

A Non-Newtonian fluid [21] is a type of fluid whose flow properties differ in many ways from those of Newtonian fluids. Most commonly, the viscosity (resistance to deformation or other forces) of non-Newtonian fluids depends on the shear rate and many Non-Newtonian fluids have a finite yield stress (below which the fluid does not flow).

3.2.2 Bubble generation in micro/millifluidic geometries

Milli- and micro-fluidic techniques [4, 11, 25-30] have proven to be extremely useful for the generation of liquid foams with well-controlled structural properties. In fact, a wide variety of micro- and millifluidic foaming devices with different configurations and dimensions are nowadays used [24-27, 31-33]. Generally, most of the geometries have channels of milli- or microscopic dimensions which are connected in such a way that a laminar co- or cross-flow [13] of gas and the foaming solution(s) is generated in a configuration which is physically unstable and breaks up periodically to form extremely monodisperse bubbles. As illustrated in Figure 3.1, the most commonly used geometries can be classified into three main classes according to their shape [4]:

1. The **co-flowing** geometry (Figure 3.1a) where the dispersed phase (gas) and the liquid (continuous phase) co-flow along a channel within which they form bubbles [24].

2. The **flow focussing** geometry (Figure 3.1b) is a special case of co-flow in which the fluid inlet channels and the gas are "focussed" in a constriction where the bubble break-up occurs.
3. The **cross flow** geometry (Figure 3.1c) is generally designed using a T-junction where the gas and the liquid inlet channels are perpendicular.

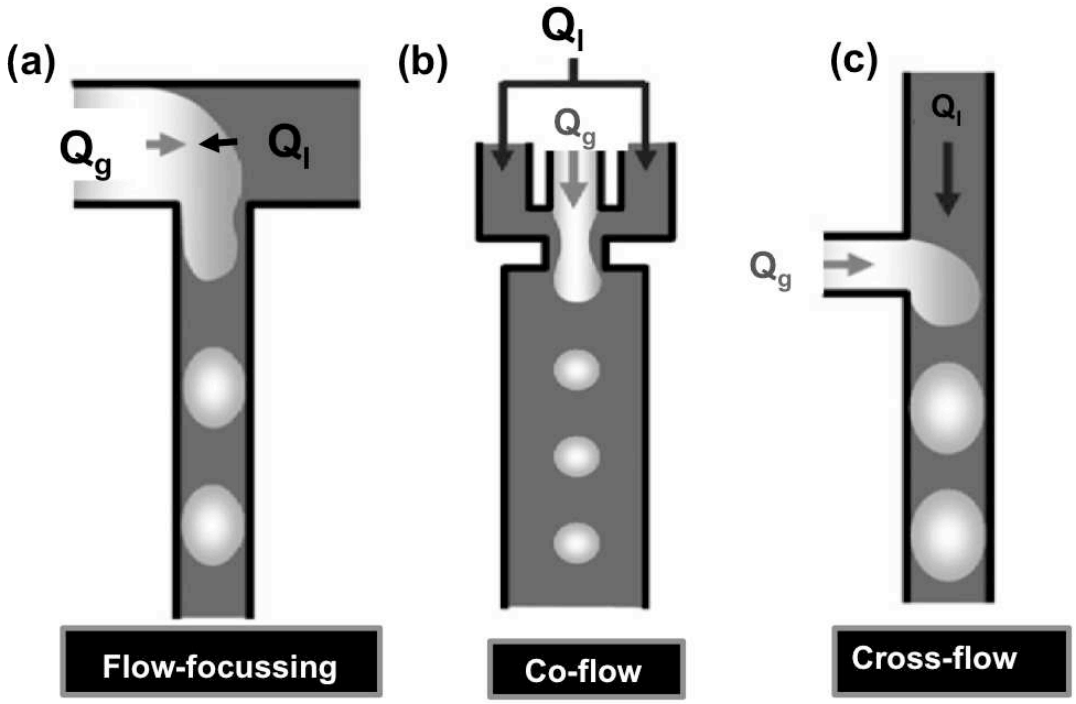

Figure 3.1: Illustration of the most used millifluidic geometry configurations

The fluidic devices used nowadays for the generation of monodisperse foams are easy to fabricate, disposable and inexpensive. They are integrated into a polymeric medium and fabricated using simple techniques which include soft lithography, hot embossing and micro milling [34-37]. Thanks to the properties of the polymer they are made of, the fluidic channel systems have plenty of advantages such as transparency, rigidity, high resistance to chemical reactions or high resistance to pressure and heating, enhancing thus the interest for the use of micro/millifluidics in various fields. We developed for our study a technique of fabrication of millifluidic Lab-on-a-Chip via *hot embossing* which is detailed in Section 4.3.2.

3.2.3 Bubble break-up regimes

The dynamics and mechanism of bubble break-up in different channel geometries have been extensively discussed by many authors [26, 28, 38-43] since they represent a key step in the process of foaming using micro- or millifluidic techniques. Understanding the break-up mechanism not only allows understanding the foaming process but also provides an accurate control over it. The formation of bubbles in micro/millifluidic devices is based essentially on a competition between the shear stresses applied by the liquid on the gas thread

and the surface tension forces which resist to the expansion of this gas thread [27]. Across the different configurations of the bubble generation geometries, the fundamental mechanism of bubble break-up is similar and commonly consists of three main steps which repeat each other in a periodic manner [4, 41, 44] and which are illustrated in Figure 3.2:

1. The gas and the liquid, which are continuously injected into the micro/millifluidic device, meet and create an interface. As both continue to flow downstream, a gas tip surrounded by the liquid is formed and expands into the main channel forming a gas thread.

2. The gas thread is deformed and collapses by one way or another (according to the flowing regimes).

3. Finally a bubble is pinched off and moves out of the device.

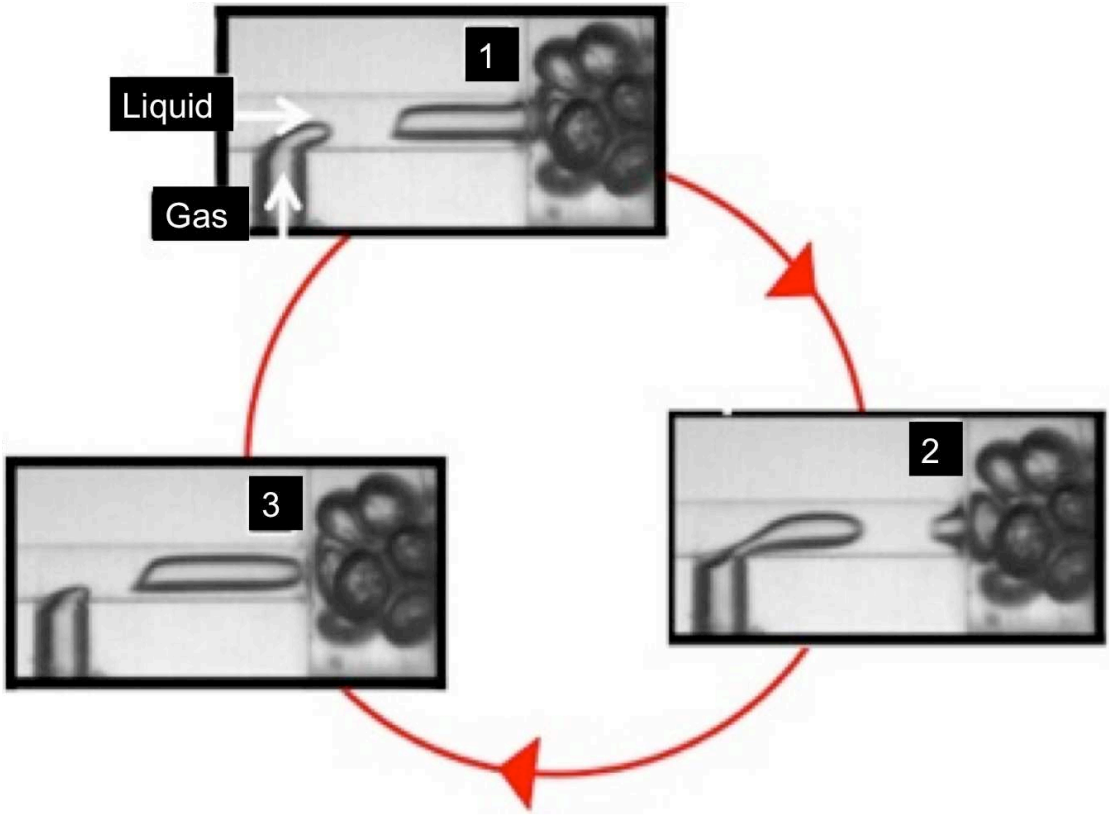

Figure 3.2: The cyclic steps of bubble detachment in the case of a cross-flow device (T-junction). (1) The gas and liquid flows meet at the junction of their respective channels. (2) As the two phases continue to flow, the tip gas stream continues growing inside the downstream channel forming a growing bubble. (3) The neck connecting the inlet of the gas with the growing bubble breaks thus releasing finally the bubble.

For different microfluidic geometries and different flowing conditions, the foaming mechanism occurs periodically following these three steps. However, the driving forces behind the break-up mechanism depend strongly on the flow conditions which lead to a difference in the way how bubbles are created. There are therefore different break up regimes which are tightly coupled to the balance

of interfacial, viscous and inertial forces during bubble generation. One distinguishes three main regimes:

1. ***The confined*** or ***squeezing regime*** [22, 45, 46] is pressure-driven [22] and occurs at low capillary numbers (Ca << 1, typically Ca < 0.002), where the gas thread blocks the channel and prevents the continuous phase from flowing further (Figure 3.3a). The liquid flows only slowly throw a narrow film between the gas thread and the channel walls. The gas thread continues to grow forming a long slug until it obstructs the upstream of the channel leading to a high increase in pressure which finally pinches-off the gas thread forming a bubble of a size usually bigger than the channel width (few mm). In this regime the bubble sizes $\boldsymbol{D_B}$ are highly monodisperse and of the order of the channel width. Furthermore, the bubble size is commonly found to be independent of the liquid viscosity [25, 46-49].

2. The unconfined or ***dripping regime*** ($0.01 < Ca < 0.3$) [45, 46], in which the gas thread is small in comparison to the channel dimension and does not get into contact with the channel walls during the whole bubbling process. Separated bubbles are formed mainly thanks to liquid shear stress which is high enough to balance interfacial forces and induce the bubble break-up. Viscous forces play therefore an important role in bubble detachment and the bubble size becomes (also) a function of the capillary number. An illustration of this regime is shown in Figure 3.3b. Bubble sizes in this regime tend to be highly monodipserse and are smaller than the channel width.

3. The jetting regime [50] occurs at high *Reynolds* numbers and typically at fast flows which form a thin stream that breaks into drops far from where the gas and liquid meet (see Figure 3.3c).

Some studies [45, 46] reported a fourth regime known as "*The partly-confined* or *transition regime"* ($0.002 < Ca < 0.01$) which takes place between the confined and unconfined regimes. The break-up is controlled by both the squeezing pressure and the shear stress which forms short slugs. Our work is mostly concerned with regimes 1 and 2, including the transition regime between both.

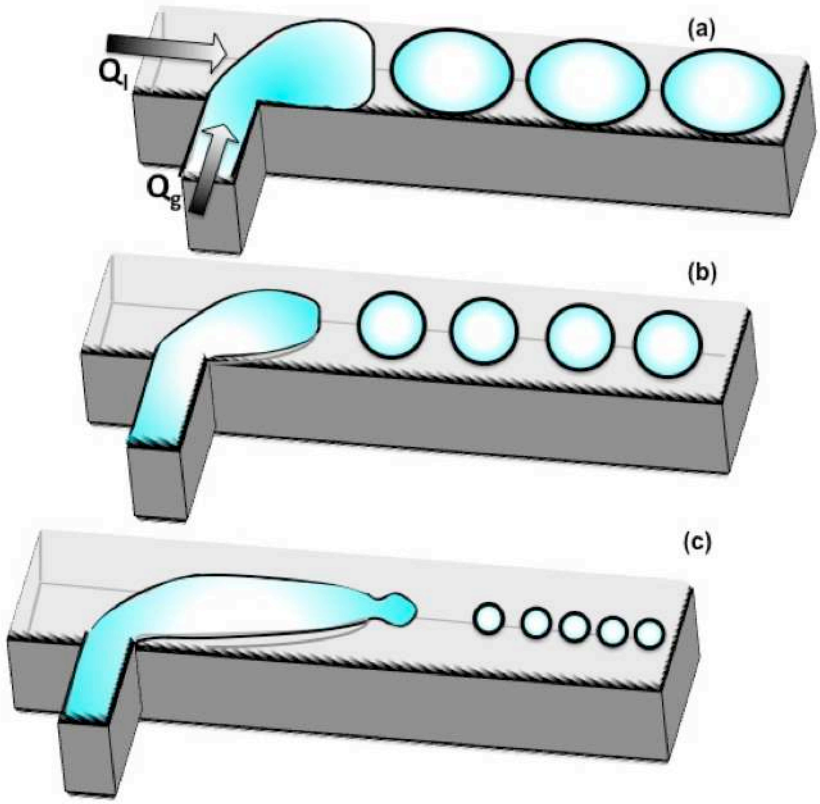

Figure 3.3: Illustration of the main bubbling regimes observed in micro/millifluidic devices. a) Squeezing regime. b) Dripping regime. c) Jetting regime.

Across these regimes, and in very general terms, one can say that the obtained bubble diameters DB are of the order of the channel dimensions DC (order of 10 μm – 1 mm) and proportional to some power α to the ratio of the gas and the liquid flow rates, Qg and Ql, (see Section 3.2.4 for more details). It holds

$$D_B \propto \beta \left(\frac{Q_g}{Q_l}\right)^{\alpha} \text{ with } \beta \propto D_C \qquad \textbf{(3. 3)}$$

All of these techniques allow achieving a high uniform bubbling with foaming rates up to a few thousand bubbles per second and with polydispersities less than 2%. The liquid fraction φ_l of the obtained foam is then given by

$$\varphi_l = \frac{Q_l}{Q_l + Q_g} \qquad \textbf{(3. 4)}$$

Equ. (3.3) and (3.4) show that one generally cannot have an independent control over all the processing parameters at the same time as liquid fraction and bubble

size tend to be coupled. It is therefore needed to make compromises between bubble sizes, range of foam densities, monodispersity or foam generation rate.

3.2.4 Calibration of the micro/millifluidic foaming device

Using the same microfluidic geometry, one can typically generate bubbles with sizes ranging over two orders of magnitude. As shown in Equ.(3.3) this can be achieved by adjusting the gas and the liquid flow rates Q_g and Q_l. For a given microfluidic geometry and foaming solution, it is easy to set the « limit of performance » of the studied system in terms of monodispersity, foam density and bubble size. By changing the gas to liquid flow rate ratio Q_g/ Q_l different bubble sizes are obtained. Plotting then the bubble diameter D_B as a function of the flow rate ratio gives a **calibration curve** which provides a good control over the bubble size, i.e. for a desired bubble size one simply needs to refer to this curve to determine the corresponding flow rate ratio. This calibration is usually performed to explore the « efficiency area » of different systems and of different foaming techniques (cross-flow, co-flow and flow-focussing) [51].
The characteristics of the foam generated at each pair of gas and liquid flow rates such as the polydispersity index P_{index} and the liquid fraction φ_l, permit to draw a phase diagram in which the foam type and transition lines are plotted with the gas and the liquid flow rates as coordinates (Figure 3.4).

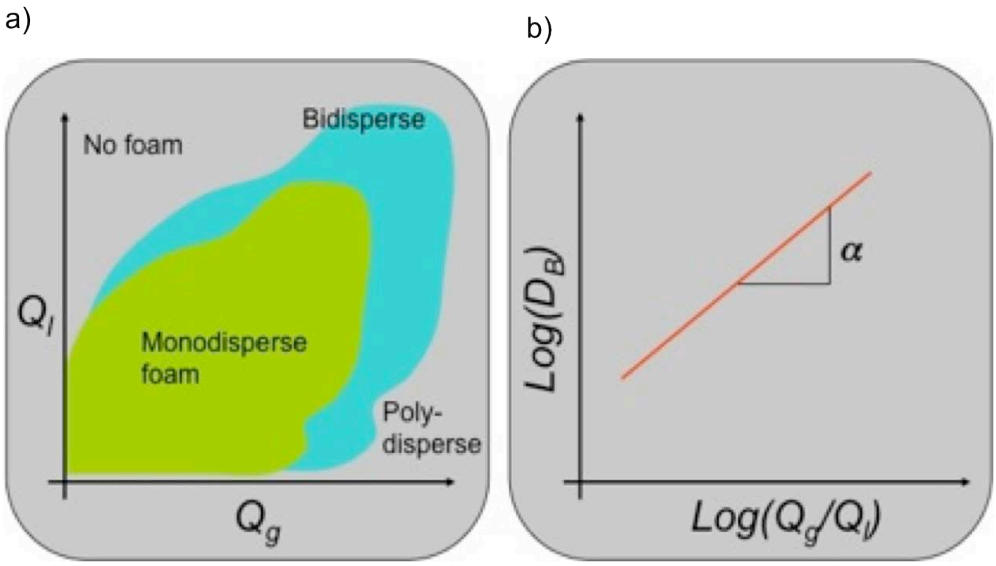

Figure 3.4: a) Sketch of a phase diagram showing the foam dispersity for different couples of gas and liquid flow rates. b) Calibration of micro-millifluidic device curve showing the power law which relates the bubble diameter and the ratio of gas and liquid flow rates.

The device performance depends strongly on the nature of the fluid. While our understanding of bubble generation using millifluidics in the case of Newtonian fluids is by now quite advanced [4, 27, 28, 30, 39, 45, 52, 53], systematic research into the behaviour of complex fluids is at its infancy [54-56]. Since some of the polymer systems employed in this thesis are non-Newtonian, we will briefly discuss in the following how the previously discussed behaviour changes with a non-Newtonian fluid.

3.2.5 Bubble generation with non-Newtonian fluids

Many of the microfluidic applications deal with polymeric, colloidal and multiphase systems such as polymer solutions/melts, gels emulsions or dispersions which are complex fluids. They exhibit a combination of viscous and elastic properties leading to non-Newtonian flow behaviour. In fact, the fluids used in microfluidic techniques have very often shear-thinning properties which can change considerably the flow behaviour and bubble formation mechanism in microfluidic flow-focussing devices [56].

The calibration of micro/millifluidic devices in the case of non-Newtonian fluids is therefore more complex and delicate than in the case of Newtonian systems [54]. For example, when comparing the power law behaviour of Newtonian fluids with that of a shear thinning polymer as in the case of one of our systems (Section 5.2.2) it is observed that in the non-Newtonian case, the bubble size increases with the gas to liquid flow rate ratio but not as a power law. Some authors like *Fu et al.* [56] have investigated the effect of the rheological properties of different fluids on bubble or droplet formation in microfluidic devices. However, the understanding of the generation of foams using microfluidics in non-Newtonian fluids remains limited [56-58].

Nevertheless, despite the delicate rheology of complex fluids under confinement [54], we find throughout this thesis that even in the case of complex polymer solutions appropriate flow regimes can be found in which bubble generation remains reliable and reproducible (Section 5.4.2).

3.3 FLOW-CHEMISTRY INSIDE MICRO/MILLIFLUIDIC LAB-ON-A CHIP

Microfluidic reactors can undertake multicomponent reactions where different compounds can react. For such purposes, mixing units or « micromixers » are integrated into the Lab-on-a-Chip in order to ensure blending, mixing, emulsification, etc. of the multiple injected reactants [59, 60]. They represent the heart of the microfluidic chip and the most complex part. They are essential to guarantee the homogenisation of the reacting solutions inside the microfluidic device where the Reynolds number *Re* is usually below 100 [61] which prevents turbulent flow and efficient mixing. Additionally, some applications require rapid fluid flow rates which decreases significantly the mixing time of the reacting fluids to only a few seconds. This leads to an inefficient mixing. In fact, at a small scale, the mixing is governed by diffusion [21] where the approximate average time τ for a small portion of a fluid to diffuse a distance L, is given by

$$\tau = \frac{L^2}{D} \qquad \textbf{(3. 5)}$$

where D is the diffusion constant. This means that the mixing time scales quadratically with the width L of the channel which implies that one can reduce significantly the mixing time by reducing the diffusion length needed for mixing

or increasing the contact area between the fluids for a given volume. The length scale of the mixing unit, the contact area and the mixing time are thus three key parameters to consider in order to ensure an efficient mixing [62].

When the dimensions of the channels are relatively big (hundreds of microns), the mixing by molecular diffusion is very slow. Moreover, reactions taking place at the interface between two components may hinder diffusion. Hence, in order to ensure a good mixing in a reasonable time, the diffusional path has to be decreased. This is generally intricate in microfluidic systems, in particular when the chemicals component react with each other, i.e. when the problem is not only diffusion-controlled. In order to overcome these problems, a range of mixing techniques for microfluidic systems has been developed in the past [63]. Among these techniques are hydrodynamic focussing, splitting and recombination [64], or injection of many substreams. These techniques and various others [65] use micromixers which can be classified in three main categories:

1. Passive [66],
2. Active [67, 68] and
3. Aided micromixers [61, 69].

In the following we shall briefly describe each of these.

Mixing in **passive micromixers** relies on the contact between fluids and aims increasing the interfacial area. This is ensured by making fluids get in contact with each other using, for instance, repeated lamination and/or splitting and recombining flows. For this purpose, there are various designs for the mixing channels and chambers which can have plenty of shapes as shown in **Figure 3.5**a.

Active micromixers use external triggers to enhance mixing quality. The external forces used can be of different nature: magnetic, electric, ultrasonic, or thermal. They all introduce turbulence in the fluid flow inside the microfluidic channels.

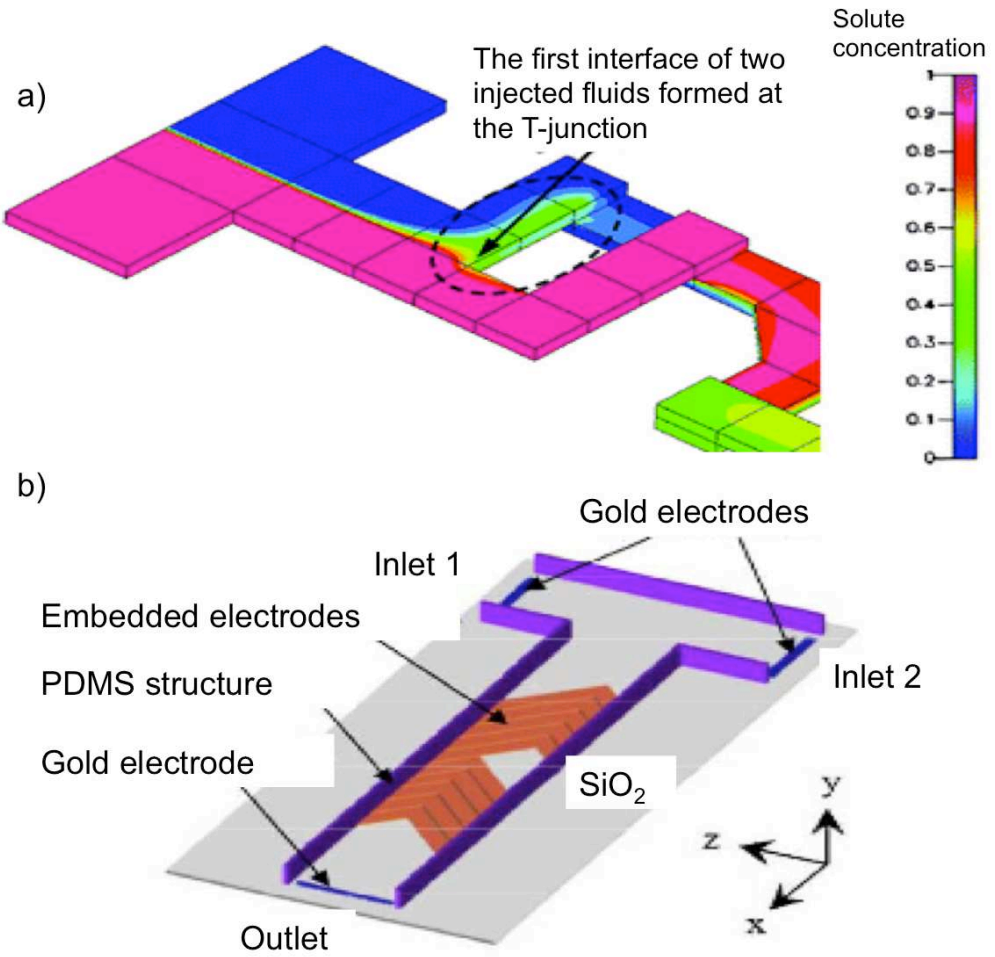

Figure 3.5: Examples of a) a passive micromixer using serpentine splitting recombination geometry from Sung Kim et al. [70] and b) an active micromixer with "T" shape microchannel with aluminium electrodes embedded on the bottom wall to enhance mixing (from Wu et al. [67]).

A new class of micromixers is beginning to appear which we have decided to call "**aided micromixers**". In this case, objects like bubbles, droplets or particles are injected into the flow. Their presence disturbs the flow field and therefore enhances mixing. An example of using bubbles to block branched channel systems in an alternating fashion has been proposed by Gastecki et al. (Figure 3.6). Another example has been developed by Mao et al. [71] which is very close to our approach (Section 7.5.3): closely packed bubbles rearrange in a chaotic fashion whilst travelling along a channel whose width changes continuously.

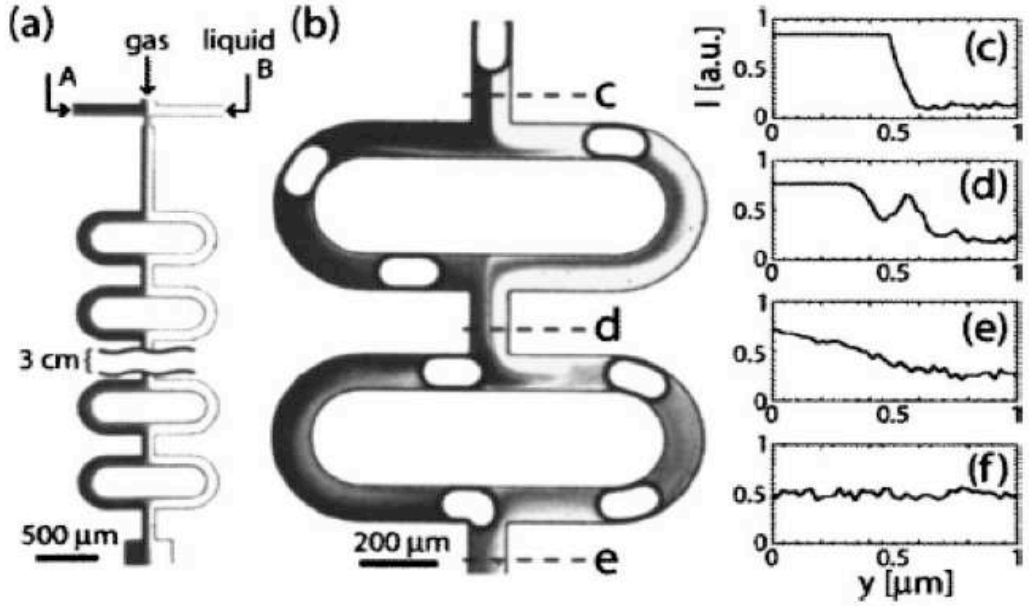

Figure 3.6: Approach the most similar to the approach used by us from [72, 73], using bubbles for mixing but with a very different concept (blocking of channels).

BIBLIOGRAPHY

1. Wereley, N.-T.N.S.T., *Fundamentals and Applications of Microfluidics*2006: Arttech house.
2. Tabeling, P., *Introduction to Microfluidics*2005: Oxford university press.
3. Whitesides, G.M., *The origins and the future of microfluidics.* Nature, 2006. **442**(7101): p. 368-373.
4. Martinez, C.J., *Bubble generation in microfluidic devices.* Bubble Science, Engineering & Technology, 2009. **1**(1-2): p. 40-52.
5. Prakash, M. and N. Gershenfeld, *Microfluidic bubble logic.* Science, 2007. **315**(5813): p. 832-835.
6. Chow, A.W., *Lab-on-a-chip: Opportunities for chemical engineering.* AIChE Journal, 2002. **48**(8): p. 1590-1595.
7. Soon-Eng Ong, S.Z., Hejun Du, Yongqing Fu *Fundamental principles and applications of microfluidic systems* Frontiers in Bioscience, 2008. **13**(January 1): p. 2757-2773.
8. Figeys, D. and D. Pinto, *Lab-on-a-Chip: A Revolution in Biological and Medical Sciences.* Analytical Chemistry, 2000. **72**(9): p. 330 A-335 A.
9. Yip Cheung Sang, Y., *Vers des micromousses stimulables (Toward smart microfoams)*, in *MSC*2009, University of Denis Diderot Paris 7: Paris.
10. Chung, K.Y., et al., *Fabricating scaffolds by microfluidics.* Biomicrofluidics, 2009. **3**(2).
11. Marmottant, P. and J.P. Raven, *Microfluidics with foams.* Soft Matter, 2009. **5**(18): p. 3385-3388.
12. van der Net, A., et al., *Highly structured porous solids from liquid foam templates.* Colloids and Surfaces a-Physicochemical and Engineering Aspects, 2009. **346**(1-3): p. 5-10.
13. Testouri, A., et al., *Highly Structured Foams from Chitosan Gels.* Macromolecules, 2010. **43**(14): p. 6166-6173.
14. Rodriguez-Arriaga, L., et al., *Elucidating the (in)stability of foams stabilized by mixtures of nano-particles and oppositely charged surfactants.* Soft Matter, 2011. **submitted**.
15. Palmieri, A., et al., *A microfluidic flow chemistry platform for organic synthesis: the Hofmann rearrangement.* Tetrahedron Letters, 2009. **50**(26): p. 3287-3289.
16. Doku, G.N., et al., *On-Microchip Multiphase Chemistry — A Review of Microreactor Design Principles and Reagent Contacting Modes.* ChemInform, 2005. **36**(25): p. no-no.
17. Dittrich, P.S. and A. Manz, *Lab-on-a-chip: microfluidics in drug discovery.* Nat Rev Drug Discov, 2006. **5**(3): p. 210-218.
18. Stone, H.A., A.D. Stroock, and A. Ajdari, *Engineering flows in small devices: Microfluidics toward a lab-on-a-chip.* Annual Review of Fluid Mechanics, 2004. **36**: p. 381-411.
19. Zhang, H., et al., *Microfluidic Production of Biopolymer Microcapsules with Controlled Morphology.* Journal of the American Chemical Society, 2006. **128**(37): p. 12205-12210.

20. Ong, S.E., et al., *Fundamental principles and applications of microfluidic systems.* Front Biosci, 2008. **13**: p. 2757-73.
21. Tadros, T.F., *Rheology of Dispersions Principles and Applications*2010: Wiley-VCH Verlag & Co.
22. Garstecki, P., et al., *Formation of droplets and bubbles in a microfluidic T-junction - scaling and mechanism of break-up.* Lab on a Chip, 2006. **6**(3): p. 437-446.
23. Wereley, N.-T.N.S.T., *Fundamentals and applications of microfluidics*. MEMS2002: Artech House.
24. Zhao, C.-X. and A.P.J. Middelberg, *Two-phase microfluidic flows.* Chemical Engineering Science, 2011. **66**(7): p. 1394-1411.
25. Christopher, G.F. and S.L. Anna, *Microfluidic methods for generating continuous droplet streams.* Journal of Physics D-Applied Physics, 2007. **40**: p. R319-R336.
26. Martinez, C.J., *Bubble generation in microfluidic devices* Bubble Science, Engineering & Technology, 2009. **1**(1-2): p. 40-52.
27. Garstecki, P., A.M. Ganan-Calvo, and G.M. Whitesides, *Formation of bubbles and droplets in microfluidic systems.* Bulletin of the polish academy of sciences technical sciences, 2005. **53**(4): p. 361.
28. Garstecki, P., et al., *Formation of droplets and bubbles in a microfluidic T-junction - scaling and mechanism of break-up (vol 6, pg 437, 2006).* Lab on a Chip, 2006. **6**(5): p. 693-693.
29. Park, J.I., et al., *A microfluidic route to small CO2 microbubbles with narrow size distribution.* Soft Matter. **6**(3): p. 630-634.
30. Wan, J., et al., *Controllable microfluidic production of microbubbles in water-in-oil emulsions and the formation of porous microparticles.* Advanced Materials, 2008. **20**(17): p. 3314-3318.
31. Garstecki, P., et al., *Formation of monodisperse bubbles in a microfluidic flow-focusing device.* Applied Physics Letters, 2004. **85**: p. 2649-2651.
32. Dollet, B., et al., *Role of the channel geometry on the bubble pinch-off in flow-focusing devices.* Physical Review Letters, 2008. **100**(3).
33. Seo, M., et al., *Microfluidic consecutive flow-focusing droplet generators.* Soft Matter, 2007. **3**(8): p. 986-992.
34. Jena, R.K., et al., *Large-strain thermo-mechanical behavior of cyclic olefin copolymers: Application to hot embossing and thermal bonding for the fabrication of microfluidic devices.* Sensors and Actuators B: Chemical. **155**(1): p. 93-105.
35. Pu, Q., et al., *On-Chip Micropatterning of Plastic (Cylic Olefin Copolymer, COC) Microfluidic Channels for the Fabrication of Biomolecule Microarrays Using Photografting Methods.* Langmuir, 2006. **23**(3): p. 1577-1583.
36. Koerner, T., et al., *Epoxy resins as stamps for hot embossing of microstructures and microfluidic channels.* Sensors and Actuators B: Chemical, 2005. **107**(2): p. 632-639.
37. Urbanski, J.P., et al., *Digital microfluidics using soft lithography.* Lab on a Chip, 2006. **6**(1): p. 96-104.
38. Drenckhan, W. and D. Langevin, *Monodisperse foams in one to three dimensions.* Current Opinion in Colloid & Interface Science, 2010. **15**(5): p. 341-358.

39. Fu, T., et al., *Bubble formation and breakup mechanism in a microfluidic flow-focusing device.* Chemical Engineering Science, 2009. **64**(10): p. 2392-2400.
40. Fu, T., et al., *Dynamics of bubble breakup in a microfluidic T-junction divergence.* Chemical Engineering Science. **66**(18): p. 4184-4195.
41. Fu, T., et al., *Squeezing-to-dripping transition for bubble formation in a microfluidic T-junction.* Chemical Engineering Science. **65**(12): p. 3739-3748.
42. Ganan-Calvo, A.M. and J.M. Gordillo, *Perfectly Monodisperse Microbubbling by Capillary Flow Focussing.* Phys. Rev. Lett., 2001. **87**: p. 274501.
43. Ohno, K.-i., K. Tachikawa, and A. Manz, *Microfluidics: Applications for analytical purposes in chemistry and biochemistry.* ELECTROPHORESIS, 2008. **29**(22): p. 4443-4453.
44. Christopher, G.F., et al., *Experimental observations of the squeezing-to-dripping transition in T-shaped microfluidic junctions.* Phys Rev E Stat Nonlin Soft Matter Phys, 2008. **78**(3 Pt 2): p. 036317.
45. Xu, J.H., et al., *Correlations of droplet formation in T-junction microfluidic devices: from squeezing to dripping.* Microfluidics and Nanofluidics, 2008. **5**(6): p. 711-717.
46. De Menech, M., et al., *Transition from squeezing to dripping in a microfluidic T-shaped junction.* Journal of Fluid Mechanics, 2008. **595**(-1): p. 141-161.
47. Garstecki, P., et al., *Formation of monodisperse bubbles in a microfluidic flow-focussing device.* Applied Phys. Lett., 2004. **85**(13): p. 2649-2651.
48. Lorenceau, E., et al., *A high rate flow-focusing foam generator.* Physics of Fluids, 2006. **18**(9): p. 097103.
49. Raven, J.P., P. Marmottant, and F. Graner, *Dry microfoams: formation and flow in a confined channel.* European Physical Journal B, 2006. **51**(1): p. 137-143.
50. Cubaud, T. and T.G. Mason, *Capillary threads and viscous droplets in square microchannels.* Physics of Fluids, 2008. **20**(5): p. 053302.
51. Antje, v.d.N., *Generation, characterisation and solidification of crystalline microfoams*, 2008, The University of Dublin: Trinity College Dublin.
52. Xu, S.Q., et al., *Generation of monodisperse particles by using microfluidics: Control over size, shape, and composition.* Angewandte Chemie-International Edition, 2005. **44**(5): p. 724-728.
53. Baroud, C.N., F. Gallaire, and R. Dangla, *Dynamics of microfluidic droplets.* Lab on a Chip, 2010. **10**(16): p. 2032-2045.
54. Nghe, P., et al., *Microfluidics and complex fluids.* Lab on a Chip, 2011. **11**(5): p. 788-794.
55. Fu, T., et al., *Bubble formation in non-Newtonian fluids in a microfluidic T-junction.* Chemical Engineering and Processing: Process Intensification. **50**(4): p. 438-442.
56. Fu, T.T., et al., *Gas-liquid flow stability and bubble formation in non-Newtonian fluids in microfluidic flow-focusing devices.* Microfluidics and Nanofluidics. **10**(5): p. 1135-1140.
57. SKURTYS, et al., *Formation of bubbles and foams in gelatine solutions within a vertical glass tube*. Vol. 22. 2008, Oxford, ROYAUME-UNI: Elsevier. 9.

58. Li, H.Z., Y. Mouline, and N.l. Midoux, *Modelling the bubble formation dynamics in non-Newtonian fluids.* Chemical Engineering Science, 2002. **57**(3): p. 339-346.
59. Nguyen, N.-T., *Micromixers - Fundamentals, Design and Fabrication*. Micro & Nano Technologies, ed. J. Ramsden2008, Norwich: William Andrew Inc.
60. Ottino, J.M. and S. Wiggins, *Introduction: mixing in microfluidics.* Philosophical Transactions of the Royal Society of London Series a-Mathematical Physical and Engineering Sciences, 2004. **362**(1818): p. 923-935.
61. Yaralioglu, G.G., et al., *Ultrasonic Mixing in Microfluidic Channels Using Integrated Transducers.* Analytical Chemistry, 2004. **76**(13): p. 3694-3698.
62. Aubin, J., et al., *Characterization of the Mixing Quality in Micromixers.* Chemical Engineering & Technology, 2003. **26**(12): p. 1262-1270.
63. Hessel, V., H. Lowe, and F. Schonfeld, *Micromixers,a review on passive and active mixing principles.* Chemical Engineering Science, 2005. **60**(89): p. 2479-2501.
64. Neils, C., et al., *Combinatorial mixing of microfluidic streams.* Lab Chip, 2004. **4**(4): p. 342-50.
65. Chung, Y.C., et al., *Design of passive mixers utilizing microfluidic self-circulation in the mixing chamber.* Lab Chip, 2004. **4**(1): p. 70-7.
66. Chen, H. and J.-C. Meiners, *Topologic mixing on a microfluidic chip.* Applied Physics Letters, 2004. **84**(12): p. 2193-2195.
67. Wu, H.-Y. and C.-H. Liu, *A novel electrokinetic micromixer.* Sensors and Actuators A: Physical, 2005. **118**(1): p. 107-115.
68. Sritharan, K., et al., *Acoustic mixing at low Reynold's numbers.* Applied Physics Letters, 2006. **88**(5): p. 054102.
69. Mansur, E.A., et al., *A State-of-the-Art Review of Mixing in Microfluidic Mixers.* Chinese Journal of Chemical Engineering, 2008. **16**(4): p. 503-516.
70. Kim, D.S., et al., *A serpentine laminating micromixer combining splitting/recombination and advection.* Lab on a Chip, 2005. **5**(7): p. 739-747.
71. Xiaole, M., et al., *Milliseconds microfluidic chaotic bubble mixer*. Vol. 8. 2010, Heidelberg, Germany: Springer. 6.
72. Garstecki, P., et al., *Mixing with bubbles: a practical technology for use with portable microfluidic devices.* Lab on a Chip, 2006. **6**(2): p. 207-212.
73. Garstecki, P., M.A. Fischbach, and G.M. Whitesides, *Design for mixing using bubbles in branched microfluidic channels.* Applied Physics Letters, 2005. **86**(24).

4 EXPERIMENTAL TECHNIQUES

The process of production of solid polymer foams used by us is composed of two main steps as shown in Figure 4.1. It consists of first foaming a polymer/monomer solution and then solidifying the liquid foam via polymerisation/crosslinking. The properties of the final solid foam are characterised in the final step.

Figure 4.1: A scheme of the main steps of our study

We present in this section the experimental techniques which we use to characterise first the liquid solutions, then the liquid foams and finally the properties of the solid foam. We will also describe briefly the principle of each measurement.

4.1 CHARACTERISATION OF THE LIQUID SOLUTIONS

The characterisation of the polymer foams which we generate in our study begins with the characterisation of the liquid monomer/polymer solutions from which they are made. It is then essential to identify key properties such as interfacial and rheological properties which have to be investigated. We use different types of techniques to characterise these liquid solutions along the whole process of their transformation into solid polymer foams. We provide here a summary of the most important techniques used for this purpose in this thesis.

4.1.1 Surface tension measurements

We performed surface tension measurements of monomer/polymer solutions containing surface active agents using *the pendant drop/ rising bubble technique*. This measurement is performed using a pendant drop apparatus (TRACKER from TECLIS) as shown in Figure 4.2. The TRACKER is able to measure the surface tension of a surfactant solution as a function of time. The results of this measurement allow obtaining the surface tension versus time curve. This instrument produces mechanically a liquid drop at the end of a needle by pushing a syringe (connected to the needle) filled with the solution to be characterised, or a rising bubble of air inside the studied solution. The principle of this measurement relies on the relation between the Young-Laplace equation and the profile of a pendant drop/rising bubble which undergoes only gravitational and surface energy forces. In some cases equilibration times can be quite long (up to 4 hours). Thus we conduct the measurements in a sealed container to avoid the evaporation of the studied solution.

Figure 4.2: Picture of the Tracker from Teclis.

Using this technique, one can easily see how fast the surfactants go to the air/liquid interfaces. The steeper the slope of the surface tension versus time curve, the shorter the time needed by the surfactants to populate the interface. When the measurements are performed for different surfactant concentrations, the CMC is given by the value of the concentration where the surface tension curve starts to show a plateau (as explained in Section 2.2.1).

4.1.2 Rheology

We performed rheological tests on the liquid monomer/solutions using a cone-plate rheometer. These tests consist of measuring the dynamic viscosity and the elastic and viscous moduli G' and G" as a function of time.

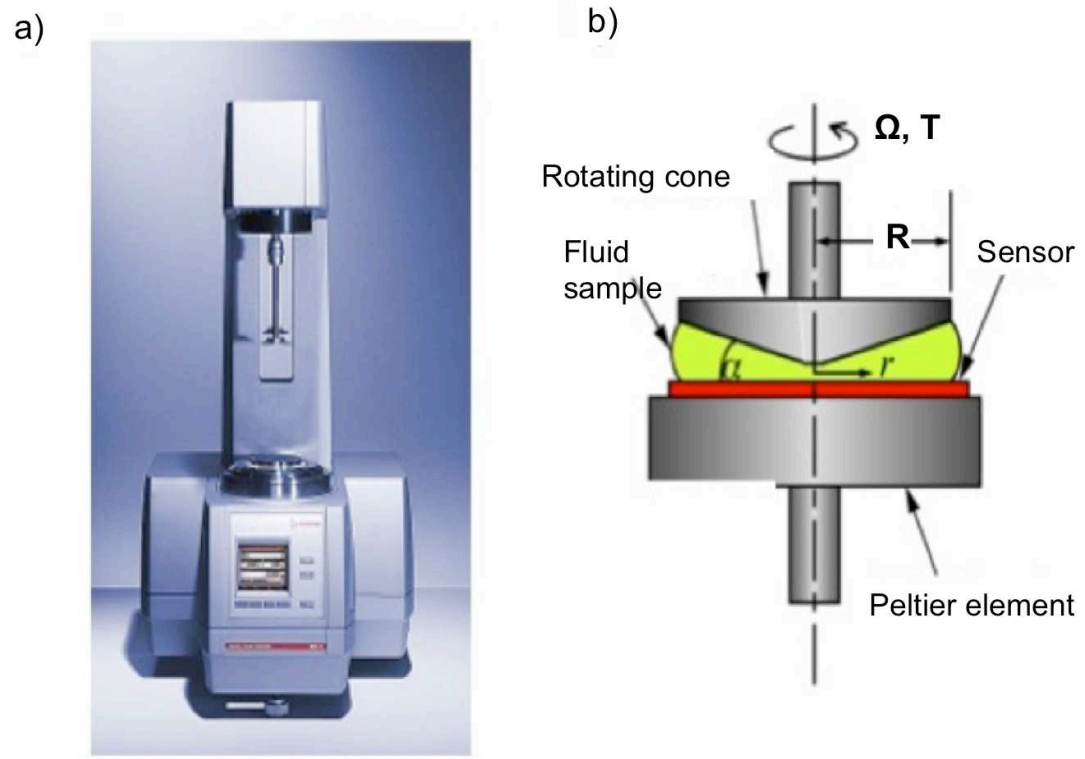

Figure 4.3: a) Picture of a rotational rheometer. b) Sketch of the cone-plate part of the rheometer where the fluid sample is deposited.

Viscosity measurement

In order to characterise the viscosity of the monomer/polymer solutions, we use a rotational rheometry technique. For this purpose, a sample of the diluted monomer/polymer solution is put into the gap of a cone-plate rheometer. In the case of our study, we used a cone-plate rheometer from Anton Paar shown in Figure 4.3a (Physica MCR 300, cone CP50-2: cone angle: 2°, diameter: 49.96mm), which is specifically designed to impose shear flow when rotated. The measuring system is driven by an ultra low-inertia motor coupled with an ultra high precision encoder of position. The whole is thermo-controlled by a temperature controller (Pelletier and thermostated bath). The samples are sealed during the measurements in order to prevent evaporation of the solvent. The temperature was kept constant at 23°C with a thermostated bath.

Measurement of elastic and viscous moduli

In order to determine the solidification time τ_S of the polymer solution, we follow the solidification process by determining the elastic and viscous moduli (G' and G'', respectively) as a function of time t after the injection and homogenisation of an appropriate solidification agent. The solution sample is injected in the cone-plate rheometer gap and oscillatory shear measurements are performed.

4.2 GENERATION AND CHARACTERISATION OF LIQUID FOAMS

4.2.1 Foam production techniques

There are different techniques of foam production depending on whether the generated foam needs to be monodisperse, bidisperse or polydisperse. In our study we are mainly interested in producing highly monodisperse foams. Nevertheless we produced polydisperse foams in order to firstly settle all the experimental parameters such as surfactant concentration, solvent concentration, or viscosity. And then we transfer the optimised parameters to the monodisperse foaming experiments. Polydisperse foam techniques are actually simpler, rapid and reproducible. We employed among these polydisperse foam production techniques the handshaking and the coupled-syringes techniques, which we explain here in more detail.

The handshaking technique consists of simply shaking powerfully a sealed container partly filled with a surfactant solution. We shake for a few minutes in order to mix the solution and the air entrapped inside the container and then we follow by imaging how the resulting foam decays with time.

In order to efficiently test and optimise the foaming properties of our solutions we designed and built a parallelised, *polydisperse foaming* device Figure 4.4a) which allows the simultaneous foaming of up to five different solutions using ***coupled syringes***. More precisely, the device contains five pairs of syringes which are connected by a capillary (Figure 4.4b). Each pair of syringes contains a foaming solution and gas. The two syringes are alternatively pushed in the two opposite directions in order to simultaneously push both, solution and gas, through the capillary which generates polydisperse bubbles of sizes of the order of a few hundred micrometres. The device is coupled with a video camera which allows following the evolution of the generated foams. An example of a typical image is shown in Figure 4.4c. One advantage of the device is to allow generating a predetermined liquid fraction of foam.

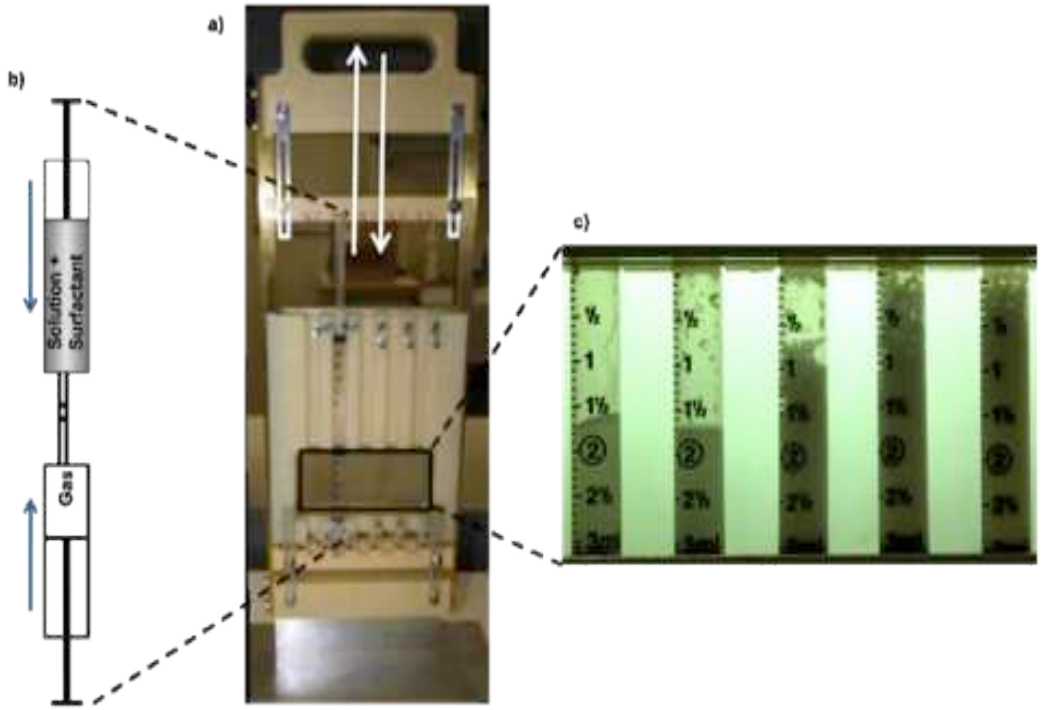

Figure 4.4: An in-house built set-up for the generation of polydisperse foams

4.2.2 Foamability/ Foam stability tests

In order to choose the working conditions for which foam stability is ensured, we performed tests revealing and comparing the ability of surfactant solutions to produce a given height of foam. In this test, we change only one parameter (for instance the surfactant concentration or the solvent concentration), and then we generate polydisperse foam using the syringes device (Section 4.2.1). The comparison of the height of the obtained foams allows choosing the one with the best foamability.

We performed also half-life time measurements by observing a given volume of foam generated with different surfactants at different concentrations in graduated containers of the same diameter, and then measured the time corresponding to the reduction of the total foam volume by half. Figure 4.5 shows an example of a half-life time measurement of a foam sample at a given surfactant concentration.

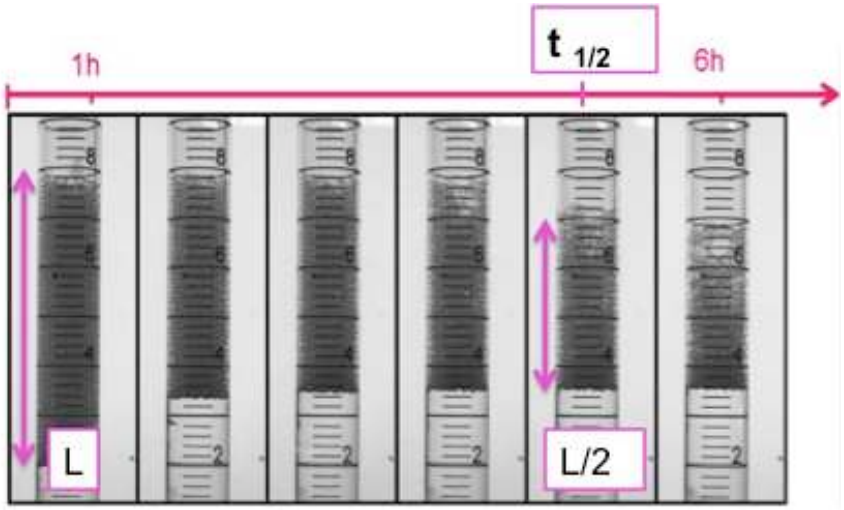

Figure 4.5: An example of half-life time measurement for a foam sample

4.3 MILLIFLUIDIC TECHNIQUES FOR THE GENERATION OF MONODISPERSE FOAM

4.3.1 Millifluidic set-up

The set-up for the generation and solidification of monodisperse foams of the studied polymers contains mainly **three common building blocks** namely

1. the *foaming geometry*,
2. the *gas and liquid supplies*
3. the *imaging system*.

Only the foaming geometry changes from one system to another.

The liquid supply is ensured by syringe pumps (KdScientific n° KDS-100-CE with Becton Dickson syringes) in a continuous manner. The injected gas can be of different nature (air, nitrogen, argon). It is supplied either by a syringe pump (syringe filled with air) or by connecting the gas inlet to a nitrogen or argon bottle equipped with a manometer to measure the gas flow rate. When we faced problems of gas compressibility, we changed the gas flow rate controller by a pressure controller which monitors the gas pressure (Elve flow pressure controller) instead. We use commercial tubing and connectors to link the foaming geometry to the gas and liquid supplies. We follow the bubble generation using a VDS Vosskuhler high-speed high-resolution CMOS camera (up to 500 frames/sec) and we characterise the foam structure using different cameras from Allied vision and Ueye IDS technologies.

Bubble diameters are measured by taking images of several monolayers of bubbles organised in a close-packed hexagonal lattice and by measuring the length of several bubbles with array of 5 – 10 bubbles.

4.3.2 Fabrication of the different foaming geometries

In our study, we are interested in foaming different kinds of polymers which have different intrinsic properties and different ways of polymerisation (cross-linking, UV-polymerisation, or polyaddition). It is therefore essential to use a specific foaming geometry and set-up for each studied system which suits the specific polymer properties. In some cases, we used commercial T-junctions which gave satisfactory foaming results. In some more complicated cases, where it was needed to integrate many sub-units we designed and fabricated millifluidic geometry in our lab with an "appropriate channel geometry" as shown in the very beginning of this manuscript in (Figure 1.3).

COMMERCIAL FOAMING GEOMETRY

We used for the foaming of *Chitosan* solutions a cross-flowing foaming device built on a commercial Kynar T- junction shown in Figure 4.6 with an inner channel diameter of 1.25 mm and cylindrical cross- sections, which is connected to the other set-up elements by Tygon R-3603 tubing with an internal diameter of 1.6 mm purchased from Fisher Scientific.

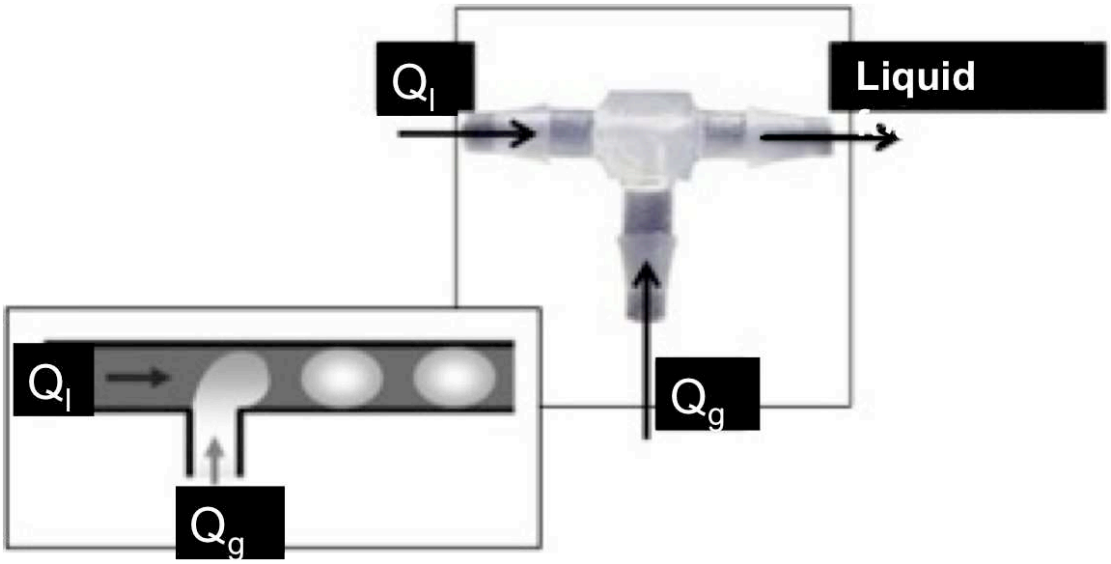

Figure 4.6: Foaming cross-flow T-junction geometry. Left: schematic illustration of the bubbling inside the T-junction. Right: The correspondent commercial Kynar T-junction

This T-junction was used to generate monodisperse *Chitosan* foams which are gelified afterwards by injecting the proper reticulent directly in the tubing (see Section 5.4.1 for more details).

IN-HOUSE MADE FOAMING GEOMETRIES

- ***Drilling technique***

In the case of the *Superabsorbent polymer SAP and polyurethane* (Section 6.6.1 and Section 7.5), we had to develop foaming geometries which fit the foaming requirement of each polymer. A built in-house T-junction using high-precision milling in polycarbonate blocks (Figure 4.7) was used in the case of SAP. This junction can host capillaries (purchased from Hirschmann) of different diameters (100-750 microns). The capillaries are first cut in the middle using an electric saw then inserted and glued manually inside the exit channel of the millifluidic geometry. Using capillaries with different diameters allows having monodisperse bubbles of different sizes (the bubble size has the same order of magnitude as the capillary diameter). This choice is justified by the fact that we were unable to obtain small bubbles with the commercial junction. Moreover, the drilled T-junction furnishes a better visibility of the bubble generation process thanks to the transparency of the polycarbonate.

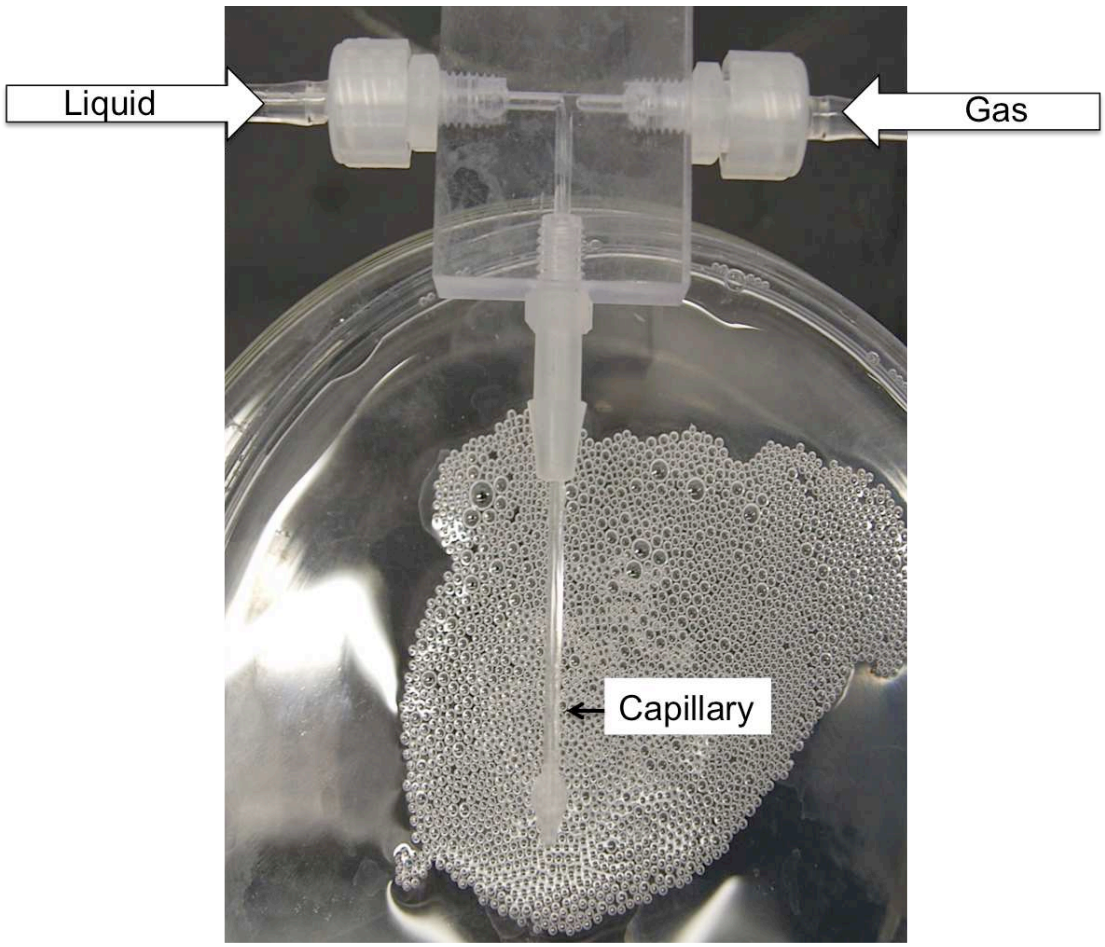

Figure 4.7: Photo of the in-house made T-junction using drilling technique on polycarbonate substrate. The bubbles are generated within micro-capillaries, which are inserted into the bottom branch of the T-junction.

- ***Hot embossing technique***

When the millifluidic Lab-on-a-Chip is composed of various sub-units and hosts many chemical reactants, it has consequently a complex design. Using the drilling technique for the fabrication of the millifluidic geometry in this case is not possible. We therefore use a *micromilling* technique, in which the channel system is milled into a plexiglass plate. Micromilling every channel would be very long and expensive, especially since the geometries are not reusable (the channels are often blocked at the end of the experiment due to polymerisation). We therefore decided to use the hot embossing technique to replicate micromilled masters. This is a very precise and inexpensive technique [1-4].

For this purpose, we set up an on-purpose hot embossing experimental protocol for the fabrication of millifluidic geometries in a very reproducible fashion. Following this protocol, we fabricate first a millifluidic master by micro-milling a polymer plate (Figure 4.8) with sufficiently high *glass transition temperatures* T_G to avoid softening or melting during milling. A wide range of polymers is available for this purpose. We chose to work with Cyclic Olefin Copolymers (COC_{170}, T_G = 170 °C, TOPAS 6017 from TICONA), which belong to a new class of inexpensive, versatile and transparent thermoplastics. The COC is widely used in the field of microfabrication [5-10] since it has a good moldability under heating/pressing which provides an excellent replication of the original master [11, 12]. Of particular advantage is that COC is available for a range of T_G (75 - 170°C), which provides easy adaptation for specific applications. In our case the COC is particularly suitable since it has a high rigidity at room temperature, which is important to avoid deformation upon the viscous fluid flow. Furthermore, it has an excellent chemical resistance and is transparent, allowing to follow in real time the foam generation.
To replicate the milled master, we cast it in Polydimethylsiloxane (PDMS, Sylgard 184 from Dow Corning) (Figure 4.8). This PDMS master is then hot embossed into a granular COC_{80} with low T_G (80 °C, TOPAS 8007). For this purpose, the PDMS mould is put into a special moulding container and covered with a layer of granular COC_{80}. The ensemble is put into a hot press (Atlas series Plateau controller from Eurolabo) where it is heated to T_G+40°C. Once the desired temperature is obtained, we press for 15 minutes at 1 bar. Afterwards the pressure is released and the ensemble left to cool down at room temperature. When cooled down, the channel system is removed and sealed with a sheet of the same COC. For this purpose, a thin layer of a mixture of cyclohexane (75%) and hexadecane (25%) is spread evenly on the surface to be sealed. The sealing sheet is pressed onto this surface in the hot press for 10 minutes at a temperature slightly below the T_G (T_G -2°C). The pressure is applied by the hand screw only in order not to deform the channels. This step is known as “the bonding of COC” which has been widely studied in order to obtain perfectly sealed microchips and avoid leakage [1, 8, 13]. The bonding can be performed using different techniques such as thermal [14], chemical [15], high-pressure bonding [16] or a combination of them.

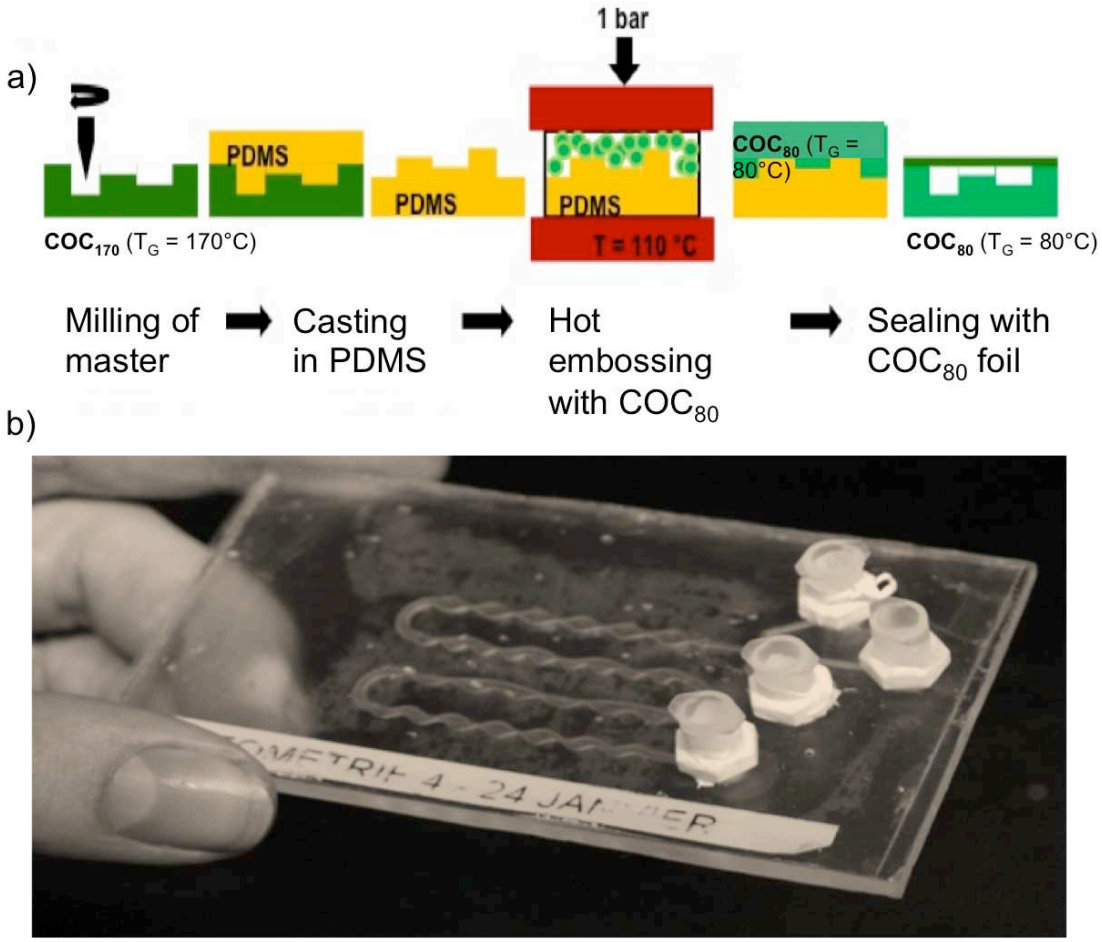

Figure 4.8: a) Typical procedure for the fabrication of the millfluidic Lab-on-a-Chip: A micromilling machine is used to mill the channel system into a COC plate (T_G = 170°C). This channel system is cast into PDMS. The PDMS master is used to mold granular COC (T_G = 80°C) in a hot embossing system. After removal of the PDMS master, the COC positive is sealed with a film of the same COC material using a mixture of 75% cyclohexane and 25% hexadecane. b) Example of a sealed Lab-on-a-Chip with Luer-Lock connectors.

4.3.3 Calibration of the foaming geometry

Before starting the production of monodisperse foams, the foaming device is calibrated using reference solutions, generally the solvent of the corresponding polymer containing an appropriate surfactant. We inject this solution in the inlet channel dedicated normally to the feeding of the liquid polymer solution. Then we vary the liquid flow rate; simply by entering the desired value on the syringe pumps, while keeping the gas flow rate constant and we report the stability/monodispersity and the average of bubble diameter of the foam. We obtain a calibration curve and a phase diagram shown in (Figure 3.4) which serve as a " ***map***" giving the coordinates (Q_l and Q_g) for a given type of foam and bubble size. Care needs to be taken when performing the calibration since for many couples of gas and liquid flow rates, the bubbling equilibration time can be sometimes very long (hours).

4.4 SOLIDIFICATION TECHNIQUES

In order to solidify the foam after its production, we employ two different techniques according to the polymer we are using. In the first technique, we inject a solution of a solidifying agent at a constant flow rate which is calculated to reproduce the same conditions used for the measurements of the solidification time τ_S. The solidifying agent is injected inside the downstream millifluidic channel at the level where the bubbles are already generated. To ensure a good diffusion of the solidifying agent, we use an appropriate mixing unit which can simply be a "delay line" of 20 cm along which we let the bubbles travel until the total diffusion of the solidifying agent occurs (Section 5.4.3). Alternatively, we integrate an on-purpose designed mixing unit, which thanks to its channel network ensures a homogeneous solidification (Section 7.5.1). The second technique used is polymerisation via UV light we use a UV polymerisation route to solidify the monodisperse foam (Section 6.3.2). The foaming solution contains a photo-initiator which triggers the polymerisation reaction when it is irradiated by a UV/VIS lamp (Oriel, 50-200 Watts).

4.5 FOAM SHAPING

Once the bubbles are generated, the foamed mixture has to be given the desired shape. We generated different foam geometries.

1. **Foamed sheets** (one or several bubble layers) and bulk foams (ordered and disordered) of various densities
2. **Foamed threads** by collecting the foam into tubes of different diameters.

For the generation of bulk foams, the foamed mix leaves the micro/milli-fluidic device in the liquid state and solidifies slowly (order of 15-60 minutes) in appropriate containers (petri dishes, bottles of different dimensions). For the generation of foamed threads, the foam needs to be collected in a lubricant tubes, in order to allow solidification in a continuous mode.

4.6 CUTTING OF SOLID FOAMS

In order to characterise the solid foams, it was necessary to cut them into samples with similar dimensions. We used generally a razor blade to cut the foam sample orthogonally at the desired dimensions. In some cases, the generated foams were very flexible; the razor blade technique was thus inappropriate since it damages the foam surface. Therefore, we employed another cutting technique in which these foam samples are first put in a liquid nitrogen bath for 15 minutes in order to render them temporarily more rigid. Then, we cut them using an electric ribbon.

4.7 CHARACTERISATION OF SOLID FOAMS

We used imaging techniques (Ueye digital camera and optical microscope) and the software ImageJ to characterise the solid foam structure for the three

polymer systems (bubble size, polydispersity index, open/closed cell structure, crystalline structures). In the case of PU, we studied the viscoelastic property of the pure polymer and the solid PU foams by dynamic mechanical analysis (DMA) using a compression machine shown in Figure 4.9 (Adamel DY 34 from MDE). In this technique, a force (stress σ) is applied to a material and the resulting displacement (strain) is measured.

Figure 4.9: DMA machine used for the compression tests on the polyurethane foams.

BIBLIOGRAPHY

1. Kricka, L.J., et al., *Fabrication of plastic microchips by hot embossing.* Lab on a Chip, 2002. **2**(1): p. 1-4.
2. Koerner, T., et al., *Epoxy resins as stamps for hot embossing of microstructures and microfluidic channels.* Sensors and Actuators B: Chemical, 2005. **107**(2): p. 632-639.
3. Juang, Y.-J., L.J. Lee, and K.W. Koelling, *Hot embossing in microfabrication. Part I: Experimental.* Polymer Engineering & Science, 2002. **42**(3): p. 539-550.
4. Heckele, M., W. Bacher, and K.D. Müller, *Hot embossing - The molding technique for plastic microstructures.* Microsystem Technologies, 1998. **4**(3): p. 122-124.
5. Rohr, T., et al., *Surface Functionalization of Thermoplastic Polymers for the Fabrication of Microfluidic Devices by Photoinitiated Grafting.* Advanced Functional Materials, 2003. **13**(4): p. 264-270.
6. Pu, Q., et al., *On-Chip Micropatterning of Plastic (Cylic Olefin Copolymer, COC) Microfluidic Channels for the Fabrication of Biomolecule Microarrays Using Photografting Methods.* Langmuir, 2006. **23**(3): p. 1577-1583.
7. Nunes, P., et al., *Cyclic olefin polymers: emerging materials for lab-on-a-chip applications.* Microfluidics and Nanofluidics. **9**(2): p. 145-161.
8. Sunkara, V., et al., *Simple room temperature bonding of thermoplastics and poly(dimethylsiloxane).* Lab on a Chip. **11**(5): p. 962-965.
9. Jena., R.K., et al., *Rheological (visco-elastic behaviour) analysis of cyclic olefin copolymers with application to hot embossing for microfabrication.* Journal of Micromechanics and Microengineering. **21**(8).
10. Jena, R.K., et al., *Large-strain thermo-mechanical behavior of cyclic olefin copolymers: Application to hot embossing and thermal bonding for the fabrication of microfluidic devices.* Sensors and Actuators B: Chemical. **155**(1): p. 93-105.
11. Leech, P.W., *Hot embossing of cyclic olefin copolymers.* Journal of Micromechanics and Microengineering, 2009. **19**(5): p. 055008.
12. Jena, R.K., et al., *Large-strain thermo-mechanical behavior of cyclic olefin copolymers: Application to hot embossing and thermal bonding for the fabrication of microfluidic devices.* Sensors and Actuators B: Chemical, 2011. **155**(1): p. 93-105.
13. Tsao, C.-W. and D. DeVoe, *Bonding of thermoplastic polymer microfluidics.* Microfluidics and Nanofluidics, 2009. **6**(1): p. 1-16.
14. Sunanda Roya, C.Y.Y., Z.Y. Wanga, L. Ananda, *Thermal bonding of microfluidic devices: Factors that affect interfacial strength of similar and dissimilar cyclic olefin copolymers.* Sensors and Actuators B Chemical, 2011.
15. Gu, P., et al., *Chemical-Assisted Bonding of Thermoplastics/Elastomer for Fabricating Microfluidic Valves.* Analytical Chemistry, 2010. **83**(1): p. 446-452.
16. Mair, D.A., et al., *Room-Temperature Bonding for Plastic High-Pressure Microfluidic Chips.* Analytical Chemistry, 2007. **79**(13): p. 5097-5102.

5 CHITOSAN FOAMS

5.1 INTRODUCTION

Chitosan hydrogels have been widely studied and used for decades in different applications, including drug delivery, wound healing treatment and thickening agents in the food industry [1-7]. *Foamed* chitosan gels are already used in some applications such as wound bandage, scaffolding or tissue engineering [1, 4, 8-10]. The *controlled* foaming of hydrogels using micro- or millifluidic techniques has been attempted in recent years in particular for alginate gels [11, 12] in a search for well-controlled material properties, for example towards scaffold development, in which pore-size control is a key parameter to ensure and optimise cell-growth [1, 8-11, 13-16].

The polymer we use is **chitosan** which is a biopolymer which is produced from chitin [4, 15, 17-20], the most abundant natural polymer after cellulose. Chitosan (Figure 5.1) forms biocompatible and biodegradable hydrogels via covalent reactions with dialdehyde groups (cross-linking).

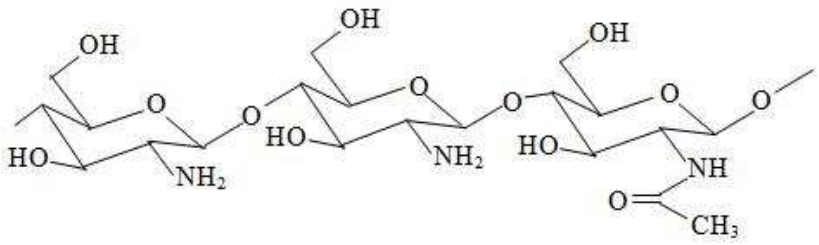

Figure 5.1 : Molecule of Chitosan

It is soluble only in acidic media thanks to the protonation of its amine groups and reacts following the reaction [21 and refernces therein].

$$\text{Chit-NH}_2 + \text{H}_3\text{O}^+ \leftrightarrows \quad \text{Chit-NH}_3^+ + \text{H}_2\text{O} \qquad \textbf{(5. 1)}$$

5.2 CHARACTERISATION OF CHITOSAN SOLUTIONS

5.2.1 Material

We purchased medium molecular weight Chitosan from Sigma-Aldrich (CAS: 9012-76-4). We prepared a chitosan stock solution of C_{ch} = 2wt% by dissolving the corresponding amount of chitosan in 0.1 mol/l acetic acid at 25°C. Dissolution and homogenisation were ensured by stirring for 48 hours at room temperature and at medium stirring speed. This stock solution was then diluted in 0.1 mol/l acetic acid to obtain a range of concentrations C_{ch} between 0.5 and 2.0 wt%. The pH of these solutions increased slightly with increasing chitosan concentration and was between 4 and 6.5.

In order to stabilize foams generated from these solutions we added the surfactant Lutensol AT25 (fatty alcohol alkoxylate with a C16/C18 chain and a degree of ethoxylation of 25, M = *1360 g.mol^{-1},* Critical micelle concentration (CMC) in water = *4.3 10^{-6} mol.l^{-1}*) provided by *BASF*. AT25 is a non-ionic surfactant chosen to avoid electrostatic interactions between the charged chitosan and the surfactant.

The chitosan solutions were gelified using the organic compound glyoxal ($C_2H_2O_2$, 40% in water, CAS number: 107-22-2) which has an aldehyde group and which was purchased from Sigma-Aldrich. Following the protocol provided by L. Payet [21], we added the glyoxal at a proportion of 20 µl for 5 g of chitosan.

5.2.2 Study of the rheological properties of chitosan solutions

All rheological measurements were carried out over a range of shear rates $\dot{\gamma}$ (from 0.1 s^{-1} to 100 s^{-1}) and for chitosan concentrations between 0.3 to 2 wt% using a rotational rheometer (Section 4.1.2). We find that the viscosity of concentrated chitosan solutions decreases non-negligibly with *shear rate*. Since our principal interest here lies in the viscosity in the limit of zero shear rate (η_0) and a characterisation of the general behaviour of the chitosan solutions corresponding to our experimental conditions (in terms of typical shear rates and characteristic flow times), we decided on the following protocol: we measure at a small number of shear rates only, starting at the lowest shear rate (range 0.1 s^{-1} to 100 s^{-1}) with a fixed measurement time of 1000 s per data point.

Solution viscosity

Figure 5.2 shows how the viscosity η changes under these measuring conditions as a function of shear rate $\dot{\gamma}$ for a selection of chitosan concentrations (C_{Ch} =0.9, 1.5, 1.7, 1.9 and 2 wt%).

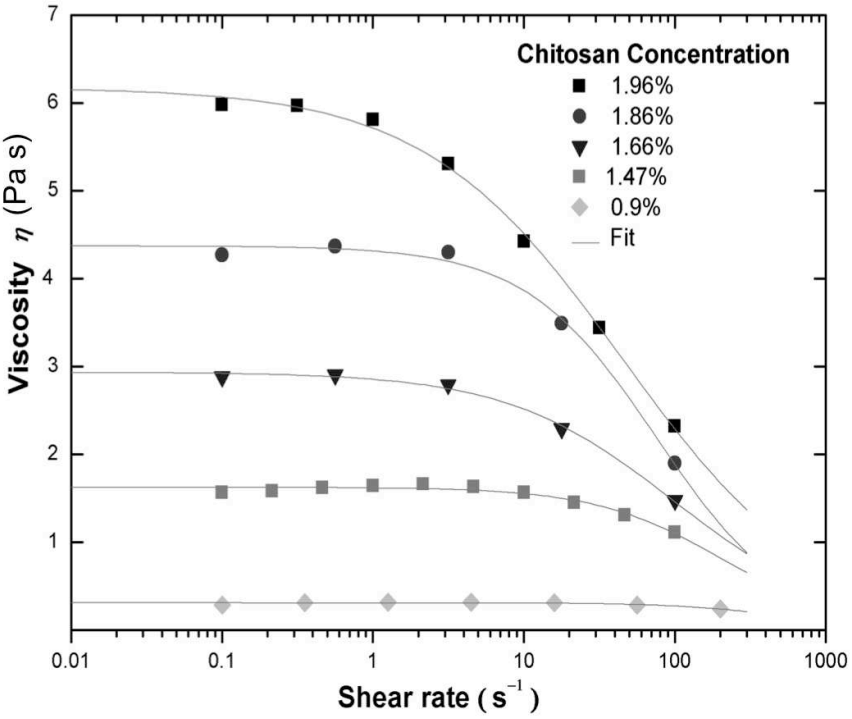

Figure 5.2: Viscosity as a function of shear rate $\dot{\gamma}$ for different chitosan concentrations.

We notice first of all that the viscosities of the solutions depend dramatically on the chitosan concentration, changing over almost four orders of magnitude as the concentration is increased from 0 % (pure water η = 0.001 Pa s) to only 2 wt% ($\eta \sim 6$ Pa s). Furthermore, with increasing chitosan concentration the solutions display an increasing shear-thinning (i.e. non-Newtonian) behaviour [22-24]. These properties indicate strong interactions between the polymers and long relaxation times, respectively, having important consequences on the generation of bubbles in millifluidic devices (Section 3.2.5). As seen in Figure 5.2, Newtonian behaviour is recovered for all solutions in the limit of low shear rates. We determined the zero-shear rate viscosities η_0 by fitting the data to the "Cross equation" [25, 26] which is commonly used to describe the behaviour of polysaccharide solutions. It holds,

$$\eta = \eta_\infty - \frac{\eta_0 - \eta_\infty}{1 + (a\dot{\gamma})^p}\ , \qquad \textbf{(5. 2)}$$

where η_∞ is the viscosity in the limit of very high shear rates, for which we use the viscosity of water (i.e. η = 0.001 Pa s), a is a typical polymer relaxation time, and p is a positive exponent. The resulting fits are shown along with the data in Figure 5.2 whilst the resulting zero-shear viscosities η_0 for the whole range of

our measurements are shown in Figure 5.4 together with the solidification time τ_S (which is discussed in more detail in the following paragraph).

The η_0 data is fitted well by a single power law

$$\eta_0 \propto AC^B , \qquad \textbf{(5. 3)}$$

with A = 0.32 ± 0.05 Pa s and B = 4.2 ± 0.3. The exponent of 4.2 is much higher than what is expected for polyelectrolyte solutions ($B \leq 1.5$ [27]). The reasons for this are manifold. First of all, the ionic strength of our solutions (≈ 0.1 M) is sufficiently large to have Debye lengths of the order of 1 nm, meaning, that charges are strongly screened and that the polymers interact more like neutral polymers. However, even for neutral polymers in the concentrated, entangled regime standard reptation theory predicts that B ≤ 15/4 [28]. This additional deviation for chitosan solutions has been discussed intensively in the recent literature ([29] and references therein) and is now commonly assigned to the fact that chitosan molecules experience additional (attractive) interactions which are not taken into account in standard reptation models. Of particular importance is the effect of hydrogen bonding and hydrophobic interactions [30] requiring the consideration of "sticky-reptation" type models [31] which predict exponents of up to 8.5. Comparison with chitosan solutions investigated under similar conditions in the literature [29] and [24] also allows us to conclude that our measurements are done for a range of chitosan concentrations corresponding to the concentrated, entangled regime, hence justifying the fact that they are well described by a single power law.

The solidification time

In order to determine the solidification time τ_S of the chitosan solutions in the presence of glyoxal we follow the gelification process by determining the elastic and viscous moduli (G' and G'', respectively) of the samples as a function of time t after the injection and homogenisation of glyoxal.

A typical example for a chitosan concentration of 1.6 %wt at excitation frequencies of 5, 10 and 15 Hz is shown in Figure 5.3. All curves are in line with the classical behaviour of solidification: whilst the viscous modulus G'' goes through a small maximum, the elastic modulus G' increases significantly with time then reaches a plateau when the solidification process terminates. The cross-over of both curves is generally taken as the gelification point, since at this point the material goes from one dominated by viscous behaviour to one dominated by elastic behaviour. This cross-over is, however, sensitive to the excitation frequency, which is why we preferred to follow the approach suggested by Chambon *et al.* [32] and successfully employed for chitosan gelification [24, 32-34]: Following from the fact that the material structure becomes scale-invariant at the gelification point, the ratio of the viscous and the

elastic modulus G''/G' is independent of the excitation frequency at τ_g. This means that considering G''/G' as a function of time provides a unique cross-over of all curves at τ_g. An example of a resulting curve is shown in the inset of Figure 5.3 for the chitosan concentration of 1.6 %wt with a cross-over at G''/G' = 1.05 at τ_g = ~1500 s.

Using this approach we determine the gelification time τ_g for a range of chitosan concentrations. The results are displayed together with the zero shear rate viscosities η_0 in Figure 5.4. This figure allows us to choose an appropriate window of chitosan concentrations based on the requirements of the foaming process: the viscosity has to be sufficiently low and the solidification time sufficiently long to allow reliable foaming. Yet the solidification time needs to be sufficiently short to ensure foam stability before gelification. In our case we decided to work with a chitosan concentration of C_{Ch} = 1.9 %wt which responds to the latter conditions (gelification time of τ_g= 820± 80 s and a zero shear rate viscosity of η_0 = 4.37 ± 0.13 Pa s).

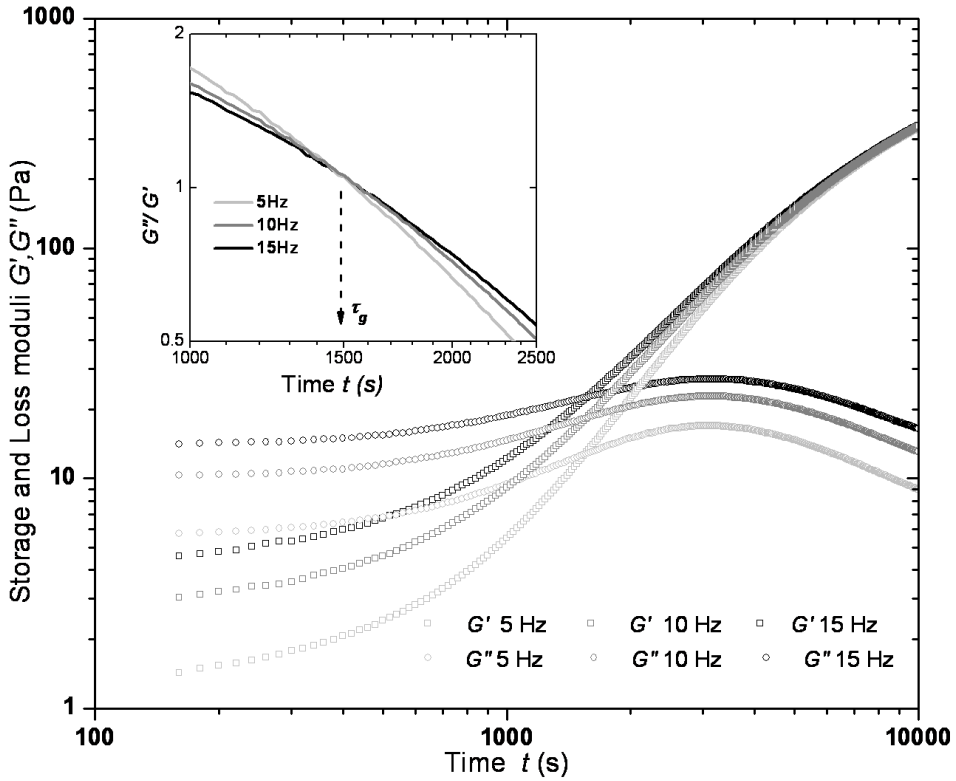

Figure 5.3: A typical example (Chitosan concentration C_{Ch} = 1.6 %wt) of how the elastic and viscous moduli, G' and G'' respectively, change upon gelification at different excitation frequencies. Insert: Plotting G''/G' provides a unique cross-over point at the gelification point and hence a well-defined (frequency-independent) measure of the gelification time.

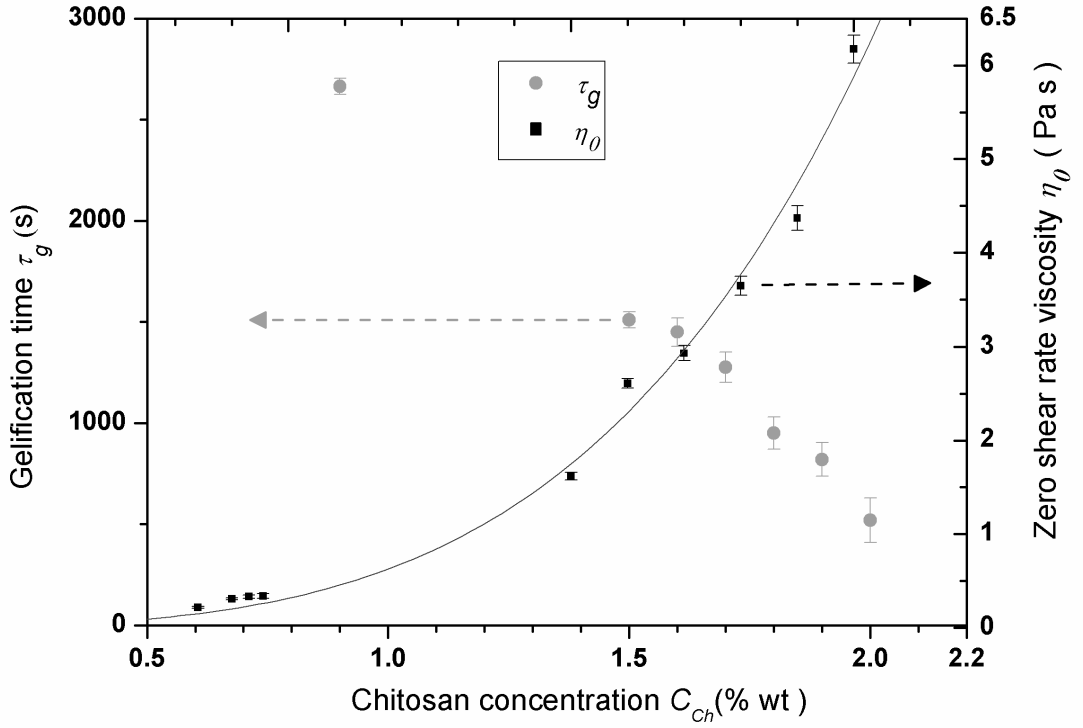

Figure 5.4: Gelification time τ_g and zero shear rate viscosity η_o as a function of chitosan concentration C_{Ch} . The viscosity is fitted by the equ.(5. 2) with A = 0.32 ± 0.05 Pa s and B = 4.2 ± 0.3

5.3 CHARACTERISATION OF THE LIQUID CHITOSAN FOAMS

In order to stabilise the foams against coalescence, an appropriate surface active stabiliser needs to be chosen. Already the chitosan by itself is highly surface active. This fact is illustrated in Figure 5.5, where we show how the surface tension γ of our standard chitosan solution (1.9 wt% Chitosan in 0.1 mol/l Acetic Acid) changes as a function of time after rapid generation of a gas/liquid interface (Tracker device, Section 4.1.1). Whilst the surface tension of pure water and the water/acid mixture remain literally unchanged with time (72 and 71 mN/m, respectively, sketched in Figure 5.5, that of the chitosan solution drops significantly but slowly to about 52 N/m, indicating the slow arrival of surface active species at the interface. This observation is confirmed by the fact that reasonably stable foams can be generated from these chitosan solutions without adding any additional surfactants. This could be due to the presence of surface active impurities in the chitosan powder, but we believe it to be a true effect of the hydrophobicity of the chitosan. Firstly, with a degree of deacetylation between 75 and 85%, the chitosan molecules contain significant hydrophobic sections. Secondly, a low pH is required to sufficiently protonate the amino groups of the chitosan to render the remaining parts hydrophilic. In our case, we find a pH of 6-6.5 pH for the highly concentrated chitosan solutions, meaning

that the free amino groups become less protonated leading to a further increase of hydrophobicity of the chitosan chains and hence a strong surface activity [35-37]. The tendency of the molecules to arrange their hydrophobic and hydrophilic parts at the gas liquid interface may be further enhanced by the fact that electrostatic intra-molecule interactions are strongly screened in our solutions providing therefore more flexible polymer chains.

The typical equilibration times of the chitosan-enriched interfaces are of the order of 10 minutes (Figure 5.5), which is too slow for our foaming process, in which foams of closely-packed bubbles are generated within a few seconds, and in which the coalescence of bubbles needs to be absolutely avoided to maintain the monodispersity and ordered structure of the final foam. We therefore add a low-molecular weight surfactant, which, on average and at sufficiently high surfactant concentration, diffuses to the interface in a few milli-seconds. Since the chitosan is charged, we chose the non-ionic surfactant Lutensol AT25 for this purpose. As is shown in Figure 5.5, the addition of this surfactant at a concentration of 0.59 wt% (which corresponds to 1000 times its CMC in pure water) not only decreases further the surface tension (42 mN/m) but also greatly accelerates the main decrease to a few seconds.

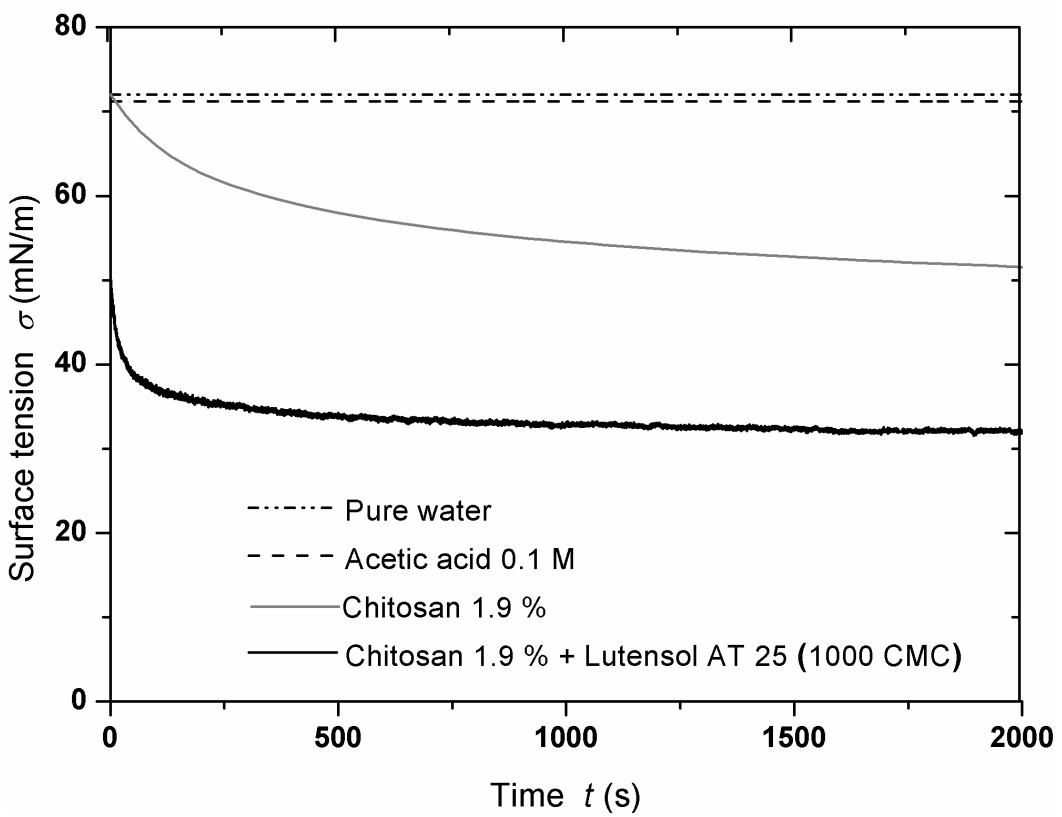

Figure 5.5: Evolution of the surface tension σ of a rapidly generated gas/liquid interface ("rising bubble" in the TRACKER device) for pure water, the acid/water mixture (sketched), the standard chitosan solution (C_{Ch} = 1.9 wt%) and the chitosan solution with added surfactant (1000 CMC of AT25).

Since the AT25 has a very low critical micelle concentration (CMC = 4.3 10-6 mol/l in pure water), relatively low surfactant concentrations need to be used to ensure that all the interfaces in a foam can be covered sufficiently (and sufficiently quickly) to ensure foam stability. This is due to the fact that foams have a very large surface to volume ratio. In order to choose the appropriate surfactant concentration we performed simple foaming tests by shaking (Section 4.2.1) for a range of concentrations of AT25 in pure water.

Results are shown in Figure 5.6a, where the left image, taken immediately after shaking the tubes (t = 0 min), provides an indication of the foamability, while the right image, taken after 30 minutes (t = 30 min), provides an indication of the foam stability over a period relevant to our typical experimental time scale. Although surprising, it is obvious from these results that very high concentrations of AT25 are required to ensure both, foamability and foam stability, which is why we fixed the working concentration at C_{AT25} = 1000 CMC (corresponding to 0.59 wt%).

Since the presence of the chitosan increases significantly the viscosity of the solution, the foams are stabilised additionally by the fact that gravity-driven drainage of liquid is reduced sufficiently to avoid the otherwise rapid formation of thin films which are very sensitive to rupture. This is illustrated in Figure 5.6b, which shows how foamability and foam stability improve with increasing chitosan concentration for a constant surfactant concentration (1000 CMC).

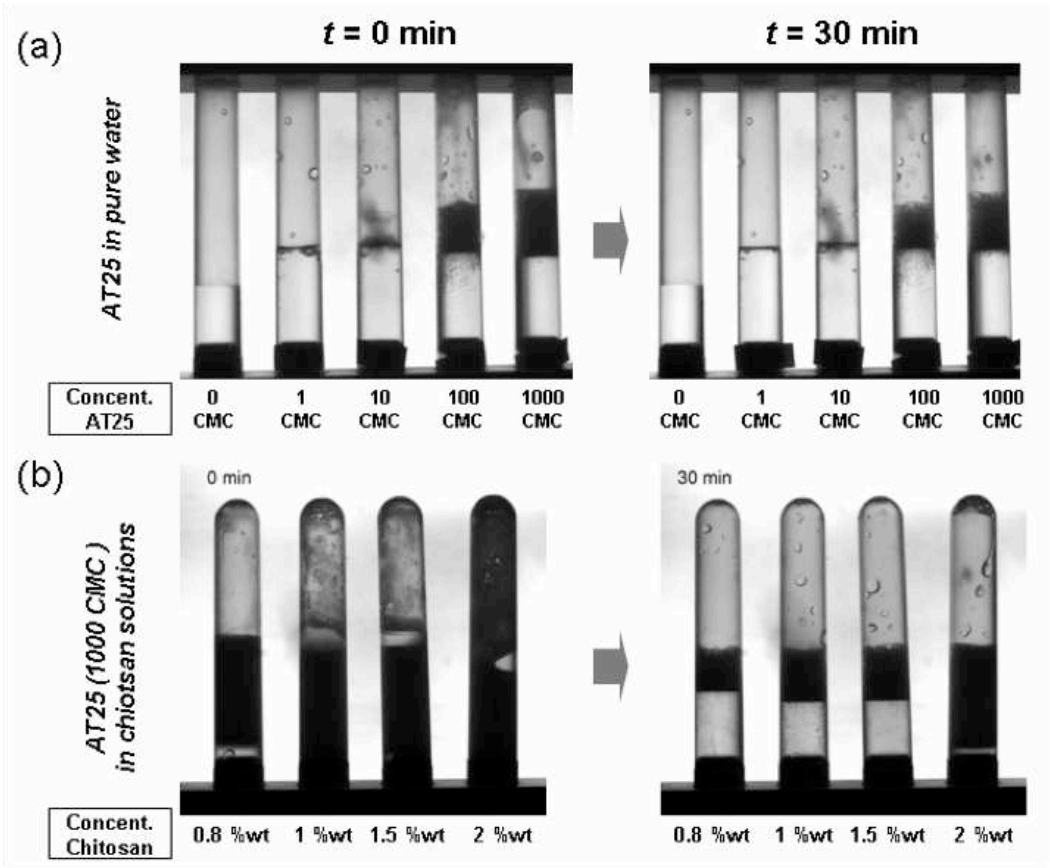

Figure 5.6: *Foamability* (left, t = 0 min) and *foam stability* (right, t = 30 min) of (a) aqueous solutions of the surfactant AT25 expressed as multiples of the critical micelle concentration (CMC = 4.3 10^{-6} mol.l^{-1}); and (b) chitosan solutions with increasing chitosan concentration at constant surfactant concentration (AT25 at 1000 CMC).

5.4 GENERATION OF HIGHLY MONODISPERSE FOAMS FROM CHITOSAN

5.4.1 The millifluidic set-up

As sketched in Figure 5.7, we generate highly monodisperse Chitosan foams with polydispersity < 5 % using a T-junction device (Section 3.2.2). When working in the right flow rate ranges (in our case both flow rates are of the order of 1-100 ml/h), the forming gas thread is pinched off by the liquid flow in an extremely regular manner, producing very monodisperse bubbles. One period of the periodic bubbling process is shown in Figure 5.8a and typical images of obtained bubbles in Figure 5.8b. The diameter of the generated bubbles is of the order of the geometric dimensions of the T-junction, which in our case around 1mm.

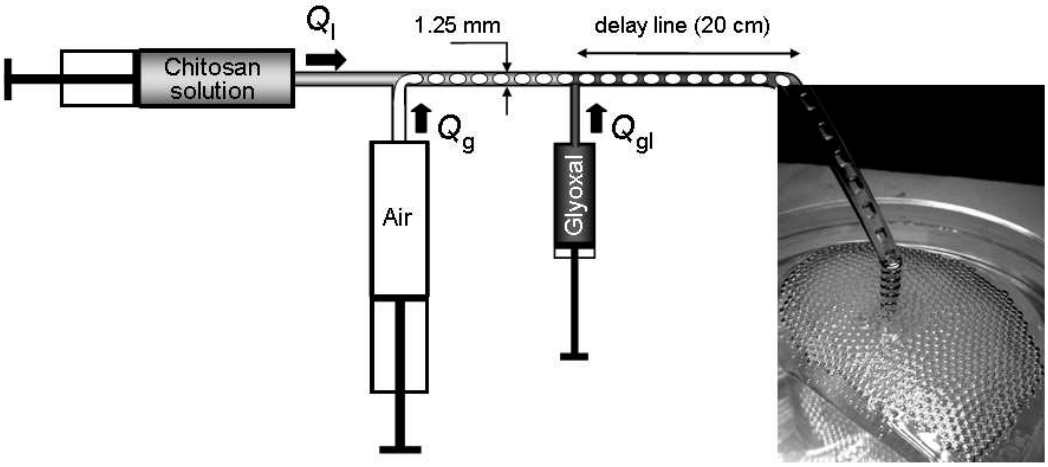

Figure 5.7: Set-up of the generation of monodisperse foams: Two syringe pumps deliver the chitosan solution and air at constant flow rate into a T-junction, where the gas thread breaks up into extremely monodisperse bubbles. These travel further down a tube where a second T-junction is used to inject the glyoxal solutions (here: Q_g = Q_l = 25ml/h, Q_{gl} =2.5 ml/h, C_{CH} = 1.9% + 0.59 %wt AT25). A "delay line" of 20 cm allows the glyoxal to diffuse into the solution before the foam exits the tube and is collected in appropriate dishes.

5.4.2 The calibration of the millifluidic set-up

We calibrated our T-junction device with two reference solutions: pure water (η = 0.001 Pa s) and pure glycerol (η = 1.5 Pa s), both containing the surfactant AT25 at a concentration of 1000 CMC. The surface tension of both solutions is close to 45 mN/m. The resulting bubble sizes (diameter D_B) are found to be extremely reproducible and are shown in Figure 5.9 as a function of flow rate ratio Q_g/Q_l. Each data point consists of data taken for different liquid and gas

flow rates keeping their ratio constant (50 ml/h < Q_l < 125 ml/h; 10 ml/h < Q_g < 400 ml/h).

The two calibration curves are well captured by the power law shown in Section 3.2.3 with α = 1.92 ± 0.02 mm and β = 0.17 ± 0.01 for the case of water and α = 1.38 ± 0.02 mm and β = 0.18 ± 0.01 for the case of glycerol. Whilst the exponent remains virtually unchanged, the pre-factor drops in the case of glycerol due to the increased viscosity. This is an expected result since at the low flow rates used by us the device is driven in the squeezing regime (Section 3.2.3) which is controlled by the surface tension of the solution and independent of the viscosity of the solution.

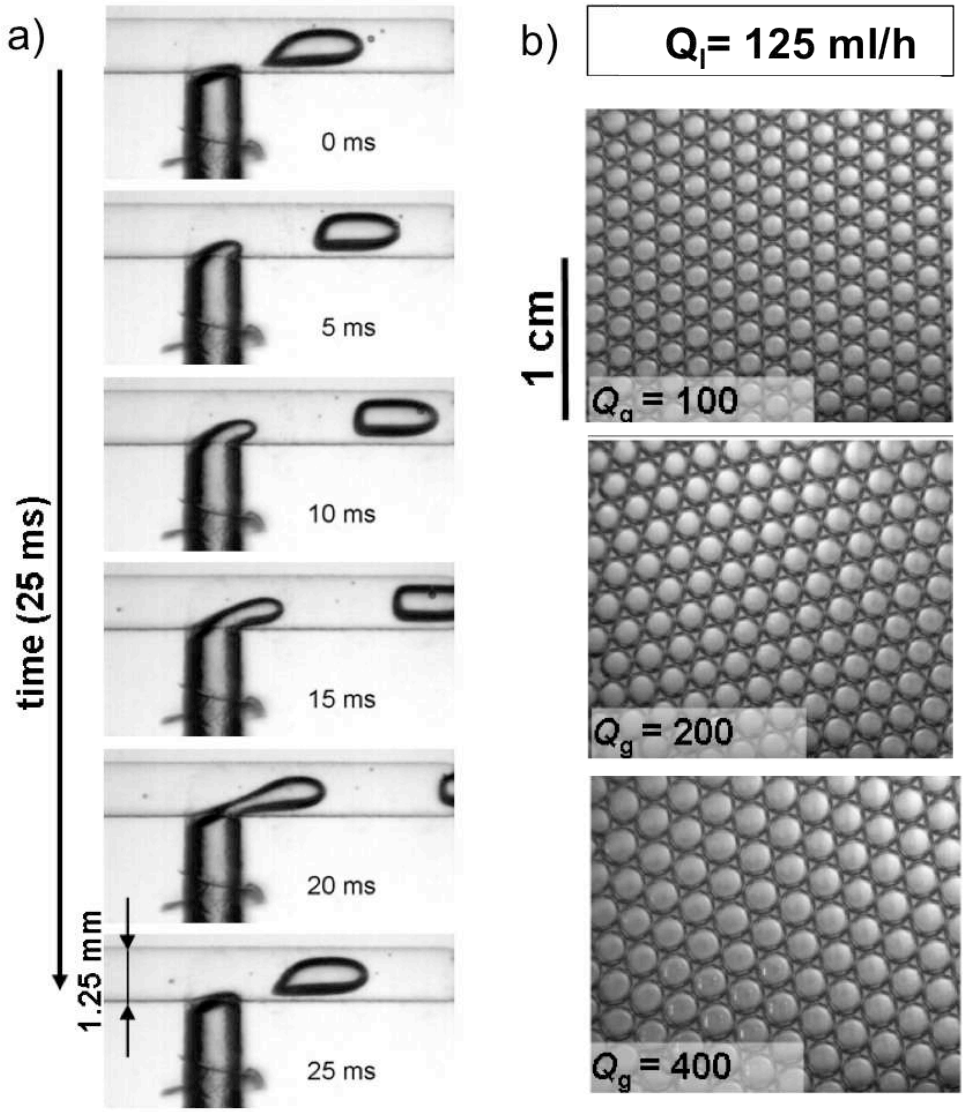

Figure 5.8: (a) One period of the bubble generation in the T-junction device for glycerol/surfactant mixutre (Q_g = Q_l = 30 ml/h). (b) Resulting bubbles for water/surfactant solution for increasing gas flow rates Q_g.

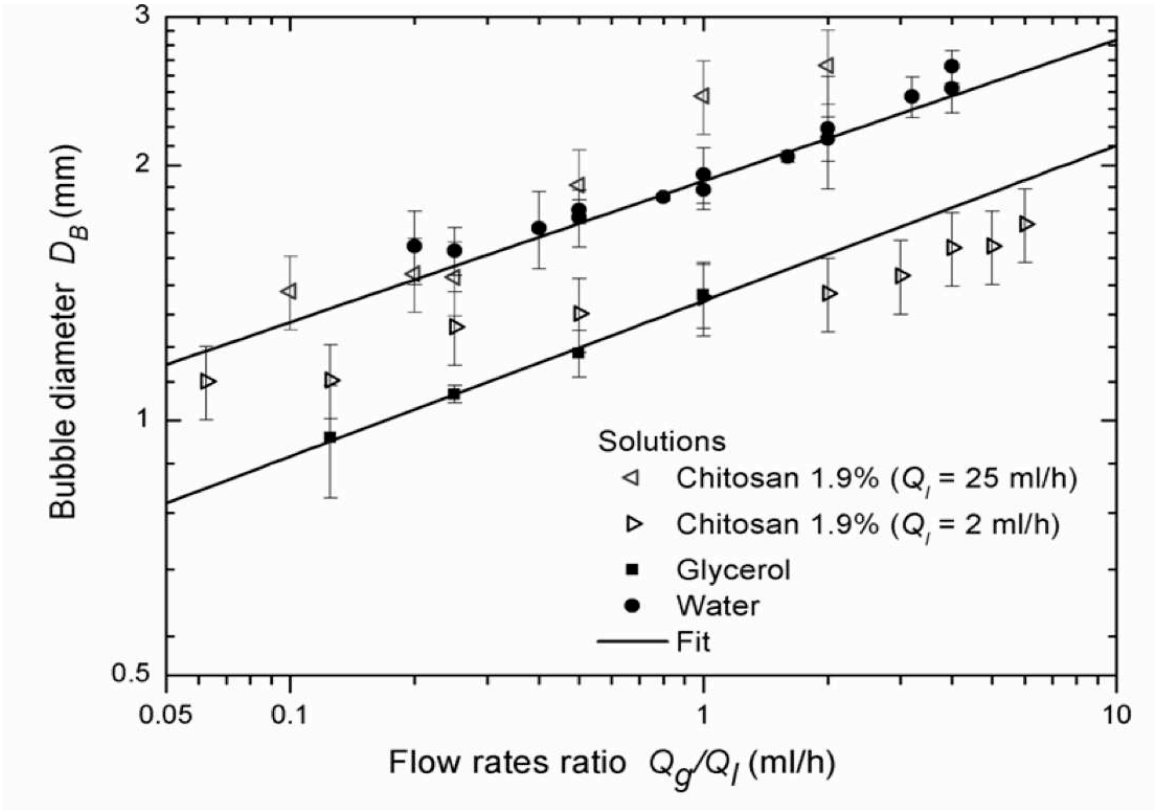

Figure 5.9: Calibration of the T-junction: for the Newtonian solutions (water and glycerol + 0.59 %wt AT25), the relationship between the bubble diameter D_B and the flow rate ratio Q_g/Q_l is well described by a power law (Equ.3.4 with: Water: α = 1.92 ± 0.02 mm, β = 0.17 ± 0.01; Glycerol: α = 1.38 ± 0.02 mm, β = 0.18 ± 0.01). This is not the case for the strongly shear-thinning chitosan solutions (here C_{CH} = 1.9 wt% + 0.59 %wt AT25), for which the absolute liquid flow rate Q_l is also a decisive parameter.

Unfortunately, this is less straightforward for non-Newtonian liquids, such as the chitosan solutions employed here. Figure 5.9 shows two data sets for our standard chitosan solution (C_{Ch} = 1.9 wt%) for two different liquid flow rates Q_l = 2 ml/h and Q_l = 25 ml/h (only the gas flow rate Q_g is varied in each curve). Unlike in the case of Newtonian liquids, the data cannot be collapsed in order to be expressed as a function of flow rate ratio Q_g/Q_l only, but depends strongly on the absolute liquid flow rate Q_l. This is a natural consequence of the strongly non-Newtonian flow behaviour of such highly concentrated chitosan solutions subjected to the flow conditions in the T-junction device. The flow of the solution being confined to the liquid film formed between the wall and the bubble surface leads to shear rates $\dot{\gamma}$ of the order of 10 – 1000 s^{-1} (assuming a film thickness of the order of 100 μm). Comparing this with the viscosity results of Figure 5.2, we see that in this regime the chitosan solution is strongly shear thinning. One would therefore expect that bubble sizes increase with increasing liquid flow rate. The same general argument may also explain why the slope cannot be the same as that of Newtonian liquids: changing the gas flow rate Q_g changes the confinement of the liquid flow and therefore its local shear rate.

However, as in the case for the Newtonian solutions, we find that the calibration of the chitosan solutions is sufficiently reliable from an experimental point of view, meaning that if care is taken to work always under the same conditions, the generated bubble sizes are very monodisperse and reproducible.

5.4.3 The mixing

In order to solidify the foam we add another T-junction just after the bubble generation (Figure 5.7) where we inject a glyoxal solution (0.16 wt%) (diluted in aqueous acetic acid solution), at constant flow rate Q_{gl}, calculated to reproduce the same conditions used for the measurements of the gelification time τ_g in Section 5.2. To allow the glyoxal to diffuse into the liquid, we let the bubbles travel along a "delay line" of 20 cm. This also enhances significantly the stability of the final foam, which we collect in containers at the end of the delay line.
We injected a black ink solution (with the same density as the glyoxal solution) in the inlet of the glyoxal in order to study the mixing of the chitosan and the glyoxal solutions. We found that as the bubbles move along the "delay line", the ink diffuses between the bubbles. The bubbles collected at the exit of the tube are totally surrounded by the black solution.

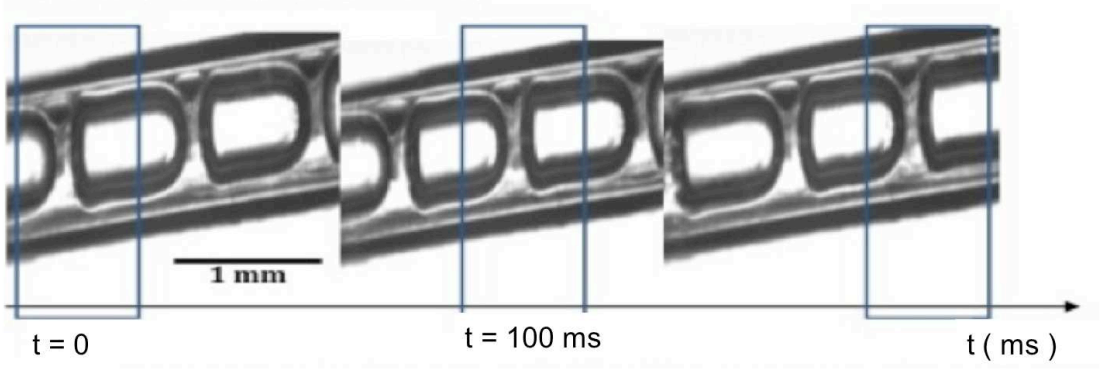

Figure 5.10: Diffusion of a black ink solution (which mimic the reticulent solution) in the delay line. The ink solution diffuses well after few seconds.

5.5 CHARACTERISATION OF CHITOSAN FOAMS AFTER SOLIDIFICATION

Some general examples of the obtained gelified foams are shown in Figure 5.11 with some close-up images of different numbers of hexagonally close-packed layers of bubbles spontaneously obtained by depositing the foams in Petri dishes. In the left column of Figure 5.11 we show what the foams look like just after gelification, i.e. containing the original amount of water. As the number of bubble layers increases, one sees clearly the appearance of three black rings in each bubble, which is an image of the three touching bubbles in the layer underneath [38]. The right column shows what these foams look like after they have been dried under ordinary room conditions for 24 h. Whilst the wet foams

are very robust gels, the dry ones become very brittle since they break and loose their structure after drying (bottom right of Figure 5.11).

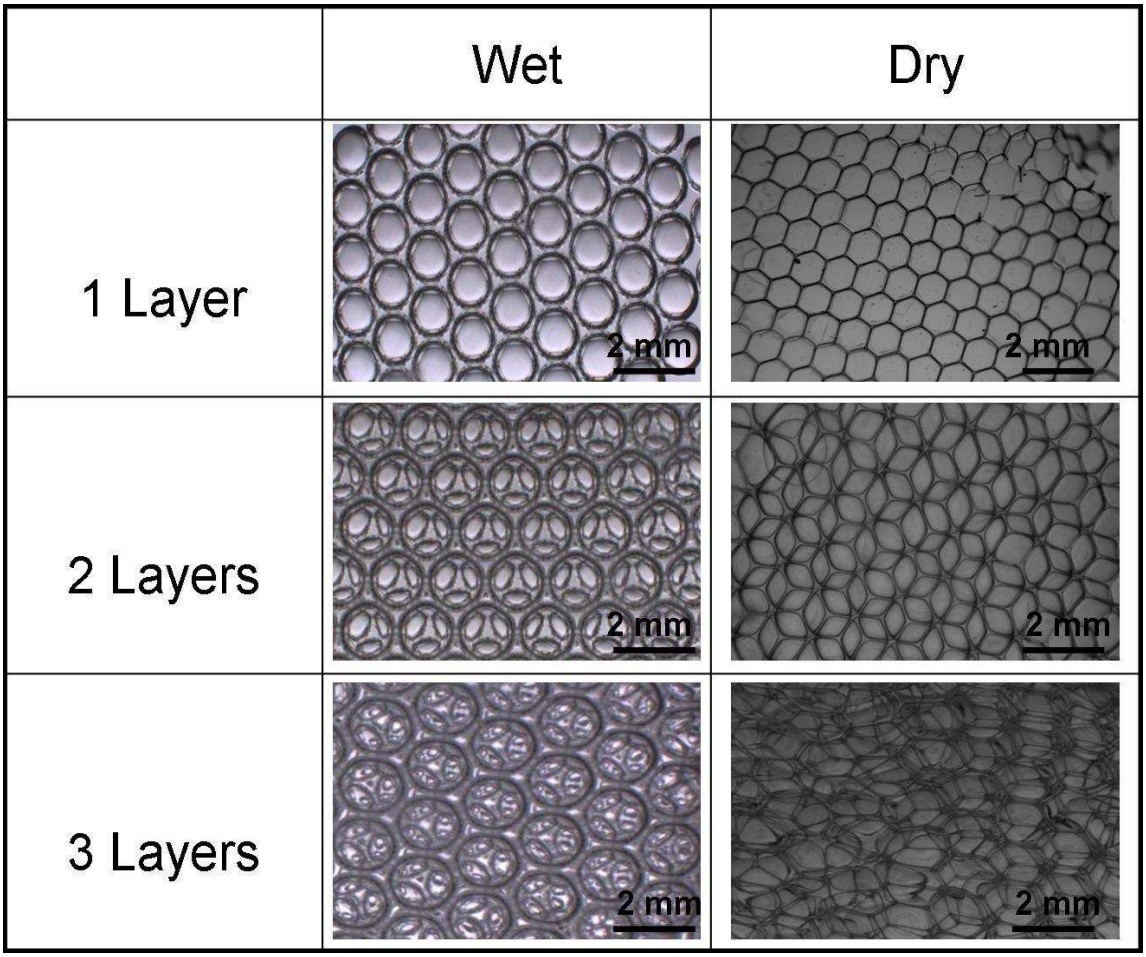

Figure 5.11: Close-up examples of obtained foam structures in the wet state immediately after gelification and when dried at the open air.

5.6 CONCLUSION

We have demonstrated a simple technique which can be used to generate extremely monodisperse, ordered foam structures from chitosan gels using milli-fluid cross-flow techniques. This work puts an emphasis on the general introduction of the technique in conjunction with the characterisation of the physical properties and the gelifying behaviour of the employed polymer. Future work should exploit in depth its potential to generate a range of foam structures of different bubble sizes and densities (spherical vs. polyhedral bubbles), and to explore in detail the physical properties of those foams.

BIBLIOGRAPHY

1. Choi, S.W., J.W. Xie, and Y.N. Xia, *Chitosan-Based Inverse Opals: Three-Dimensional Scaffolds with Uniform Pore Structures for Cell Culture.* Advanced Materials, 2009. **21**(29): p. 2997.
2. Chenite, A., et al., *Rheological characterisation of thermogelling chitosan/glycerol-phosphate solutions.* Carbohydrate Polymers, 2001. **46**(1): p. 39-47.
3. Alargova, R.G., et al., *Foam superstabilization by polymer microrods.* Langmuir, 2004. **20**(24): p. 10371-10374.
4. Rinaudo, M., *Chitin and chitosan: Properties and applications.* Progress in Polymer Science, 2006. **31**(7): p. 603-632.
5. Alsarra, I.A., *Chitosan topical gel formulation in the management of burn wounds.* International Journal of Biological Macromolecules, 2009. **45**(1): p. 16-21.
6. Deng, C.M., et al., *Biological properties of the chitosan-gelatin sponge wound dressing.* Carbohydrate Polymers, 2007. **69**(3): p. 583-589.
7. Yi, H., et al., *Biofabrication with Chitosan.* Biomacromolecules, 2005. **6**(6): p. 2881-2894.
8. Chaterji, S., I.K. Kwon, and K. Park, *Smart polymeric gels: Redefining the limits of biomedical devices.* Progress in Polymer Science. **32**(8-9): p. 1083-1122.
9. Van Vlierberghe, S., P. Dubruel, and E. Schacht, *Biopolymer-Based Hydrogels As Scaffolds for Tissue Engineering Applications: A Review.* Biomacromolecules, 2011. **12**(5): p. 1387-1408.
10. Zhang, H., et al., *Microfluidic Production of Biopolymer Microcapsules with Controlled Morphology.* Journal of the American Chemical Society, 2006. **128**(37): p. 12205-12210.
11. Chung, K.Y., et al., *Fabricating scaffolds by microfluidics.* Biomicrofluidics, 2009. **3**(2).
12. Yip Cheung Sang, Y., *Vers des micromousses stimulables (Toward smart microfoams)*, in *MSC*2009, University of Denis Diderot Paris 7: Paris.
13. Sung-Wook, C., X. Jingwei, and X. Younan, *Chitosan-Based Inverse Opals: Three-Dimensional Scaffolds with Uniform Pore Structures for Cell Culture.* Advanced Materials, 2009. **21**(29): p. 2997-3001.
14. Griffon, D.J., et al., *Chitosan scaffolds: Interconnective pore size and cartilage engineering.* Acta Biomaterialia, 2006. **2**(3): p. 313-320.
15. Kim, I.Y., et al., *Chitosan and its derivatives for tissue engineering applications.* Biotechnology Advances, 2008. **26**(1): p. 1-21.
16. Li, J., et al., *Culture of hepatocytes on fructose-modified chitosan scaffolds.* Biomaterials, 2003. **24**(13): p. 2317-2322.
17. Desbrieres, J., *Viscosity of semiflexible chitosan solutions: Influence of concentration, temperature, and role of intermolecular interactions.* Biomacromolecules, 2002. **3**(2): p. 342-349.

18. Mucha, M., *Rheological characteristics of semi-dilute chitosan solutions (vol 198, pg 483, 1997).* Macromolecular Chemistry and Physics, 1997. **198**(3).
19. Koide, S.S., *Chitin-chitosan: Properties, benefits and risks.* Nutrition Research, 1998. **18**(6): p. 1091-1101.
20. El-Hefian, E.A., R.A. Khan, and A.H. Yahaya, *Study of the parameters affecting the viscosity of chitosan solutions.* Journal of the Chemical Society of Pakistan, 2008. **30**(4): p. 529-531.
21. Payet, L., *Viscoelasticité et structure de gels à base de Chitosane - Relations avec les proporiétés diffusionnelles de macromolécules dans ces biogels* 2005, UNIVERSITE PARIS 7: Paris.
22. Desbrieres, J., C. Bousquet, and V.G. Babak, *Interfacial properties of ionic amphiphilic systems. based on polysaccharides.* Revue Roumaine De Chimie, 2007. **52**(4): p. 423.
23. Martinez, A., E. Chornet, and D. Rodrigue, *Steady-shear rheology of concentrated chitosan solutions.* Journal of Texture Studies, 2004. **35**(1): p. 53-74.
24. Payet, L., *Viscolelasticity and gel structure from chitosan (in French)* in *Macroscopic Physics*2005, University of Paris 7 Denis Diderot: Paris.
25. Kluge, T., et al., *Concentration and molecular weight dependence of the quenching of Ru(bpy)(3)(2+) by ferricyanide in aqueous solutions of synthetic hyaluronan.* Macromolecules, 2000. **33**(2): p. 375-381.
26. Arditty, S., et al., *Some general features of limited coalescence in solid-stabilized emulsions.* The European Physical Journal E: Soft Matter and Biological Physics, 2003. **11**(3): p. 273-281.
27. P.G. de Gennes, P.P., R. M. Velasco, F. Brochard, *Remarks on polyelectrolyte conformation.* Le journal de physique, 1976. **37**: p. 1461-1473.
28. Gennes, P.G.d., *Scaling concepts in polymer physics*, 1979: Cornell university Press, Ithaca.
29. Cho, J., et al., *Viscoelastic properties of chitosan solutions: Effect of concentration and ionic strength.* Journal of Food Engineering, 2006. **74**(4): p. 500-515.
30. Muthukumar, M., *Dynamics of polyelectrolyte solutions.* Journal of Chemical Physics, 1997. **107**(7): p. 2619-2635.
31. Rubinstein, M. and A.N. Semenov, *Dynamics of entangled solutions of associating polymers.* Macromolecules, 2001. **34**(4): p. 1058-1068.
32. Chambon F. , W.H., *Linear viscoelasticity at the gel point of a crosslinking PDMS with imbalanced stoichiometry.* Journal of rheology, 1987. **31**(8): p. 683-697.
33. Moura, M.J., M.M. Figueiredo, and M.H. Gil, *Rheological Study of Genipin Cross-Linked Chitosan Hydrogels.* Biomacromolecules, 2007. **8**(12): p. 3823-3829.
34. Mours, M. and H.H. Winter, *Relaxation patterns of nearly critical gels.* Macromolecules, 1996. **29**(22): p. 7221-7229.
35. Elsabee, M.Z., R.E. Morsi, and A.M. Al-Sabagh, *Surface active properties of chitosan and its derivatives.* Colloids and Surfaces B: Biointerfaces, 2009. **74**(1): p. 1-16.
36. Babak, V., et al., *Interfacial properties of dynamic association between chitin derivatives and surfactants.* Colloids and Surfaces a-Physicochemical and Engineering Aspects, 1999. **147**(1-2): p. 139-148.

37. Sagnella, S. and K. Mai-Ngam, *Chitosan based surfactant polymers designed to improve blood compatibility on biomaterials.* Colloids and Surfaces B-Biointerfaces, 2005. **42**(2): p. 147-155.
38. van der Net, A., et al., *Simulating and interpretating images of foams with computational ray-tracing techniques.* Colloids and Surfaces A: Physicochemical and Engineering Aspects, 2007. **309**(1-3): p. 159-176.

6 SUPERABSORBENT POLYMER FOAMS

6.1 INTRODUCTION AND APPROACH

Superabsorbent polymers (SAP) are materials that have the ability to absorb and retain large volumes of water and aqueous solutions up to 100 times their own weight [1, 2] (Figure 6.1). They are thus ideal for liquid absorbing applications such as baby nappies, adults' incontinence pads [3] and absorbent medical dressings [4]. Superabsorbent polymers are also extensively used for their liquid uptake properties in agriculture and soil treatment applications [5 , 6]. They are typically made from partially neutralised cross-linked poly (acrylic acid) [7 , 8] and are generally available as granular white solids.

Figure 6.1: The swelling behaviour of SAP foam.

Here we generated monodisperse ordered foams from these polymers using millifluidic techniques in order to obtain superabsorbent ordered foams. The preparation of these polymer foams consisted of different steps which follow the general two-step process of our study (Chapter 1). The principal steps required in the case of SAP systems are shown in Figure 6.2. First we prepare the monomer solution by mixing different components following a recipe provided by BASF [9], then this solution is degassed in such a way that all the oxygen dissolved in it is removed. We generate foams from the degassed solution using different techniques. These foams are afterwards polymerised under UV light and then dried. The structural properties of the obtained foams are determined using qualitative optical techniques.

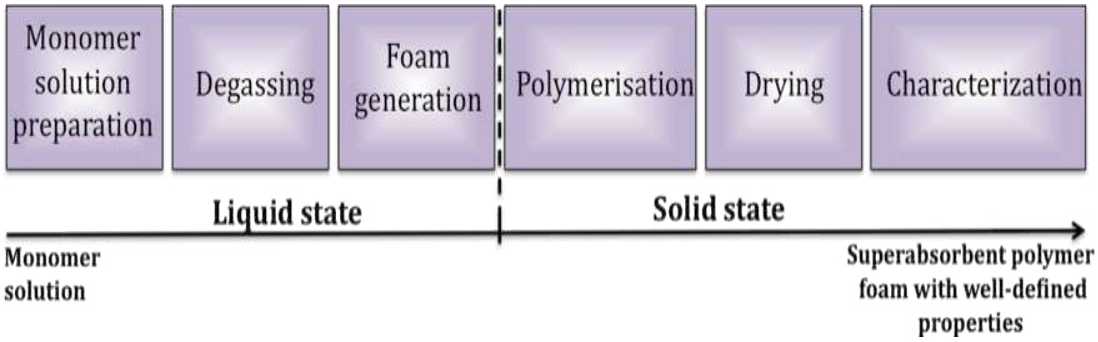

Figure 6.2: Principal steps of the preparation of superabsorbent polymer foam from the monomer solution (left) to the final superabsorbent polymer foam (right).

We report here the results of this study. First, a background of the chemistry of superabsorbent polymer is presented in Section 6.2 where all key points necessary to the good understanding of this study are given. In the following, we discuss in detail the properties of the monomer solution employed and demonstrate how to optimise its preparation in order to improve the final foam "quality" (Section 6.3). Furthermore, we present detailed investigations into the foaming properties of these monomer solutions (Sections 6.4 and 6.5). Finally, we show how to generate highly monodisperse monomer, liquid foams using a millifluidic flow-focussing technique (Section 6.6) and we present some of the final ordered polymerised foam structures obtained (Section 6.7). In the following, the superabsorbent polymer will be noted SAP when needed.

6.2 BACKGROUND

Acrylic acid is the basic component of SAP since it is the monomer that once neutralised and then polymerised will turn into SAP (Figure 6.3a). In fact acrylic acid represents the repetitive unit of the final SAP polymer which owes its high ability of absorbance to several mechanisms among which there are (Figure 6.3b):

1. The release of ions such as Na^+, originally present in the neutralising solution, increases the **osmotic pressure** inside the polymer gel which leads to the take-up of water by the polymer network.
2. The interactions between the hydrophilic polymer backbone which contains water-loving carboxylic acid groups (-COOH) with water. These include **hydration** and the **formation of hydrogen bonds**. The hydration consists of the attraction of water molecules by the COO- and Na+ ions presents in the neutralised solution. And the formation of hydrogen bonds occurs between water molecules. Both interactions encourage the attraction of water molecules inside the polymer network.
3. The COO^- ions from the acrylic acid repel each other and hence, expand polymer coils.

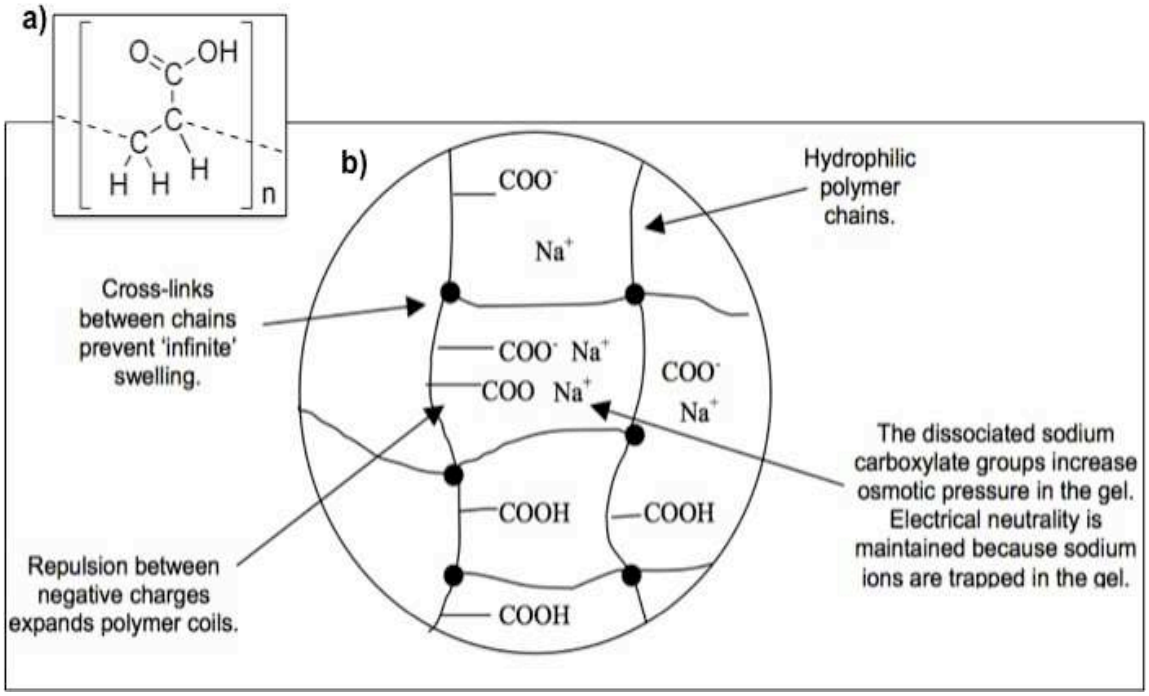

Figure 6.3: a) Chemical structure of poly (acrylic acid). b) A schematic illustration of the mechanisms involved in the high swelling ability of SAP from [10]

A **cross-linker** is used in order to link the polymer chains together forming hence the polymer network and preventing it from "swelling to infinity", i.e. dissolving.

6.3 RECIPE AND PROTOCOL

6.3.1 Recipe

The superabsorbent monomer solution is prepared following a recipe provided by BASF [9]. Some ingredients of the original recipe and some experimental details of the preparation protocol (such as stirring times or the order of adding chemicals) have been changed to fit the techniques used by us. The components used in our recipe are presented in Table 6.1 where their chemical structures, their CAS number and the exact quantity used for each of them are mentioned. Table 6.1 lists also the role played by each component in the formation of the final "superabsorbent polymer foam" (SAP foam) and the notation used by us to replace the component long names.

Table 6.1: Recipe of the preparation of the neutralised monomer solution

Component name	Role	Notation	Chemical structure	Quantity (wt %)	CAS number
Acrylic acid	Monomer	**AA**	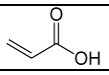	0.340	79-10-7
Sodium acrylate solution	Neutraliser	**NaAcryl**	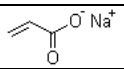	0.131	7446-81-3
Triethanolamine	Neutraliser	**TEA**	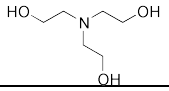	0.390	102-71-6
N,N' methylene bisacrylamide	Cross-linker	**Bisacrylamide**	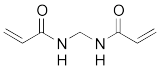	0.027	-
2,2'-azobis 2-amidinopropane dihydrochloride (3% aqueous solution)	Initiator	**Initiator**	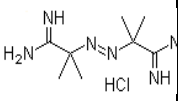	0.026	2997-92-4
Distilled water	Solvent	**Water**	H_2O	0.065	-
Lutensol AT80 (90% aqueous solution)	Surfactant	**AT 80**	$RO(CH_2CH_2O)_x H$ R=Linear, saturated $C_{16}C_{18}$ fatty alcohol	0.021	-

The monomer solution is obtained by mixing these components following a given order. Each component contributes at a given moment of the experiment to the formation of the final SAP foam product.

Since we need to foam the monomer solution, a sufficient amount of surfactant is also added to ensure a good foamability and foam stability. The surfactant used here is a non-ionic surfactant provided by BASF and which belongs to the same family (Lutensol type surfactant with fatty alcohol alkoxylate with a C16/C18 chain and a degree of ethoxylation of 80, CMC = 1.2 10^{-5} mol/l, M = 3780 g/mol) than the one used in Section 5.

6.3.2 Set-up and protocol

The principal set-up used to mix and prepare the neutralised monomer solution is shown in Figure 6.4. We obtain the solution by mixing the components listed in Table 6.1 in an order ensuring optimal dissolution of the chemicals in the solvent and a final homogenous monomer solution. The preparation of the neutralised monomer solution is composed of three major steps: mixing, neutralisation and degassing.

1. Mixing

First, we dissolve the surfactant in acrylic acid by stirring for 2 hours at room temperature. Then we add the cross-linker which is also dissolved by stirring for 2 hours under the same conditions. We add then water and we stir again for 12 hours. This solution is noted S_{BN} (Before Neutralisation).

2. Neutralisation

The neutralisation of acrylic acid is an exothermic reaction and the neutraliation degree increases with increasing temperature. We therefore need to control the temperature of the solution in such a way that it does not exceed 16°C in order to obtain the desired degree of neutralisation. We use for this purpose, during the whole neutralisation step, an ice bath in which we place the beaker containing the reacting mixture (Figure 6.4). A thermometer is used to check continuously the temperature of the solution. The neutralisation is done using two neutralising solutions: first sodium solution (sodium hydroxide or sodium acrylate solution NaAcryl), then triethanolamine (TEA) are added to the solution drop by drop in order to avoid too rapid heating (we stop the dripping if the temperature exceed 16°C). We neutralise such that a final degree of neutralisation of approximately 60 % is obtained[11].

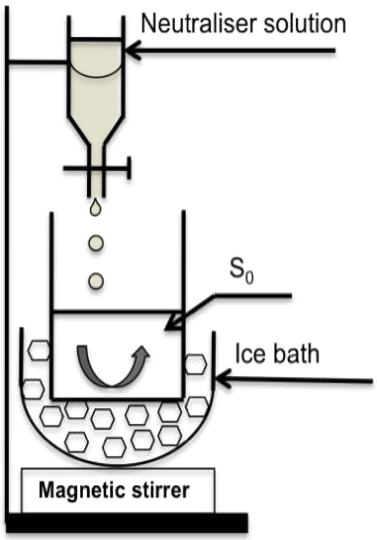

Figure 6.4: Set-up of the preparation of the neutralised monomer solution. The monomer is first well mixed with the surfactant, the cross-linker and water. This mixture is noted S_{BN}. Then, two different neutralising solutions are added drop by drop while stirring. The final neutralised solution is noted S_{NM}.

3. Degassing

Oxygen greatly reduces or even entirely inhibits the polymerisation process by combining with free radicals. It is therefore very important to remove any dissolved oxygen from the solutions in order to ensure a rapid and homogeneous polymerisation. Degassing of the solutions is therefore a very

important step and every solution used in the recipe needs to be degassed before the final polymerisation step. Care should also be taken while transferring solutions from one container to another (for instance from the degassing vessel to the foaming device) by transferring it as fast as possible and by sealing all the containers.
The degassing process starts by putting the monomer solution in a four-neck round-bottom sealed vessel having 4 orifices which ensure simultaneously the circulation of nitrogen (inlet and outlet), the injection of the initiator and the removal of the degassed solution which is then supplied to the foaming device (Figure 6.5). We then degas the neutralised monomer solution for 30 min using a flow rate of nitrogen of 10 l/min and we repeat the degassing for 15 min after the injection of the initiator. The degassing time used by us is higher than what is mentioned in the recipe of the patent provided by BASF [9]. This is due to the fact that the nitrogen flow rate that we use is much lower than the one used in the patent mentioned above. Once the degassing is finished, we fill a syringe with the degassed solution (liquid) and another syringe with nitrogen (gas) which we seal immediately to avoid oxygen contamination. These syringes will ensure the liquid and gas supply in the foaming device(s).
Following this procedure, we reduce the typical polymerisation time of our solutions and foams from half an hour for non-degassed solutions to a few minutes for degassed solutions.

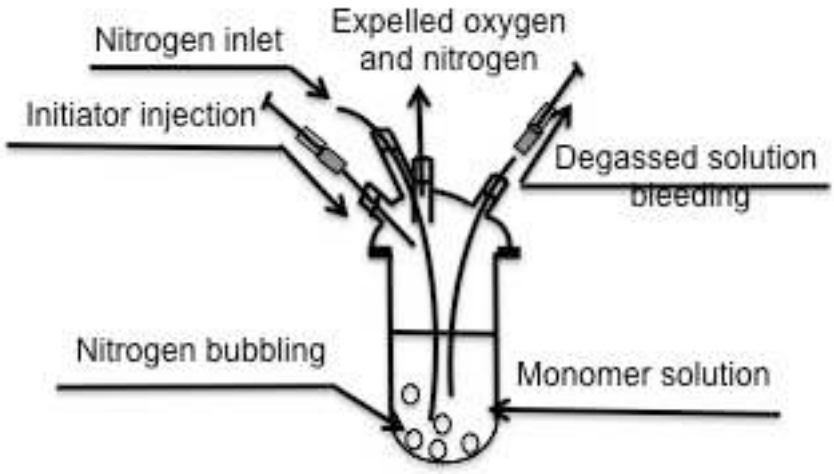

Figure 6.5: Deagassing set-up. The neutralised monomer solution is put into a four-neck round-bottom sealed vessel having 4 orifices which ensure simultaneously the circulation of nitrogen (inlet and outlet), the injection of the initiator and the final removal of the degassed solution.

The polymerisation process starts when the neutralised monomer solution (containing initiator) is put under UV light. In fact, the initiator used is photosensitive. Under the influence of UV light, it gets into an excited state leading to the formation of free radicals and the foam starts to polymerise.
In our study, care had to be taken not only to avoid any contamination with oxygen of the foam generated from the degassed monomer solution but also to

control the polymerisation conditions (heating), in particular the polymerisation time, in order to avoid the destabilisation of the foam.
Experimentally, the monomer foam is placed in different containers of different diameters and different thicknesses and is then immediately irradiated from above with a UV/VIS lamp. The distance between the sample and the lamp is equal to 10 cm. The polymerisation time depends on the thickness and the surface of the sample and tends to be of the order of a few minutes for properly degassed solutions. The obtained solid foams were dried at room temperature for 24 hours.

6.4 CHARACTERISATION OF LIQUID SOLUTIONS

In an attempt to optimise the foaming properties of the neutralised monomer solutions we noticed a strong surface activity of the neutraliser TEA. We verified this by measuring the surface tension (Section 4.1.1) of the monomer solution before and after adding the TEA (with and without adding the surfactant AT80 at a concentration of 1.92 wt%). The resulting surface tensions are presented in Figure 6.6 as a function of time.

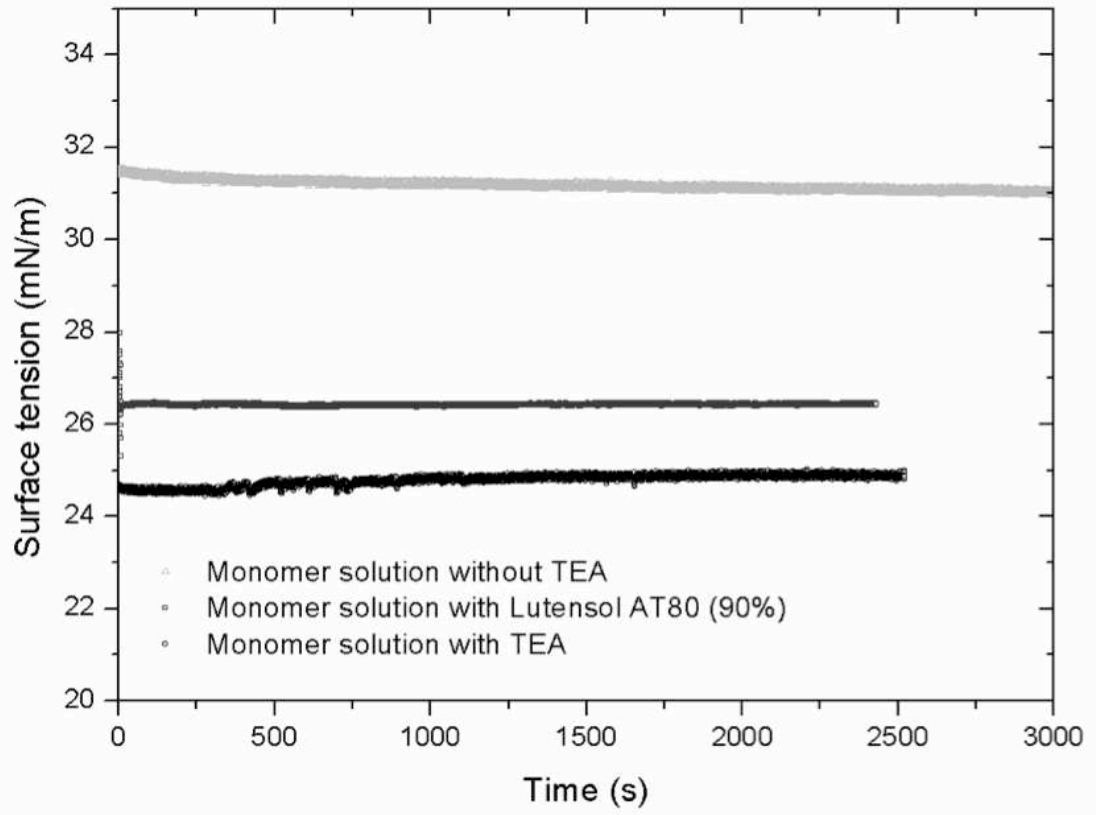

Figure 6.6: Evolution of the surface tension with time for the neutralised monomer solution without AT80 and TEA, the monomer solution with only TEA and the monomer solution with only AT80. AT80 and TEA show significant surface activity since they decrease measurably the surface tension of the monomer solution. These measurements are done using a pendant drop device ("Tracker", TECLIS).

The results show that the surface tensions of all solutions equilibrate quite quickly and are stable with time. They also confirm that the addition of TEA significantly reduces the surface tension from approximately 32 to 25 mN/m, indicating a strong surface activity of TEA (pure TEA has approximately 47 mN/m). This observation is supported by the literature, where it is well documented that the tertiary amine is protonated in an acidic medium and gives a quaternary ammonium salt with high surface activity which is extensively used as a cationic surfactant in cosmetics and several other applications [12].
Moreover, the surface tension of the TEA and AT80 mixture is lower than the surface tensions obtained using these two pure species separately. This shows that interface of the system is covered by both AT80 and TEA and is known as the synergistic effect of surfactant mixture.
This has been verified by simple foaming tests (Figure 6.7) which showed that we need the interplay between both ingredients, as only solutions containing both TEA and AT80 produce stable bubbles (right tube in Figure 6.7). At this stage it is not clear to us which role each of the two ingredients play since both are surface active agents (with different adsorption times) and viscosifier. Indeed, we measured the viscosity of the solutions and we found that it increased four-fould when adding the AT80.

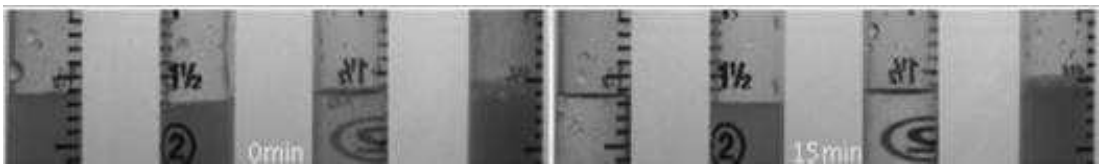

Figure 6.7 : Foamability (left, t = 0 min) and foam stability (right, t = 15 min) of the neutralised monomer solution (without initiator) containing from left to right: neither TEA nor AT80; only TEA; only AT80; both TEA and AT80.

6.5 CHARACTERISATION OF THE FOAMS

Foamability and foam stability tests are performed with the monomer solution containing 1.92 % of surfactant AT80.
We varied **the water content** of the monomer solution, and then we performed foamability tests. Since we commonly find that the foamability/stability of neutralised monomer solutions depends on the foaming technique, we cross-checked the results obtained using polydisperse and monodisperse foaming tests. In the first case, as shown in Figure 6.8, we obtained polydisperse foams whose initial volume (Figure 6.8a) and stability (Figure 6.8b) increases significantly with increasing water content.

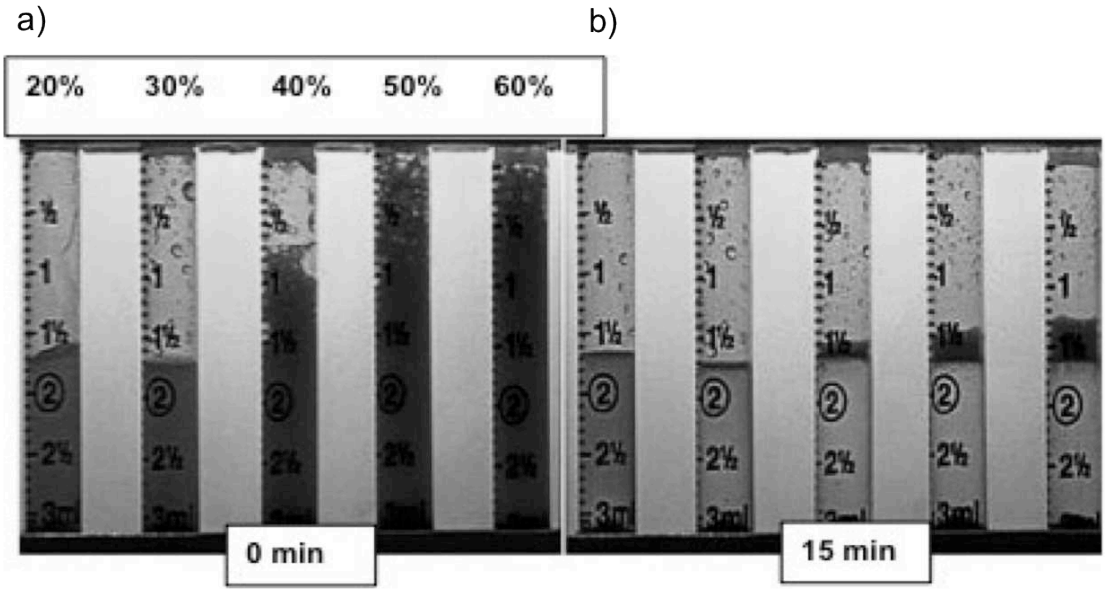

Figure 6.8: a) Foamability of neutralised monomer solutions (with Bisacrylamide) with different water percentages (from left to right: 20%, 30%, 40% and 60%). b) Foam stability after 15 min.

This is slightly different when using the same solutions to generate monodisperse foams. In fact, after the production of monodisperse foams with the T-junction cross-flow device (Section 3.2.2 and Section 6.6.1) using equal gas and liquid flow rates (25 ml/h for the different solutions), we found that under these conditions the solution containing 40% of water is the one which gives the most monodisperse and stable foam (Figure 6.9). By varying the gas and liquid flow rates, we were also able to generate extremely stable (more than half an hour) and monodisperse foams with lower water contents, which is why we decided to maintain the original recipe by using 20% of water in the monomer solutions.

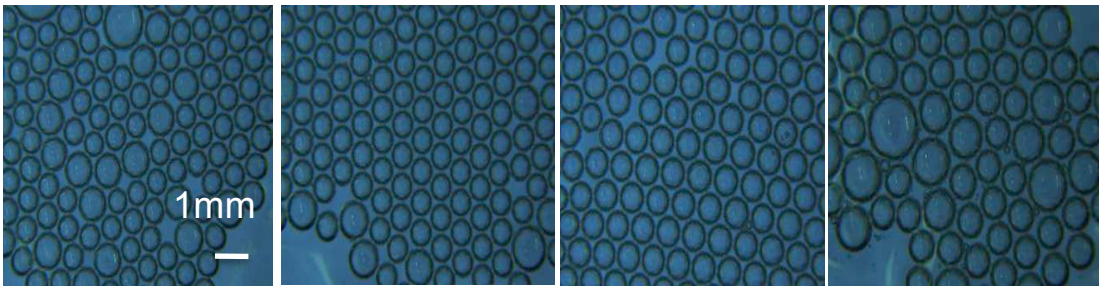

Figure 6.9: Foaming test at a constant surfactant concentration (1.92 %) for different water percentages in the monomer solution (from left to right: 20%, 30%, 40% and 50%). The images are taken immediately after foaming. The stability increases with monodispersity (30 % and 40 % are the most stable (few minutes))

6.6 GENERATION OF MONODISPERSE SAP FOAMS

6.6.1 The millifluidic set-up

For the generation of monodisperse foams we used a millifluidic flow-focussing technique (Section 3.2.2). The corresponding set-up, shown in Figure 6.10, contains two syringe pumps which are connected to the foaming device (T-junction made in polycarbon blocks with an inner channel diameter of 720 micrometers).

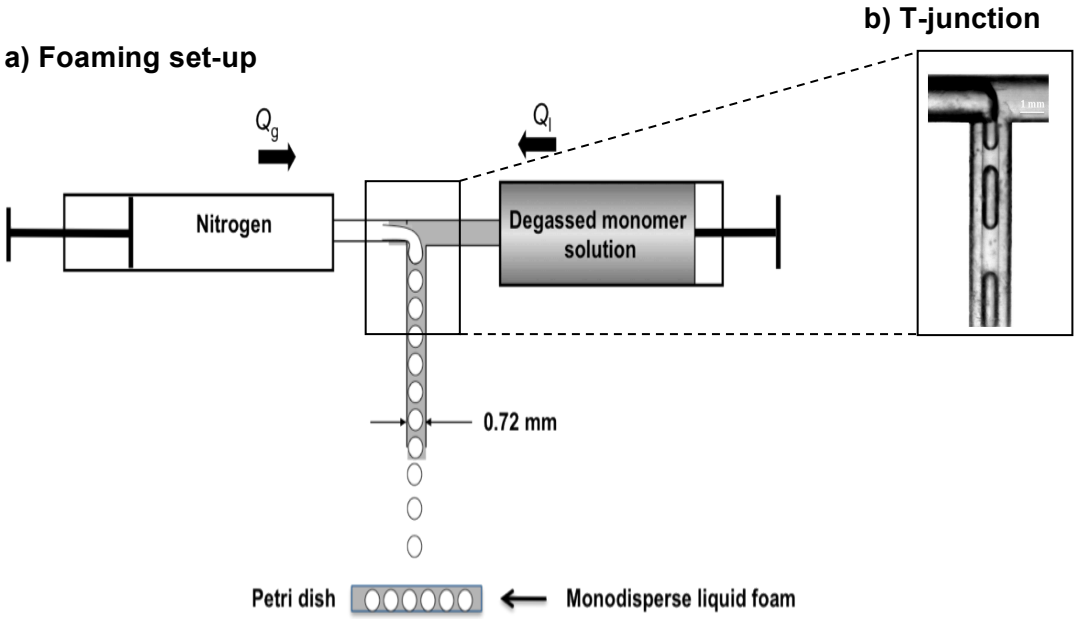

Figure 6.10: Set-up for the generation of monodisperse foams: Two syringe pumps deliver the monomer solution (collected in a sealed syringe) and nitrogen at constant flow rate into a T-junction, where the gas thread breaks up into extremely monodisperse bubbles. Different break up regimes are observed depending on the flow rate ratio. a) Millifluidic set-up, b) T-junction.

6.6.2 Calibration of the millifluidic device

In order to calibrate the foaming device we used simple aqueous surfactant solutions (containing 1000 CMC of Lutensol AT11) as a reference system. A high surfactant concentration is needed to cover all the foam interfaces sufficiently rapidly. These solutions have certainly lower viscosities than the typical monomer solutions we are working with. But, since the viscosities of the monomer solutions change with their chemical composition, and since we do not know exactly the final composition, we decided to use water as a reference system to understand the fundamental behaviour of the device. Using this understanding, we can predict its performance for solutions of different viscosities from physical arguments.

We investigated the monodispersity and the dependence of the obtained bubble size D_B on the gas and liquid flow rates, Q_g and Q_l, respectively. We first varied the liquid flow rate Q_l for different fixed gas flow rates and we estimated qualitatively the monodispersity of the obtained foam. The results are presented in Figure 6.11 in form of a phase diagram which shows a well-defined zone (Q_g–Q_l–couples) in which monodisperse foams can be reliably and reproducibly generated (turquoise points) (see appendix B for more details). Outside this area, the foams are either bi- or polydisperse. In principle, one can also control the final liquid content of the foam (from bubbly liquid to hexagonally close-packed bubbles to dry foam) by choosing an appropriate flow rate ratio within this zone. However, as is indicated by the dashed line in Figure 6.11.a, with our device we do not manage to directly generate foams with liquid fractions less than 26% (hexagonally close-packed bubbles). This is due to the fact that the narrow capillary, in which the bubbles are generated, is connected to a very large channel. However, we easily generate low-density foams by draining the liquid from higher density ones. If the *direct* generation of drier foams is necessary at some point of this project, we need to adapt the device geometry (see for example Section 7.5). We know from the literature that with appropriate device geometries one can go down to liquid fractions of a few percent [13].

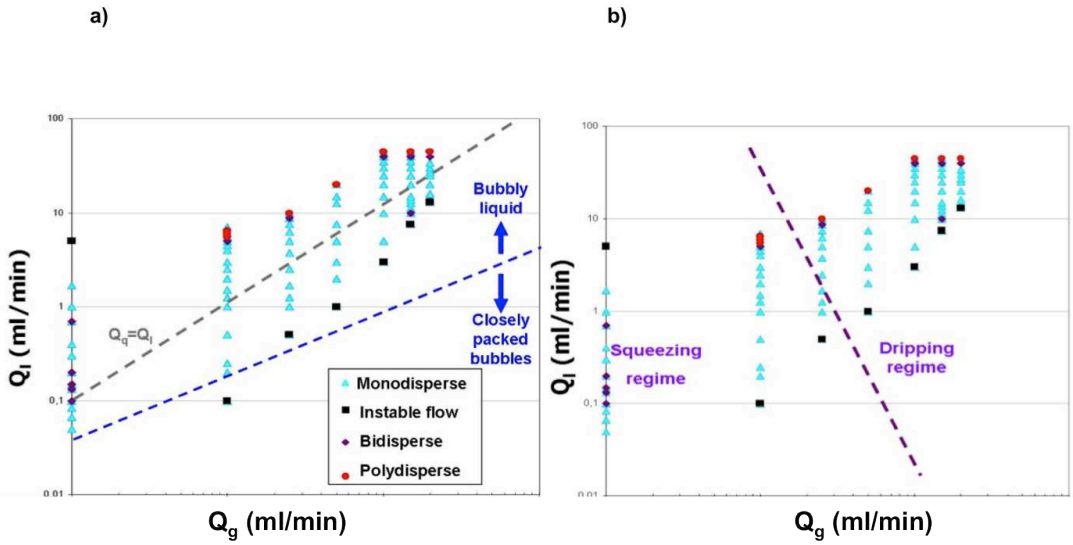

Figure 6.11: Phase diagram of the monodispersity of foams generated using the flow-focussing device. The continuous phase is an aqueous solution of the surfactant Lutensol AT 11 at 1000 CMC, and the dispersed phase is air. a) The blue dashed line represents the limit between the bubbly liquids and wet foams composed of hexagonally close-packed spherical bubbles (26% liquid fraction). Below this limit, a dry foam is obtained with thin liquid films between the bubbles which are closely packed. b) The same phase diagram indicating the transition (dashed line) between the squeezing and the dripping regime.

In our case we encounter two different flow regimes, which are described by the same fundamental power law (Section 3.2.4) but with different exponents. The data for flow rates in between these extreme cases consist of two sections described by each of these power laws, as is visible in Figure 6.12a. More quantitatively we find the following fitting parameters: α = 0.89 ± 0.04 mm and

β = 0.23 ± 0.01 for the squeezing regime, and α = 0.75 ± 0.01 mm and β = 0.56 ± 0.03 for the dripping one. The two extreme cases (low gas and liquid flow rates for the squeezing regime {blue line} and high gas and liquid flow rates for the dripping regime {purple line} (Section 3.2.3) are shown in Figure 6.12b. As expected, we observe bubble sizes smaller than the capillary diameter (0.7 mm) for the dripping regimes and bubble sizes larger than the capillary diameter for the squeezing regime.

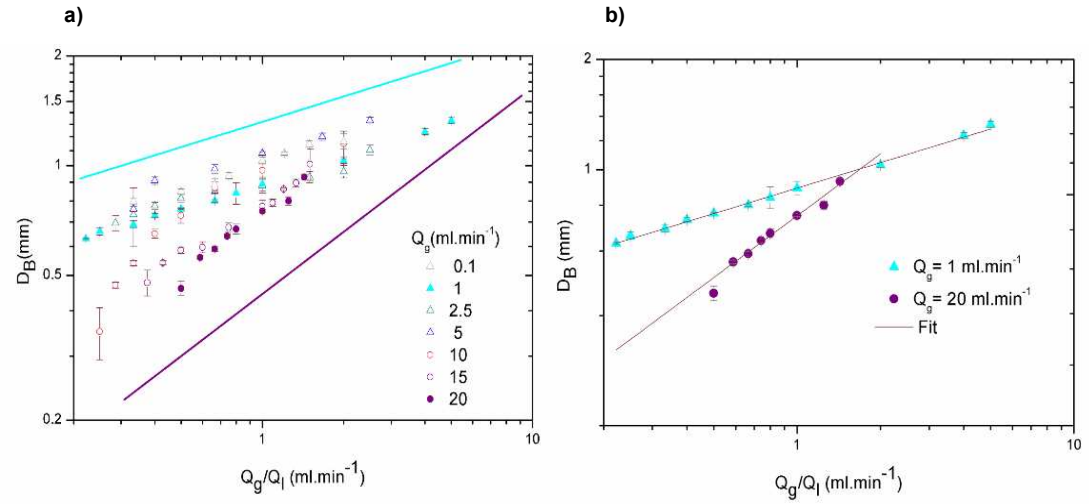

Figure 6.12: Calibration of the foaming set-up. For a fixed gas flow rate, we determine the effect of liquid flow rate on the bubble size. a) The data are enveloped by two main power laws corresponding respectively to the squeezing regime (blue line) and the dripping regime (purple line). b) The two power laws corresponding to the two different regimes.

6.7 POLYMERISATION AND ORDERED POLYMERISED FOAM STRUCTURES

The SAP foams generated using the millifluidic device (Section 6.6.1) are collected in containers of different shapes. We found that the foam generation works very reliably and that the foams are very stable (Figure 6.13). Examples of polymerised foams are presented on Figure 6.14.

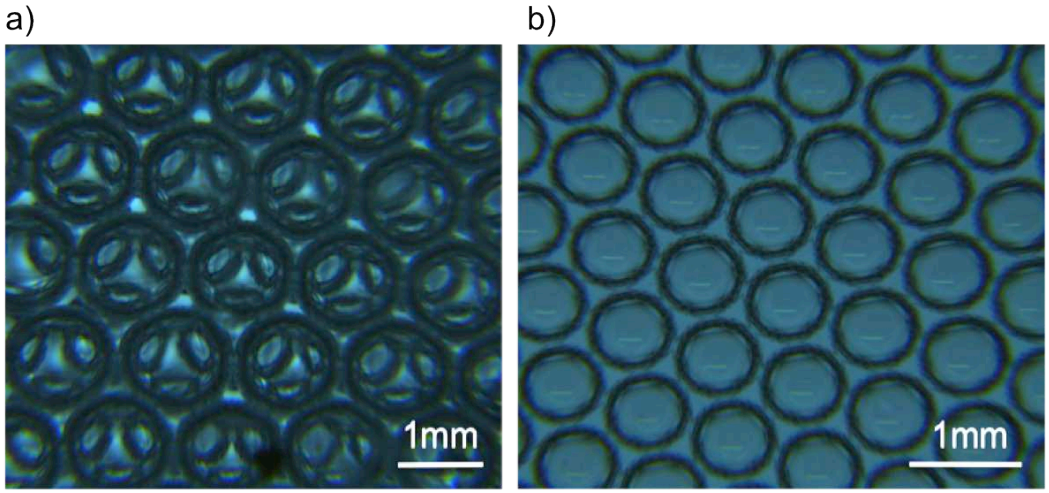

Figure 6.13: Monodisperse liquid foam generated using our millifluidic T-junction (Section 6.6.1) with gas and liquid flow rates equal to 25 ml/h. Foams are generated from the degassed monomer solution containing the initiator. a) Two layers of bubbles. One can see through each bubble from the upper layer, the three bubbles from the layer underneath. b) One layer of equal-size bubbles.

The foams were collected by gathering the bubbles inside appropriate containers. The bubbles fell down spontaneously from the exist channel of the millifluidic device under the effect of gravity. They were left to self-organise inside the containers, into one, two and three layers which are then polymerised under UV. We found that the foam structures polymerise very well within a few minutes **without loss of structure**. In fact, the solid foams preserve the same structure of the initial liquid foam. Examples of these structured superabsorbent polymer foams are presented in Figure 6.14 where it is apparent that the foams have mostly open-cell structures. Of particular interest is that one of our key goals was confirmed: the periodicity of the foam structure ensures periodicity in more microscopic structural properties. For example, the dimensions of the holes created in the films are the same for all the films within the same foam structures (compare top left and top right of Figure 6.14). Moreover, the hole dimensions are likely to be fine-tuned by properly adjusting the physico-chemical parameters of the solutions and the liquid fraction of the liquid foam template. For example, foams with higher liquid contents, with higher liquid viscosities or foams which solidify more rapidly (higher initiator concentrations) should have smaller holes in the films. One should even be able to generate closed-cell foams.

We did not observe phase separation between water and polymer, as reported by *Antje Van Der Net* for the preliminary studies for this work [14]. We believe this to be due to the fact that we manage to work with much lower water contents and a polymerisation strategy which, through the neutralisation, allows the integration of much larger quantities of water in the polymer network. Much more detailed and systematic investigations are needed to investigate these kinds of questions.

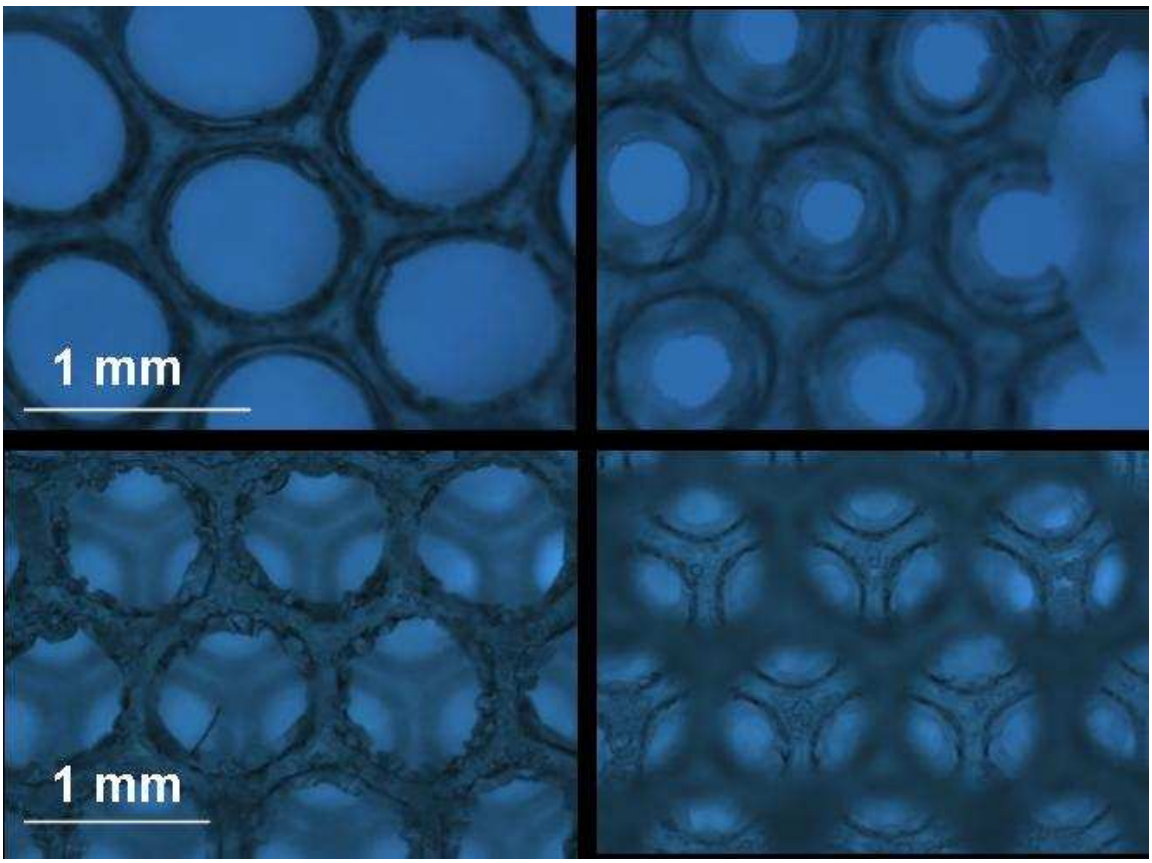

Figure 6.14: two layers of superabsorbent polymer monodisperse foams. The upper image shows monolayers of monodisperse solid foams with an open-cell structure. The bottom image presents two layers of bubbles (left: outer layer and right: inner layer). The foam conserves in both cases its structure after polymerisation.

In order to obtain threads, we collected the generated foams in narrow tubes where they organise under confinement. We observed, as shown in Figure 6.15, different bubble structures which vary with tube diameters.

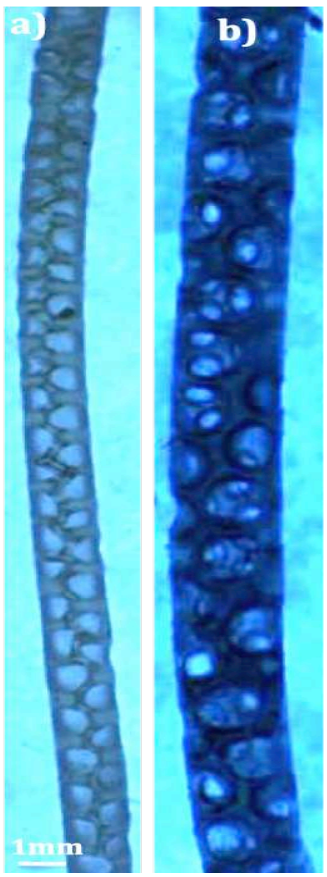

Figure 6.15: Thread-like foam structures formed by polymerising under confinement in tubes of different diameters (a) 2mm, (b) 3mm. Different bubbles patterns are observed (a) zigzag structure, (b) monodisperse random structure

The monomer solution drains while generating the foam. We extracted with a nozzle the drained liquid then we polymerised the foam for 1 min. An example of a polymerised foam is shown in Figure 6.15. Although the drained liquid has been removed (sucked with a syringe) before polymerisation, the drainage continues during the polymerisation step (although very short step) and a non-foamed bottom phase is obtained.

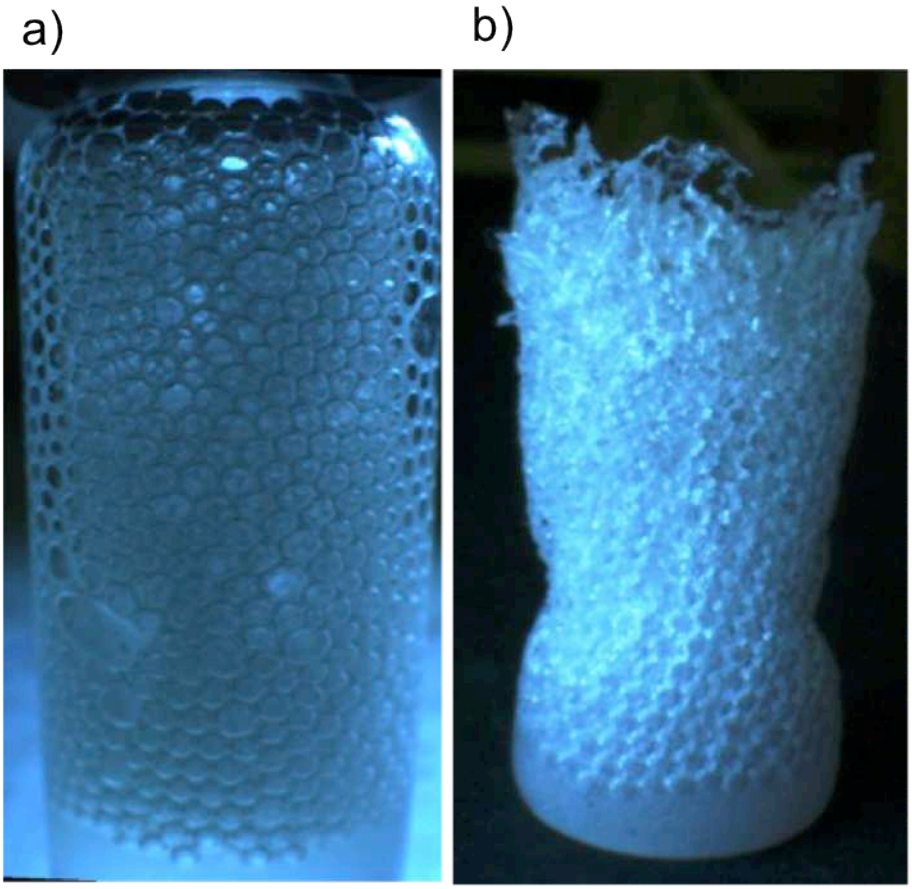

Figure 6.16: 3D foams obtained by polymerising a foam contained in a bottle. a) polymerised foam in the mould. b) foam extracted from the mould. The foam conserves the mould shape. The foam shrinks when the mould is removed, due to evaporation of water, but the bubble structure is generally conserved. Some imperfections are noticed (deformed bubbles) due to mechanical shear between the foam and the bottle walls.

The polymerised foams do not always conserve their liquid structures. Under confinement they are frequently deformed due to mechanical shear when the foam starts to polymerise (buckling). In fact, these deformations or imperfections are especially observed in the case of the bubbles in close contact with the container. If the shear is not very strong (slower polymerisation), the foam regains its normal structure when extracted from the confining container as it is shown on Figure 6.16a. In some cases, the foam deformation is irreversible.

6.8 CONCLUSION

This study demonstrates that the generation of highly structured monodisperse foam from a superabsorbent polymer network is an interesting issue, although very delicate. Thanks to our investigation, we now master the generation of monodisperse foams with well-defined properties in terms of bubble size, structure and density – all of which allows controlling and improving the final

properties of the superabsorbent polymer foam. The generation of very ordered foams with equal-sized bubbles using a millifluidic flow-focussing technique was found to be very well reproducible. All relevant parameters influencing the quality of the final superabsorbent polymer foam were considered. We could not due to a lack of time, study all of them but we have already an appreciative idea (by simple estimation, observed tendency) about their qualitative behaviour. However, the major part of them was well studied under the most suitable conditions, such as surfactant concentration, cross-linker nature, millifluidic technique, etc.

We have identified a large zone in the flow rate phase diagram where we reliably generate monodisperse foams with bubbles of diameters between 0.5 and 1.5 mm using a capillary with 0.7 mm diameter. In order to obtain smaller bubble sizes one could simply use a smaller capillary.

We do not expect significant changes in the device operation when working with liquids of higher viscosity. If the viscosities remain reasonable, they will simply shift the monodisperse region in the phase diagram (Figure 6.11) and the transition between the two flow regimes towards lower flow rates.

The questions left without answers need to be studied more deeply in order to obtain an improved final product. This implies a revision of all the superabsorbent polymer foam recipe steps in order to optimise all the important parameters (polymerisation time, water percentage, type of cross-linker, homogenisation time, etc).

Even though we did not have the time to investigate in detail the generated SAP foams, one can easily imagine the advantages, which the monodisperse foam structures will have for different applications. Applications of hydrogel foams for scaffolding [15-17] or the 3D culture of bacteria [18] are asking for a precise control over the pore architecture. Moreover, the absorption rate of SAP foams depends strongly on the average bubble size and the degree of open-cellness. Both can be controlled to high accuracy with our approach, which should therefore provide fundamental insights into the complex absorption processes of SAP foams.

BIBLIOGRAPHY

1. Zhang, J., et al., *Water absorbency of poly(sodium acrylate) superabsorbents crosslinked with modified poly(ethylene glycol)s.* Journal of Applied Polymer Science, 2003. **90**(7): p. 1851-1856.
2. Mohammad J. Zohuriaan-Mehr, K.K., *Superabsorbent Polymer Materials: A Review.* Iranian Polymer Journal, 2008. **17**(6): p. 451-477.
3. Raju, M.P. and K.M. Raju, *Design and synthesis of superabsorbent polymers.* Journal of Applied Polymer Science, 2001. **80**(14): p. 2635-2639.
4. Sannino, A., et al., *Biomedical application of a superabsorbent hydrogel for body water elimination in the treatment of edemas.* Journal of Biomedical Materials Research Part A, 2003. **67A**(3): p. 1016-1024.
5. Chen, P., et al., *Synthesis of superabsorbent polymers by irradiation and their applications in agriculture.* Journal of Applied Polymer Science, 2004. **93**(4): p. 1748-1755.
6. Woodhouse, J. and M.S. Johnson, *Effect of superabsorbent polymers on survival and growth of crop seedlings.* Agricultural Water Management, 1991. **20**(1): p. 63-70.
7. Liu, Z.S. and G.L. Rempel, *Preparation of superabsorbent polymers by crosslinking acrylic acid and acrylamide copolymers.* Journal of Applied Polymer Science, 1997. **64**(7): p. 1345-1353.
8. Raju, K.M., M.P. Raju, and Y.M. Mohan, *Synthesis and water absorbency of crosslinked superabsorbent polymers.* Journal of Applied Polymer Science, 2002. **85**(8): p. 1795-1801.
9. Hans-Joachim Hahnle, U.S., Wolfgang Heider, Gunnar Schornick, Thomas anstock, *Water-absorbing, cellular, cross-linked polymers with improved distribution effect, method for their production and their use*, 2004, BASF Aktiengesellschaft: Germany. p. 19.
10. M., E., *Superabsorbent polymer*, BASF, Germany.
11. Testouri A., D.W., *BASF visit report 2009*, 2009.
12. Pantchev, I. and D.J. Hunkeler, *Influence of quaternary ammonium salt addition on the surface activity of polyacrylic dispersants.* Journal of Applied Polymer Science, 2004. **92**(6): p. 3736-3743.
13. Raven, J.P., et al. *Microfluidics with foams*. in *3rd French Microfluidics Conference.* 2006.
14. Van Der Net A., D.W., *Ordered fluid foams as a templates for new cellular fibers*, 2007.
15. Karp, J.M., P.D. Dalton, and M.S. Shoichet, *Scaffolds for Tissue Engineering.* Mrs Bulletin, 2003. **28**(04): p. 301-306.
16. Griffon, D.J., et al., *Chitosan scaffolds: Interconnective pore size and cartilage engineering.* Acta Biomaterialia, 2006. **2**(3): p. 313-320.
17. Chung, K.Y., et al., *Fabricating scaffolds by microfluidics.* Biomicrofluidics, 2009. **3**(2).
18. Choi, S.W., J.W. Xie, and Y.N. Xia, *Chitosan-Based Inverse Opals: Three-Dimensional Scaffolds with Uniform Pore Structures for Cell Culture.* Advanced Materials, 2009. **21**(29): p. 2997.

7 POLYURETHANE FOAMS

7.1 INTRODUCTION

Polyurethane foams are the most frequently and widely used polymer foams of which several million tons are produced every year with a market of more 10 billion Euro [1, 2]. Ranging from flexible to rigid and from open- to closed-cell foams, polyurethane foams span a particularly wide range of uses from seating applications to thermal and acoustic insulation [2, 3] (Figure 7.1).

Figure 7.1: Examples of some applications of PU foams

The polyurethane industry now masters extremely well the polyurethane chemistry. However, two main challenges remain even after many decades of research:

1. Explicit control over pore sizes, pore size distribution and pore arrangement
2. Explicit control over the degree of the pore connectivity (open vs. closed cells)

The lack of "explicit" control results from the complexity of the physical chemistry of the initially liquid foam and of the chemical reactions (Section 7.2.1) involved. The latter generates side products of the main polymerisation reaction, which influence both bubble size distribution and pore connectivity in a non-negligible way.

Decades of industrial experience in combination with scientific efforts [4-11] have led to sufficient control in order to optimise product performance. However, "explicit" control, in which the influence of the different formulation and generation parameters may be justified by scientific arguments, is still far from reach.

The first goal of this work was therefore to reduce the chemical reactions to a minimum, i.e. to the polymerisation reaction without the presence of side reactions and therefore side products which may influence the final foam properties. **The second goal** was to implement this well-controlled chemistry with a well-controlled foam formation/solidification in order to obtain equally well-controlled foam structures which may provide insight into the key mechanisms which control the pore connectivity and, moreover, into the detailed structure/property relationships of polyurethane foams.

The latter is joining an experimental perspective to a growing research effort which aims to understand in detail how the *microstructure* of a solid foam is related to its *macroscopic* properties [12-14]. Typical questions at the core of this subject are: In which way are the mechanical or acoustic properties of a monodipserse foam different from those of a polydisperse foam? Which role does the organisation of the bubbles play, i.e. in what way are the properties of crystalline foams different from disordered ones? How does the size of the cell-opening influence mechanical, acoustic or thermal properties?

In this part of the thesis we have been able to develop millifluidic Lab-on-a-Chip techniques which, in combination with the simples possible polyurethane chemistry, provides us with the possibility to generate well-controlled foam structures (Section 7.7) with equally well-controlled polymer properties (Section 7.8). Due to time constraints, the characterisation of these foams remains preliminary, but should nevertheless provide a glimpse into the great possibilities provided by the application of our approach.

7.2 BACKGROUND

7.2.1 Polyurethane chemistry

Polyurethane is a polymer composed of organic units joined by urethane links. The urethane linkage is the result of the reaction between an isocyanate group –N=C=O- and a hydroxyl group –OH (like alcohol or amine) [2, 3]. As shown in Figure 7.2, polyurethanes are produced by the polyaddition reaction of a polyisocyanate with a polyalcohol (polyol) in the presence of a catalyst and other additives [3]. In this case, a polyisocyanate is a molecule with two or more

isocyanate functional groups, and a polyol is a molecule with two or more hydroxyl functional groups. The reaction product is a polymer containing the urethane linkage, -RNHCOOR':

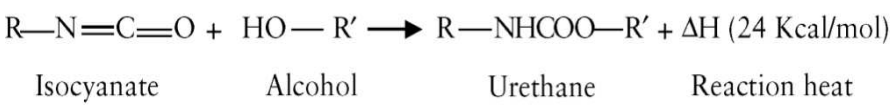

(7. 1)

Polyols are the predominant reagents used in the polyurethane formation. They are polyhydroxyl compounds of two main classes: polyesterols and polyetherols. They are star-like molecules (see Figure 7.2) which are characterised by the number of branches (i.e. the number of hydroxyl groups per molecule), and by their functionality. The molecular weight of the polyols used in polyurethane synthesis varies generally between 300-10000 g/mol, and the number of hydroxyl groups/molecule of polyol is generally in the range of 2-8 OH groups/molecule.

Isocyanates are characterised by their molecular weight and by the NCO content which indicates how many NCO groups a molecule contains [3]. The two most used isocyanates in industry are the isocyanates MDI (diphenylmethane diisocyanate) and TDI (toluene diisocyanate).

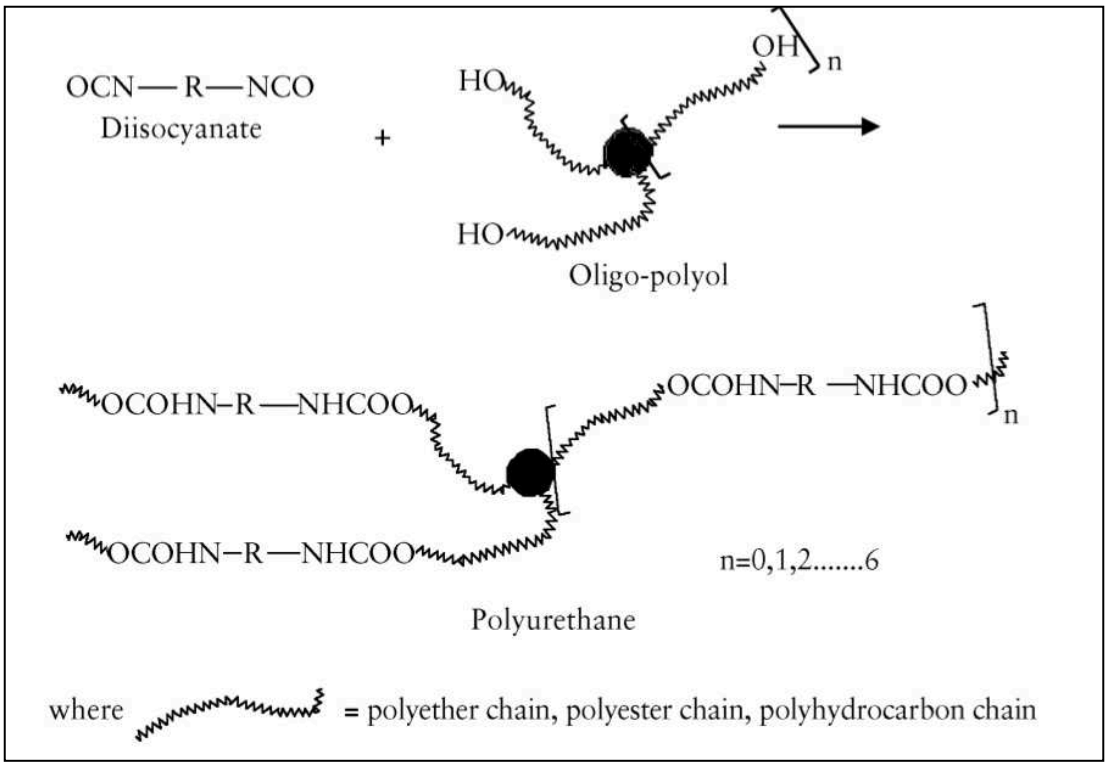

Figure 7.2: General reaction of polyurethane synthesis taken from [1]

Polyurethanes are commonly classified in two categories: flexible and rigid polyurethanes. This classification is mainly based on the polyol structure, which controls the topology and cross-link density of the final polymer network. As

sketched in Figure 7.2, a polyol of low functionality, having around 2-3 hydroxyl groups/molecule and with a high molecular weight of 2000-10000 g/mol leads to an elastic polyurethane and on the contrary, a low molecular weight polyol of 300-1000 g/mol, with a high functionality of around 3-8 hydroxyl groups/mol leads to a rigid polyurethane [3].
Figure 7.3, within this network the urethane and urea linkages generate the "hard domain" or "hard segment" of polyurethane. The polyol chains which are more "mobile" represent the "soft domain" or "soft segment" [1].

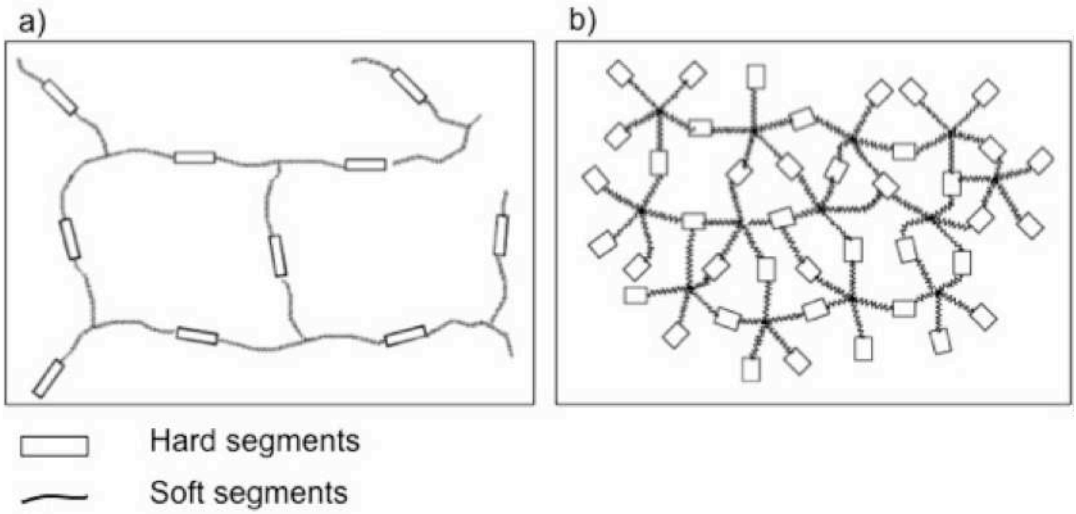

Figure 7.3: Crosslinked structure of: a) flexible and b) rigid polyurethane from [1]

Furthermore, the structure of polyurethanes depends strongly on the ratio between the OH and the NCO contents, which is known as the "mixing ratio". In fact, the NCO/OH ratio influences strongly the molecular weight of the final polyurethane as shown in Figure 7.4 and consequently the properties of polyurethane foams. The maximum molecular weight is obtained for a ratio NCO/OH = 1, since each OH group will react with one NCO group to make a fully connected polymer network. An excess of polyol leads to OH terminated polyurethane with smaller molecular weight and a sticky texture due to the free OH groups which did not react. On the hand, an excess of isocyanate leads to NCO terminated polyurethane in which all the « extra » NCO groups react with each other leading to a very rigid polyurethane [1].

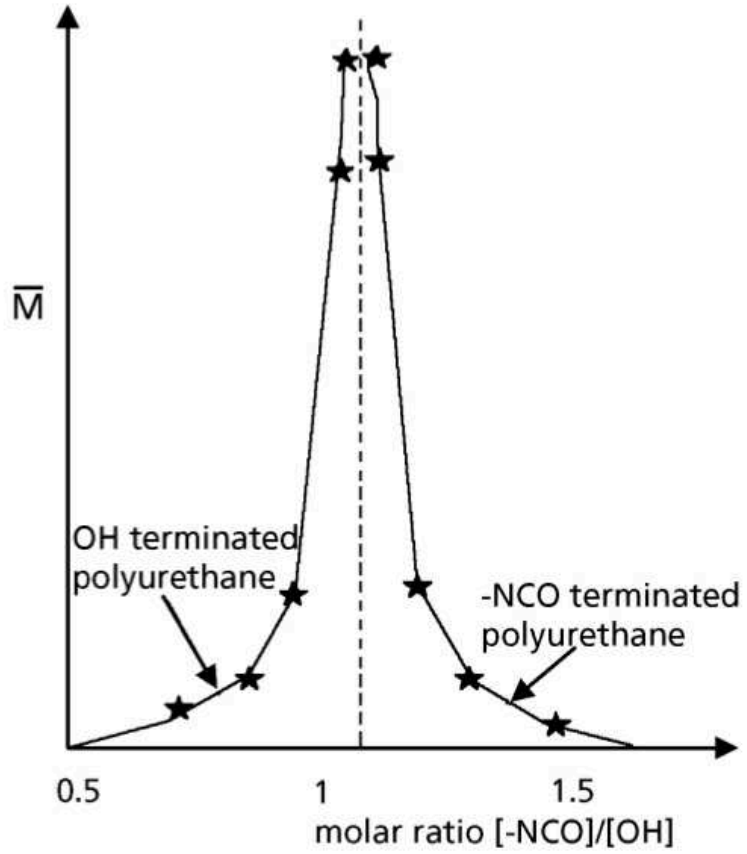

Figure 7.4: Influence of the "mixing ratio NCO/OH" on the molecular weight of polyurethane from [3]

Another important ingredient of polyurethane chemistry is the fact that when the isocyanate groups react with water, gaseous CO_2 and an amine group are formed. This latter reacts again with the isocyanate groups which did not react yet to form urea as shown in Equ. (7. 2).

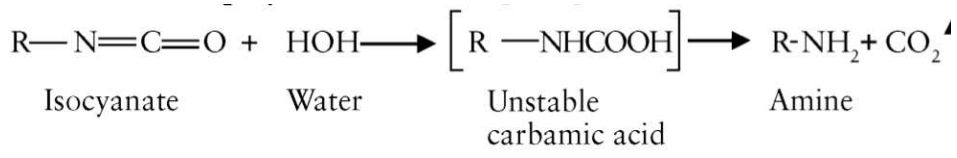

(7. 2)

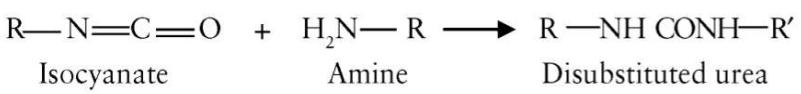

Many other side reactions can occur when isocyanates and polyols are mixed together. For example, the urethane and urea groups can further react with

isocyante groups since they contain themselves hydrogen atoms. These side reactions produce allophanates and biurets which lead to further branching/crosslinking of the polymer chains [2, 3]. We will not address such side reactions since they are of no interest for our study.

7.2.2 PU foaming

The reaction of isocyanate with water releases gaseous CO_2 (Equ. (7. 2)) which serves as blowing agent for the production of polyurethane foams. This reaction is thus very important for the polyurethane foam industry since it represents the most commonly used foaming technique, which is illustrated in Figure 7.5. It is called "*the one shot technique*" and consists of a rapid mixing in one step only of all the ingredients needed for the production of polyurethane foam. The success of this technique depends on an extremely efficient mixing which has to be rapid enough in order to mix all the components in the initial stage of the reaction while the solution is still liquid.

In order to simplify this procedure, "a master batch" – called *solution A* - which contains all the components that do not react with each other is prepared before mixing and contains polyols, water, catalysts and additives. This solution A is then mixed with solution B which contains the isocyanates only.

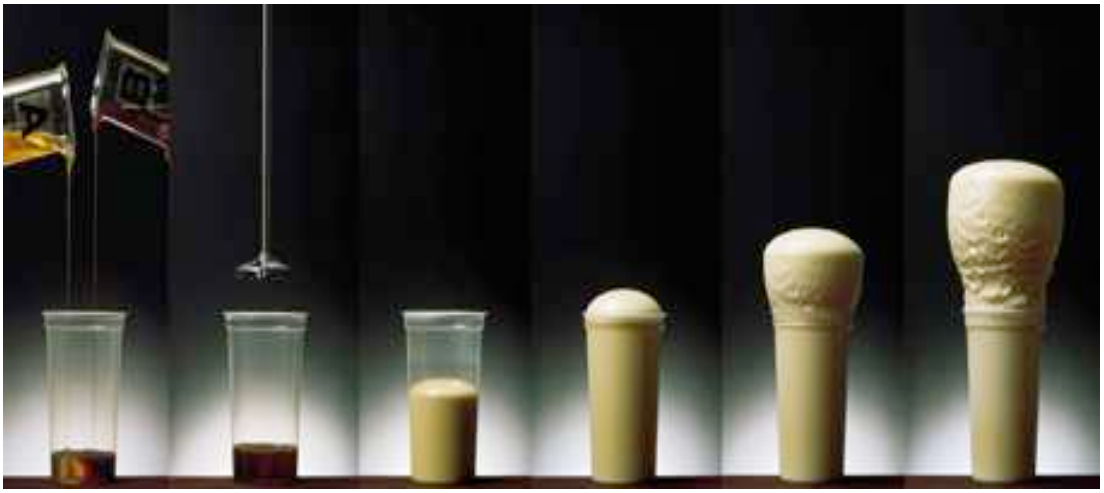

Figure 7.5: The most commonly used technique of production of polyurethane foams in industry: solution A and solution B are mixed releasing gaseous CO_2 and forming therefore the final foam (from [2]).

In the case of our study, the reaction of isocyanate with water is considered as a « *side reaction* » which has to be avoided using solutions which contain only traces of water (water content < 0,4%). In fact, our project is new in the world of polyurethane foams in the sense that we use physical blowing of bubbles, in which an inert gas is injected in a controlled manner to generate bubbles. More specifically, we use **for the first time millifluidic techniques** to generate **highly structured monodisperse polyurethane foams**.

7.2.3 PU surfactants (silicone surfactants)

The surfactants used in the polyurethane foam formulation are basically *silicone surfactants* [15, 16], which are polymeric amphiphiles. They were introduced to the polyurethane market in the 1950s as foam stabilisers. Their applications have spread afterwards thanks to their surface activity in both aqueous and non-aqueous media and their ability to achieve very low surface tension in comparison with conventional hydrocarbon surfactants (left of Figure 7.6).

As shown on the right of Figure 7.6 and in Figure 7.7, silicone surfactants are composed of a permethylated siloxane backbone (hydrophobic part) which is coupled to one or more polar groups (hydrophilic part). The polar groups are commonly polyethylene oxides. Silicone surfactants owe their strong surface activity to the presence of the methyl groups ($-CH_3$) and to an entropic effect provided by the flexibility of the siloxane backbone. The surface energy of a methyl-saturated component is known to be around 20mN/m and it is the lowest surface energy attainable by any surfactant [17].

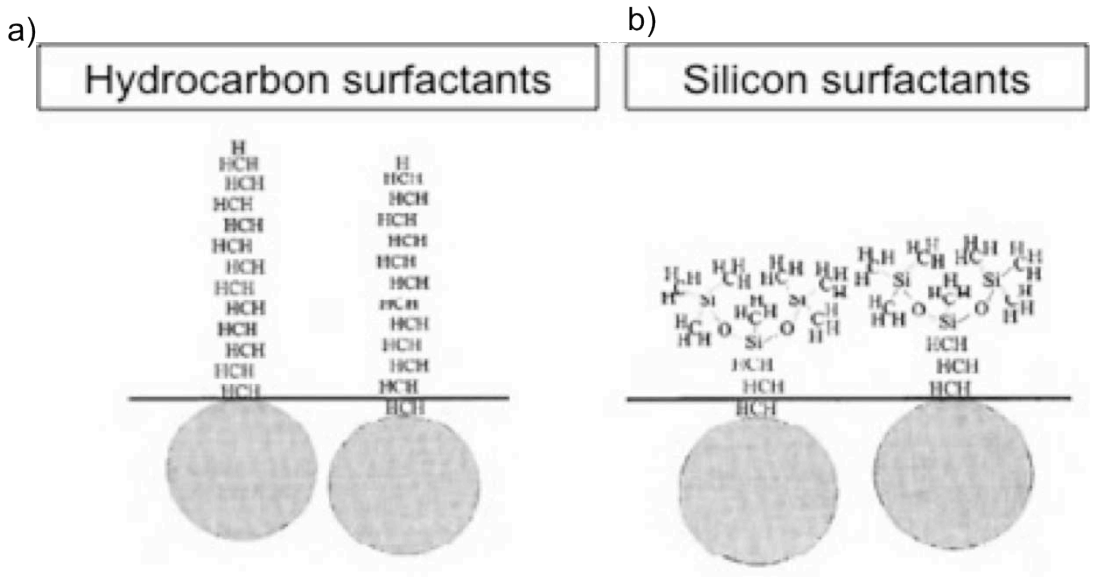

Figure 7.6: Schematic presentation of a hydrocarbon surfactant (a) and a silicon surfactant (b) (taken from [17]).

The three most commonly used architectures of silicone surfactants are comb-like copolymers, ABA copolymers and trisiloxane copolymers. They are presented in Figure 7.7.

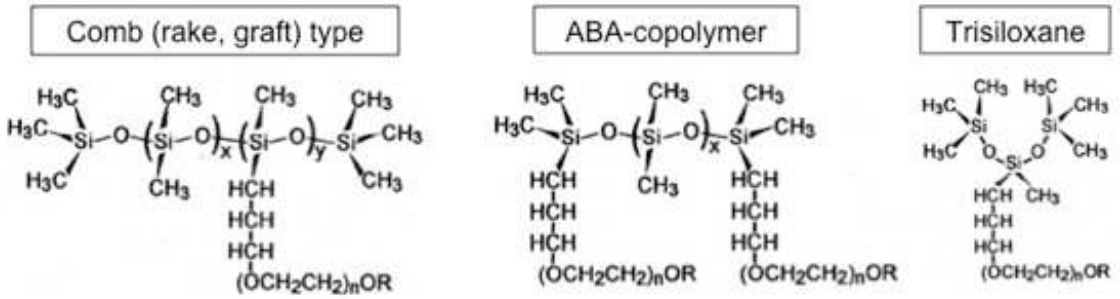

Figure 7.7: The most common three types of silicone surfactants [17]

Despite the structural differences between silicone surfactants and hydrocarbon ones, they have many common properties, e.g.

- the variation of surface tension with surfactant concentration is similar
- they both self-aggregate into micelles.

7.3 OPTIMISATION OF POLYURETHANE FOAM FORMULATION

The chemical components we used in the preparation of our polyurethane solutions are listed in Table 7.1 where their chemical structures and viscosities are listed. They are all provided by *Elastogran* and *BASF*. After a number of investigations (Section 7.3.2) we chose these chemicals among various others (three isocyanates from different natures and two different surfactants). In fact, different ingredients have been studied by us (Sections 7.3) in order to optimise the recipe of the preparation of polyurethane such that it validates the following criteria:

1. sufficiently low **solution viscosity** to generate foams using millifluidic techniques (Section 3.2.4),
2. sufficiently high **solution viscosity** to ensure foam stability against drainage,
3. sufficient **foam stability** (order of one hour),
4. sufficient control over the **solidification time** (between few minutes and few hours).

Throughout our study, we aimed to keep the chemical composition of the polyurethane foams as simple as possible. Many studies [2, 14, 18, 19] have shown that it is sufficient to work with five principal ingredients only:

1. Polyol
2. Isocyanate
3. Surfactant
4. Catalyst
5. Dispersed phase (Gas).

While the polyol and the isocyanate react to form the polyurethane, the surfactant stabilises the foam produced using millifluidic technique (by injecting gas), and the catalyst is used to control the reaction kinetics to adjust to the specific foaming application. Table 7.1 lists the final ingredients used by us and also shows the used notation in this section to replace the long names of the components.

Table 7.1: Ingredients used for the preparation of our physically blown polyurethane foams (except DPM which is used to mimic isocyanate when needed).

Component name	Component commercial name	Notation	Principal Chemical structure	Viscosity (25°C) mPa.s
Polyol	Lupranol	Polyol	-OH	1100
Isocyanate	M20W	M20W	-N=C=O-	155-235
Surfactant	Tegostab B8002	Tegostab	Polyether modified polysiloxane	500
Catalyst	Jeffcat ZR50	Jeffcat ZR50	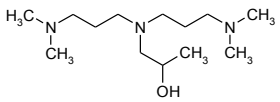	17
Isocyanate-like molecule	Diphenyl methane	DPM	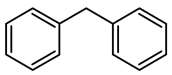	70

7.3.1 Study of the interfactial properties of PU liquid solutions

Elastogran provided us with four surfactants known for their stabilising effect in non-aqueous media. These surfactants are well-known in the polyurethane literature for their ability to decrease the surface tension of the polyol to very low values (around 20 mN/m)[8]. We received three surfactants from the Tegostab series (Tegostab 2470, Tegostab B8002, Tegostab 8232) and the Niax Silicone L620. The Tegostabs are comb-like surfactants (Figure 7.7) while the Niax surfactant is an ABA siloxane surfactant. All the surfactants are colourless, liquid with relatively high viscosities.

We characterised both surfactants since we did not have information about either the structure or their characteristics. We investigated their surface activity in polyol solution and their critical micelle concentration (CMC) using the TRACKER device (Section 4.1.1). This allowed us to choose the best surfactant, which not only stabilises the foam the best.
As shown in Figure 7.8, the equilibrium surface tension of all the surfactants in pure polyol (Table 7.1) at the same concentration (10 wt%) gives a general idea of their surface activity. The surface tension of the solutions drops from about 33 mN/m to about 21 mN/m for all the surfactants. The latter value is typical of Silicone surfactants in various media, the CH_3-groups promoting very low surface energies [17, 20]. Since all surfactants seem to have a similar surface

activity when used at high concentration, we chose to study only two surfactants: the medium one of the Tegostab serie **Tegostab B8002** and the **Niax Silicone L620**.

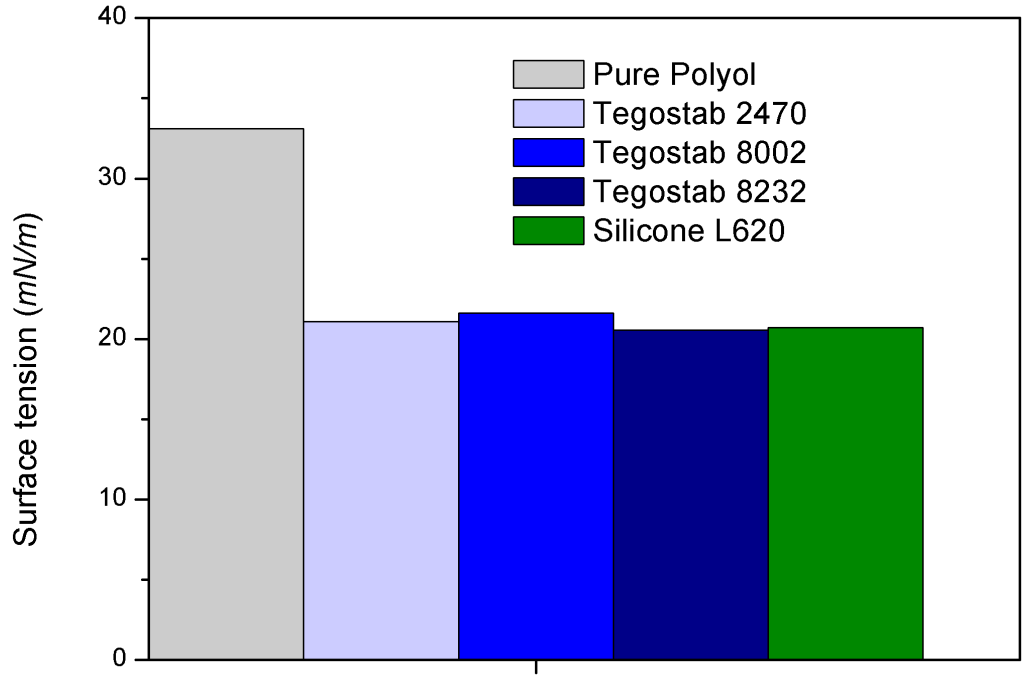

Figure 7.8: Equilibrium surface tension of pure polyol and the four surfactants at 10 wt% in pure polyol

We measured the surface tension of these surfactant solutions at different concentrations in polyol. The results are presented in Figure 7.9 as a function of the surfactant concentration (logarithmic scale).

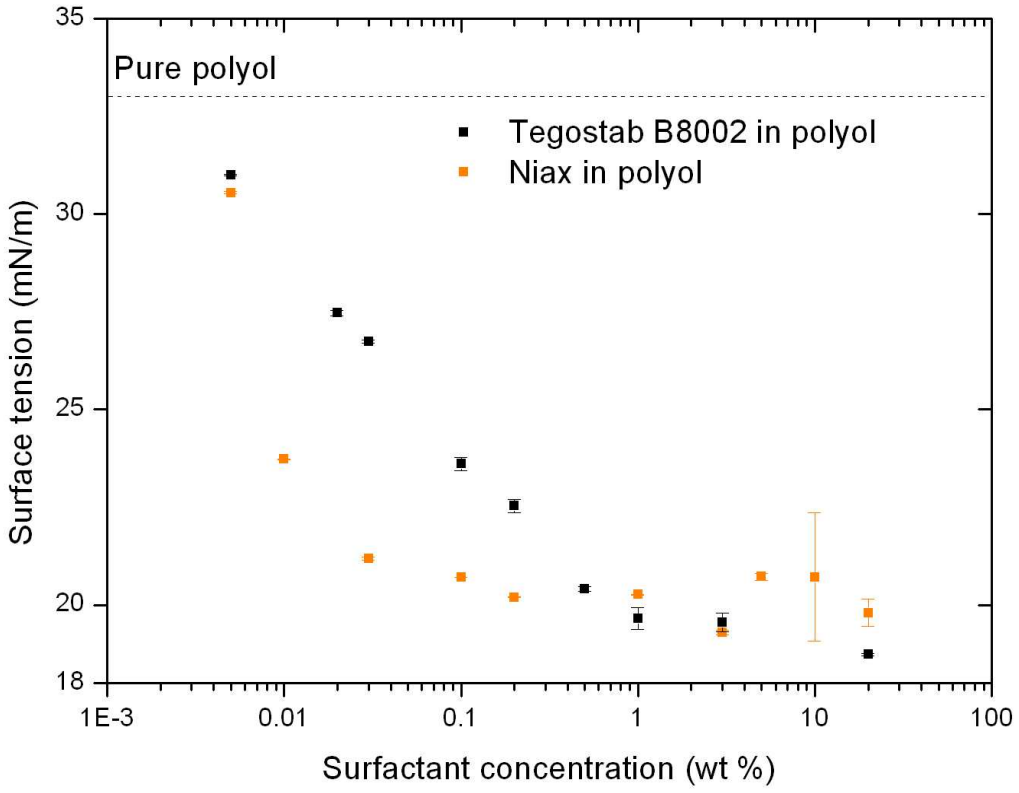

Figure 7.9: Evolution of the surface tension of Tegostab and Niax as a function of their concentration in polyol

Both surfactants display a concentration behaviour very similar to that of standard, low-molecular weight surfactants as discussed in Section 2.2.2: the surface tension decreases significantly when the surfactant concentration increases and remains constant above the CMC. In the case of Tegostab B8002 the CMC is about 1 wt% and for the Niax, it is lower, around 0.1 wt% (Table Table 7.2).

Table 7.2: CMC values for the two standard surfactants in pure polyol used throughout this work as reference.

Surfactant	CMC
Tegostab B8002	1 wt%
Niax	0.1 wt%

We also show (Figure 7.10) the dynamic surface tension for Tegostab, i.e. the variation of the surface tension with time as it approaches equilibrium (Section 2.2.2). This allows following the surfactant dynamics (slow ad- or desorption, surfactant exchange etc.), which is very important to match the adsorption and the foaming time scales.

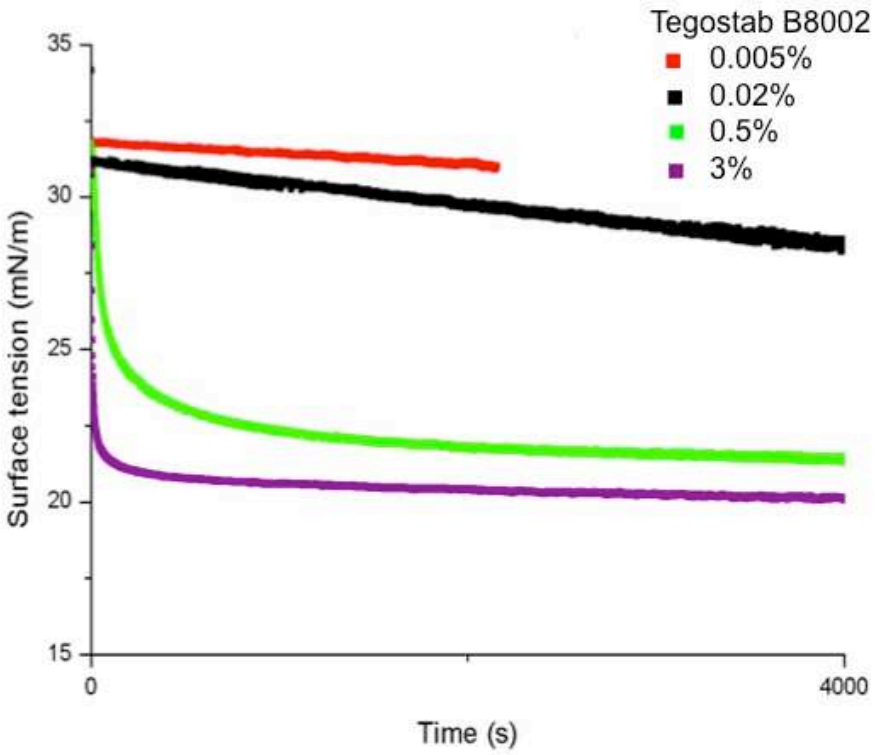

Figure 7.10: Evolution of the surface tension with time for the Tegostab solutions. These measurements are performed using a pendant drop device ("Tracker", TECLIS). The higher the surfactant concentration, the faster the equilibrium surface tension is reached.

The surface tension decreases with time until it reaches a plateau corresponding to the equilibrium surface tension. The higher the surfactant concentration, the faster the decrease of the surface tension: while equilibration below the CMC can take more than an hour, it takes only a few minutes above the CMC. Choosing a value of the surfactant concentration corresponding to few times the CMC, allows not only to have a good foamability but also to make sure that all the air/solvent interfaces of the foam are covered well and fast enough. Since we typically generate a bubble in 10^{-2} s (Section 3.2.3) we chose to work with a surfactant concentration of 5 wt% throughout the work reported here.

Up to now, we have investigated the surface activity of the two surfactants in pure polyol which is the principal solvent (around 90 wt%) used for the preparation of the polyurethane pre-mix. However, the behaviour of these surfactants can be different once the polyol is mixed with the isocyanate. It is then very important to study their behaviour in polyol and isocyanate mixture. Since it is very difficult to measure correctly the surface tension of a reacting solution, we decided to measure the surface tension of the Tegostab in a solution containing a 50/50 mixture of polyol and diphenyl methane (DPM). Diphenyl methane is a reactant which is very similar chemically to the isocyanate (Figure 7.11) and hence expected to "simulate" the presence of the isocyanate.

The advantage of using the diphenyl methane is that not only it mimics well the isocyanate, but also allows one to perform long experiments since it does not polymerise avoiding thus the possible surface tension changes. Moreover, diphenyl methane is not hazardous whereas isocyanate is a harmful and toxic product which has to be handled only under a fumed hood making experiments difficult.

From the results of the surface tension measurements which are shown in Figure 7.12, one observes that the addition of the DPM reduces the surface tension from approximately 33 mN/m to 25.5 mN/m. This is a classical behaviour of mixtures in which the solvent with lower surface energy concentrates at the interface. However, once the Tegostab B8002 is added, the surface tension reduction with concentration is very similar to that of polyol alone, and in particular its final value above the CMC. We therefore conclude that the presence of the isocyanate should not change significantly the behaviour of the surfactant and that the measurements performed on pure polyol can serve as a reliable reference. This should be even more so the case since the isocyanate concentration in the final polyurethane solution will be very small (around 7 wt%), whilst the DPM concentration used here was 50 wt%.

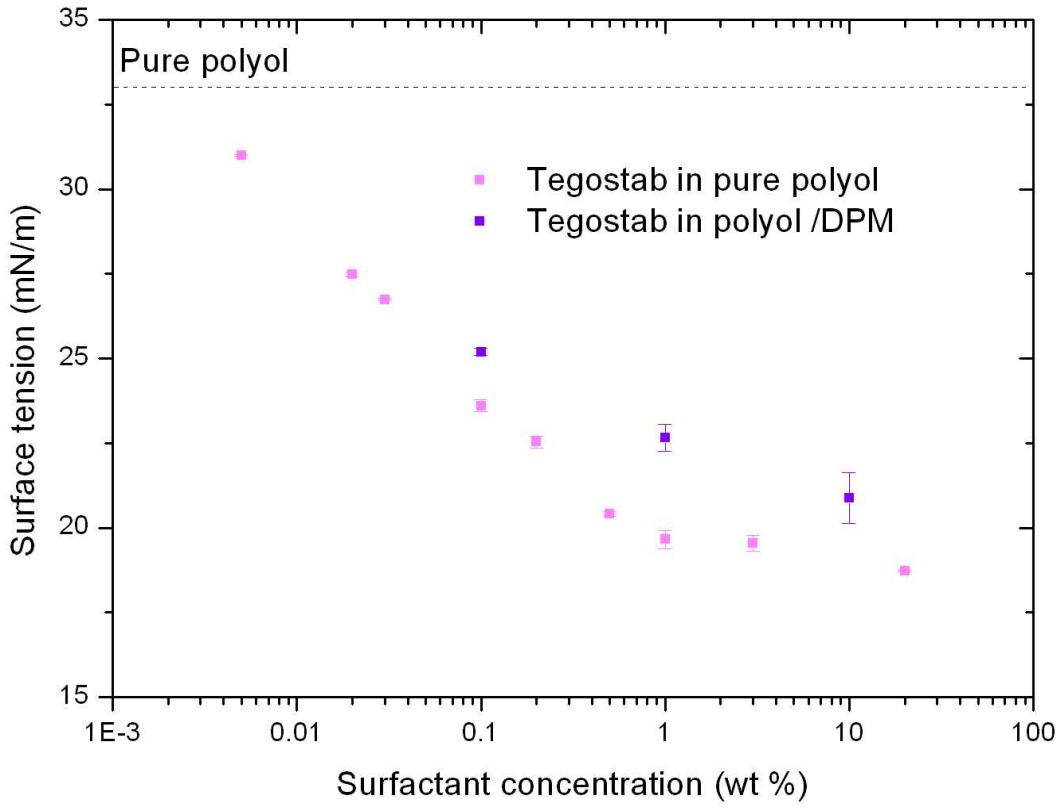

Figure 7.11: Surface tension as a function of the surfactant concentration (Tegostab 8002) in pure polyol and in a 50/50 mixture of polyol and diphenylmethane (DPM) to simulate the presence of an isocyanate

7.3.2 Characterisation of liquid PU foams

Foamability

To cross-check the surface tension results shown in Section 7.3.1, we prepared solutions of different concentrations of the chosen surfactants in polyol, then we foamed them using a commercial T-junction. We compared then the foamability of each solution for the two surfactants as shown in Figure 7.12a. The foamability is also checked for Tegostab solutions containing 50% diphenylmethane (Figure 7.12b) to simulate the presence of isocyanate (Section 7.3.1).

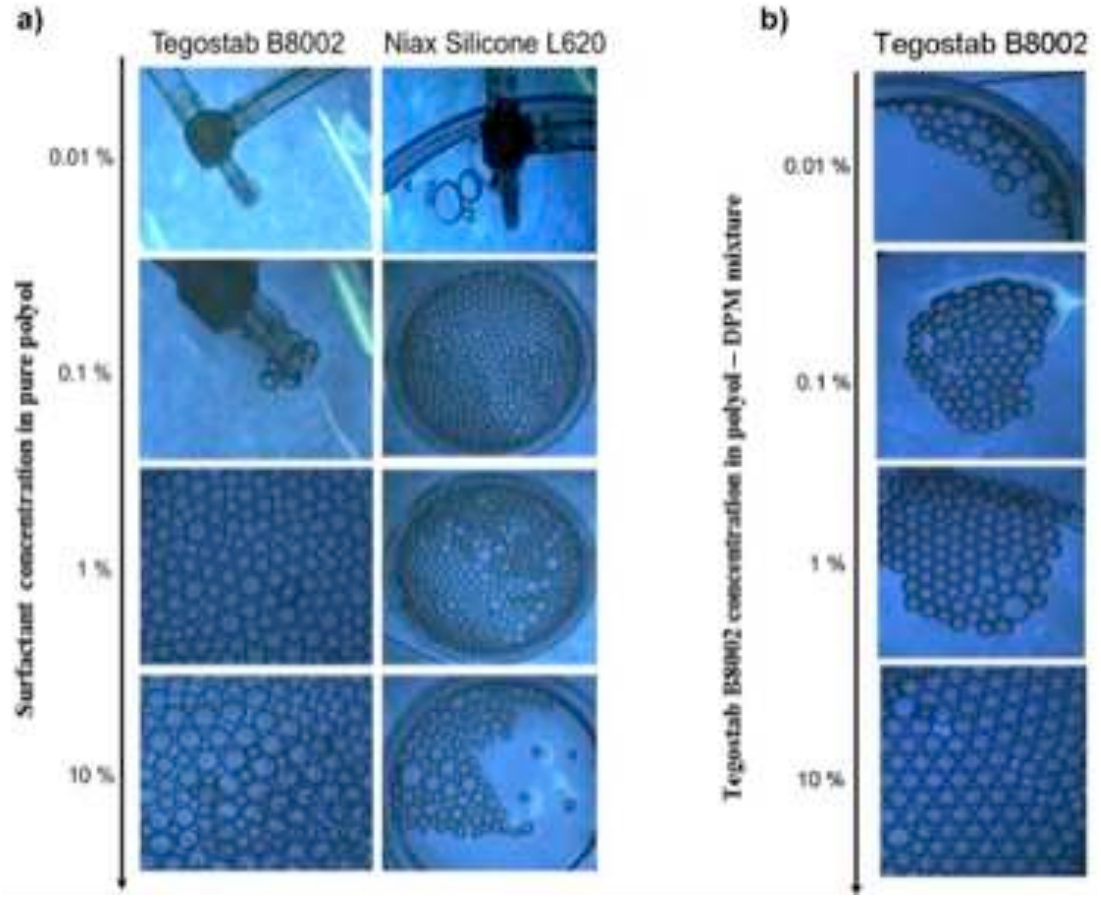

Figure 7.12: a) Foamability test of polyol solutions containing Tegostab and Niax repectively at different concentrations. b) Foamability test of a 50/50 mixture of polyol and diphenylmethane (DPM) containing Tegostab at different concentrations

As we can see in Figure 7.12, the solutions foam very badly for concentrations of Tegostab which are below the CMC (1wt%). Only a small number of bubbles are stabilised, we increase the concentration to about and above the CMC (> 1 wt%) of Tegostab, we achieve a better foamability. In this strip of concentration, we can say that the higher the concentration of Tegostab, the better the foamability.

For the Niax solutions, one can clearly notice that at very low concentration we obtain only some bubbles which burst immediately. When the concentration increases to the CMC (0.1wt%), a considerable amount of stable foam starts to be formed. Once the Niax concentration reaches a limit value (around 1 wt%), the foamability starts to decrease.

Foam stability

In order to choose the working conditions for which **foam stability** is ensured, we performed half-life measurements (Section 4.2.2) in pure polyol then in a 50/50 mixture of polyol and diphenyl methane (DPM). We collected the same amount of each monodisperse foam generated with the two chosen surfactants at different concentrations in graduated containers of the same diameter, then we measured the time corresponding to the reduction of the total foam volume by half (Figure 7.13a).

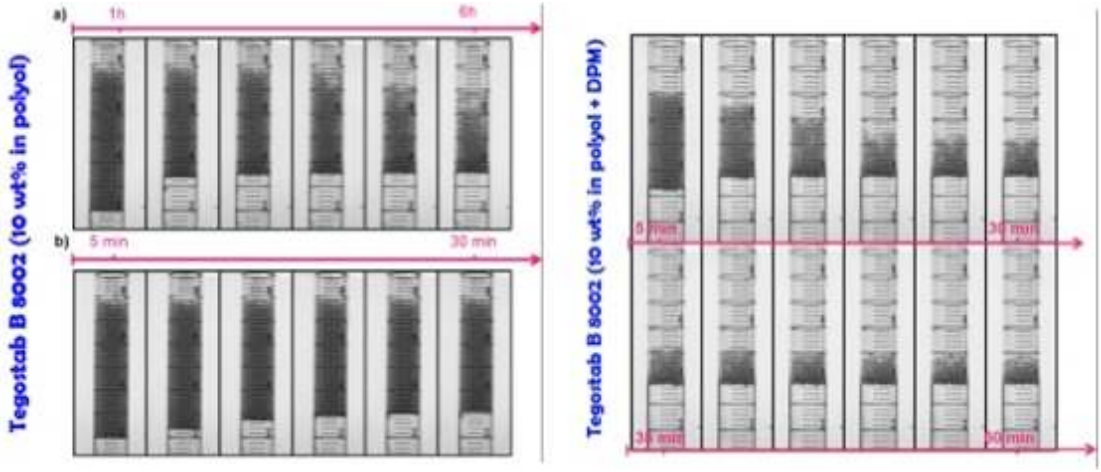

Figure 7.13: a) Foam stability of 10 wt% Tegostab solution in pure polyol. a) The foam stability is checked for quite long duration (the foam is stable for few hours). b) The foam stability is checked for the typical duration of our foaming process. b) Foam stability of 10 wt% Tegostab solution in a mixture of polyol and diphenyl methane. The presence of diphenylmethane affects the foam stability.

We notice a difference in the liquid foam stability with and without diphenylmethane, which is very likely due to the reduced viscosity of the DPM. However, in both cases, the foam shows sufficient stability on typical experimental time scales. This confirms the results of the surface tension measurements shown in Figure 7.11.

Figure 7.14 shows the results of the foam half-life time (Section 4.2.2) for the two surfactants in pure polyol. These correlate with the observations for the foamability (Section 7.3.2): for Tegostab, the higher the concentration, the more stable the foam. Whereas, for the Niax, the foamability and the foam stability improves as the concentration increases then, around a surfactant concentration

of 0.1wt% starts to decrease. This could be due to depletion effects caused by the formation of complex species in the bulk solutions at high surfactant concentrations.

Combining the surface tension and foaming results of the various surfactant solutions, we chose therefore to use the Tegostab B8002 at a concentration of 5wt% for the preparation of our polyurethane foams.

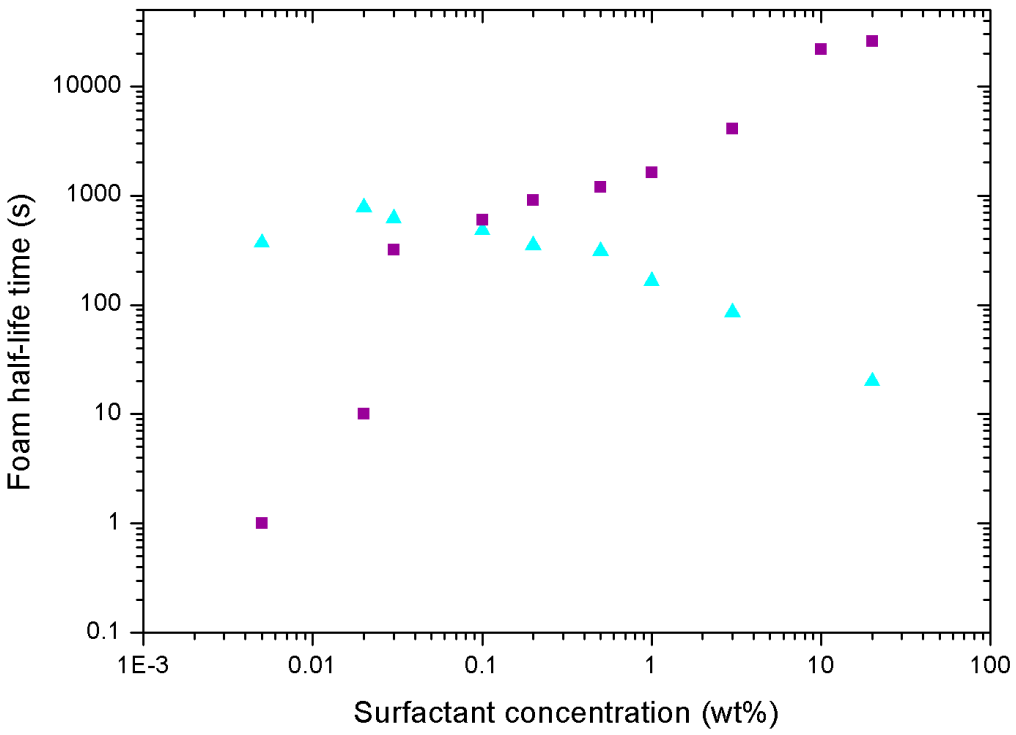

Figure 7.14: Evolution of the half-life time with surfactant concentration of foams generated with Tegostab B8002 and Niax Silicone L620.

7.3.3 Determination of the solidification time of the PU liquid solutions

In order to determine the solidification time τ_s of the polyol – isocyanate mixtures (with mixing ratio 1:1) in the presence of a catalyst (Jeffcat ZR50), the solidification process was followed by determining the elastic and viscous moduli (G' and G'', respectively) of the samples as a function of time t. We take the cross-over of both curves as the solidification point (Section 2.8), since at this point the material goes from one dominated by viscous behaviour to one dominated by elastic behaviour. The results provided by Elastogran for our solutions using different catalyst concentrations are presented in Figure 7.15a where the viscoelastic moduli are plotted as a function of the time rescaled by the solidification time. It is obvious from the excellent overlapping of these curves that the catalyst accelerates very homogeneously the solidification process without having an influence on the transitory and final material

properties. The solidification time is plotted as a function of the catalyst concentration in Figure 7.15b where the data has been fitted by an exponential law following

$$\tau_S\ (\mathrm{s}) = 4800 \exp\left(-9.5\, C_{Cat}(\mathrm{wt\%})\right). \qquad (7.3)$$

This function will allow extrapolating to the desired solidification time and determining the corresponding catalyst concentration.

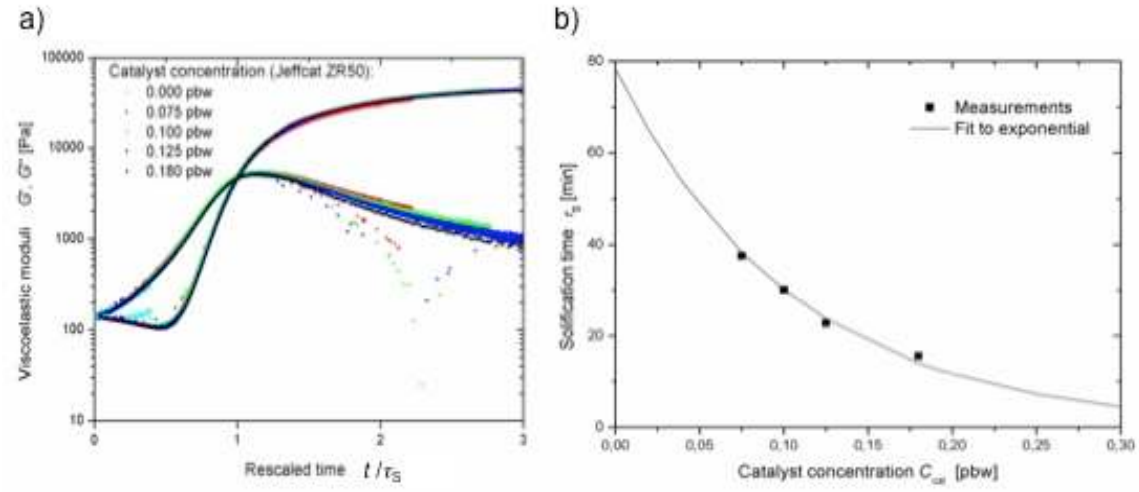

Figure 7.15: a) Variation of the viscoelastic moduli upon solidification for the polyol/isocyanate mixture at mixing ratio 1:1 for a range of catalyst concentrations. The time t has been rescaled by the solidification time τ_S which are shown in b) as a function of catalyst concentration C_{Cat}. The data was fitted by the exponential function provided in Equ. (7.2).

Thanks to these results, we can easily tune the polymerisation time of our solutions and foams from few seconds to few hours according to the desired shape and application of the final foam. The solidification time is chosen in a such a way to allow the generation of a monodisperse foam where the bubbles have enough time to flow slowly out of the foaming device due to the high viscosity of the premix solution and then self-organise under gravity before solidification.

7.4 THE FINAL POLYURETHANE RECIPE

The study of the properties of the liquid polyurethane solutions and foams (Section 7.3.1 to Section 7.3.2) allowed us to choose the "best ingredients" and their quantities. Table 7.3 presents the final recipe for the preparation of polyurethane foams which we shall use in the following studies.

Table 7.3: Standard recipe used in this work

Ingredient	Commercial name	Concentration	Solution
Polyol	Lupranol	*Cpol* ≈ 89 wt%	**A**
Isocyanate	N20W	*Ciso* ≈ 6 wt%	**B**
Surfactant	Tegostab	*Csurf* = 5 wt%	**A**
Catalyst	Jeffcat ZR50	*Ccat* = variable (0.05 – 0.3 wt%)	**A**
Gas	Air	Depends on desired foam density	**Gas**

The concentration of polyol and isocyanate are chosen in this recipe in such a way to obtain a **mixing ratio** 1:1 (Section 7.2.1) in almost all the experiments. This ratio changes only in some measurements in order to study its effect on the polymer and the polymer foam properties.

It is important to mention that, in our study, as in the "one shot technique" commonly used in PU industry (Section 7.2.2), the liquid/solubilised ingredients are separated into two principal liquid mixtures, SOLUTION A (master batch) containing the polyol(s) and all the additives, and SOLUTION B the isocyanate (Table 7.3). The composition of the solutions is chosen such that individually they are stable with time but start to react and solidify once they are mixed. Whenever possible, we shall describe our procedure in terms of these two principal solutions.

7.5 THE MILLIFLUIDIC FOAMING SET UP

7.5.1 Millifluidic channel network

Since the millifluidic Lab-on-a-Chip which we use to generate polyurethane foams is composed of various units (Section 1) and hosts many chemical reactants, it has consequently a complex design. Using micromilling techniques for the fabrication of each of the millifluidic geometries in this case would be very long and expensive, especially since the geometries are often not reusable (the channels are often blocked at the end of the experiment due to polymerisation). We decided thus to use the hot embossing technique (Section 4.3.2) which is very precise and inexpensive.

Figure 7.16 shows the design of the millifluidic geometry used by us to inject, foam and mix the chemicals involved in the polyurethane formation reaction (Table 7.3). This Lab-on-a-Chip contains two sub-units, which form the channel network: **foaming** and **mixing unit**. Both are discussed in more detail in the following.

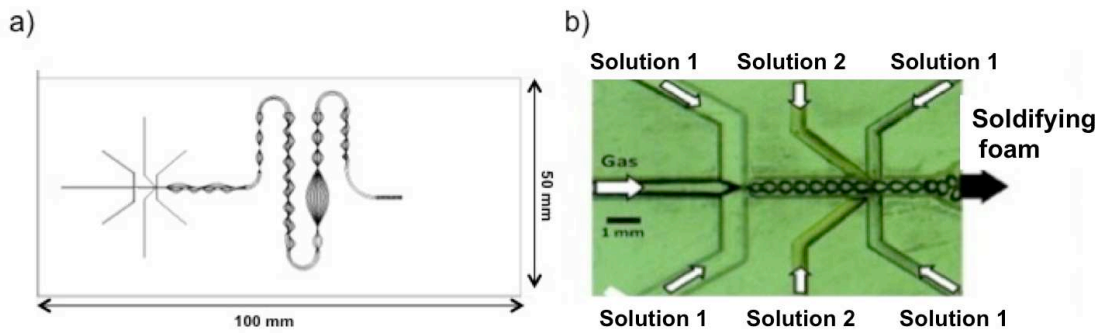

Figure 7.16: a) Design of the geometry using the software *Galaad*. b) Top view of a typical millifluidic channel system with injection of gas and various chemicals for on-chip reactions.

7.5.2 The foaming unit

The foaming unit consists of a flow focussing geometry (Section 3.2.2) which serves to generate the bubbles by focussing into a constriction two outer inlets of solution A and a gas inlet in between. The gas is injected into the solution at constant flow rate, ensuring well-controlled generation of bubbles. We generate foams with bubbles of different sizes (tens of microns - 2mm). We also established a successful technique for the generation of monodisperse and multi-disperse foams.

In fact, our new contribution here is that we have established a simple way to tune foam dispersity and bubble size. This can be reached by tuning the ratio of the length of the constriction (through which the bubble generation takes place) to its smallest width. One can thus design channel geometries which give large flow rate ranges in which well-controlled foam generation can tune between bi-, tri-, or multi-disperse foams and the ratio of the bubble sizes. Bi- and tri-disperse bubbling regimes have been witnessed in the literature [21, 22] but never explored scientifically. Figure 7.17 shows examples of bidisperse foam generation.

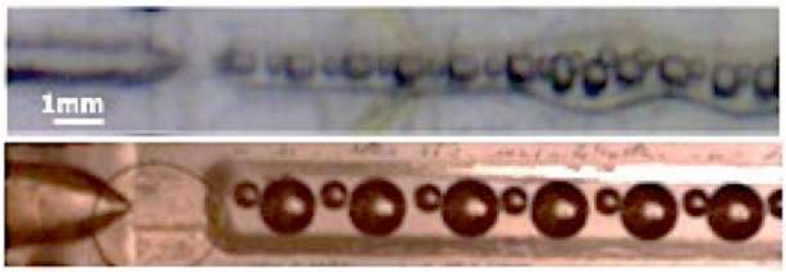

Figure 7.17: Examples of generation of bidisperse foam.

Furthermore, by changing the gas to liquid flow ratio; we generated foams with relative densities in the range 1%-100% (without bubbles) (Section 2.7.2), knowing that densities above 10 % are achieved easily whilst densities below 10% require some special efforts. Examples of obtained foams can be seen in Figure 7.18.

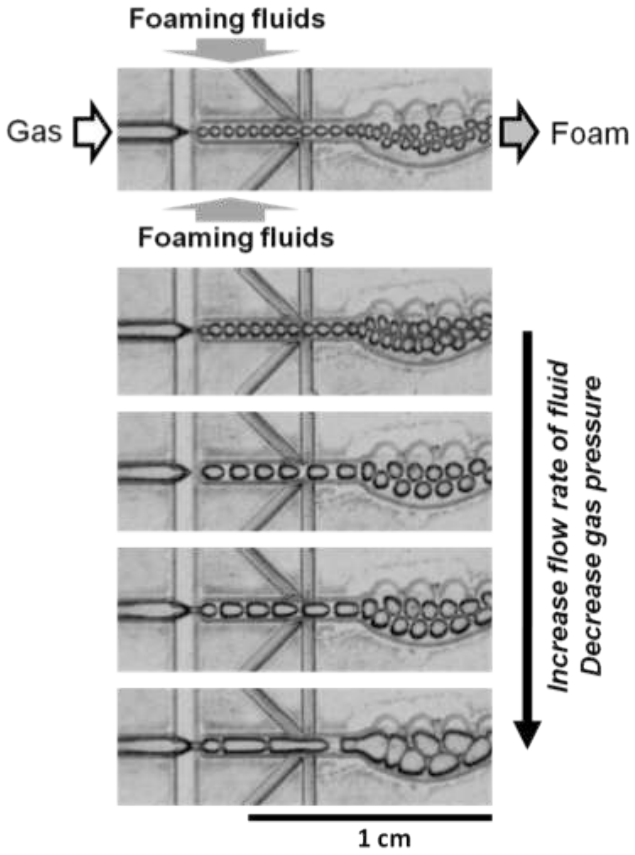

Figure 7.18: a) An illustration of the generation of foams with different densities obtained by tuning the gas and liquid flow rates. In order to decrease the bubble size one can either increase the liquid flow rate or decrease the gas flow rate (from top to bottom).

Typical flow rates Q and pressures P used by us with resulting bubble sizes D_B are given in Table 7.4.

Table 7.4 : Typical flow rates and pressures used for the Lab-on-a-Chip

$Q_{A,1} + Q_{A,2}$ (ml/min)	$Q_{A,3} + Q_{A,4}$ (ml/min)	$Q_{B,1} + Q_{B,2}$ (ml/min)	P_{N2} (bar)	D_B (µm)
Polyol + surfactant + catalyst		**Isocyanate**	**Nitrogen gas**	**Bubble diamter**
9.2	0.84	0.84	0.25	300
4.6	0.42	0.42	0.2	700

Comments on the injection of chemicals

When injecting reacting chemicals into the channel network, particular care needs to be taken to

1. ensure that the chemicals are mixed properly, and to
2. avoid the clogging of the channels.

The injection of the different solutions occurs before the mixing unit and we use two different channel designs.

In the **first design** (see Figure 1.3), which is the main technique which we use for the generation of PU foams, the bubbling takes part in the solution A only and the solution B is injected just after bubbling and before (or directly into) the mixing unit. With this option, it is straightforward to vary the NCO/OH ratio (and hence the final polymer properties) by simply varying the ratio of the flow rates of solution A and B.

In the **second design** (see Figure 1.3), the solution A and B are "pre-mixed" using a mechanical stirring technique, then the pre-mix solution is injected into the channel network before the foaming unit such that solidification starts before bubbling. There is no need to use a mixing unit in this case since all the ingredients are already mixed. The catalyst concentration needs to be adjusted in order to avoid channels blocking. Each design has its advantages and disadvantages, which are listed in Table 7.5.

Table 7.5: The advantages and disadvantages of the two designs of foaming used in our study

	Advantage	**Disadvantage**
Design 1	Solidification starts after bubbling and just before or in the mixing unit. Hence, bubble generation is reproducible and can be well calibrated	A non-negligible amount of liquid (~10%) is injected after the bubbling, hence the generated foams will have at least 10% density
Design 2	Low density foams can be obtained more easily	Solidification starts before bubbling and each composition of the solutions will have a different effect on the solution visco-elasticity, hence on the bubble generation (i.e. calibration of bubbling more difficult and less general)

Particular care needs to be taken when injecting solution B into a channel system in which solution A is already flowing (which is generally the case). In order to ensure that the solution B does not remain (and solidify) on the channel walls or in the corners of the commonly rectangular channels, the channel design must ensure that solution B is carried into the center of the flow. This is ensured by injecting the solutions into the principal channel in the way sketched in Figure 7.19a which creates stable "layers" of each solutions due to the fact that he flow of viscous solutions in milli/microfluidic geometries is laminar.

The outer layer in contact with the wall needs to be made of solution A (which can be thin). Towards the interior, many different layers can be created, ensuring a large contact area between the two solutions – an important stage before the MIXING UNIT in order to ensure homogeneous reaction conditions and therefore

reproducible polymer properties. An experimental realisation of this principle is shown in Figure 7.19b.

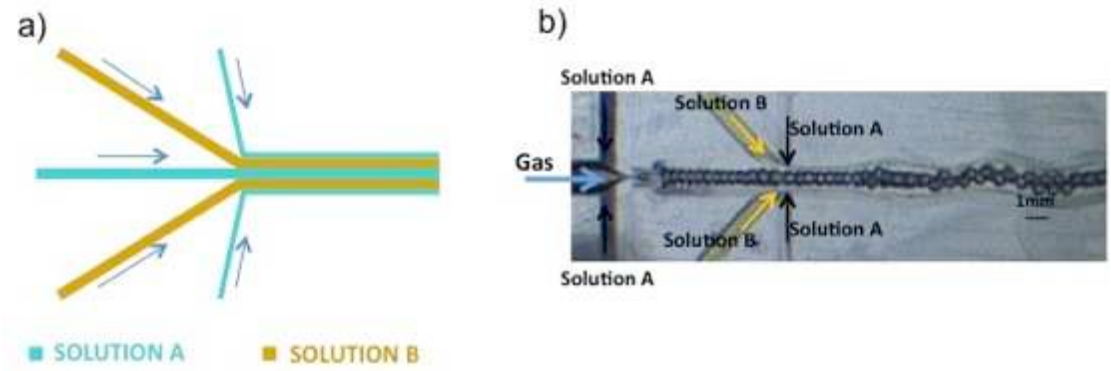

Figure 7.19: a) Sketch of the channel geometry which ensures that solution B is not in contact with the channel walls. Many multiple layers can be constructured which simultaneously ensure a large contact area between the two solution. b) Photograph of experimental realisation showing the sequence of injection of SOLUTION A, then B and then A to avoid deposition of SOLUTION B on the wall.

7.5.3 The mixing unit

We established a new mixing technique which relies on the presence of the bubbles and uses their motion to mix efficiently the various solutions contained between them. For this purpose, the channel system of the mixing unit is designed in such a way that bubbles are continuously forced to change their relative positions in a manner which is as "chaotic" as possible.

As can be seen in Figure 7.16a, we have successfully solved this problem by designing channels which have a "wiggly" shape, given by sinusoidal channel geometries described by $A = A_0 \sin(kx)$, as shown in the top graphs of Figure 7.20. More specifically, the shapes of two opposite walls are sinusoids of different wave vectors k_1 and k_2, chosen in such a way that the channel width changes in a complex manner along the channel (bottom graphs of Figure 7.20). Figure 7.20c, for example, shows a non-periodic variation of the channel width, which forces the bubbles to rearrange in a complex manner. One condition for this to happen is that the bubble size needs to be smaller than the average channel width. It is also essential that the channel width is at least several times the size of one bubble in such a way to have enough bubbles moving along the channel and ensuring a good mixing.

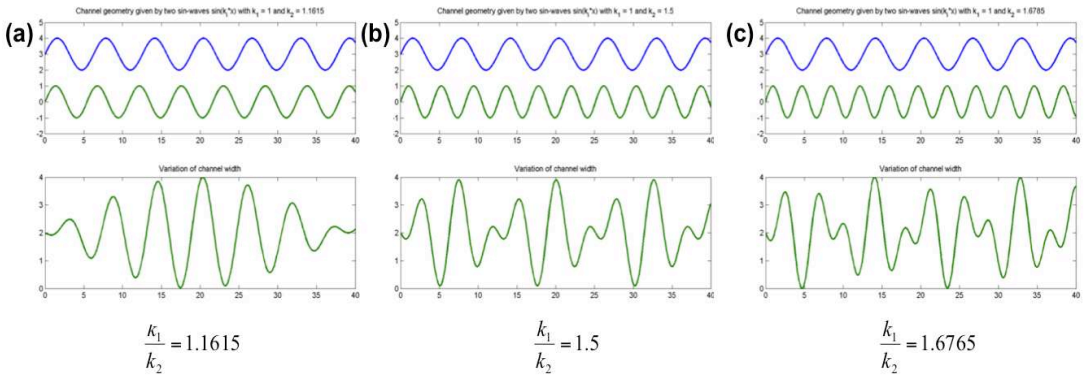

Figure 7.20: Channel geometry (top graphs) and resulting variation of the channel width along the channel (bottom graphs) of channels constructed by two sin-curves with different wavelengths

Since the oscillations of the channel width vary over one order of magnitude, the same mixing geometry works for a range of bubble sizes, rendering one single set of channel designs applicable for a range of bubble sizes (which are simply modified by changing the flow rates).
In order to optimise mixing, we put several sequences of such "wiggly" channels together, often in a serpentine pattern to save space (Figure 7.21a). Figure 7.21b shows the efficiency of the mixing channel for different bubble sizes.

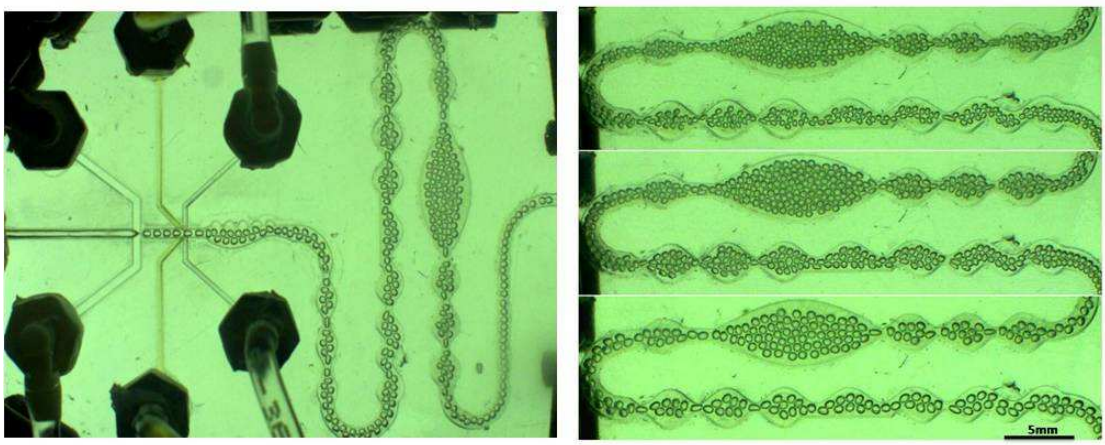

Figure 7.21: LEFT: Specific example to show the mixing of two fluids (transparent and yellow, injected on the left of the image thanks to the flow of closely packed bubbles (from left to right) through a channel system in which the channel width varies. RIGHT: Examples of the same mixing channel for different bubble sizes. Here the bubbles are generated in-situ. Also droplet or particles can be used for the same purpose.

7.6 QUALITY OF MIXING OF THE INGREDIENTS WITHIN THE MILLIFLUIDIC DEVICE

The mixing quality is also tested experimentally by using dye solutions and following the change in colour of the solution surrounding the bubbles which flow inside the millifluidic zigzag channels (here symmetric channel geometry). We see clearly that the movement of the bubbles leads to a mixing of the two solutions (grey and white solutions). In fact, these two solutions do not mix at all in the absence of bubbles and we see two adjacent laminar flows.

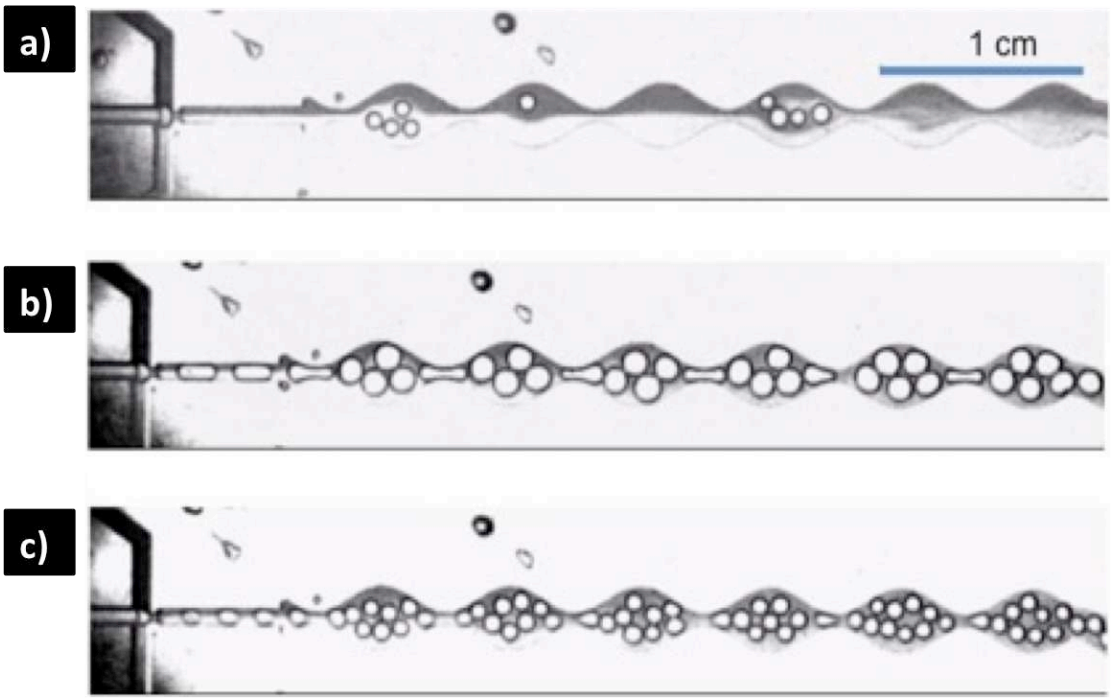

Figure 7.22: Characterisation of the wiggly mixing channels. In the absence of bubbles (upper image) the flow is laminar and there is no mixing. The movements of bubbles help to obtain a "chaotic" mixing (two bottom images).

7.7 POLYURETHANE FOAMS

We generated different types of PU solid monodisperse foam (2D, 3D, threads as shown for instance in Figure 7.26 in order to study their structures and mechanical properties. We chose a solidification time around 1h (Section 2.8), in such a way to allow the generation of a monodisperse foam where the bubbles have enough time to self-organise under gravity. The foam was then generated, collected out of the millifluidic device in containers having different shapes and then left in these containers until they are completely solidified. We took pictures of the foams immediately after their generation (still liquid and sticky) and after their complete solidification. Pictures of some of these foams are presented in Figure 7.23 and Figure 7.24.

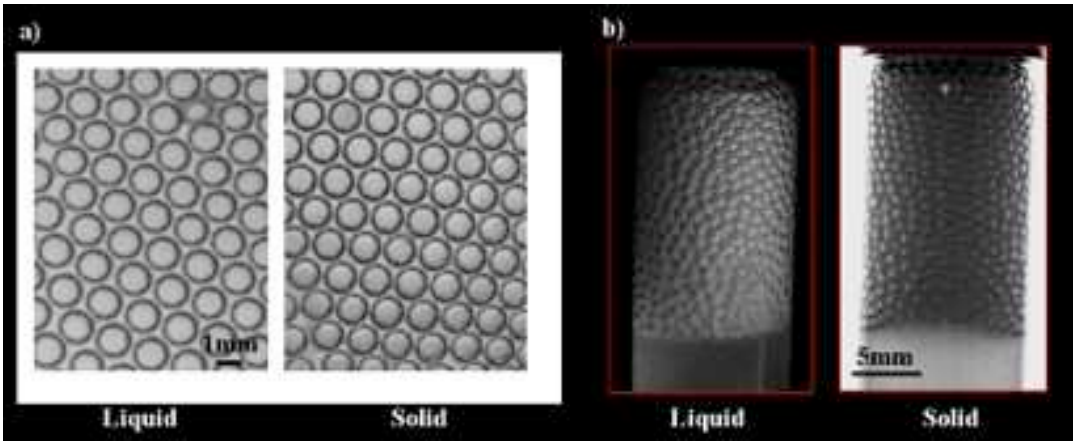

Figure 7.23: Images of PU monodisperse foams a) 2D foam and b) 3D foams at the liquid state (left side of each image) and solid state (right side).

The foams were very stable and kept the same shape/structure during the solidification. We notice from Figure 7.24 that the foams obtained using the catalyst are more stable then those without catalyst which drain and destabilise after a few hours. Reducing the solidification time from 6-7 hours without catalyst to 1 hour using the catalyst, freezes the foam and preserves its structure. The absence of catalyst has nevertheless a significant advantage since it permitted us to obtain foams with low density, which are more complicated to generate, by simply prelevating the upper part of the drained foam sample. This is illustrated in Figure 7.25 where one can see the liquid fraction difference between the upper and the lower part of the drained foam.

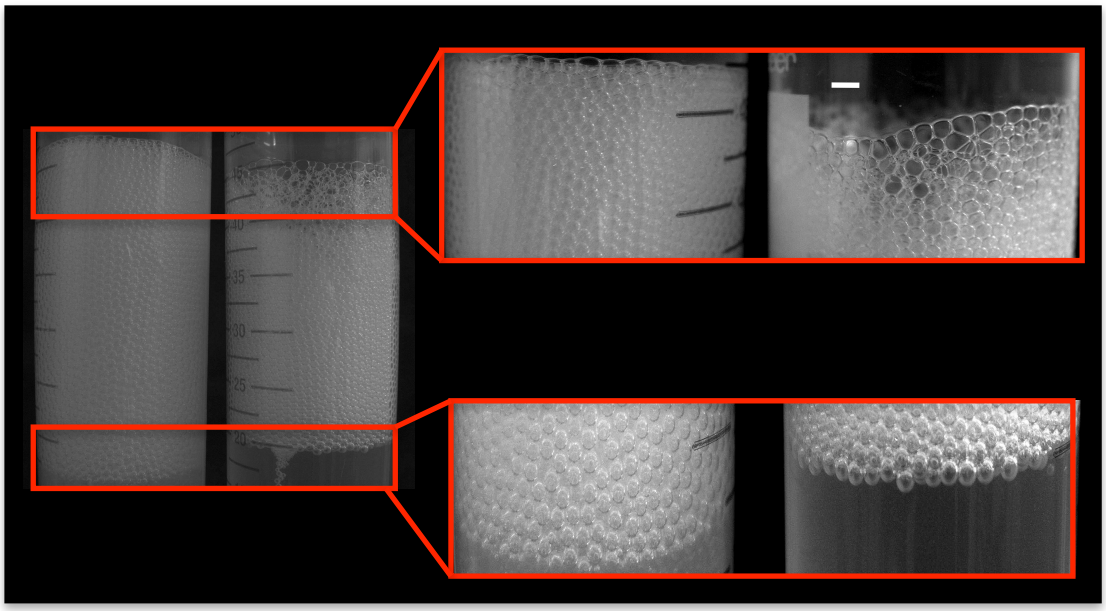

Figure 7.24: Monodisperse solid PU foam obtained with (left) and without (right) catalyst. The foams are obtained using the same T-junction and the same flow rates. The images are zoomed to see clearly the effect of the catalyst on foam density and structure.

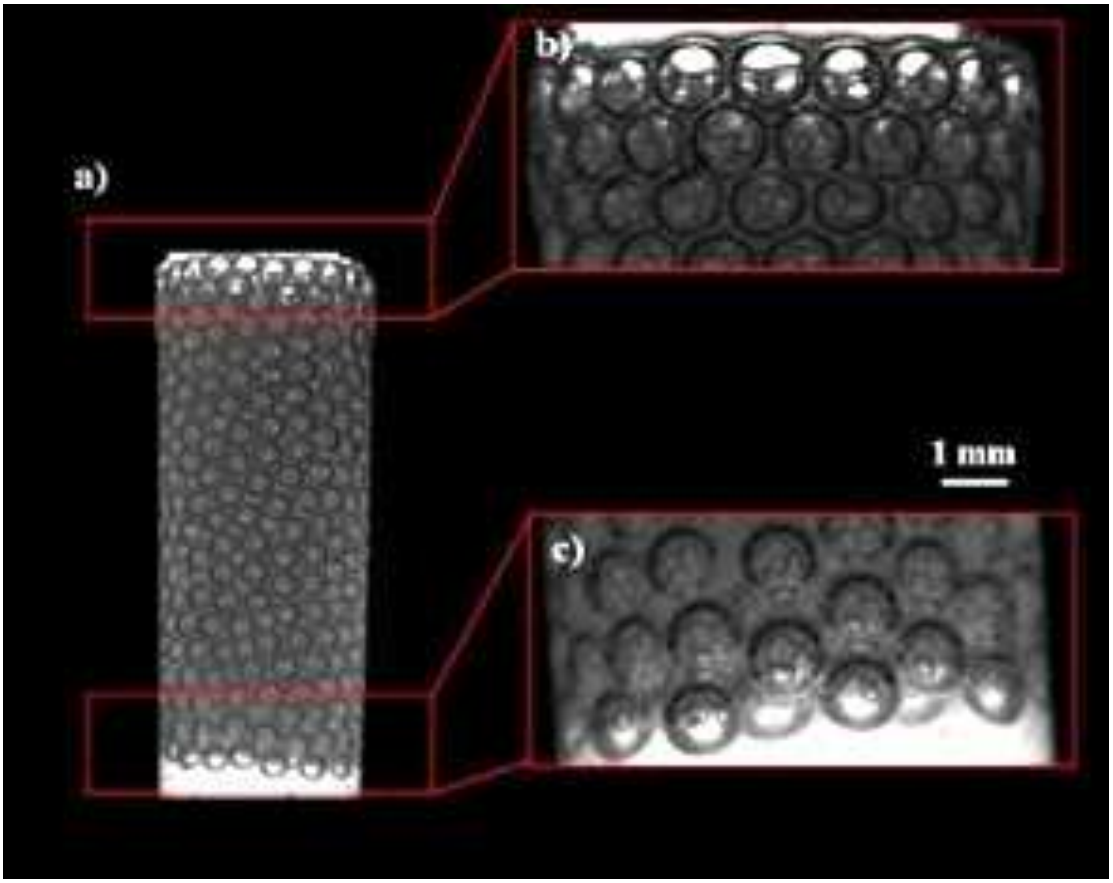

Figure 7.25: a) PU solid foam. b) Effect of drainage on the foam structure: Polyhedral bubbles at the top of the foam (dry foam). c) Effect of the drainage on the foam structure: Spherical bubbles in the bottom of the foam (wet foam).

We were able to obtain foams with a wide range of shapes, order, cell structures, density and bubble sizes as is well illustrated in Figure 7.26.

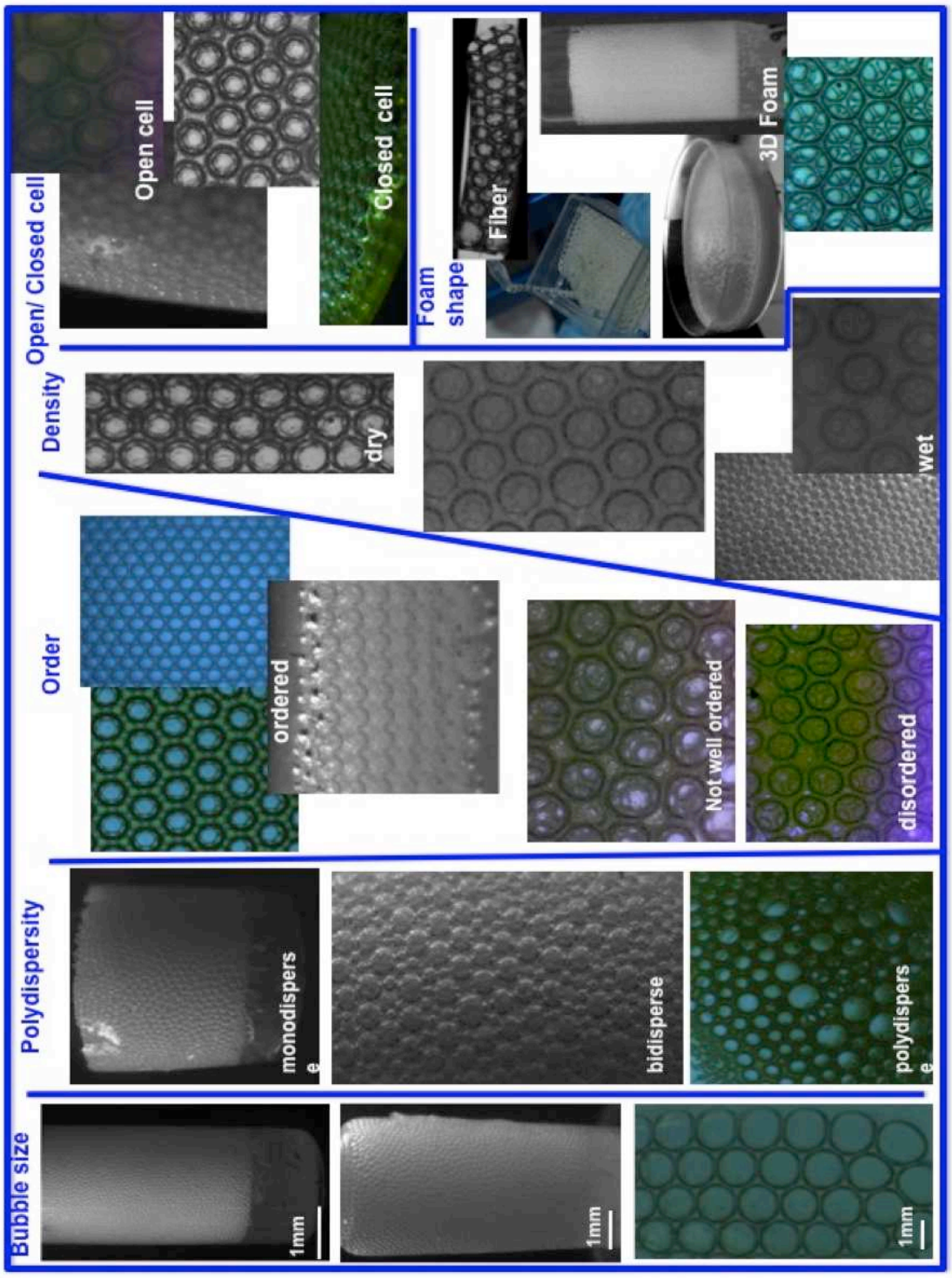

Figure 7.26: Solid polymer foams having different shapes and structures

The freshly generated foams were left to dry for two days, then they were extracted from their containers and observed under the microscope in order to study their crystalline structures. We found that the bubbles have a preference to self-organise into FCC structure (Section 2.5.2) as shown in Figure 7.27b.
We were also interested in the open/closed cell structures of these foams. Figure 7.28 shows the different cell structures obtained.

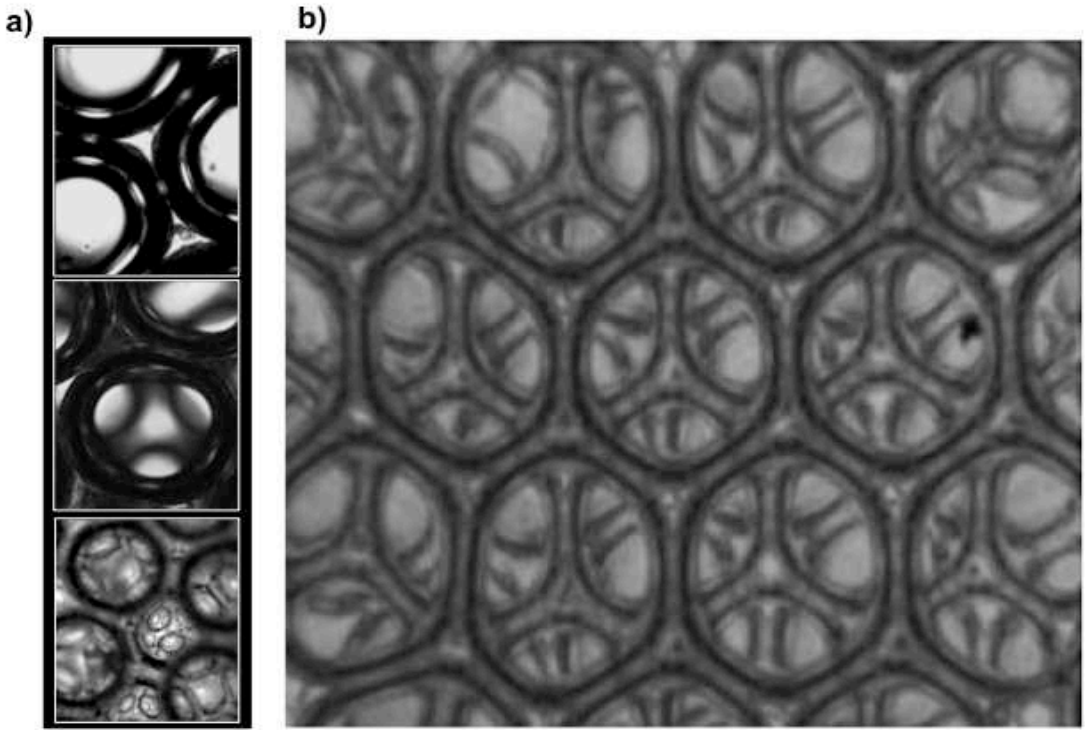

Figure 7.27: a) A microscope view of the different bubble structures. From up to down: one, two and three bubble layers. The average bubble size is about 1.1 mm. b) Close-up example of an FCC structure (ABC) of solid PU foam after its complete solidification.

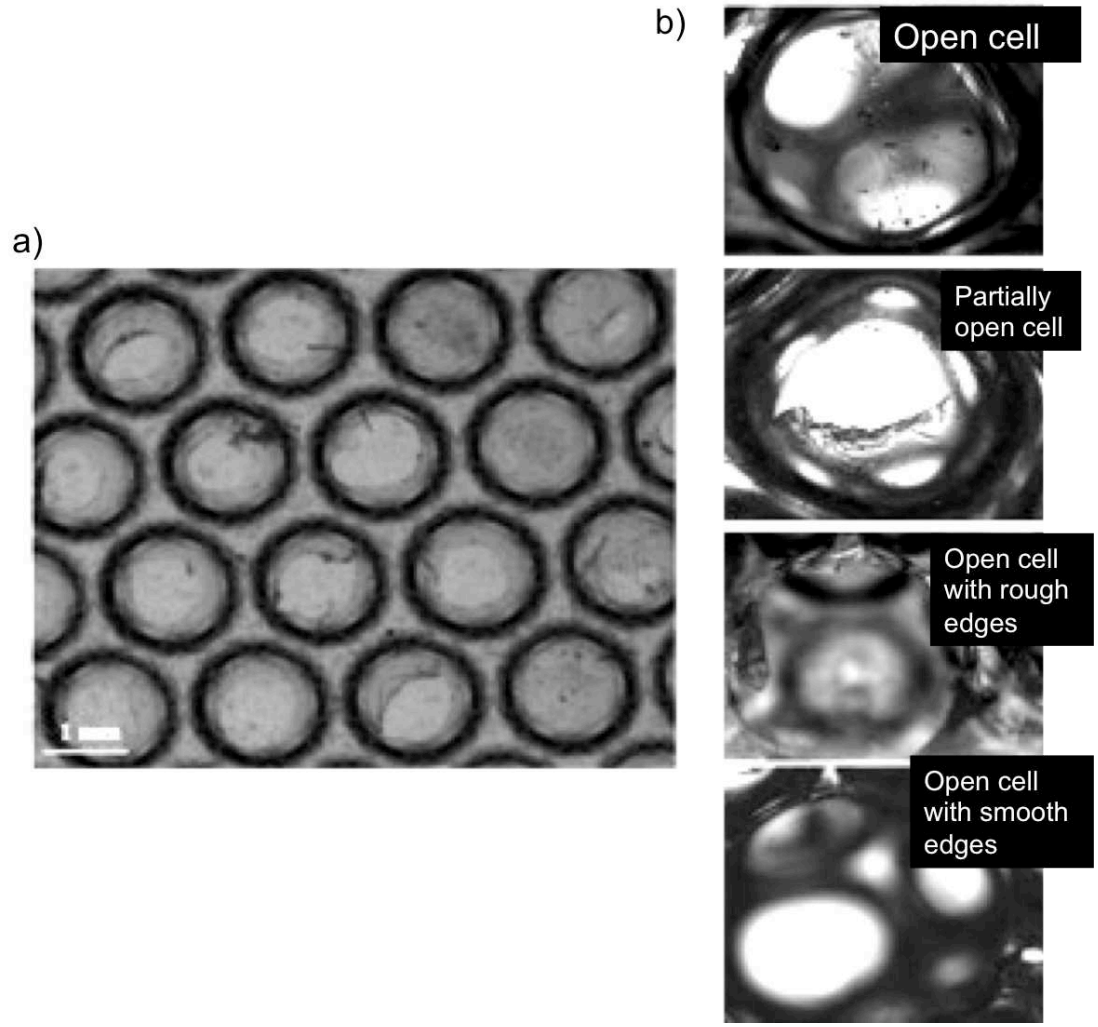

Figure 7.28: a) 2D PU solid foam having different cell structures. b) A microscope view of different cell structures. From top to bottom: Closed cell, partially open cell, completely open cell with rough edges and completely open cell with smooth edges.

We also changed the mixing ratio during the foaming process, and we observed that for a mixing ratio superior to 1:1, the foam is very rigid due to the formation of urea. This is illustrated in Figure 7.29 where two foams having different mixing ratios present two different mechanical behaviours under the same applied force.

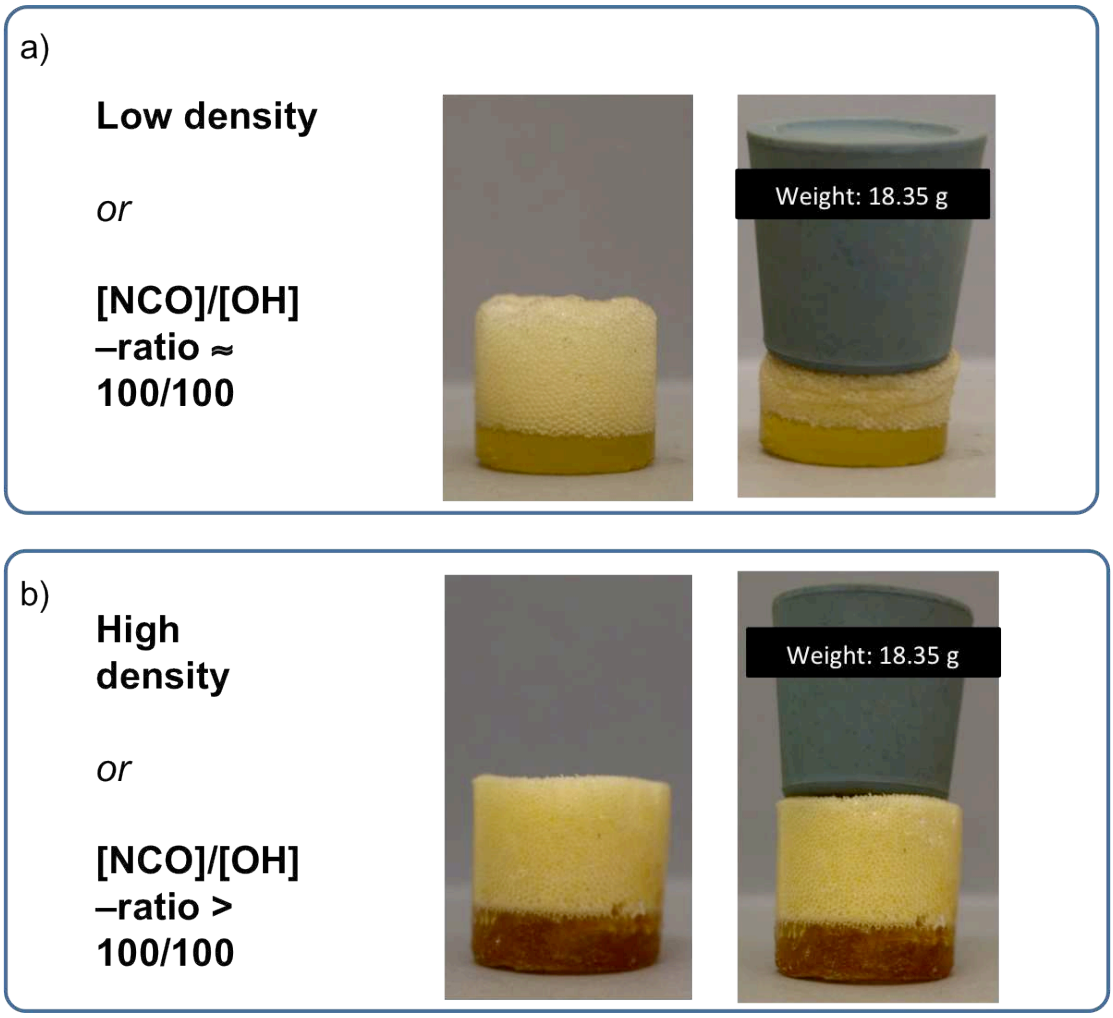

Figure 7.29: Pictures illustrating the influence of the mixing ratio on the mechanical properties of PU foam : a) Low density foam. b) High density foam.

7.8 CHARACTERISATION OF THE MECHANICAL PROPERTIES OF PU FOAMS

7.8.1 Introduction

The mechanical properties of solid foams arise from an intricate interplay between the mechanical properties of the polymer itself and the foam structure (Section 2.7.2). A simple macroscopic deformation of the foam results in a range of microscopic deformations of different elements of the foam structure, leading to a macroscopically complex response. For example, the Plateau borders may be compressed, bent, then can buckle or break, the films may stretch or rupture.

Foam can be deformed in different ways, combining shear and compression. Of particular interest here is the response of foam to simple (uni-axial) compression. Figure 7.30a and b show typical stress (σ) – strain (ε) responses of an elastomeric foam and an elastic-plastic foam, respectively. Both curves are characterised by an initially linear regime, whose slope gives the **Young's modulus** of the foam.

$$E_F = \frac{\Delta\sigma}{\Delta\varepsilon} \qquad \textbf{(6. 4)}$$

The linear regime is followed by a non-linear one in which the Plateau borders buckle elastically (Figure 7.30a) or deform plastically (Figure 7.30b) leading to the appearance of a more or less pronounced plateau in the stress-strain relation, which is characterised by a **pleateau stress σ_{el} or σ_{pl},** respectively. This plateau is followed by a strong increase towards the **densification strain** ε_0 at which the structure collapses, opposite bubble walls start to touch each other and one starts to probe the mechanical properties of the polymer of which the foam is made.

In the linear regime, the uni-axial compression of a material is described by the Young's modulus and the Poisson ratio ν, which describes the deformation of the material in the direction orthogonal to the compression. A uni-axial compression is a combination of a pure shear and a purely compressive deformation, which is why it can alternatively be described using the shear modulus K and bulk modulus μ of the material, in isotropic materials, and one has (both descriptions are related by the simple relationships)

$$E = \frac{9K\mu}{3K + \mu} \qquad \textbf{(6. 5)}$$

$$\nu = \frac{3K - 2\mu}{2(3K + \mu)}. \qquad \textbf{(6. 6)}$$

The stress-strain curves shown in Figure 7.30a and b are universal in the sense that they can be normalised by the Young's modulus E_P of the polymer. As a result, the quantitative features depend almost entirely on the **foam structure** and the **foam density ρ_F**. Figure 7.31 shows how the stress-strain response of an elastomeric foam varies with the normalised foam *density* $\rho_r = \rho_F / \rho_P$, which is equivalent to the solid fraction of the foam. The curves display the pronounced increase of the elastic modulus E_F and the plateau stress σ_{el} of the foam with density and the accompanying decrease of the densification strain ε_0 (i.e. shortening of the plateau length).

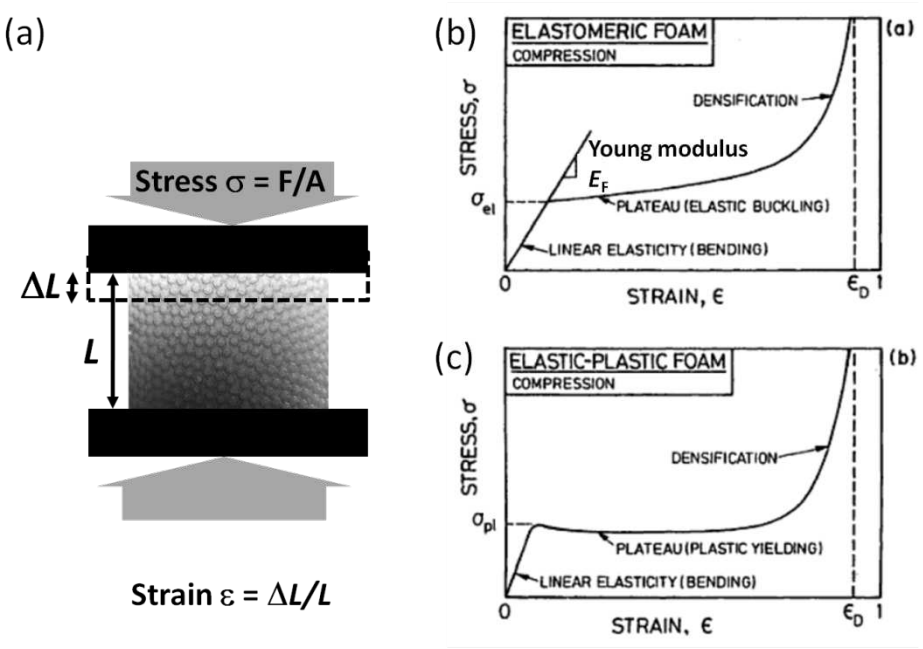

Figure 7.30: (a) Schema of a typical compression test. (b) and (c) Typical stress-strain response curves of elastomeric and elastic-plastic foams, respectively (from [23]).

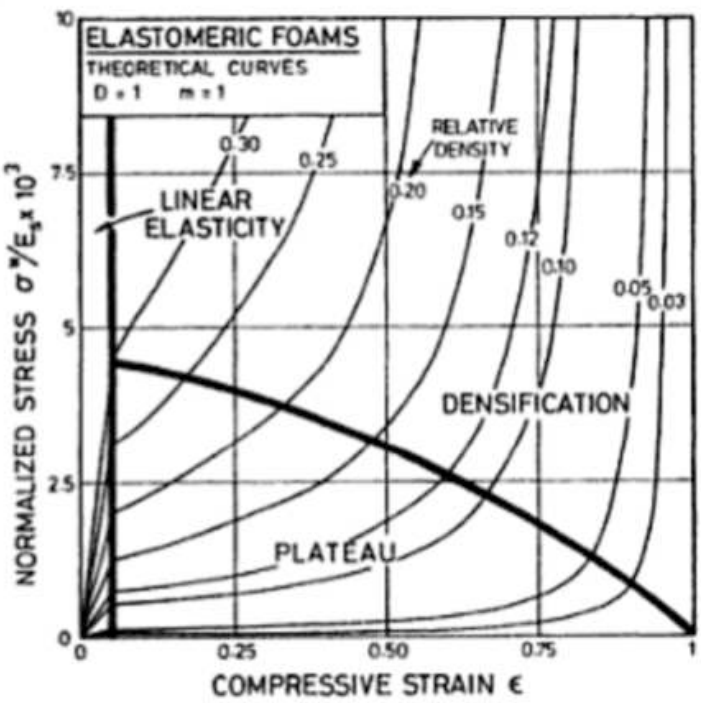

Figure 7.31: Variation of the stress-strain behaviour with foam density from (Figure 5.35 in [23]). The stress has been normalised by the Young's modulus of the polymer.

Up to now, quantitative investigations of the influence of the *macro- and micro-structure* of foams, has mostly been left to computer simulations [24-26], due to the difficulty of generating foams with sufficiently well-controlled micro- and

macro structuring and density. The goal of this part of the thesis was therefore to provide a technique to generate such well-controlled foam samples.

Due to time constraints, the mechanical investigations of our foams have to remain indicative and limited to measurements of the Young's modulus of different foam structures, which should be much less sensitive to the foam structure than other stress-strain features, like the onset of the plateau stress. However, we believe that our investigations illustrate nevertheless the beginning of a new area in which polymer foams with well-controlled structures will be exploited in order to avail of purpose-designed properties. This is very likely to go well beyond the exploitation of simple mechanical properties. In particular, acoustic properties come to mind.

7.8.2 Models

Foams are a sub-class of **composite materials**, in which the dispersed composite is a gas. The modelling of effective mechanical properties of composites has experienced a great boost over the last few decades. On the one hand this is due to the outstanding properties of these materials, which find increased use in applications. On the other hand, this results from the availability of ever-increasing computer power and computational models which now allow to simulate the complex behaviour of such materials and therefore provide quantitative comparison with experiments and analytical models. At the current stage, modelling efforts have concerned mostly the influence of the volume fraction of the dispersed phase. With the increasing possibility to control also the structural organisation of the dispersed phase, researchers are now beginning to show a growing interest in linking the *microstructure* and resulting *micro-mechanics* to the *macroscopic* mechanical response. Apart from simplified systems (such as explorations of two dimensional systems [27]), the latter subject is very much at its infancy.

Modelling efforts of gas inclusions in elastic solids can be divided into two main groups (Figure 7.32), which are scientifically and historically anchored in two different scientific communities. On the one hand there is the *solid foam community*, which considers relative densities around and below the close-packed configurations of gas inclusions (typically $0 < \rho^* < 0.5$) (Section 2.5). On the other hand, there is the *porous media community*, which considered densities around and above the close-packed configuration (typically $0.3 < \rho^* < 1$). The close-packed configuration consists of close-packed spherical holes, with the overall material density depending on the size distribution and organisation of the spheres (Section 2.5.2).

In the **low-density limit** the inclusions deform into polyhedral shapes, which may either be open- or closed cell (2.7.2). Here, modelling efforts tend to consider the behaviour of interconnected strut networks [23] with well-defined topologies, in which the struts are connected either by their end-points only (open-cell), or, additionally, by the presence of thin films (closed-cell). In the **high-density limit**, spherical inclusions are evenly distributed throughout the solid matrix. At sufficiently low density, the mechanical action of these inclusions

can be considered as independent ("dilute limit") whilst they start to interact increasingly below this limit.

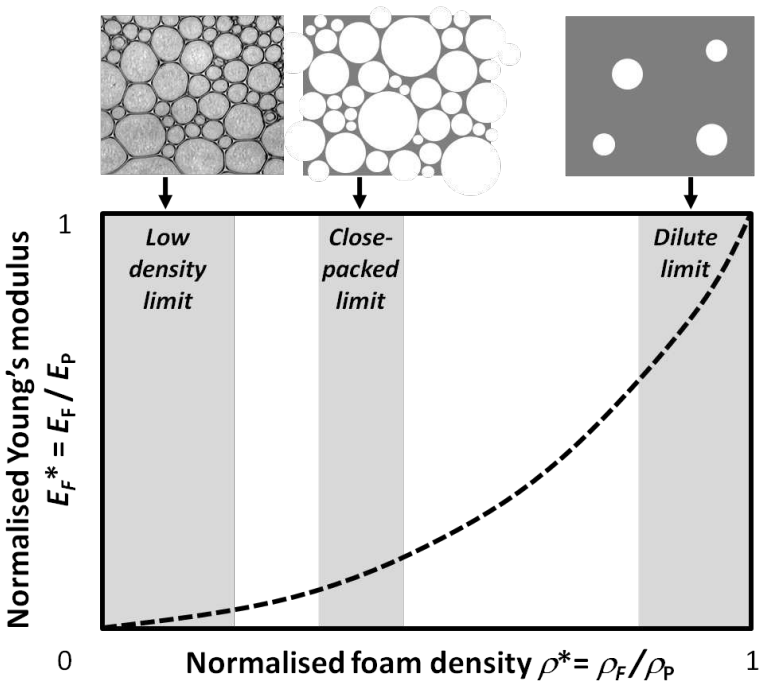

Figure 7.32: Variation of Young's modulus with foam density. The precise shape of the curve depends on the structural properties of the foam, i.e. on the polymer distribution, and on the polymer properties. Modelling tends to be divided into different density regimes, as indicated by the different zones.

As we have seen in Section 7.8.1, the mechanical response of composite materials is very complex. In the following we shall therefore limit our discussion to the Young's modulus only. The various results are summarised in Figure 7.33.

In the **low density limit**, Gibson and Ashby [23] established models which have proven to capture well the general behaviour of foams after a wide range of experimental and computational investigations [26, 28-30]. Using micro-mechanic approximations of simple geometrical models, Gibson and Ashby showed that the main mechanism which determines the Young's modulus of **open-cell foams** results from the bending acting of the struts. Due to the three-connected foam geometry (section 2.7.2) this leads to the following power-law dependence

$$E_F{}^* = C(\rho^*)^2, \qquad \textbf{(6. 7)}$$

Where C is a numerical prefactor close to unity.

In the case of **closed-cell foams**, the stretching of the films needs to be taken into account additionally to the strut bending mechanics. This stretching makes the foam stronger, which is why Equ. (6. 4) is modified to give

$$E_F{}^* = C_1\vartheta^2(\rho^*)^2 + C_2(1-\vartheta)\rho^*. \qquad \textbf{(6. 8)}$$

Here C_1 and C_2 are numerical constants of the order unity. ϑ is the fraction of polymer contained in the struts, hence (1-ϑ) is the fraction of of polymer contained in the films. Commonly, researchers assume that $0.6 < \vartheta < 0.8$. Figure 7.33 shows results of this model for $\vartheta = 0.6$ and for $\vartheta = 0.8$. In the low density limit, the Young's modulus is expected to depend little on the structure of the foam, since it is dominated by its topology, which is fixed by the liquid foam topology (Section 2.3). However, some fine differences have been seen in the case of ordered foam structures, but the work is too preliminary to be discussed here.

In the **high density limit** a wide range of models is available [31-34], relating the Young's modulus to the density of the composite material and the Poisson ratio of the polymer. Most models which have proven to capture well the properties of high density foams, follow closely a power law dependence

$$E_F^* \sim (\rho^*)^n, \qquad \textbf{(6. 9)}$$

With n depending on the Poisson ratio and $n \approx 2$ for typical Poisson ratios encountered with standard polymers. The higher the Poisson ratio, the higher the exponent, i.e. the more the $E(\rho)$-curve curves away from a straight line. Equ. (6. 9) had been established for n = 2 in an empirical model by Moore [33] (see Moore's law in Figure 7.33) and has been derived more rigorously using differential schemes [35, 36]. Interestingly, this power law dependence is the same as the one derived by Gibson and Ashby for open cell foams in the low-density limit (Equ. (6. 7)) using completely different arguments. However, as we shall see later, the prefactors differ between the two cases (attention, this difference in prefactor is not shown in Figure 7.33). Hence, as a rule of thumb, this law may be used to obtain a first approximation of how the Young's modulus varies with density over the entire density range.

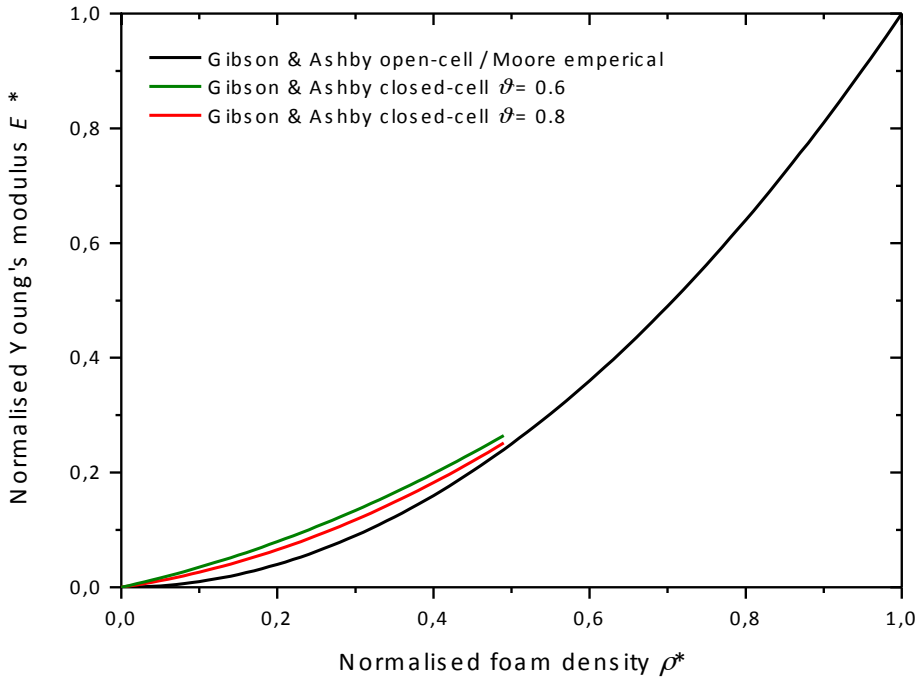

Figure 7.33: Summary of different models discussed in this section.

In general, one sees that the elastic modulus depends much more strongly on the foam density than on the detailed foam structure or polymer properties.

7.9 COMPARISON WITH EXPERIMENTS

7.9.1 Pure polymer properties

As discussed in Section 7.8, the results of the characterisation of the foam properties are normalised by those of the pure polymer in order to obtain homogeneous and comparable results. We thus performed compression tests firstly on the pure polymer using the compression machine (Section 4.7). The corresponding stress-train curve is presented in Figure 7.34. The stress increases smoothly with the increasing strain and the curve does not show a Plateau due to the high density of the polymer. The Young's modulus is given by the slope of the linear regime shown on the inset of Figure 7.34 and is found to be equal to E_P = 0.9 MPa which is similar to the results of the compression tests performed in BASF (see Appendix D). We will be using this value of the Young's modulus to normalise the Young's modulus of the studied foam samples.

It may be surprising to the reader that the linear regime does not start from zero deformation. This is due to the fact that the samples are not cut in a perfectly parallel manner. Homogeneous bulk compression of the entire polymer is therefore achieved only for deformations above approximately 0.1.

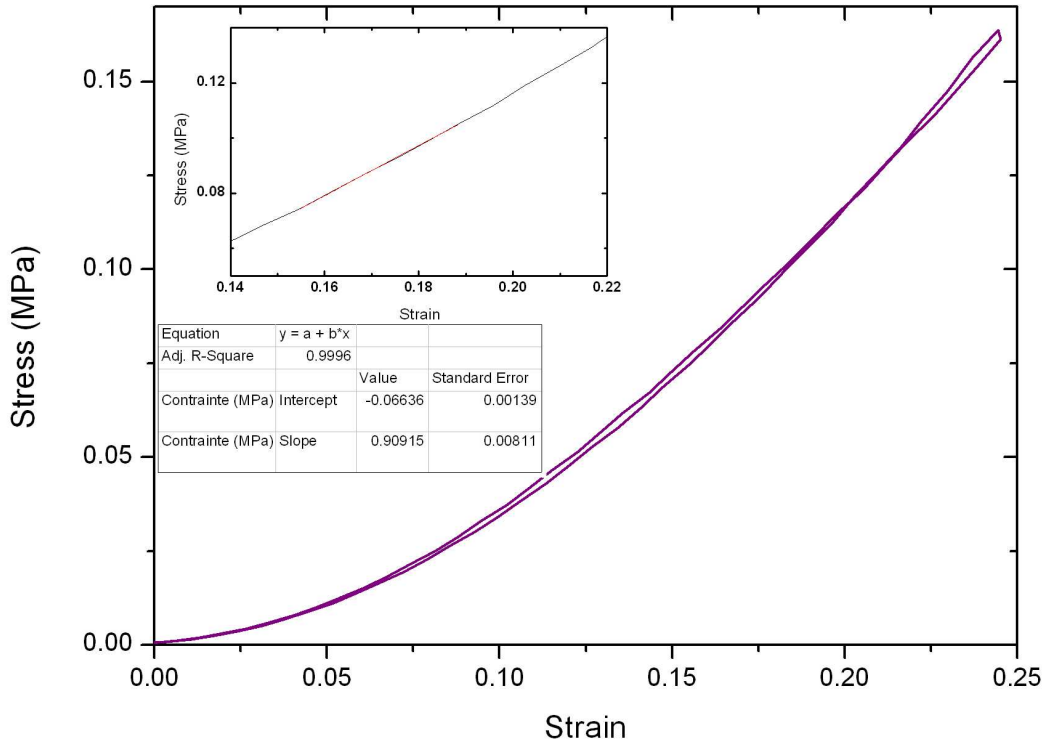

Figure 7.34: Stress-strain curve of the pure polymer. The inset curve shows a linear fit in the linear regime. The Young's modulus $E_P \sim 0.9$ MPa is given by the slope of this linear region.

7.9.2 Foam properties

Figure 7.35 shows a typical stress-strain curve of a monodisperse polyurethane foam which has undergone an orthogonal uni-axial compression. One can clearly see the different features discussed in Section 7.8.1. The initial linear regime where the material deforms elastically corresponds to the linear region whose slope corresponds to the Young's modulus. As the stress increases, the material starts to buckle and the curve shows a plateau which is more pronounced for low density foams. In Figure 7.35 the plateau is short because of the relatively high density (270 g/l) of the corresponding foam. This plateau is followed by a high increase in stress towards the densification strain (here ε_0=0.82).

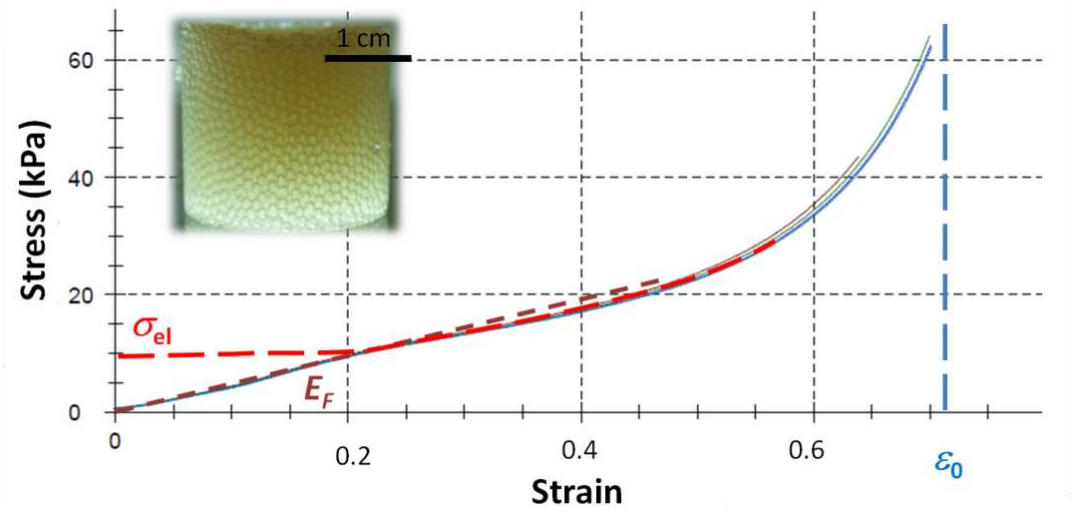

Figure 7.35: Typical stress-strain curve of a PU monodisperse foam. Here we indicate the linear regime with slope E_F, the plateau stress σ_{el} and the densification strain ε_0.

The influence of the foam density on the length of the plateau and on the Young's modulus value is illustrated in Figure 7.36 where the stress-strain curves of four monodisperse foams with different densities are plotted in the same graph. These curves display the expected increase in the Young's modulus with density and a shortening in the plateau length as the density increases as predicted in the literature (Figure 7.35). The curves for the high-density foams are less smooth than the curves for the low density one since the samples were much smaller (1 cm^3 instead of 10 cm^3) and we were having problems to cut them in a properly parallel manner.

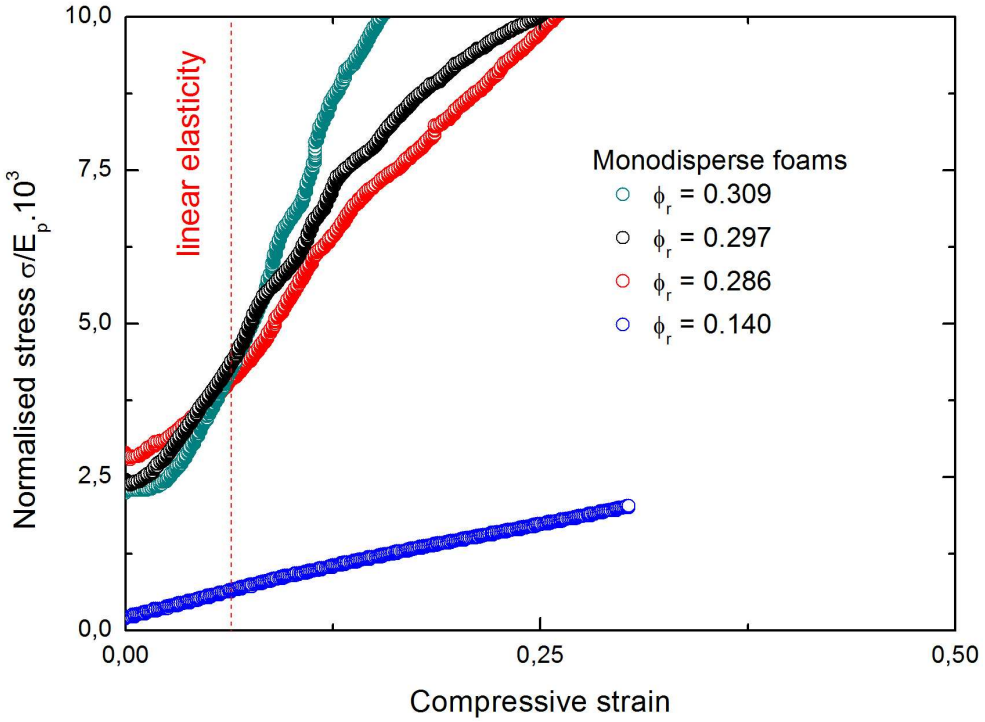

Figure 7.36: stress-strain curves obtained for four monodisperse foams with different densities. The mechanical response of these foams change drastically with density.

As mentioned before, the mechanical investigations performed by us were focused only on the measurements of the Young's modulus of different foam structures due to limited time. The results of these measurements are gathered in one main curve (Figure 7.37), which displays the normalised Young's modulus E_F/E_P for each foam sample as a function of the relative foam densities. Additionally to the monodiserse foams, this curve contains measurements of polydisperse foam samples which we generated by simple beating using the same chemical formulation as the one used for the generation of the monodisperse foams.

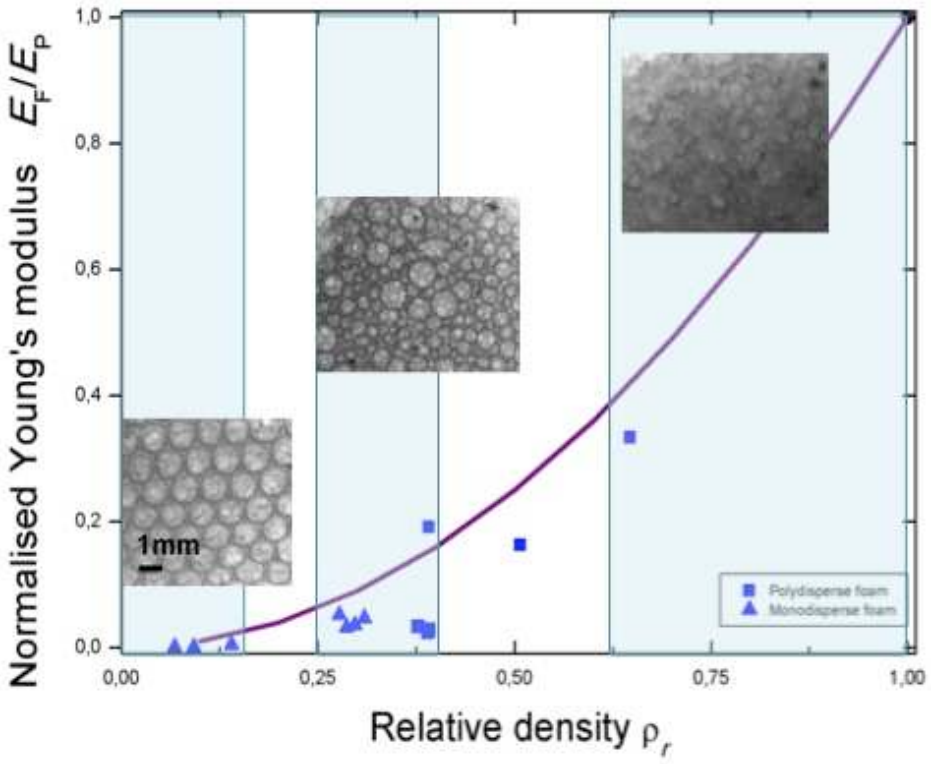

Figure 7.37: Variation of the normalised Young's modulus of monodisperse and polydisperse PU foams with the normalised foam density. A picture of a typical foam is shown for each density zone. The line corresponds to Moore's law (Equ.(6. 9)).

We notice from Figure 7.37 that the monodisperse foams are concentrated in the low to "medium" density regions, whereas the polydisperse foams are denser and have thus higher elastic modulus. This is mainly due to the foam generation technique: while the millifluidic technique allows reaching very low foam density values by adjusting the gas and liquid flow rates, the generation of low-density, polydisperse foams from highly viscous solutions is a more complicated issue. This is due to the fact that polydisperse foaming techniques do not control the final foam density and entrain a lot of liquid which does not have time to drain before solidification.

When we plot the normalised Young's modulus as a function of the relative density in a log-log scale (Figure 7.38), we can clearly see that the data fit very well the quadratic dependence on the density: Gibson and Ashby law (Equ. (6. 5) for open cell foam in the low-density limit and the Moore model (Equ. (6. 9)) in the high-density one. However, even though these two models have the same power law dependence, they have clearly different pre-factors. These prefactors are equal to 0.157 and 1 in the low and high-density case, respectively.

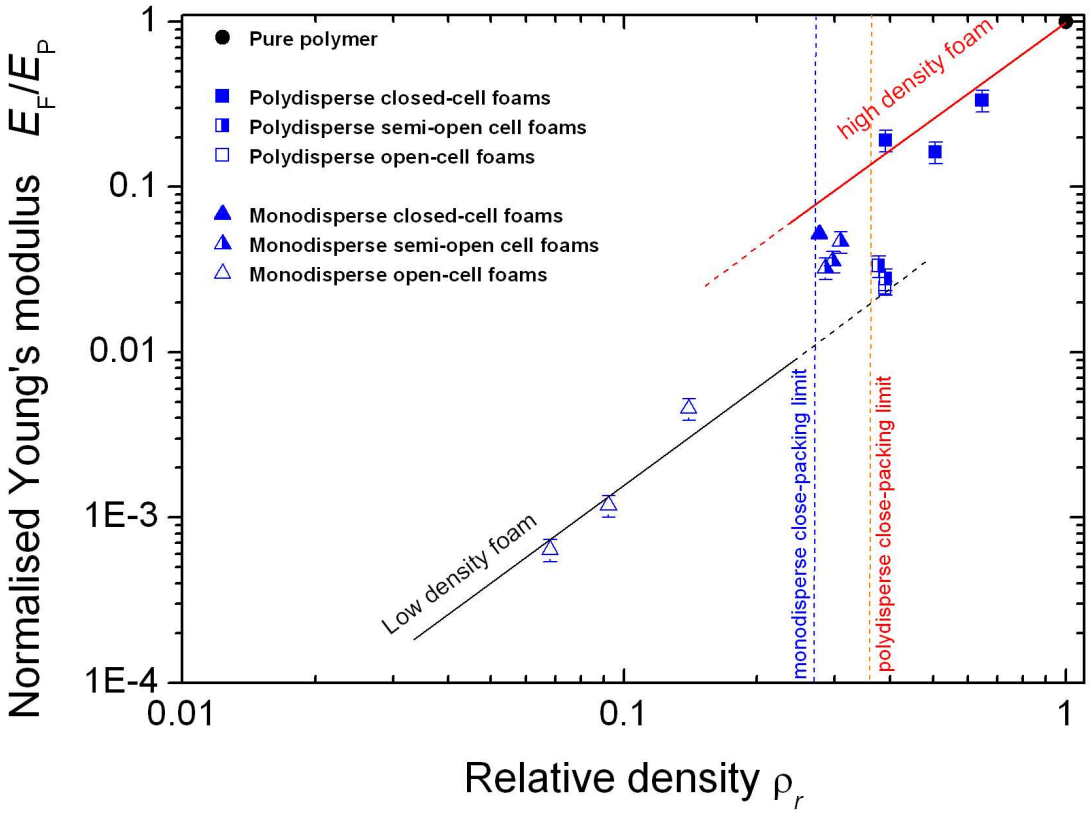

Figure 7.38: Variation of the Young's modulus of monodisperse and polydisperse PU foams with the foam density in a log-log scale

7.10 DISCUSSION

The low-density limit is characterised by the presence of essentially open-cell foams with polyhedral structure. In fact, the thin films are very fragile and often rupture before or during their solidification under the effect of drainage and/or the liquid suction by the Plateau borders which creates an open-cell structure (section 2.7.2). Pictures of some of the open-cell foams obtained in the low-density limit are shown in Figure 7.39.

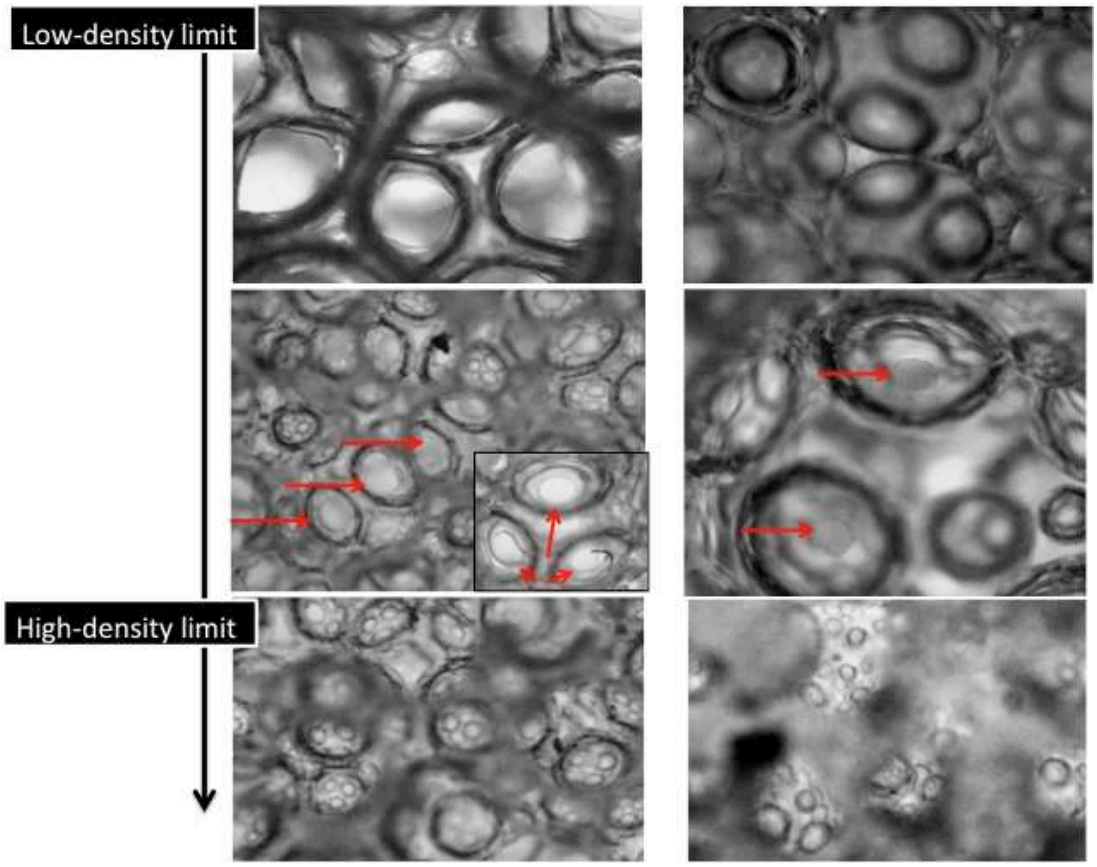

Figure 7.39 : Pictures of the cell structures of the PU LEFT) monodisperse and RIGHT) polydisperse foams generated by us for different densities. The red arrows show the open windows of the foam films. In the low density limit all the cells are open.

In the high-density limit, the foams have spherical bubbles which are separated by thick polymer films and thus a closed-cell structure (Figure 7.39). This is is described well by Moore's law.

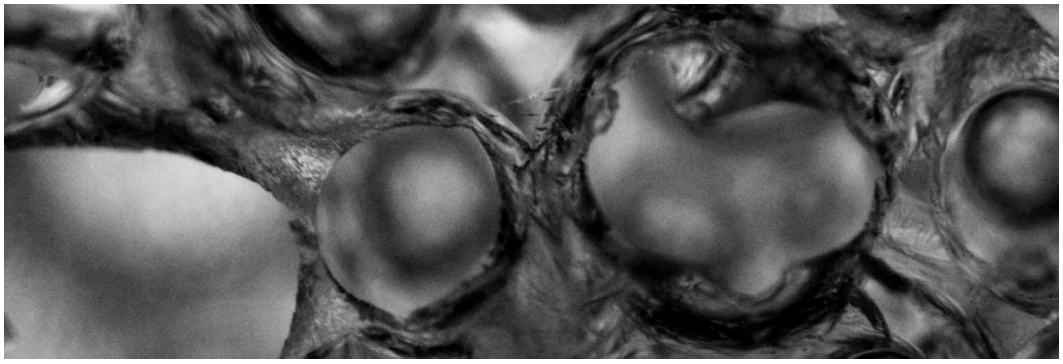

Figure 7.40: Picture of a high-density foam with open cells. This sample was prelevated from the top of a polydisperse foam obtained without catalyst.

Surprisingly, even the foams approaching the close-packed limit ($\rho_r \approx 0.3$) are captured well by the description of open-cell foams, even though this model is supposed to hold only for low-density foams [23]. However, a close look to the structure of these foams under the microscope (Figure 7.40) revealed reveals that even these foams have either semi-open or totally open structures. This is due to the fact that these foams remain liquid for at least one, often more than two hours before solidification. The foams undergo thus a pronounced drainage and an important attraction of the liquid to the Plateau borders (or struts). These samples taken from the upper part of the drained foam have therefore very thin films which most of the time rupture partially or totally during the long solidification process.

Moreover, even if the films to not rupture, they will be very thin. This is translated in terms of modelling by the fact that almost all the liquid is concentrated into the foam struts (ϑ high) and that the remaining polymer in the thin films is negligible (1-ϑ *negligible*). Therefore, the equ.(6. 6) changes to become $E_F{}^* = C_1\vartheta^2(\rho^*)^2$, which is the same power law of the Gibson and Ashby model for open cell foams. In this sense, our foams are very different to those produced with common industrial techiques, which solidify more quickly and therefore maintain a ϑ around 0.7 and therefore a pronounced influence of the film stretching.

The two fit curves of the low- and the high-density limits happen to be two "envelope curves" for all the PU foams produced by us which have different structures. Between these two density limits, one can find partially open foams with either monodisperse or polydisperse structures. This gives to these foams an elasticity higher than that of low-density foams due to the stretching of the films, which they contain. Nevertheless, their Young's moduli remain lower than the high-density foams since they contain only a given percentage of closed cells.

Interestingly, the transition between the two limiting cases is surprisingly sharp, probably due to the negligible role of the films even at high densities (as discussed above). Moreover, depending on the monodispersity and bubble organisation, the transition itself seems to have two envelopes (vertical, dashed lines in Figure 7.38): the first transition occurs at the "monodisperse close-packing limit" ($\rho_r \approx 0.26$, blue dashed line) and the second one at the "polydisperse close-packing limit" ($\rho_r \approx 0.36$, red dashed line) which are transitions from the dry foam limit to the wet foam one. This observation must be a natural consequence of the fact that it is around this limit that bubbles start to loose contact and that thick polymer films can be maintained between bubbles during solidification.

It is important to note that we have not specified the different bubble sizes of the samples. We find that as predicted by the modelling, the Young's modulus is independent of the bubble size.

Even though we do not have enough quantitative data to make a solid statement here, we would therefore like to propose the following hypothesis for our foams

(see Figure 7.41), taking into account our measurement, our observations and the modelling/theoretical efforts from the literature:

The Young's modulus of PU foams generated by our approach (physical blowing and simple chemistry) is **independent of the bubble size**. The key parameter in the two regimes (low and high-density regimes) is the foam density with

$$\frac{E_F}{E_P} = \alpha\rho^2, \qquad \textbf{(6. 8)}$$

However, both limits are described by different pre-factors with α =0.157 in the low-density limit and α= 1 in the high density limit. The foam structure plays a role for intermediate densities, notably around the close-packed density. The latter provides limiting densities around which the transition between the low and high-density limit occurs.

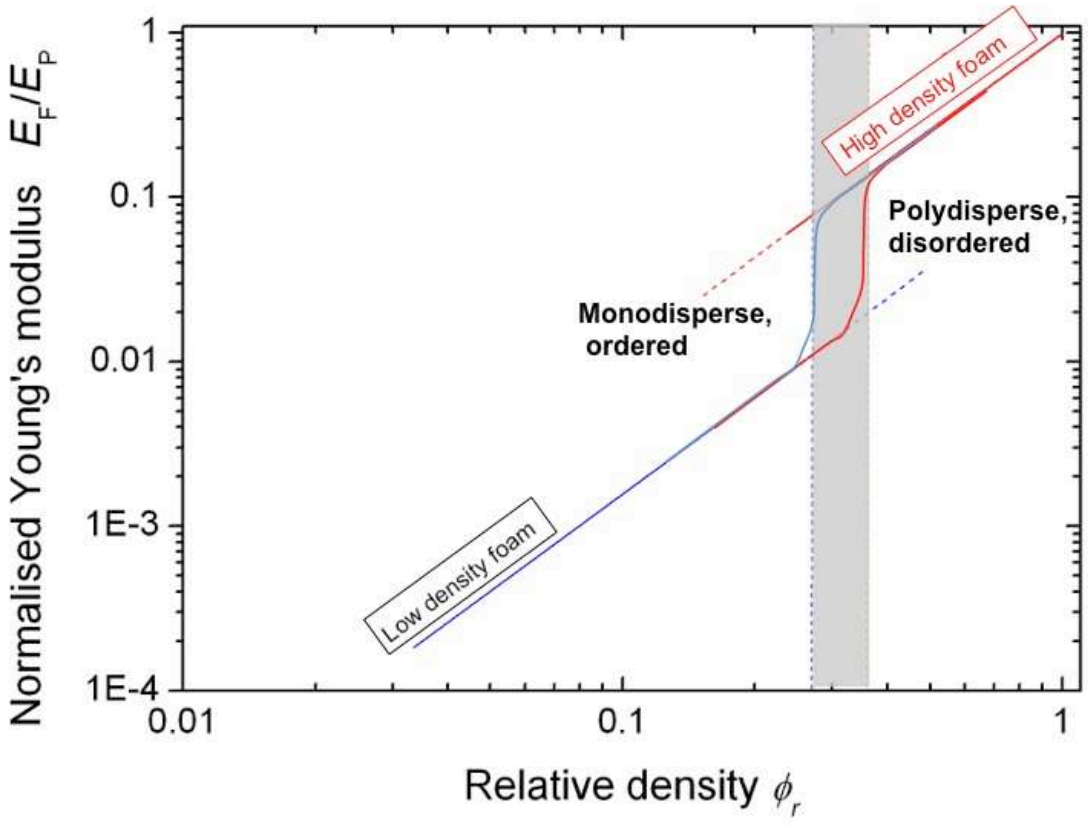

Figure 7.41: A schematic illustration of the transition in the wet limit for monodisperse and polydiserse foams

This hypothesis will have to be verified in the near future with more systematic measurements, in which bubble size, bubble size distribution and polymer properties are systematically varied. It will also be of interest to tune

solidification times in a manner to control more quantitatively the parameter ϑ in Equ. (6. 6). The two-step approach provided by us using millifluidics provides such control.

7.11 CONCLUSION AND OUTLOOK

We proposed here a new reliable approach for the generation of ordered monodisperse polyurethane foams using Lab-on-a-Chip flow chemistry. We showed in our study how this technique offers a good control over some foam properties such as bubble size and foam density. The foam cell structure was correlated to the foam density. It was in fact found that low-density foams tend to have open cells and high-density foams tend to have closed cells. This issue is of a high interest in both academic and industrial fields. It has been indeed the subject of various scientific studies during the last five decades which related the open-cell structure of polyurethane foams to many phenomena among which there are the effect of the surfactant siloxane backbone to the polyether ratio, the precipitation of urea as an extension to the solid precipitation defoaming mechanism, and many other hypothesis [16, 20, 37-40]. Investigations should therefore be pursued in a more systematic fashion in order to elucidate the mechanisms behind the foam cell structure.
We also studied quantitatively the mechanical properties of polyurethane foams and correlated them to the structure of the corresponding foams. It was found that the general behaviour of the stress-strain curves obtained for all foam samples are similar to those found in the literature [23]. We have validated the effect of the foam density on the mechanical behaviour of the foam (shortening of the plateau length and increase of the Young's modulus with density) using our data.

The mechanical characterisation data fit well with what is predicted in the elastic foam mechanics literature: In the high-density limit, foams have mainly closed-cell structures and the Young's modulus vs. density follows a power law (ρ^2). In the low-density limit (or dry limit), the bubbles are polyhedral and have most of the time an open structure or films which are so thin that their contribution to the mechanical properties may be neglected. In this case the contribution of the film stretching can be neglected in the mechanical response and again a quadric dependence of the Young Modulus with foam density is obtained yet with a prefactor of about one order of magnitude lower than the one in the high-density limit.

The foams with densities around the close-packing limit present a partially open-structure and form a well-defined transition between the two limit models.

Within our investigations, the bubble size (200 micrometer – 2 mm) was found to have no influence on the general mechanical response of all the foams, which we produced.

The influence of monodispersity on the Young's modulus is negligible since no significant difference between monodisperse and polydisperse Young's moduli was observed. However, the monodispersity was found to change the trend of the overall stress-strain curve. In fact the monodisperse foam curve has a more pronounced plateau than the polydisperse one which is seemingly due to the homogeneous response under load of equal-sized bubbles which deform all at the same time and in the same manner.

These results represent a first step in the investigations of the mechanical behaviour of polyurethane foams. The study of the effect of monodispersity on the general mechanical response may be of high interest for both academic and industrial questions.

Moreover, an exploration of the effect of the chemical composition of the polyurethane foams on the mechanical properties should be conducted by using polyols of different structures and by studying different mixing ratios which is expected to change drastically the properties of the final polyurethane foams.

BIBLIOGRAPHY

1. Ionescu, M., *Chemistry and Technology of Polyols for Polyurethanes*2005, Shawbury, Shrewsbury, Shropshire, SY4 4NR, UK: Rapra Technology Limited.
2. Leppkes, R., *Polyurethanes Material with many faces*, ed. V.m. industrie2003.
3. Ionescu, M., *Chemistry and Technology of Polyols for Polyurethanes*2005, Shawbury, Shrewsbury, Shropshire: UK:Rapra Technology Limited. 586.
4. Frey, J.H., et al., *Low emission, cell opening surfacants for polyurethane flexible and rigid foams*, 1998.
5. Han, M.S., et al., *Effects of Silicone Surfactant on the Cell Size and Thermal Conductivity of Rigid Polyurethane Foams by Environmentally Friendly Blowing Agents.* Macromolecular Research, 2009. **17**(1): p. 44-50.
6. Harikrishnan, G. and D.V. Khakhar, *Effect of monomer temperature on foaming and properties of flexible polyurethane foams.* Journal of Applied Polymer Science, 2007. **105**(6): p. 3439-3443.
7. Kaushiva, B.D., et al., *Surfactant level influences on structure and properties of flexible slabstock polyurethane foams.* Polymer, 2000. **41**(1): p. 285-310.
8. Kendrick, T.C., et al., *The surface chemistry of polyurethane foam formation : I. Equilibrum surface tensions of polysiloxane-polyether block copolymer solutions.* Journal of Colloid and Interface Science, 1967. **24**(2): p. 135-140.
9. Krämer, R.H., et al., *Heat release and structural collapse of flexible polyurethane foam.* Polymer Degradation and Stability. **95**(6): p. 1115-1122.
10. Sonnenschein, M., et al., *The relationship between polyurethane foam microstructure and foam aging.* Polymer, 2008. **49**(4): p. 934-942.
11. Winter, H.H., P. Morganelli, and F. Chambon, *Stoichiometry Effects on Rheology of Model Polyurethanes at the Gel Point.* Macromolecules, 1988. **21**(2): p. 532-535.
12. Dounis, D.V. and G.L. Wilkes, *Structure-property relationships of flexible polyurethane foams.* Polymer, 1997. **38**(11): p. 2819-2828.
13. Kaushiva, B.D., *Structure-Property Relationships Of Flexible Polyurethane Foams*, 1999, Virginia Polytechnic Institute and State University: Blacksburg, Virginia.
14. Thomson, T., *Polyurethanes as Specialty Chemicals. Principles and Applications*, ed. C. PRESS2005.
15. Hill, R.M., *Silicone surfactants--new developments.* Current Opinion in Colloid & Interface Science, 2002. **7**(5-6): p. 255-261.
16. Zhang, X.D., et al., *Role of silicone surfactant in flexible polyurethane foam.* Journal of Colloid and Interface Science, 1999. **215**(2): p. 270-279.
17. Hill, R.M., *Silicone surfactants*. Surfactant Science Series, ed. A.T. Hubbard1999, New York: Marcel Dekker.
18. Testouri, A., et al., *Highly Structured Foams from Chitosan Gels.* Macromolecules, 2010. **43**(14): p. 6166-6173.

19. Drenckhan, W. and D. Langevin, *Monodisperse foams in one to three dimensions.* Current Opinion in Colloid & Interface Science, 2010. **15**(5): p. 341-358.
20. Owen, M.J., et al., *The surface chemistry of polyurethane foam formation : II. The role of surface elasticity.* Journal of Colloid and Interface Science, 1967. **24**(2): p. 141-150.
21. Martinez, C.J., *Bubble generation in microfluidic devices* Bubble Science, Engineering & Technology, 2009. **1**(1-2): p. 40-52.
22. Garstecki, P., A.M. Ganan-Calvo, and G.M. Whitesides, *Formation of bubbles and droplets in microfluidic systems.* Bulletin of the polish academy of sciences technical sciences, 2005. **53**(4): p. 361.
23. Gibson , J.L. and M.F. Ashby, *Cellular Solids: Structure and Properties*. 2nd ed. Cambridge Solid State Science Series, ed. D.R. Clarke, S. Suresh, and I.M. Ward FRS1997, Cambridge: Cambridge University Press.
24. Jang, W.-Y., A.M. Kraynik, and S. Kyriakides, *On the microstructure of open-cell foams and its effect on elastic properties.* International Journal of Solids and Structures, 2008. **45**(7-8): p. 1845-1875.
25. Warren, W.E. and A.M. Kraynik, *Linear elastic behavior of a low-density Kelvin foam with open cells.* Journal of Applied Mechanics-Transactions of the Asme, 1997. **64**(4): p. 787-794.
26. Mills, N., *Polymer Foams Handbook: Engineering and Biomechanics Applications and Design Guide*2007, Oxford: Butterworth-Heinemann.
27. Day, A.R., et al., *The elactic moduli of a sheet containing circular holes* Journal of the Mechanics and Physics of Solids, 1992. **40**(5): p. 1031-1051.
28. Green, D.J. and P. Colombo, *Cellular Ceramics: Intriguing Structures, Novel Properties, and Innovative Applications.* Mrs Bulletin, 2003. **28**(04): p. 296-300.
29. Lee, S.T., C.B. Park, and N.S. Ramesh, *Polymeric foams: science and technology*2006: CRC/Taylor & Francis.
30. Lee, S.T. and N.S. Ramesh, *Polymeric foams - Mechanisms and Materials*. Polymeric foams series, ed. S.T. Lee2004, Bica Raton, Flrida, USA: CRC Press.
31. Milton, G.W., *The theory of composites*. Cambridge monographs of applied and computational mathematics ed. A.I. P. G. CIARLET, R. V. KOHN, M. H. WRIGHT2004, Cambridge: Cambridge University Press.
32. Zhang, Y., D. Rodrigue, and A. Ait-Kadi, *High density polyethylene foams. II. Elastic modulus.* Journal of Applied Polymer Science, 2003. **90**(8): p. 2120-2129.
33. Moore, D.R. and M.J. Iremonger, *The Prediction of the Flexural Rigidity of Sandwich Foam Mouldings.* Journal of Cellular Plastics, 1974. **10**(5): p. 230-236.
34. Hashin, Z., *The elastic moduli of heterogeneous Materials.* ASME J. Appl. Mech., 1962. **29**: p. 143-150.
35. McLaughlin, R., *A study of the differential scheme for composite materials.* International Journal of Engineering Science, 1977. **15**(4): p. 237-244.
36. Farber, J.N. and R.J. Farris, *Model for prediction of the elastic response of reinforced materials over wide ranges of concentration.* Journal of Applied Polymer Science, 1987. **34**(6): p. 2093-2104.

37. Mondal, P. and D.V. Khakhar, *Regulation of cell structure in water blown rigid polyurethane foam.* Macromolecular Symposia, 2004. **216**: p. 241-254.
38. Owen, M.J. and T.C. Kendrick, *Surface chemistry of polyurethane foam formation : III. Effect of gas diffusion between bubbles and surface viscosity on bubble stability.* Journal of Colloid and Interface Science, 1968. **27**(1): p. 46-52.
39. Semsarzadeh, M.A. and A.H. Navarchian, *Effects of NCO/OH ratio and catalyst concentration on structure, thermal stability, and crosslink density of poly(urethane-isocyanurate).* Journal of Applied Polymer Science, 2003. **90**(4): p. 963-972.
40. Zhang, X.D., H.T. Davis, and C.W. Macosko, *A new cell opening mechanism in flexible polyurethane foam.* Journal of Cellular Plastics, 1999. **35**(5): p. 458.

8 GENERAL CONCLUSION AND OUTLOOK

The work presented in this thesis describes a new approach of generating highly structured solid polymer foams using Lab-on-a-Chip techniques. We have been able to demonstrate the efficiency of such an approach which relies on using a two-step process in which a liquid foam with well-controlled properties is first generated and then solidified in-situ. Having being applied to three different polymer systems (biohydrogel chitosan (Chapter 5), synthetic superabsorbent hydrogel (Chapter 6) and polyurethanes (Chapter 7)) this two-step process has proven to preserve the liquid foam structure during its solidification. In our applications this leads to the formation of solid foams with equal-volume bubbles which are arranged in highly ordered bubble crystals (Figure 8.1). This is of great interest for many applications such as scaffolding, cellular culture and the improvement of many of the foam "performances".

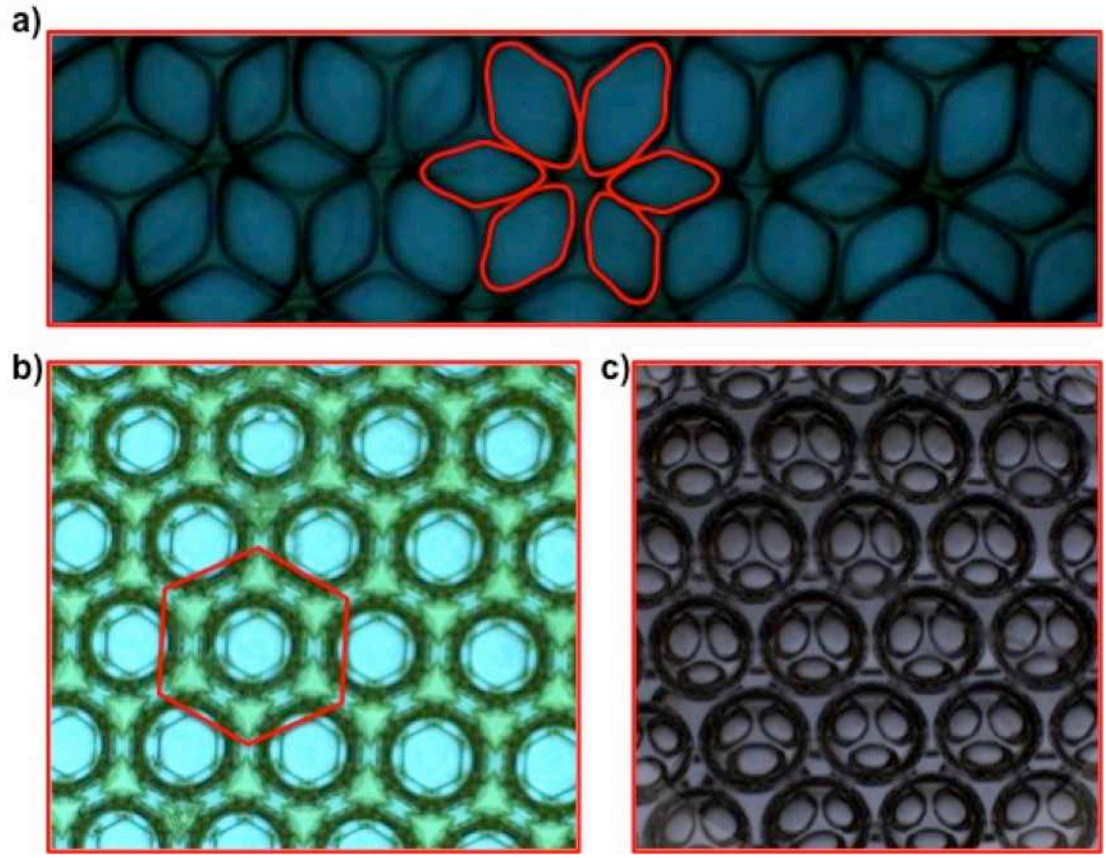

Figure 8.1: Some artistic pictures (with names invented by us) of a) Chitosan "flower structure". b) Polyurethane "star-like" bubbles. c) "Alien-faced" chitosan foam.

We have been able to demonstrate that for these three polymer systems one can master with high precision the generation of monodisperse foams using millifluidic flow techniques. These provide well-defined foam properties in terms of bubble size, structure and density – all of which allows controlling and improving the properties of the final polymer foam. This was ensured by

calibrating the millifluidic foaming device which permits to obtain a simple power law given by $D_B=D_c(Q_g/Q_l)^b$.

The generation of very ordered foams with equal bubble size using millifluidic techniques was found to be very well reproducible. As a result, we were able to generate foams with controlled bubble sizes and densities by choosing the appropriate pairs of gas and liquid flow rates, and by adjusting appropriately the millifluidic device geometry. For convenience, the bubble sizes generated by us have typically been of the order of 0.3-1.5 mm. In principle, these sizes can be driven down to a few tenths of micrometers. Working with smaller bubbles will help to overcome an important issue: due to the high difference in liquid/gas densities, gravity driven drainage leads easily to inhomogeneous foam densities. The foam height over which the foam remains homogeneous may be approximated by (see Appendix A)

$$h \approx 3.4\sqrt{\frac{1}{\varphi}}\frac{l_c^2}{R_B}$$

where φ is the liquid fraction, R_B the bubble radius and l_c the capillary length. This shows that the smaller the bubbles and the lower the liquid fraction, the larger the height of the foam over which it remains homogeneous.

We observed different crystalline bubble structures as reported in the literature [1-3], mostly FCC and HCP. These structures are obtained only if the polymer solidification time is fine-tuned to let the bubbles, which exit from the millifluidic device, self-organise under gravity/confinement before the polymerisation occurs. Although we did not perform a systematic study on the crystalline structure of our foams, the "qualitative" optical characterisation of the crystalline foam samples demonstrated that these structures could be easily obtained using the two-step process.

Thanks to the modular nature of microfluidic techniques, it is possible to integrate mixing processes, chemical reactions and foam generation in a way which provides an important degree of control over each processing step. The separation of our work into independent steps (Section 1), which were translated into sub-units inside the lab-on-a-chip channel network used for the generation of the crystalline foams has proven to be very efficient. This allowed to study each sub-unit in an independent fashion and rendered easier the adjustment of the channel network according to the requirements of each studied system.

It was also deduced that one needs to work initially with foams which have a liquid content of more than 30 % to ensure that bubbles remain spherical and glide easily one past another to find their optimal location in the hexagonally close-packed structure. In dryer foam, rearranging neighbouring bubbles is energetically too costly and therefore does not occur spontaneously. Ordered, solidified foams with lower liquid content and therefore with non-spherical bubbles can be formed by allowing the liquid to drain, either due to gravity or through the application of pressure gradients [3]. With highly viscous liquids,

such as the chitosan or polyol solutions we used, this draining process takes time, which requires an even more delicate fine-tuning of foam stability and solidification time.

There should, however, also be a great interest in generating monodisperse foams with disordered structures. These can be achieved by tuning the liquid and gas flow rates in such a way as to produce immediately foams of low liquid fractions.

In some preliminary tests we have seen that this may also be a promising route to generate open-cell foams. Whilst the foams generated at high liquid content seem to maintain closed cells upon solidification, those containing a smaller amount of liquid and hence larger and thinner films separating the bubbles seem to experience film rupture upon solidification such that holes are created between bubbles, whilst the overall bubble structure is "frozen", leaving behind a sponge-like material.

In a more particular way, our study showed the following details.

In the case of **Chitosan** (Chapter 5), we demonstrated the feasibility of generating ordered equal-sized foams from hydrogel via crosslinking, which are extensively used for biomedical applications. In particular, applications of hydrogel foams for scaffolding [4, 5] or the 3D culture of bacteria are asking for a precise control over the pore architecture. The generation of these gelified foams entrains two particularly interesting fundamental questions, which are already receiving increasing attention due to their relevance to applications: the first concerns the understanding of the functioning of a number of micro- or millli-fluidic techniques for non-Newtonian solutions. The second concerns the long-term "stability" of the gelified porous materials. For example, in some cases, we were not able to permanently "freeze" the gelified foam structures. In those cases the elastic modulus of the gel-network was not sufficient to counterbalance pressure differences between bubbles, hence driving a self-amplifying gas exchange from the smaller to the bigger bubbles known as *foam coarsening* [6]. Important fundamental questions are therefore related to the existence of a limiting elasticity of the continuous phase to entirely stop the coarsening, or, in more general terms to the bubble size distribution obtained in a coarsening foam which has a non-negligible network elasticity.

Producing ordered foams from the **superabsorbent polymer** (Chapter 6) was an attempt to demonstrate the flexible and universal feature of our technique of generating structured foam. We qualitatively showed that the SAP with ordered foamed structure inside have more homogeneous absorption. Even though we did not have the time to investigate in detail the generated SAP foams, one can easily imagine the advantages of the monodisperse foam structures for different applications. Efforts are made to replace the currently used granular SAP systems by foamed ones. The absorption rate of SAP foams depends strongly on the average bubble size and on the degree of open-cellness. Both can be

controlled to high accuracy with our approach which should therefore provide fundamental insights into the complex absorption processes of SAP foams.

The quantitative characterisation of the mechanical properties of the **polyurethane** (Chapter 7) ordered foam gave a preliminary insight into the effect of the foam structure on its mechanical response. We confirmed that the foam density is the key parameter which influences the elastic modulus of the foam and we could show that the polyurethane foams produced by us are well captured by two power laws taken from the literature (Section 7.8.2). The foams in the high-density limit were found to have closed-cell structures, whereas low-density foams have open-cell ones. We found that the effect of monodispersity on the Young's modulus of the foams was not very significant in the low and high-density limit. However, it plays a role at intermediate densities around the close-packed limit of the foam structure, which depends on the bubble size distribution. Combining our results with modelling efforts from the literature, we propose two limiting curves for the Young's modulus of monodisperse and polydisperse foams and porous media over the entire density range. Future investigations should study this hypothesis more systematically. They should also concentrate on the effect of the monodispersity on the mechanical response at high strains, for which we expect a more pronounced influence of the monodispersity.

The versatility of our approach has been demonstrated for a range of materials, including polymer and particle gels [5, 7-10]. It should easily be transferable to a large range of polymers and reticulants. In the case of monomeric acrylamid solutions, which are polymerised and cross-linked simultaneously in the solidifying foam, this has been demonstrated by Van der Net *et al.*[8]. Sang et al. successfully used physically cross-linked (ionic) alginate solutions containing ferrofluid particles to render the foamed gels stimulable [7]. In general, using milli- or microfluidic techniques for the well-controlled generation of multi-phase systems with one solidifying component presents a very promising and versatile "lego-type" route to the fabrication of a wide range of materials with equally well-controlled properties.

The upscaling of monodisperse foaming techniques is of great interest for industrial applications but remains very challenging. The parallelisation is seemingly the most suitable and easiest way to generate large foam samples. This approach has been used recently by Stoffel et al. [11] who successfully designed a microfluidic bubble generator with 256 parallel production channels which operate simultaneously. Bubble production in this case is described by a different power law but remains reliable and reproducible.

The near future will certainly see this range extended to serve the needs of different domains which require precise control over porous structures. In this process, solid foams may also conquer entirely new domains. To make this happen, manifold challenges need to be faced. These concern in particular more control over the creation and stabilisation of foams formed from chemically complex liquids, many of them non-aqueous; or the comprehension and control

of foam and thin film stability during the liquid/solid transition. The modular approach proposed here may help to advance our scientific understanding in these domains and may provide a significantly improved control over the final foam properties (for example the degree of open-cellness). Simultaneously, the availability of well-controlled solid foam structures may help to investigate more deeply important questions related to the structure-property relationship of porous solids. As such, the subject is not only of interest for applied questions, but it also raises - and will hopefully help answering - much more fundamental ones.

BIBLIOGRAPHY

1. van der Net, A., et al., *The crystal structure of bubbles in the wet foam limit.* Soft Matter, 2006. **2**(2): p. 129-134.
2. van der Net, A., et al., *Crystalline arrangements of microbubbles in monodisperse foams.* Colloids and Surfaces a-Physicochemical and Engineering Aspects, 2007. **309**(1-3): p. 117-124.
3. Hoehler, R., et al., *Osmotic Pressure and Structures of Monodisperse Ordered Foam.* Langmuir, 2007. **24**(2): p. 418-425
4. Griffon, D.J., et al., *Chitosan scaffolds: Interconnective pore size and cartilage engineering.* Acta Biomaterialia, 2006. **2**(3): p. 313-320.
5. Chung, K.Y., et al., *Fabricating scaffolds by microfluidics.* Biomicrofluidics, 2009. **3**(2).
6. Weaire, D. and S. Hutzler, *The Physics of Foams*1999, Oxford: Clarendon Press.
7. Yip Cheung Sang, Y., *Vers des micromousses stimulables (Toward smart microfoams)*, in *MSC*2009, University of Denis Diderot Paris 7: Paris.
8. van der Net, A., et al., *Highly structured porous solids from liquid foam templates.* Colloids and Surfaces a-Physicochemical and Engineering Aspects, 2009. **346**(1-3): p. 5-10.
9. Testouri, A., et al., *Highly Structured Foams from Chitosan Gels.* Macromolecules, 2010. **43**(14): p. 6166-6173.
10. Rodriguez-Arriaga, L., et al., *Elucidating the (in)stability of foams stabilized by mixtures of nano-particles and oppositely charged surfactants.* Soft Matter, 2011. **submitted**.
11. Stoffel, M., et al., *Bubble Production Mechanism in a Microfluidic Foam Generator.* Physical Review Letters, 2012. **108**(19): p. 198302.

9 APPENDICES

Appendix A

Results of the calibration of the T-junction used for the generation of monodisperse Chitosan foams

The detailed results of the calibration of the foaming geometry (T-junction) with different capillaries are shown in the tables below.

Table 9.1: Calibration of T-junction using Water + Fairy in a channel of 1mm width

			Volume de liquide injecté (mL)													
			2				5,5				9					
Qgaz(ml/h)	Qliq(ml/h)	Qgaz/Qliq	L(cm)	Nbre de bulles	D(mm)	Monodisperse	L(cm)	Nbre de bulles	D(mm)	Monodisperse	L(cm)	Nbre de bulles	D(mm)	Monodisperse	Moyenne	Ecart type
25	50	0,5	0,878	6	1,46	~	1,303	9	1,45	~	0,941	7	1,34	~	1,417	0,213066
50	50	1	1,261	8	1,58	X	1,235	10	1,24	X	1,823	12	1,52	X	1,447	0,580721
100	50	2	1,627	10	1,63	X	2,044	13	1,57	X	1,457	9	1,62	X	1,607	0,102866
200	50	4	0,928	5	1,86	X	2,038	11	1,85	X	1,659	9	1,84	X	1,85	0,032
400	50	8	2,617	12	2,18	X	1,951	9	2,17	X	1,59	7	2,27	X	2,207	0,176242
800	50	16	1,482	6	2,47	~	1,271	5	2,54	~	1,261	5	2,52	~	2,51	0,115378
25	100	0,25	1,329	7	1,9	~	1,486	8	1,86	~	1,304	7	1,86	~	1,873	0,073901
50	100	0,5	2,148	11	1,95	~	3,831	19	2,02	~	3,87	19	2,04	~	2,003	0,151226
100	100	1	4,004	18	2,22	X	3,801	17	2,24	X	3,417	15	2,28	X	2,247	0,097762
200	100	2	2,215	10	2,22	X	3,93	16	2,46	X	3,433	14	2,45	X	2,377	0,434462
400	100	4	3,352	12	2,79	X	2,564	9	2,85	X	3,748	13	2,88	X	2,84	0,146642
800	100	8	2,293	7	3,28	~	3,495	10	3,5	~	3,088	9	3,43	~	3,403	0,359674
25	200	0,125	0,927	7	1,32	~	1,98	14	1,41	~	0,841	6	1,4	~	1,377	0,157852
50	200	0,25	1,534	10	1,53	~	1,086	7	1,55	~	1,557	10	1,56	~	1,547	0,048881
100	200	0,5	2,843	17	1,67	X	2,204	13	1,7	X	2,362	14	1,69	X	1,687	0,048881
200	200	1	3,089	17	1,82	X	2,419	13	1,86	X	2,873	16	1,8	X	1,827	0,097762
400	200	2	1,701	8	2,13	X	0,855	4	2,14	X	0,923	4	2,31	X	2,193	0,323712
800	200	4	1,858	7	2,65	~	2,055	8	2,57	~	1,855	7	2,65	~	2,623	0,147802
100	25	4	1,843	8	2,3	~	0,94	4	2,35	~	1,586	7	2,27	~	2,307	0,129326
100	50	2	2,189	12	1,82	X	1,959	11	1,78	X	2,329	13	1,79	X	1,797	0,066613
100	100	1	1,669	10	1,67	X	1,861	11	1,69	X	1,375	8	1,72	X	1,693	0,080532
100	200	0,5	2,497	19	1,31	X	1,519	11	1,38	X	1,233	9	1,37	X	1,353	0,12115

Table 9.2: Calibration of T-junction using Water + Fairy in a channel of 1.25mm width

			Volume de liquide injecté (mL)													
			2				5,5				9					
Qgaz(ml/h)	Qliq(ml/h)	Qgaz/Qliq	L(cm)	Nbre de bulles	D(mm)	Monodisperse	L(cm)	Nbre de bulles	D(mm)	Monodisperse	L(cm)	Nbre de bulles	D(mm)	Monodisperse	Moyenne	Ecart type
25	50	0,5	1,415	8	1,77	~	1,432	8	1,79	~	1,41	8	1,76	~	1,773	0,04888
50	50	1	1,329	7	1,9	X	1,583	8	1,98	X	2,18	11	1,98	X	1,953	0,1478
100	50	2	1,264	6	2,11	X	1,546	7	2,21	X	1,623	7	2,32	X	2,213	0,33613
200	50	4	1,811	7	2,59	~	1,565	6	2,61	~	1,596	6	2,66	~	2,62	0,11538
25	100	0,25	1,283	8	1,6	~	1,29	8	1,61	~	1,397	9	1,55	~	1,587	0,10287
50	100	0,5	1,24	7	1,77	X	1,747	10	1,75	X	1,185	7	1,69	X	1,737	0,13323
100	100	1	1,523	8	1,9	X	1,475	8	1,84	X	1,88	10	1,88	X	1,873	0,09776
200	100	2	1,492	7	2,13	X	1,705	8	2,13	X	1,98	9	2,2	X	2,153	0,12933
400	100	4	1,262	5	2,52	~	1,452	6	2,42	~	1,236	5	2,47	~	2,47	0,16
25	125	0,2	0,781	5	1,56	~	1,165	7	1,66	~	0,8	5	1,6	~	1,607	0,16106
50	125	0,4	1,162	7	1,66	X	1,318	8	1,65	X	1,052	6	1,75	X	1,687	0,17624
100	125	0,8	1,461	8	1,83	X	1,475	8	1,84	X	2,577	14	1,84	X	1,837	0,01848
200	125	1,6	2,467	12	2,06	X	1,434	7	2,05	X	1,635	8	2,04	X	2,05	0,032
400	125	3,2	1,681	7	2,4	~	1,721	7	2,46	~	1,43	6	2,38	~	2,413	0,13323

Table 9.3: Calibration of T-junction using Glycerol + Fairy in a channel of 1.25mm width

			Volume de liquide injecté (mL)													
			2				5,5				9					
Qgaz(ml/h)	Qliq(ml/h)	Qgaz/Qliq	L(cm)	Nbre de bulles	D(mm)	Monodisperse	L(cm)	Nbre de bulles	D(mm)	Monodisperse	L(cm)	Nbre de bulles	D(mm)	Monodisperse	Moyenne	Ecart type
6,25	50	0,125	0,554	6	0,92	~	0,699	8	0,87	~	1,028	11	0,93	~	0,907	0,102866
12,5	50	0,25	0,643	6	1,07	X	0,747	7	1,07	X	1,169	11	1,06	X	1,067	0,018475
25	50	0,5	0,804	7	1,15	X	0,692	6	1,15	X	0,99	8	1,24	X	1,18	0,166277
50	50	1	1,129	8	1,41	~	1,019	7	1,46	~	1,024	7	1,46	~	1,443	0,092376
12,5	100	0,125	0,653	7	0,93	~	1,098	11	1	~	0,858	9	0,95	~	0,96	0,115378
25	100	0,25	0,611	6	1,02	X	0,776	7	1,11	X	0,892	8	1,12	X	1,083	0,176242
50	100	0,5	0,765	7	1,09	X	0,875	7	1,25	X	0,876	7	1,25	X	1,197	0,295603
100	100	1	0,7	6	1,17	~	0,708	5	1,42	~	1,056	7	1,51	~	1,367	0,563721
15,625	125	0,125	0,804	8	1,01	~	1,07	11	0,97	~	1,013	10	1,01	~	0,997	0,073901
31,25	125	0,25	0,527	5	1,05	X	0,554	5	1,11	X	0,529	5	1,06	X	1,073	0,102866
62,5	125	0,5	0,753	6	1,26	X	0,485	4	1,21	X	0,724	6	1,21	X	1,227	0,092376
125	125	1	0,928	7	1,33	~	0,734	5	1,47	~	0,714	5	1,43	~	1,41	0,230755

Appendix B

Phase Diagram of the calibration of the flow-focussing foaming geometry

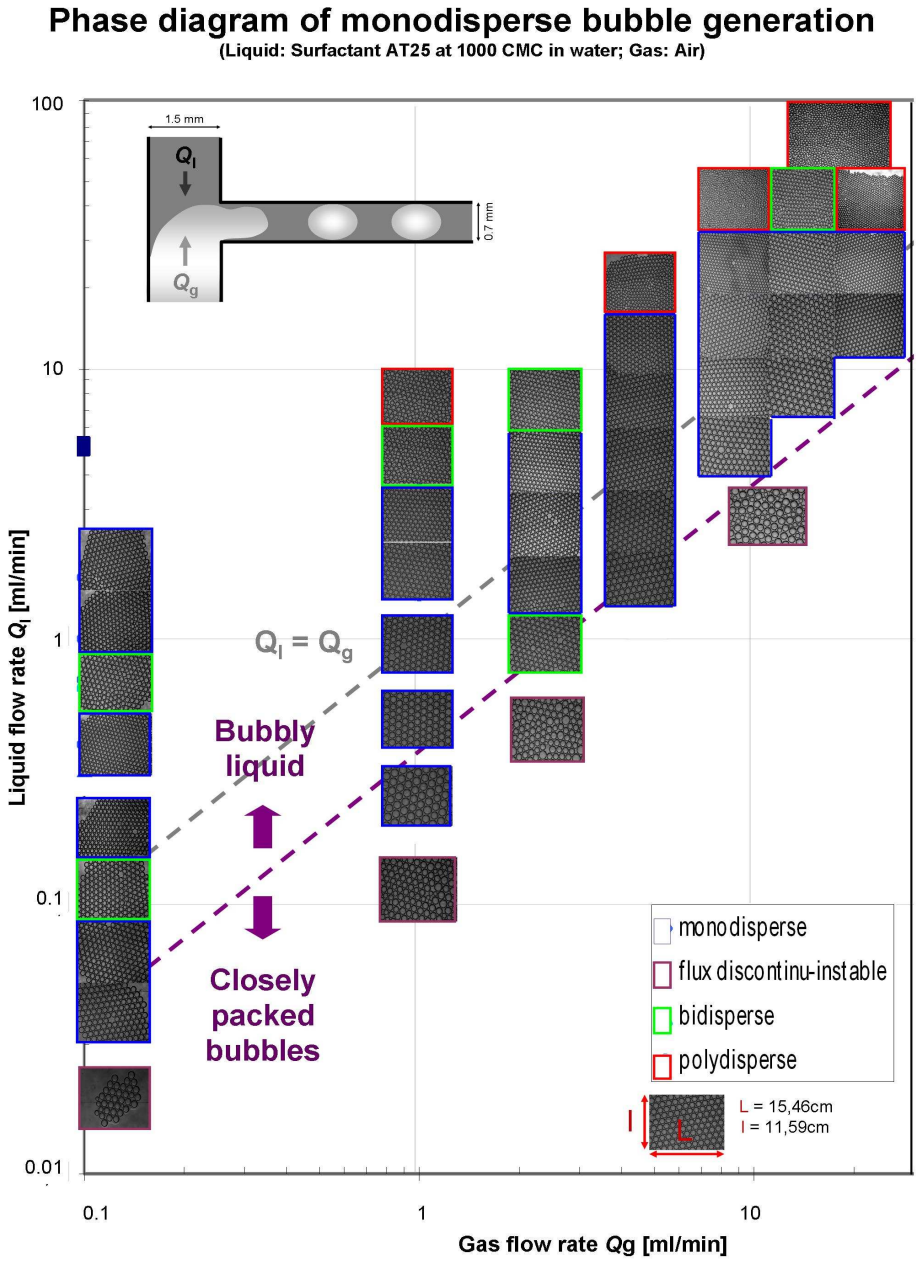

Figure 9.1 : Phase diagram of monodiserspe foam generation

Appendix C

How to approximate how much a foam with initial liquid fraction φ_L and bubble radius R_B drains?

Assumptions:

1. Kelvin foam
2. Foam sufficiently dry in order to approximate it by Plateau borders only (otherwise need to take into account the vertices)

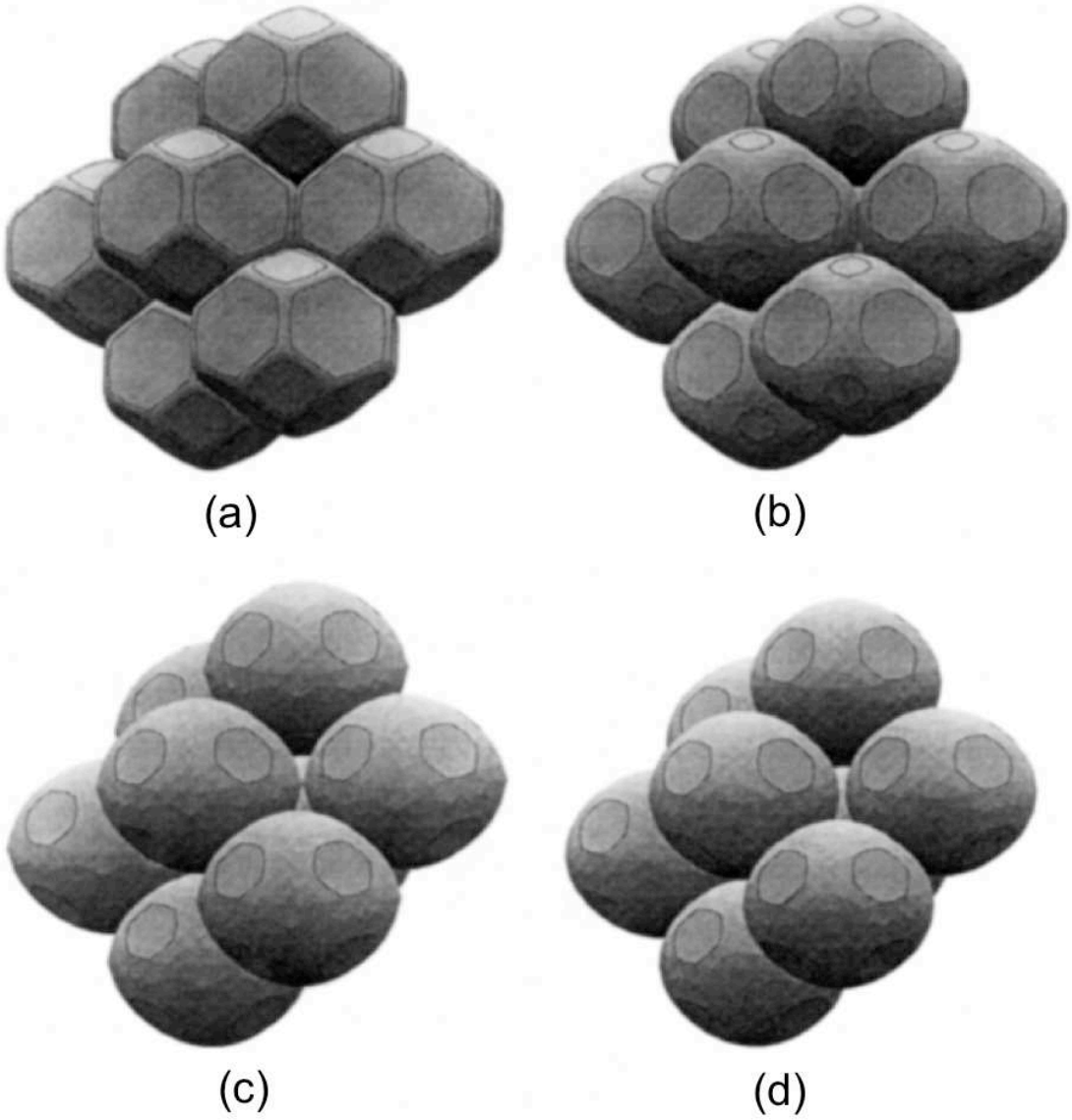

Figure 9.2 : Kelvin bubbles for different liquid fractions

We know for the Kelvin structure that

$$\varphi_{Kelvin} \approx 1.18\left(\frac{h}{l}\right) + 0.17\left(\frac{r}{l}\right)^2 + 0.16\left(\frac{r}{l}\right)^3$$

With *r* being the radius of curvature of the Plateau border, *h* the thickness of the films and *l* the edge length of the facets (all of them are equal in a Kelvin structure). In reasonably dry foams we can neglect the contribution of the films and the vertices to the liquid fraction (first and last term, respectively). We also know that

$$R_B = l(6\sqrt{2}/\pi)^{1/3}$$

Now : In equilibrium, the hydrostatic pressure should be of the order of the Laplace pressure of the Plateau borders which have radius of curvature *r*. We therefore have

$\rho g h = \frac{\gamma}{r}$,

Assuming that the Plateau borders are straight, i.e. the second radius of curvature of the Plateau border infinitely large. γis, of course, the surface tension. For a Kelvin structure we know from above that

$$r = \sqrt{\frac{\varphi}{0.16}}\left[\frac{6\sqrt{2}}{\pi}\right]^{-1/3} \approx 0.29\sqrt{\varphi}R_B$$

We therefore obtain that

$$h \approx 3.4\sqrt{\frac{1}{\varphi}}\frac{l_c^2}{R_B}$$

with lc being the capillary length. Hence we can say that if h is much higher than the actual height of the foam, the corresponding foam samples is considered as homogeneous.

Using Kelvin foams is not a crude approximation. All these type of calculations are very insensitive to the foam structure, since they depend on the surface energy which depends little on the foam structure.

Appendix D

First results of the effect of the mixing ratio on the mechanical behaviour of polyurethane polymer

Results of the measurements of the elastic moduli for different mixing ratio performed in BASF.

Compression tests were performed on polymer films generated using four different mixing ratios in BASF laboratory (with and without catalysts). The results are presented in Figure 1 and Figure 2. Due to time constraints, we were not able to pursue these investigations. It remains nevertheless a good starting point for future more systematic studies.
We have generally noticed that the higher the mixing ratio, the higher the elastic modulus which is due to the formation of NCO terminated polyurethane in presence of an excess of isocyanate (mixing ratio 110:100).

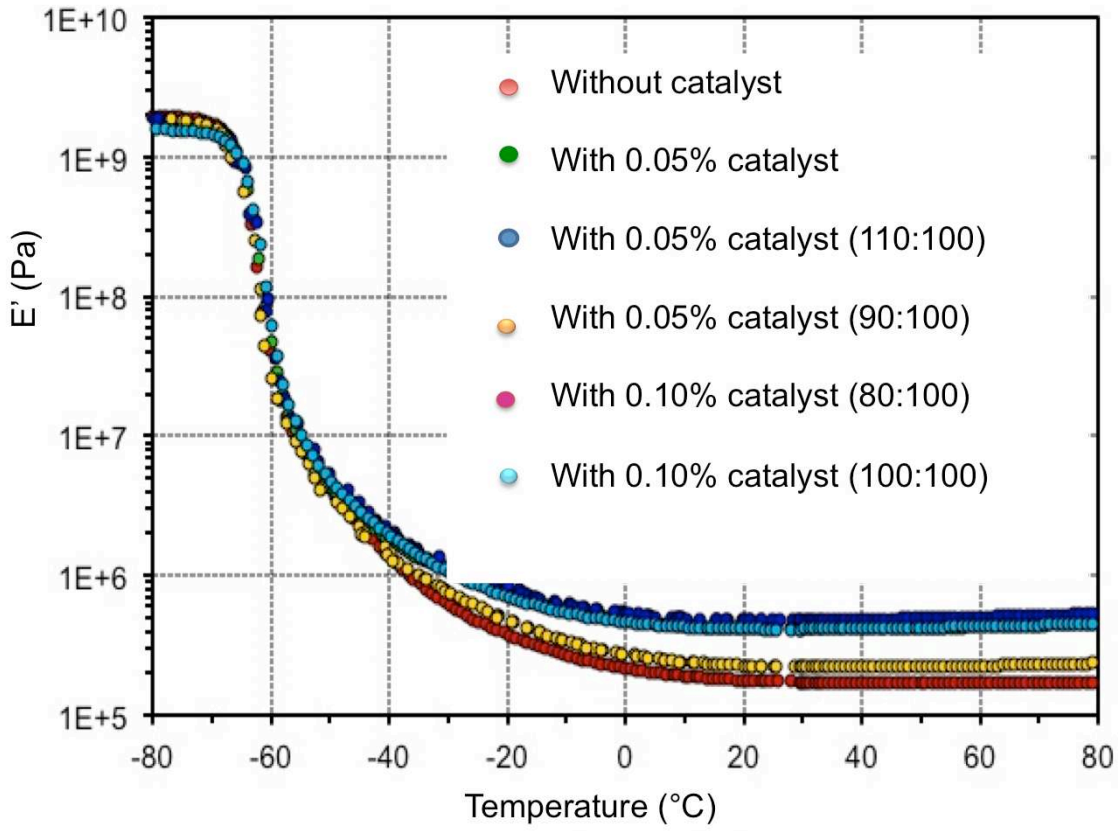

Figure 9.3: Results of the measurements of the elastic modulus for different polymer chemical compositions performed in BASF laboratory

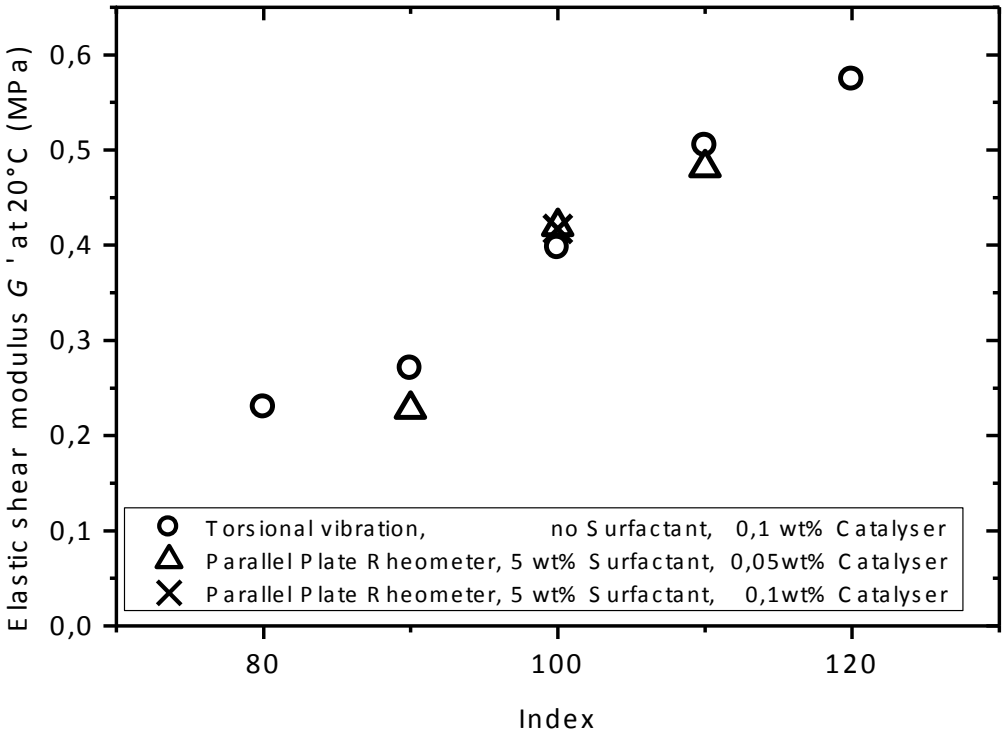

Figure 9.4: Results of the measurements of the Young modulus of foam samples with different mixing index performed in BASF